Mechanical behavior of RC walls under seismic activity strenghtened with CFRP

Samiullah Qazi

N° d'ordre 2013ISAL0003
Année 2013

Thèse

COMPORTEMENT MÉCANIQUE SOUS SOLLICITATIONS ALTERNÉES DE VOILES BÉTON ARMÉ RENFORCÉS PAR MATÉRIAUX COMPOSITES

Présentée devant
L'institut national des sciences appliquées de Lyon

Pour obtenir
Le grade de docteur

Formation doctorale
Laboratoire de Génie Civil et d'Ingénierie Environnementale

École doctorale
École doctorale MEGA de Lyon

Par
Samiullah QAZI
(Ingénieur)

Soutenue le 17 Janvier 2013 devant la Commission d'examen

Jury MM.

Nathalie ROY	Professeur, Université de Sherbrooke	Rapporteur
David BIGAUD	Professeur, Université d'Angers	Rapporteur
Joaquim BARROS	Professeur à l'Université de Minho	Examinateur
Ali LIMAM	Professeur, Insa Lyon	Examinateur
Marc QUIERTANT	Chargé de recherche, IFSTTAR	Invité
Patrice HAMELIN	Professeur émérite, Université Lyon 1	Invité
Emmanuel FERRIER	Professeur, Université Lyon 1	Directeur de thèse
Laurent MICHEL	Maitre de Conférences, Université Lyon 1	Co-directeur de thèse

Laboratoire de recherche: Laboratoire de Génie Civil et d'Ingénierie Environnementale

To my parents
To all those who are dear to me

Acknowledgements

First, I would like to thank my supervisor, Dr. Emmanuel Ferrier, for offering me the opportunity to work at the "Laboratoire de Génie Civil et d'Ingénierie Environnementale site BOHR" . I am highly indebted for his continuous support, encouragement, and constant discussion throughout this research. I would also like to thank Dr. Laurent MICHEL who is the co-director of this thesis. He initiated the research project and contributed significantly by advice and guidance.

It was a pleasure to work in an amicable and friendly environment with Dr Patrice HAMELIN, Dr Aron GABOR, Dr Amir SI LARBI, Dr Bruno JURKIEWIEZ, Dr Laurence CURTIL, Dr Nadège REBOUL, Dr Xuang Hong VU, Dr Raphaël CONTAMINE, Dr Charlotte MEAUD and Samira SOUIDI.

My thanks also go to Freyssinet interprise for providing me with necessary equipments and materials for experimental investigations.

I would also like to thank the Higher Education Commison (HEC) of Pakistan for supporting me with the research grant from period 2009-2012 for conducting the research.

Finally, I am grateful to my parents and my family for their patience and encouragement throughout the research work.

COMPORTEMENT MÉCANIQUE SOUS SOLLICITATIONS ALTERNÉES DE VOILES BÉTON ARMÉ RENFORCÉS PAR MATÉRIAUX COMPOSITES

Résumé

Les enquêtes récentes sur les séismes ont fait ressortir l'importance des murs en béton armé en tant que partie intégrante des structures. L'évolution des règlements prend en compte ces considérations, par contre le bâti existant doit subir des renforcements dans l'objectif de leur mise en conformité. Dans cette thèse une étude expérimentale faite sur douze murs (six élancés et six courts) renforcés par un collage externe en composite a été conduite. Les murs ont été conçus en étant sous-renforcés à la flexion et cisaillement. Quatre de ces six échantillons ont été renforcés par des bandes de PRFC collées. Deux spécimens, un témoin et un renforcé, ont été soumis à un test de chargement statique et quatre échantillons, l'un témoin et trois rénovés, ont été soumis à des essais de charge cyclique. La discussion et l'analyse des tests incluent la description de la fissuration, l'analyse de la rigidité, de la capacité de charge ultime, de la ductilité.

Mots-Clés: voile - béton armé - renforcement par PRF – séisme – ancrage.

Mechanical Behavior of RC Wall under Seismic activity Strengthened with CFRP

Abstract

Recent earthquake surveys have revealed the significance of RC walls as an integral part of structures. It reduces the structure damage to some extent. However, like other structural member they too are vulnerable. Researchers on basis of their post eartthquake survey and laboratary experiments have concluded that the RC wall buildings sustained damage, mainly due to design and construction work flaws. In this thesis experimental result of shear walls is discussed. They were designed under-reinforced to fail in shear in ase of short wall and in flexure for slender walls. Three out of these six specimens, in each case, were strengthened externally with CFRP strips bonded to wall panel and mesh anchors installed at wall foundation joint. Two specimens, one RC and one CFRP retrofitted (short and slender wall each), were subjected to static load test and three specimens, one RC and two to three CFRP retrofitted, were subjected to quasi static cyclic load tests. The test result analysis discussion includes failure mode, stiffness, ultimate load capacity, ductility, and energy dissipation.

Key-words: shear wall – Reinforced Concrete (RC) – seismic strengthening – Carbon Fiber Reinforced Polymers (CFRP) – anchorage.

Table of contents

General Introduction

Earthquake is one of the major natural hazards. It is not always predictable and can occur all over the world. However, it mostly occurs on active faults that define the major tectonic plates of the earth. Ninety percent of the world's earthquakes occur along these plate boundaries (that represent about 10% of the surface of the earth). According to the U.S. geological survey estimate, up to 50 seismic activities occurs per day i.e. 20,000 per year. However, luckily most of them go undetected as either they hit remote areas or have small magnitude. An earthquake causes the worst damage when it occurs in an urban area. For example it is estimated that the 1995 Kobe earthquake cast more than 80 billion Euros, almost 5300 people died, 27000 were injured, and 30000 became homeless. Over the last five years, several devastating earthquakes of magnitude (Mw) greater than 7, took place in China (Sichuan, May 2008, Mw = 7.9), Haiti (January 2010, Mw = 7), Chile (February 2010, Mw = 8.8), Japan (Northeast Honshu, March 2011, Mw = 9), and New Zealand (Christchurch, February 2011, Mw = 7.1).

The earthquake impact on an area is directly correlated with its intensity, and the construction practice and population density of that area. The intensification and urbanization of populations in recent decades are two aggravating factors of the earthquakes consequences. Jean Jacques Rousseau (Rousseau 1756) on the basis of his observations of the damages caused by 1755 Lisbon earthquake concluded that the damage would have been much less, and may be zero if we "had not collected there twenty thousand houses of six to seven floors and if the inhabitants of this city had been dispersed more evenly and more lightly lodged."

To ensure that buildings are safe and reliable against earthquakes, countries such as Japan and United States have updated their seismic building codes. A perfect illustration of relevance of this approach lies in endurance of a large number of infrastructures in 2011 Japan earthquake (though other disorders were generated by the tsunami). For example, roads, airports and ports were opened within a week after the earthquake for emergency vehicles (The Japan Times 2011), and about in two weeks for general traffic (Daily Yomiuri online, 2011).

Ensuring the availability of reliable construction is necessary for the public safety and prevention of the major risks ([OJ, Law No. 2004-811, 2004]); however, instant reconstruction of all the civil engineering infrastructures not complying with the modern seismic safety standards is not possible. Thus, study of the structures vulnerability and means to rehabilitate it is in general interest. In France, the new national seismic zoning (JORF n°0248, décret n°2010-1254 2010) & (JORF n°0248, décret n°2010-1255 2010), related to the Eurocode 8 (EN 1998), involves the reclassification of certain structures/buildings in the areas where the seismicity has been noted: a revaluation of these structures is necessary. The Caribbean earthquake plan presented in Council of Ministers on 17 January 2007 (DGPR 2009) makes significant programs in reducing the vulnerability of structures. The aim is that within 20 years, most of the public buildings (education, health, crisis management, social housing) if necessary, should be strengthened or rebuilt to withstand a major earthquake. It is supported by OPECST (L'Office Parlementaire d'Évaluation des Choix Scientifiques et Technologiques) (OPECST 2010) statement that if an earthquake alike Fort-de-France 1839 earthquake occur today more than 30,000 will be affected by it.

For structure rehabilitation or strengthening, it is necessary to assess the vulnerability of structures and propose rehabilitation techniques for weak structural elements. Numerous techniques exist today to ensure the compliance of structures, including traditional materials such as concrete and steel. Re-strengthening structural elements by composite materials is an attractive alternative because of its light weight, ease in implementation and resistance to corrosion. However, to meet the immediate concerns of professionals and public works, it is necessary to pursue the development of design codes, for composite materials reinforcement techniques, in continuity with existing procedures, developed for example in the Eurocodes (EN 1998) or in national design guidelines.

In this context, the project ANR-INPERMISE (INgénierie PERformantielle pour la Mise en SEcurité des ouvrages par matériaux composites), involving industrial partners (Freyssinet International and Vinci Construction France) and the LGCIE (Laboratoire de Génie Civil et d'Ingénierie Environnementale, Villeurbanne), CSTB (Centre Scientifique et Technique du Bâtiment, Champs-sur-Marne) and IFSTTAR (Institut Français des Sciences et Technologies, des Transports, de l'Aménagement et des Réseaux – site de Paris), was initiated to develop qualification testing and propose methods for the design and analysis, consistent with the regulations (including the Eurocodes), of RC columns and walls (RC or masonry) subjected to axial compression and base shear. It included designing and validation of innovative construction processes by implementing composite materials and ensuring security of structures, especially in the case of accidental or extreme loads (shocks, earthquakes).

The LGCIE involved in this project focused on the development of tests and calculation methods for RC shear walls strengthened with CFRP. Shear walls are in general the major structural element in buildings in France. They are used as vertical load resistant members, and in addition to that used to resist lateral load (seismic activity). Proposal of a novel technique to rehabilitate these major elements and predict their load response behavior is a necessity. In literature, a very small number of experimental data is currently available regarding the behavior of RC walls strengthened with Fiber Reinforced Polymers (FRP) reinforcements as compared to the studies investigating the behavior of reinforced concrete walls. Therefore, it is essential to be able to analyze the effectiveness of such a solution. The anchoring of composite materials is often necessary to ensure its optimization. Thus, the study of constructive processes specific to improve the anchorage and load transfer between wall and support (beam/ foundation) is fundamental in the analysis of the effectiveness of the reinforcement techniques.

The research work presented in this dissertation focuses on the behavior RC shear walls strengthened with FRP and loaded with a static cyclic displacement load with a constant axial load ratio, representative of seismic action. Primary objectives of this research are: (a) to identify damage mechanisms, its development at local and global scale, the origin of nonlinearities in behavior and the ultimate deformation (b) to estimate and verify experimentally the variation in specimens' strength, ductility and energy dissipation capacity due to the changes made in the external CFRP reinforcement arrangements.

Although the range of FRP material used in construction is quite diverse (such as carbon fibers, glass, and aramid) CFRP is used in this study because of its implementation in majority of research work done on the RC structural elements due to its high strength.

The objective of this scientific and technical project is not to propose new reinforcement systems (except the optimization of anchoring conditions) but to propose the application of existing processes on the reinforced concrete shear walls to improve its seismic performance.

The above mentioned objectives are addressed in this research work. The dissertation is divided in to three parts as follows.

Part I provides a review of the different types of structural damages caused by an earthquake, specifically in reinforced concrete walls. Different techniques of reinforcement are discussed: techniques related to traditional materials and new materials such as FRP. Anchorage techniques used to improve the external CFRP reinforcement performance are discussed. This is important because to rehabilitate structures, it is necessary to have a certain amount of knowledge about their failure mechanisms and repair techniques.

Part II describes the experimental work conducted on test specimen, simulating the infield shear walls at 1:3 scales. Tests were designed to characterize the influence of CFRP reinforcement effect on the behavior of RC walls. Different CFRP reinforcement configurations were tested, with use of anchors in some case to evaluate its effect in controlling the intermediate crack debonding. The result discussion includes: variation in failure modes, performance gains (strength, ductility, and dissipated energy) attributed to CFRP configurations.

Part III describes analytical approach adapted to: (a) approximately evaluate specimen ultimate load capacity, ultimate displacement, and its load response behavior on global scale (b) propose avenues for development of design codes of these reinforcements specific to seismic retrofit.

The conclusion provides a summary of this work highlights its strong points its limitations and briefly discusses the possible future directions.

Part I: Literature review

1 Earthquake Damage

1.1 Introduction

Seismic activity/Earthquake is the result of a sudden release of energy in the Earth's crust that creates seismic waves. It is caused mostly by rupture of geological faults but also by other events such as volcanic activity, landslides, mine blasts, and nuclear tests. Its effects include ground shaking/rupture, landslides/avalanches, fires, soil liquefaction, and tsunami. Earthquake induced oscillations have catastrophic consequences on structures. Its severity depends on intensity of seismic activity and earth strata. Figure 1.1 shows a mere glimpse of the structural devastation caused by earthquake around the globe in different times.

(a) Damage caused by liquefaction,
Nagata, Japan, June 16, 1964.

(b) Column failure,
Loma Prieta, California, October 17, 1989.

(c) Typical masonry shear wall failure,
Northern Iran, June 20, 1990

(d) Interior frame structure collapse,
Northridge, California, January 17, 1994.

(e) Soft lower story collapse,
Duzce, Turkey, November 12, 1999

(f) Pancake collapse,
Algeria, Boumerdes, May 21, 2003.

Figure 1.1: Earthquakes induced Structural damages (NGDC USA)

Earthquakes induced structural damage results in loss of precious human life and economic devastation. Table 1.1 summarizes the devastations caused by some of the major earthquakes. The collapses of structures play a tremendous role in the death toll of an earthquake. The substandard construction practices in under-developed countries is one of the main reason of the higher number of human loss in comparison to that occurred in developed countries, in an earthquake of same magnitude. Post earthquakes surveys revealed that earthquake induced damage is severe in case of adobe, un-reinforced masonry and non ductile reinforced concrete structures

Table 1.1: Earthquake Devastations.

Earthquake	Magn-itude	People			Structure Damaged	Property loss
		Dead	Injured	Homeless		
Loma prieta California,1989	6.9	63	3757	12000	20881	$ 6-13 Billion
Iran 1990	7.4	50000	60000	400000	100000	$ 200 million
Northridge California, 1994	6.7	60	7000	20000	40000	$ 20 Billion
Kobe, Japan 1995	7.2	5300	27000	30000	110000	$ 132 Billion
Kocali, Turkey 1999	7.4	17127	43953	250000	244500	$ 3-6.5 Billion

1.2 Seismic Induced Structural Oscillations

During a seismic activity, structures undergo three types of oscillations (vibrations). These are depicted in Figure 1.2.

1.2.1 Vertical Oscillations

It is not negligible in the vicinity of epicenter. Recent analysis of strong motion data conducted in the near field sites of major earthquake indicated that during moderate to strong earthquakes, the vertical to horizontal peak acceleration ratio (V/H) often exceeds unity and violates on average by a factor of at least 30 per cent modern codified values (Ambraseys N.N. and Simpson K. A. 1996). Figure 1.3 shows the damage induced in structures due to neglected fluctuation in axial force design assumption as a result of induced vertical oscillations.

1.2.2 Horizontal Oscillations

It produces bending and shear stress at the bottom of structure. It also induces P-delta effects, resulting in cyclic compression of the load bearing element on one side of the structure and tensioning on the other side.

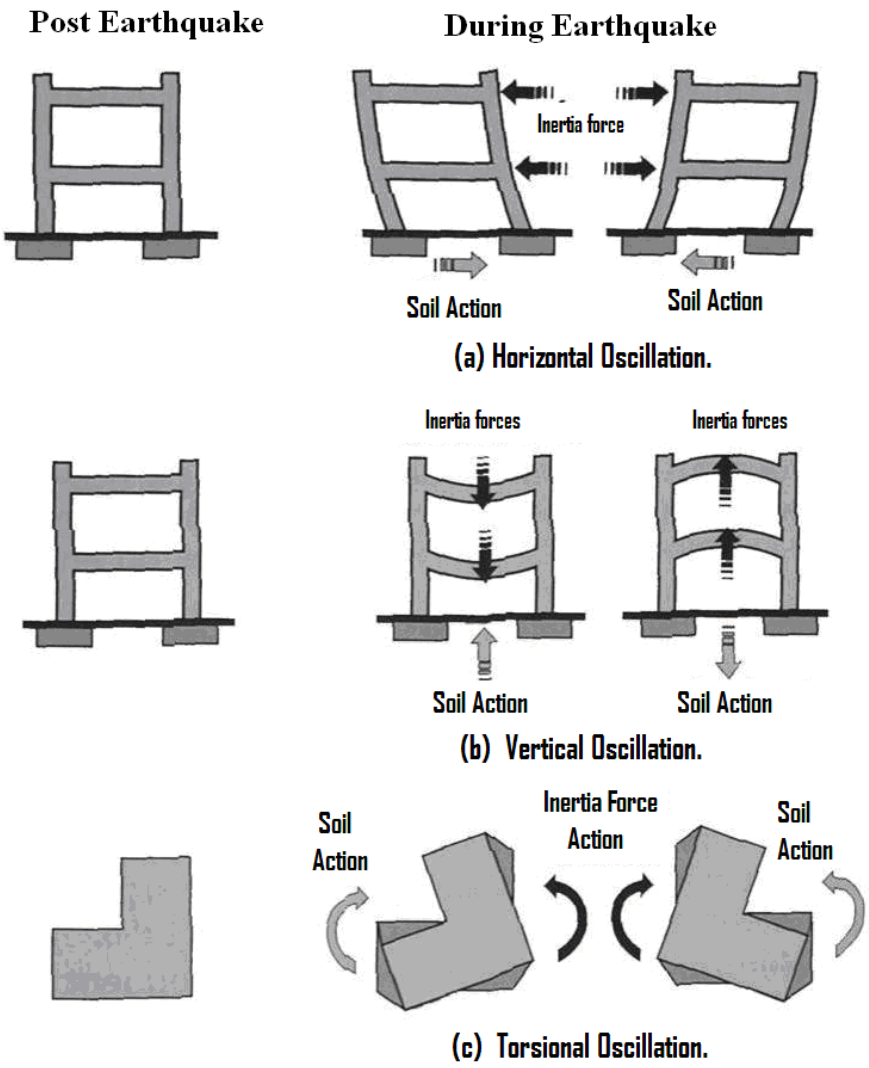

Figure 1.2: Structural Oscillations induced by Soil vibration (Milan Zacek 1996)

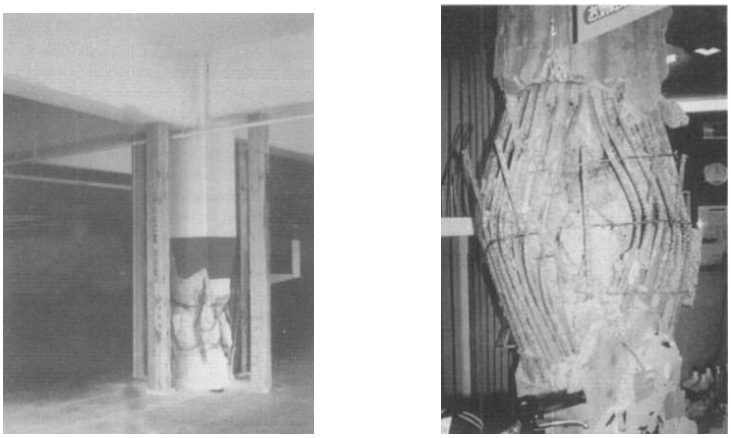

(a) Shear-compression failure in column of cast-in-place garage (b) Compressive failure of internal column of the building

Figure 1.3: Seismic induced vertical oscillation effects (Papazoglou and Elnashai 1996)

1.2.3 Torsion

Its severity depends on the direction of the seismic action and on the position of the centre of rotation that may be different at one level from other as in the case of complex buildings (Milan Zacek 1996). The rate of damage depends on the lever arm length in between the centre of rotation and centre of rigidity.

Disorders in structure occur, as the inertia forces oppose the movement induced by earthquake. Structures having greater mass, experience greater inertial force under same seismic activity i.e. heavier buildings experience stronger forces than lightweight buildings, with the same acceleration, due to differences in their masses.

1.3 Structural Damage Classification

According to European Seismological Commission (EMSK scale 1993) the structural damage is classified into five grades.

Negligible to Slight Damage (Grade 1)

- Masonry Buildings: Hairline cracks formation in wall, fall of small pieces of plaster and in few cases loosely fitted stones fall from buildings at upper portion.
- Reinforced Concrete Buildings: Fine cracks in the plaster over frame members and in the partitions.

Moderate Damage (Grade 2)

- Masonry Buildings: Cracks in many walls, fall of fairly large pieces of plaster and parts of the chimneys fall down.
- Reinforced Concrete Buildings: Hairline cracks in columns and beams, mortar falls from the joints of suspended wall panels, cracks in the partition walls, fall of pieces of brittle cladding and plaster.

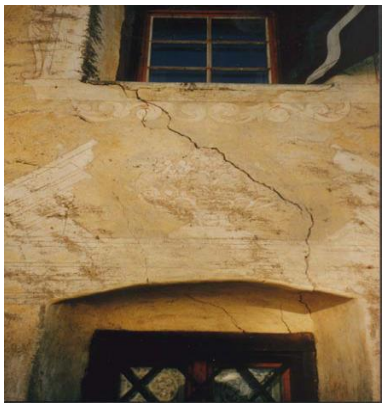

Figure 1.4: Diagonal Cracking in M. Building (Grison, Switzerland 1991 /Vaz)

Substantial to Heavy Damage (Grade 3)

- Masonry Buildings: Large and extensive cracks in most walls, pan tiles or slates slip off, chimneys breakage at the roof line, and failure of individual non-structural elements.
- Reinforced Concrete Buildings: Cracks in columns with detachment of pieces of concrete, cracks in beams.

Figure 1.5: Grade 3 damage in RC building

Very Heavy Damage (Grade 4)

- Masonry Buildings: Serious failure of walls; partial structural failure.
- Reinforced Concrete Buildings: Severe damage to the joints of the building skeleton with destruction of concrete and protrusion of reinforcing rods, partial collapse, tilting of columns.

Figure 1.6: Partial building Collapse in RC building (Mexico City 1985)

Destruction (Grade 5)

- Masonry Buildings: Total or near to total collapse.
- Reinforced Concrete Buildings: Total or near to total collapse.

Figure 1.7: Total collapse of RC building (Spitak, Armenia 1988 /Leninakan)

Earthquakes do not have the same impact on all components of a structure. In a Para-seismic study, it is desirable to differentiate the pathology developed on the short or slender column, shear wall short or slender, of reinforced concrete or masonry and even Slab.

1.4 Seismic Induced Damage to Structural Members

Defects within structure design and construction flaws are the primary sources of large scale earthquake devastations. Design defects include, use of insufficient load safety factor or capacity reduction factor, inadequate provision of reinforcement arrangements within structure elements, especially at critical sections such as column or beam plastic hinge sections and improper load transfer arrangements at joints. Earthquake induced damages within different structure elements along with their causes are explained briefly in the following paragraphs.

1.4.1 Column

In frame structures, columns are the most crucial structural elements. As they provide stability to it by transmitting load from super structure to foundation and furnish ductility. Due to their major contribution under seismic activity, they are the most vulnerable structural elements. Its failure is most vital as it may lead to additional failure and may result in complete collapse. Seismic induced damages which column may sustain are those caused due to non-ductile details, unsuitable transverse reinforcement, inadequate cross-section dimensions, unconfined lap splices, inadequate anchorage lengths, wide tie spacing at critical sections, excessive beam strength and soft story (Arslan and Korkmaz 2007; Sezen et al. 2003). Figure 1.8 depicts some of the column failure types.

Figure 1.8 (a) show the photo of the failed first story column in an eleven-stories building after 1985 Mexico city earthquake [Photo credit: E.V leyendecker, U.S.Geological survey]. A U.S geological survey team concluded that this type column failure was induced by variation in stiffness in between the first and other floors of the building, concentrating the load in the first story column. Figure 1.8(b) is the photo of overpass columns damaged in Northridge California earthquake of 1994 [Photo credit: M. Celebi, U.S.Geological survey]. Accordingly to U.S geological survey team, columns failure occurred due to poor column

confinement as an outcome of insufficient shear reinforcement. Figure 1.8(c) & (d) are photos of columns of moment-frame building in Adapazari, failed during Kocaeli, Turkey 1999 earthquake. The columns failure occurred due insufficient arrangement of lap splices, wide spacing of ties with 90-degree hooks and no cross tie arrangements (Sezen et al. 2003). Column failure shown in Figure 1.8(c) is a result of wide tie spacing and provision of lap splices in the plastic hinge zone. While Figure 1.8(d) show the buckling of longitudinal bars due to poor confinement of the concrete core as an outcome of wide tie spacing.

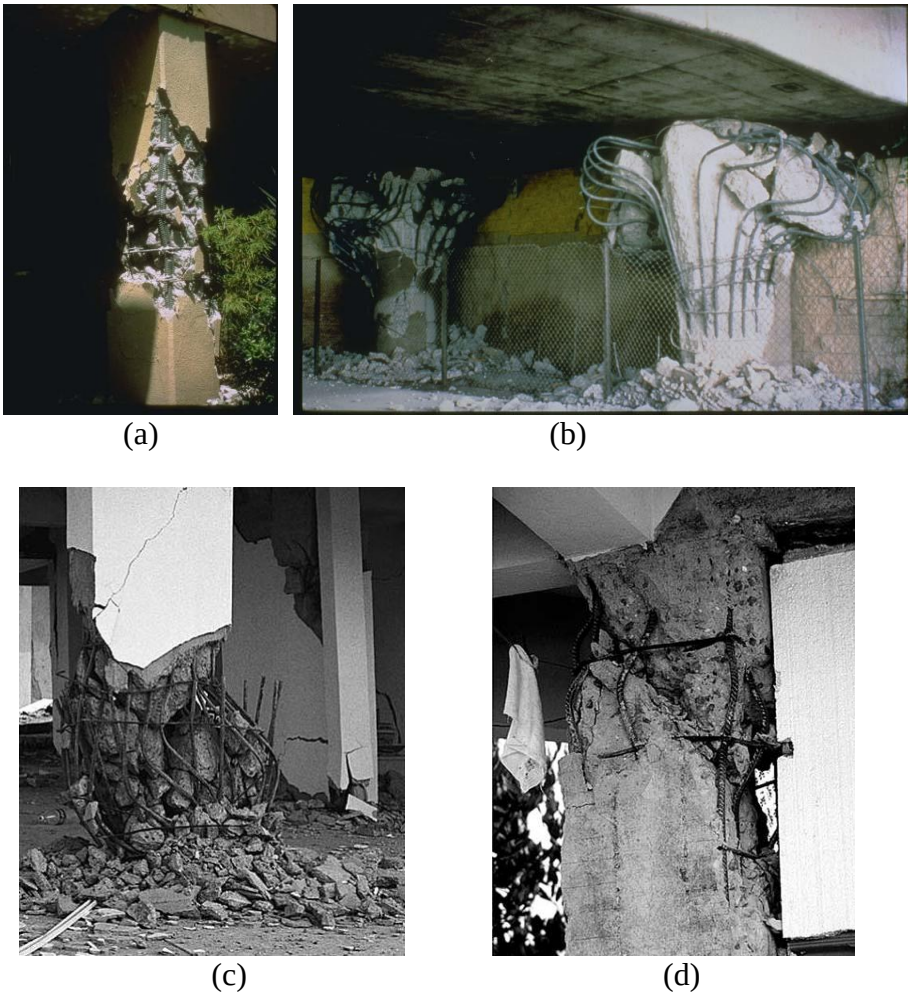

Figure 1.8: Damage/Collapse of R.C. column

1.4.2 Beam

According to Turkish earthquake code TEC-98, first plastic hinges are desired to occur at the beam end. Therefore in TEC-98, it is recommended to bend special seismic hoops and crossties up to 135°. It is also the recommendation in ACI 318 code to furnish a 135° of bend plus 6d (Dia. of bar) extension at free end in seismic zones. However in buildings, constructed former than development of these codes, consists of smooth reinforcing bars of 6-8 mm diameter with 90° hooks (Arslan and Korkmaz 2007; Sezen et al. 2003), it was concluded that beam failure occurred as a result of the general practice of using bent-up longitudinal bars, which helped in increasing the moment carrying capacity of support and shear capacity of beam but on the other hand these bent-up bars cannot resist cyclic shear forces. Figure 1.9, indicates the above mentioned flaws (Sezen et al. 2003).

(a) (b)

Figure 1.9: Damage/Collapse of R.C. Beam

1.4.3 Beam-Column Joint

Researchers concluded that the main source of beams-column joint failure was the provision of inadequate lateral ties (Arslan and Korkmaz 2007; Sezen et al. 2003). It was based on Kocaeli, Turkey 1999 post-earthquake reconnaissance survey, and is supported by other researchers (Kaplan et al. 2010; Murty et al. 2003). The columns smaller dimensions are also responsible for joint failure (Murty et al. 2003). Figure 1.10 shows photos of damaged beam column joints.

Figure 1.10: Failure of Beam-column joint

1.4.4 Shear wall

Shear walls are the main structural elements which are used to provide lateral stability to the structure and keep its lateral drift within reasonable limits by resisting in plane horizontal induced load (Park and Paulay 1975; Thomas Paulay 1975; Mau and Thomas 1986). Since 1960, shear wall structures have been practiced, for medium to high rise buildings, in many countries susceptible to earthquake such as France, Switzerland, Germany, Japan, New Zealand, Switzerland, Portugal, Mexico, Taiwan, Canada, Chile, Romania, Turkey, Colombia, The republics of the former Soviet Union, U.S.A. etc. They were basically designed as

bracing system to withstand vertical and wind load as in Switzerland (Greifenhagen and Pierino Lestuzzi 2005) and Hong Kong (Su and Wong 2007).

The post earthquake investigation revealed that shear wall structures performed well as compared to frame structures (Sezen et al. 2003; Fintel 2012). However, researcher on the basis of their post earthquake surveys concluded non ductile behavior of structure especially those fabricated in late 1960-70. These structures showed non ductile behavior as in that era buildings were designed on the basis of resistance and therefore even if these structures possess strength, they exhibit non ductile behavior. On the basis of these observations and further advancement in the field of earthquake engineering, the building design codes are now modified and these late 1960's construction do not withstands with the new safety standards (Pellissier 2004). The shear walls constructed in that era too do not fulfill the modern code safety regulations. Researchers (Greifenhagen and Pierino Lestuzzi 2005; T Paulay and Priestley 1982) after careful study on shear wall pathologies, have concluded that low reinforcement ratio, light transverse reinforcement, 90 degree bent angle, lack of cross ties and insufficient reinforcement arrangement at joints, and in some cases use of poor construction material make these walls susceptible to brittle shear failure, diagonal compression, sliding failure and ultimately restrict their deformation capacity.

Figure 1.11 show photos of damaged shear walls. The first photo shows the failure of a shear wall observed after Chile 1985 Earthquake (Wyllie et al. 1986). In Chilean earthquake the damage observed in shear wall was sliding in construction joint, spalling and degradation of concrete at the extremities to the wall base and buckling of longitudinal bars near wall boundaries. The second photo shows a damaged narrow shear wall/blade column observed after 1999 Kocaeli (Turkey) earthquake (Sezen et al. 2003). It was concluded that the wall sustained such kind of damage due to provision of light transverse reinforcement with 90-degree hooks and lack of cross ties.

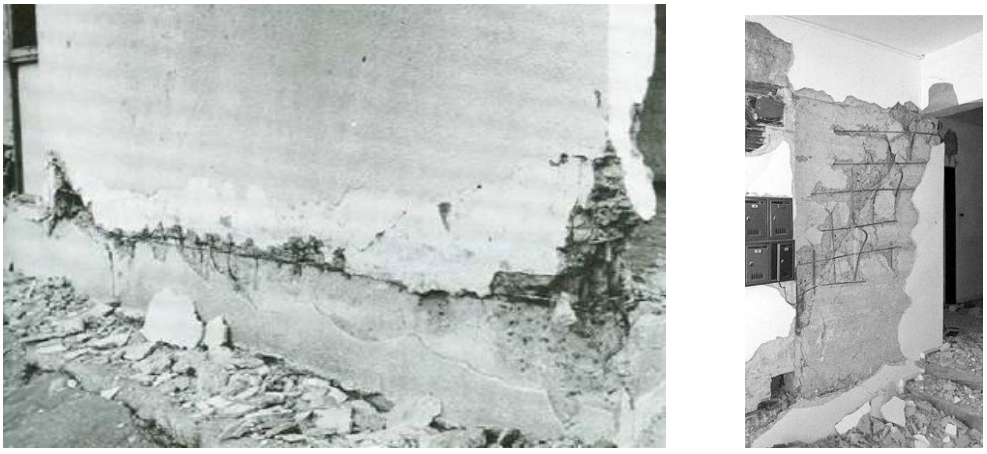

(a) Shear wall failure at the bottom (Wyllie et al. 1986) (b) Shear failure of wall/blade column (Sezen et al. 2003)

Figure 1.11: Shear wall damage/failure

Figure 1.12 shows a photo of failed shear wall. This failure occurred as a result of the existence of wide opening made within shear wall and lack of adequate reinforcement provision at window opening.

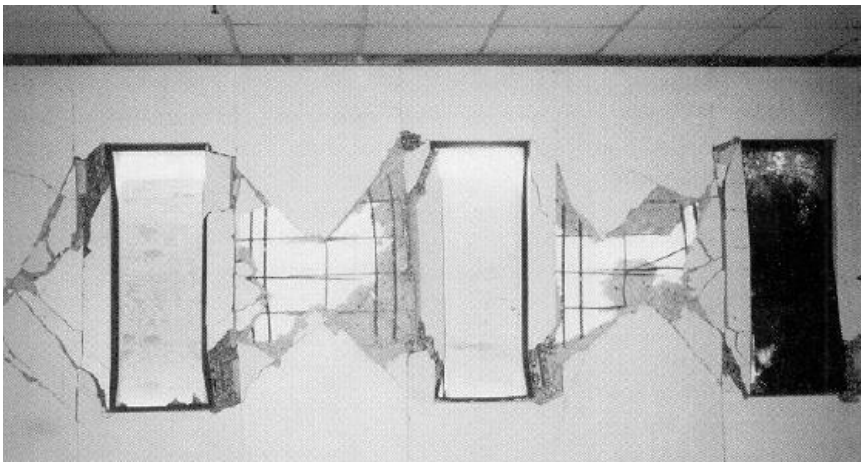

Figure 1.12: Damaged concrete shear wall (Osteraas and Somers 1996)

Figure 1.13 shows a photo of a building which collapsed at its 5th floor. The shear wall is squashed and buckled out of plane as a result of insufficient design provision for vertical load fluctuation, an outcome of earthquake induced vertical oscillation (Papazoglou and Elnashai 1996).

Figure 1.13: Building with a collapsed 5th floor (Papazoglou and A. S. Elnashai 1996)

The low tensile strength of concrete results in the development of tensile cracks within walls, even at service loads, which in turn affects the stiffness of the structural elements to a greater extent (Kara and Dundar 2009). Therefore the tensile cracks initiation and its propagation within shear wall reduces the flexural and shear stiffness, which in turn increases the structural member deflection.

2 Shear wall

2.1 Introduction

Shear walls play a vital role in dissipation of seismic activity induced energy in structure. The dissipation capacity is directly related to its transverse dimensions i.e., when thickness of RC shear wall is doubled, its energy dissipation capacity becomes twice.

The main parameters that influence (dominate) the behavior of shear walls are:

- Slenderness, defined as the ratio of height by the width of the wall, h / l.
- Provision and the percentage of reinforcement.
- Intensity of the normal load/load pattern.

Other parameters that influence its behavior are effective moment of inertia, shear modulus of concrete and presence of cracks (Mickleborough et al. 1999).

2.2 Shear wall Structural System Classification

The structural systems of buildings are classified into three types, based on the shear walls function (Figure 2.1).

Bearing wall system: Load-bearing walls for vertical loads, and shear walls or braced frames for the lateral earthquake loads resistance.

Building frame system: Space frame for vertical loads and shear walls or braced frames for the horizontal earthquake resistance.

Shear wall system: The shear walls play double or full role by providing resistance to both vertical and horizontal loads. The system is commonly practiced in France.

2.3 Shear wall Types

On the basis of its function the shear walls can be categories as follow.

2.3.1 Slender wall

Walls having height to length ratio greater than 2 (i.e. H/L > 2) are called slender walls. This type of wall exhibits three forms of load effects.

- The most obvious and important is the flexion where one can find a failure either by plastic yielding of vertical reinforcement and crushing of concrete or in some cases only concrete crushing or breakage of tensile reinforcement.
- Flexion and shear force where one can observe failure by plastic yielding of vertical and transverse reinforcements.
- Shear force where one can observe failure due to compression reinforcement breaking or shear failure of concrete.

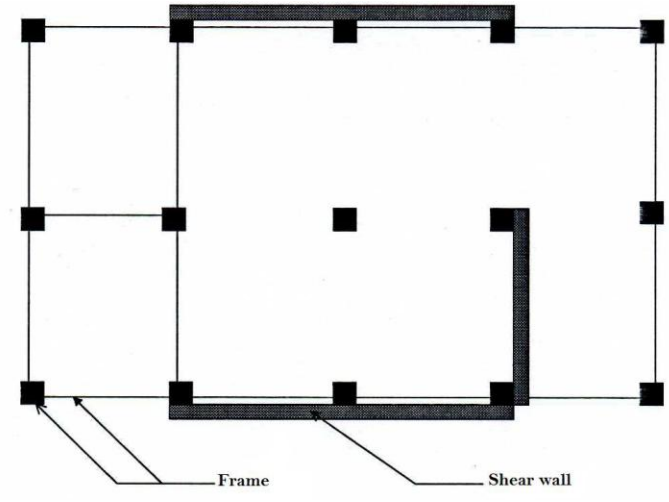

(a) Bearing wall system

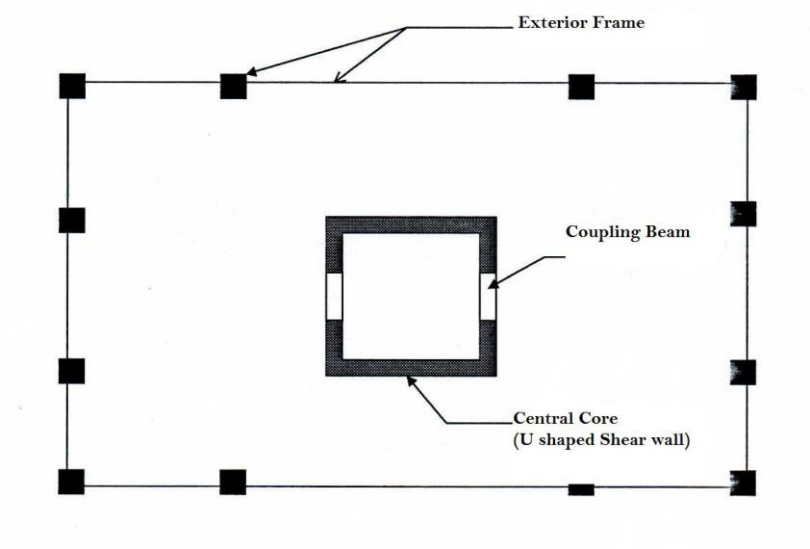

(b) Building frame system

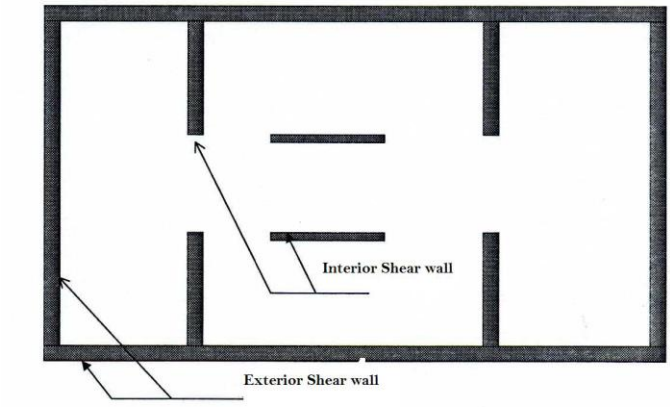

(c) Shear wall system

Figure 2.1: Shear wall Structure types (Nicolae 2000)

2.3.2 Short Wall

Wall having height to length ratio less than 2 (i.e. H/L < 2) are called short walls. In this case shear is generally dominant as compared to flexion. The shear load effects exhibited by it are:

- Sliding at the base of wall.
- Diagonal rupture of the shear wall.
- Crushing of concrete at the base.

2.4 Shear Wall Pathologies and Problems

Reinforced concrete structures built in 1960s and 1970s inc1uded many details that were detrimental in regard of their seismic performance. Some of the common deficiencies were poor confinement of longitudinal reinforcement, inadequate transverse reinforcement, poor anchorage of transverse reinforcement (90 degree hooks not anchored in confined regions), and inadequate seismic detailing such as, placement of lap splices just above the floor levels at critical sections for plastic hinging. Due to complexity of the above mentioned flaws in late 60's construction work, shear walls fabricated in that era, exhibited different behaviors.

2.4.1 Laboratory Performance of Shear wall

In order to find out the load response behavior of shear wall as a single structure member and in combination with other structure elements, researchers have carried out experimental tests on the shear walls specimens fabricated in the laboratory. The main ambition was to find out the effect of various parameters, such as concrete compressive strength, vertical and horizontal reinforcement ratio, axial force ratio, variation in thickness and slenderness ratio on the failure modes, shear strength and ultimate drifts.

Barda et al. (Barda et al. 1977) investigated the behavior of six flange shaped structural wall with transverse reinforcement in boundary elements. The specimens were tested as cantilever which had shear span-to-length ratios in the range of 0.25 to 1.0. Two out of the six specimens were subjected to cyclic load test and remaining to monotonic load test. The tests were performed under a high level of shear stress, ranging from $8\sqrt{f_c^{'}}$ to $14\sqrt{f_c^{'}}$ (psi). After the peak load, a significant loss of strength and stiffness were observed while at failure, the drift capacities were less than 1.0%. The results highlighted the ineffectiveness of horizontal reinforcement in the wall shear resistance with shear span-to-length ratios less than 0.5 while the vertical reinforcement was mostly effective for walls with shear span to length ratios between 0.25 and 0.5 and less effective for walls with a ratio of 1.0. However, it was recommended that in order to have more evenly distributed cracks with reduced widths, minimum horizontal and vertical web reinforcement should be provided in all walls regardless of their aspect ratio. It was also pointed out that a significant portion of shear introduced at the top of the wall transmits directly to the foundation by diagonal compression. The authors also investigated the influence of shear aspect ratio on shear strength. The shear strength of the specimen with a shear aspect ratio of 1.0 was found to be 20% lower than that of the specimens with smaller aspect ratios (i.e. ratios of 0.25 and 0.5).

Cardenas et al. (Cardenas et al. 1980) evaluated the performance of rectangular shaped reinforced concrete walls with a shear span-to-length ratio of 1.1 and without special boundary elements. One out of the seven specimens was subjected to cyclic loading, while the rest were tested under monotonic lateral loading. The main parameters applied were the amount and distribution of the vertical and horizontal reinforcement (Figure 2.2). The results

showed that both the vertical and horizontal reinforcement contribute to the shear strength of low-rise walls. The drifts measured at failure, under monotonic loading were in the range of 0.6% to 1.9%, whereas for the one subjected to cyclic loading, was approximately 0.5%. An upper limit in the order of $10\sqrt{f_c'}$ (psi) was proposed for the shear strength of low-rise walls. The average shear stress was based on the effective depth of the section rather than the length of the wall.

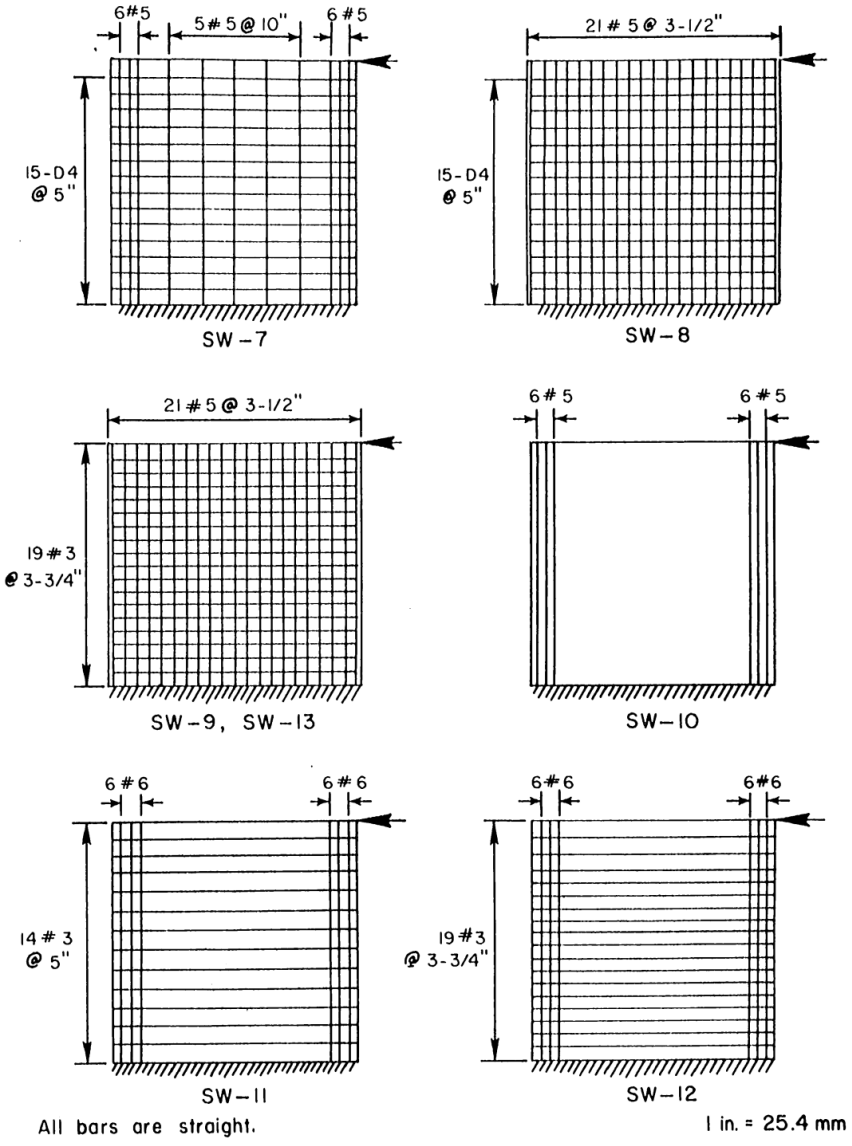

Figure 2.2: Reinforcing configuration of the tested wall specimens (Cardenas et al. 1980)

Paulay et al. (T. Paulay et al. 1982) studied the behavior of squat walls (S.R. = 0.5) subjected to static cyclic load test. The specimens were tested as cantilever and the lateral load was applied at head beam with no vertical compression. The reinforcement configuration kept in case of specimen W1 , with rectangular cross section, were: vertical reinforcement (0.807%) and horizontal reinforcement (1.608%) distributed uniformly in a single layer with additional vertical reinforcement placed at each of the two boundary zones of wall section (260 mm^2). Sliding shear failure was dominant in this case in addition with regularly formed

diagonal cracks within the wall web. At displacement ductility of $\mu_\Delta = 6$, the slip represented almost 65% of the total displacement at wall's top.

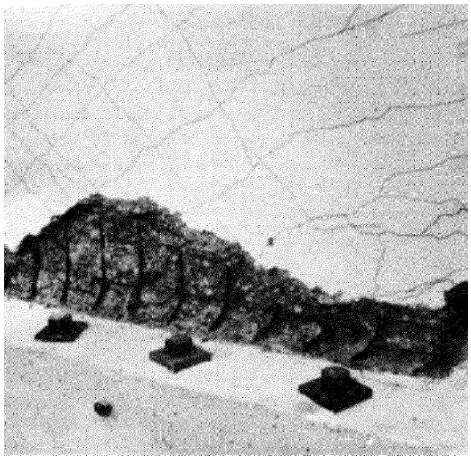

Figure 2.3: Failure of wall W1 by sliding shear

Maier and Thürlimann (Maier and Thurlimann 1985) studied the influence of horizontal reinforcement on the performance of cantilever shear wall. For this purpose two shear walls of rectangular shape with identical geometry and uniformly distributed vertical reinforcement were fabricated and a variation of 0 to 1.03% (0 for S9 and 1.03% for S4) was kept in their horizontal reinforcement ratios. The two specimens were subjected to monotonic lateral load test, keeping the normal load as constant. It was observed that the horizontal reinforcement though changed the failure mode and decreased the ultimate drift but had only minor influence on the peak load. Specimen S9 and S4 failed in diagonal tension and diagonal compression respectively.

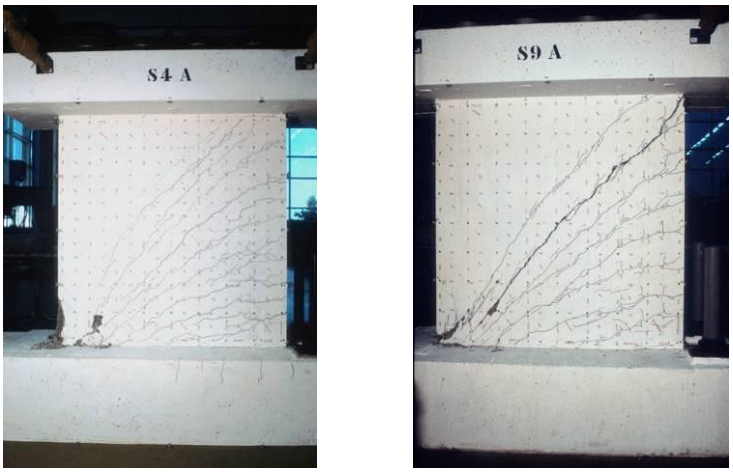

Figure 2.4: Shear wall failure mode (Maier and Thurlimann 1985)

Lefas et al. (Lefas et al. 1990) studied the influence of various parameters i.e., axial load, concrete compressive strength , H/L ratio and wall web horizontal reinforcement on shear wall behavior with concentrated vertical reinforcement at ends. The vertical

reinforcement ratio was kept equal to 2.4% and 3.1% within wall web and wall boundaries respectively. Changes were made in the wall specimens, web horizontal reinforcement ratio (0.37% and 1.1%), vertical axial load (0 to 460 kN), and slenderness ratio (h/l from 1 to 2). The test specimens were subjected to static monotonic load tests as simple cantilevers with tip load. It was observed that while axial compression reduced the vertical and horizontal deflection, it increased the load carrying capacity and secant stiffness characteristics and the increase becomes more pronounced with an increase in slenderness. It was also observed that although the amount of horizontal reinforcement was almost reduced to one third, this reduction caused minor variation in the failure mode, peak load, and achieved drift. Diagonal compression failure was observed in both cases and it was concluded that the concrete compression zone contributes significantly to the overall shear strength of the wall.

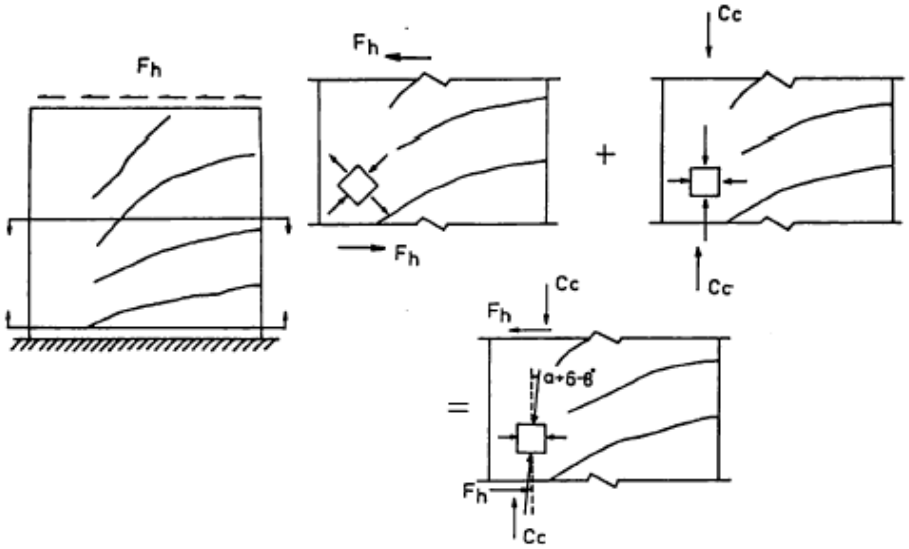

Figure 2.5: Schematic representation of failure mechanism of walls

Salonikios et al. (T.N. Salonikios et al. 1999) carried out test study on the squat walls with slenderness ratios of 1.0 and 1.5. The specimens were subjected to static cyclic load test as cantilevers. The variation made in specimen configurations includes: alteration in web reinforcement ratio (0.565% to 0.277%), boundary reinforcement (1.7% to1.3%) and presence of vertical load and diagonal reinforcement. The specimens showed failure in a predominantly flexural mode, characterized by concrete crushing and rebar buckling at the confined edges. This was accompanied with moderate diagonal cracks within the wall web and sliding at the wall bottom. Sliding was prominent in specimens with no diagonal reinforcement. It was the case in both types of walls i.e. wall with slenderness ratio 1.5 and 1.0. It was also observed that the variations made in the vertical, horizontal, and boundary reinforcements did not influence the failure mode and observed drift. An increase in the energy dissipation capacity and reduction in sliding was observed in the specimens with diagonal web reinforcement.

Rothe (Rothe 1992) investigated the performance of rectangular and flanged cross-sections walls under static monotonic, static cyclic and dynamic behavior. All specimens were tested as cantilever walls. The specimens discussed here are T01, T04, T10, and T11 because of their different failure modes. The reinforcement arrangement of these specimens was the same except for specimen T04, for which no horizontal reinforcement was provided. The specimen T01 failed because of rupture of vertical rebar while specimen T04 due to diagonal

tension. Both specimens were tested on a shaking table. Specimen T10, subjected to static cyclic test, depicted sliding shear. Specimen T11 was subjected to an axial force ratio of 0.07 and failed in diagonal compression. Based on test data the authors concluded that a sliding shear mode of failure would not occur in dynamic tests because dynamic sliding shear strength was considered to be significantly greater than that of the static case.

Figure 2.6: Failure of wall LSW3 (S.R. =1.0) and MSW3 (S.R. =1.5) in presence of vertical compression
(T.N. Salonikios et al. 1999)

Fouré (Fouré 1993) studied the influence of horizontal and vertical reinforcement on short wall of slenderness ratio of 0.5. The test specimens were subjected to axial force of almost 0.03 with a full rotational restraint at the top. The influence of horizontal reinforcement on the strength and deformation capacity was very slight while the vertical reinforcement played a major role in specimens' shear and flexure behavior.

Wiradinata and Saatcioglu (Wiradinata and Saactioglu 1986) evaluated the influence of slenderness ratio on rectangular shaped cross section wall by testing, two walls with slenderness ratio of 0.3 and 0.6. The smaller wall (slenderness ratio 0.3) exhibited a highly pinched hysteretic behavior that was attributed to excessive sliding deformations at the base of the wall, which contributed more than 70% to the lateral displacement at the end of the test. The lateral drift recorded, at failure, was 2.6%. On the other hand, taller wall failed by diagonal tension at a drift of 1.7%. In this case, even though flexural and shear deformations were both significant throughout the test, shear deformations clearly governed once the wall strength started to degrade. The authors concluded that walls with a smaller shear span-to-length ratio are more susceptible to sliding shear failures as compared to the taller walls.

Sittipunt and Wood (Sittipunt and Wood 1996) did analytical study to evaluate the influence of the diagonal reinforcement on the wall behavior. They concluded that diagonal reinforcement provides a mechanism that is more successful in transferring the lateral forces into the foundation, leads to lower shear strains close to the base of the wall, and improves energy dissipation capacity.

Salonikios et al. (T.N. Salonikios et al. 1999, 2000) tested eleven walls detailed according to the Eurocode 8 (EN 1998) provisions. The walls were reinforced for shear with an orthogonal grid of web reinforcement. The test parameters were: shear span-to-length ratio (1 and 1.5) and diagonal reinforcement in wall web. The average drift recorded in the taller wall specimens was 1.5% compared with 1.0% in the smaller one. The addition of diagonal reinforcement did not improve the wall drift capacity. All specimens exhibited diagonal cracking of the web and sliding at the wall base and failed in a predominantly flexural mode, characterized by concrete crushing and reinforcement buckling at the confined wall edges. The sliding shear resistance provided by diagonal bars improved the energy dissipation capacity of the walls with a shear span-to-length ratio equal to 1.0. However, its effect was less significant for the taller walls, particularly in the presence of axial compression. The authors pointed out that the degree of pinching was controlled by bond slip and horizontal sliding rather than by the opening of inclined shear cracks.

Sittipunt et al. (Sittipunt et al. 2001) studied the influence of diagonal reinforcement on the hysteretic response of four barbell shaped wall specimens with a shear span-to-length ratio of 1.4. Two walls were fabricated with the provision of conventional vertical and horizontal reinforcement in web, while in the other two specimens the conventional reinforcement was replaced with a grid of inclined reinforcement (Fig. 2-6). The walls with conventional reinforcement exhibited web crushing, whereas the other two specimens exhibited concrete crushing in the boundary elements. It is important to note that in the research work the transverse reinforcement in the boundary elements was not intended to provide confinement to the concrete core. The behavior of the walls with diagonal reinforcement was almost similar to that observed by Salonikios et al. (1999; 2000), and was characterized by a decline in the shear distortions at the plastic hinge region in contrast to the specimens with conventional web reinforcement. However, after the diagonal reinforcement yielded, the magnitude of shear distortions was comparable in all the specimens with no appreciable effect on deformation capacity.

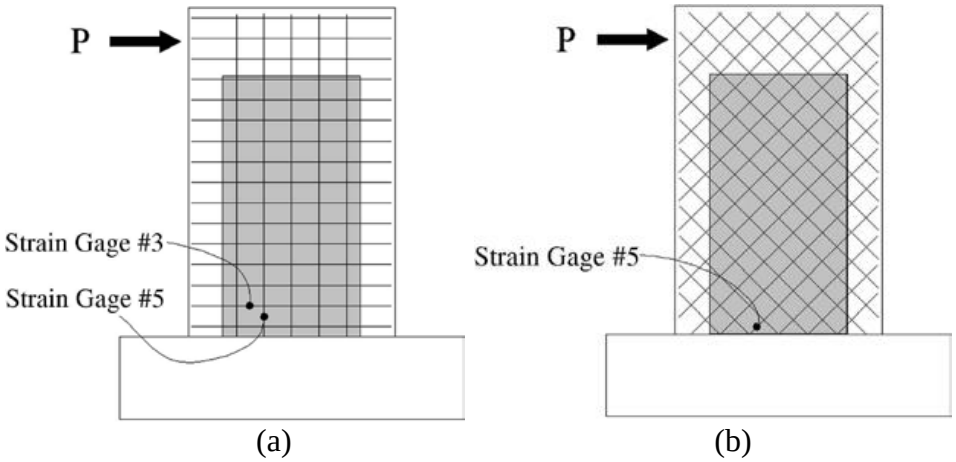

Figure 2.7: Reinforcement Layout: (a) conventional (b) orthogonal

Hidalgo et al. (Hidalgo et al. 2002) tested twenty six low-rise walls under displacement reversals. The walls shear span-to-length ratios was in the range of 0.35 to 1.0. The walls were designed to exhibit a shear failure mode in order to examine the behavior of buildings with walls displaying a non-ductile failure mode. It was observed that the walls

deformation capacity decreases as the shear span-to-length ratio decreases. Diagonal cracking was observed at 0.1% drift, while drifts at failure varied from as low as 0.3% to 1.3%. It was observed that the amount of distributed reinforcement has no significant influence on the drift at first cracking but has produced somewhat affect latter on. Contrary to the observations, in other experimental projects, it was reported that the distributed web reinforcement had little or no effect on the maximum shear strength. However, the test setup had a significant influence on the observations since these walls were tested under double curvature. It was also suggested that the energy absorption capacity of the specimens was not influenced by the variation of wall aspect ratio.

Choi (Choi 2006) evaluated the influence of diagonal reinforcement on low-rise walls with shear span-to-length ratio of 0.75. The findings were similar to the others work (Arslan and Korkmaz 2007; T.N. Salonikios et al. 1999, 2000; Sittipunt et al. 2001).

2.4.2 Shear wall Failure Modes

The variation in the failure modes of shear wall is highlighted by experimental research work (Fouré 1993; Greifenhagen and Pierino Lestuzzi 2005; Lefas et al. 1990; Maier and Thurlimann 1985). On the basis of their work the authors attributed this variation to parameters, such as reinforcement ratio, strength and detailing, cross section type, concrete compressive strength, axial load ratio, loading pattern and boundary conditions. The different failure modes are discussed briefly in the following section.

2.4.2.1 Slender Wall

Slender shear wall failure modes are depicted in Figure 2.8. Each failure mode is discussed briefly in the following text.

a) Flexural Failure

Mode f1: In this mode, failure occurs due to plastic yielding of vertical reinforcement on the tension face and crushing of concrete on the compression face. This is the most satisfactory mode of failure as it forms a plastic hinge in the lower part of the shear wall which dissipates energy to a large extent.
This sort of failure is dominant in a very long wall under weak normal and moderate shear force.

Mode f2: This mode of failure is dominant in heavily reinforced shear wall. In this case failure occurs by crushing of concrete**.** Mode f2 is less ductile than method f1, especially in the case of a rectangular section.

Mode f3: The failure occurs due to the brittle fractures of vertical reinforcements.
It happens in shear wall, weakly reinforced, and rebar distributed and not concentrated at the ends. The ductility and energy absorption capacity can be improved by concentrating the vertical reinforcement at the ends.

b) *Flexural/Shear Failure*

Mode f/t: The failure is accompanied by plastic yielding of vertical reinforcement in flexion and horizontal reinforcement. It occurs in moderately slender wall where bending is more dominant and the horizontal reinforcement is inadequate.

c) Shear Failure

Mode t: It happens due to concrete compression failure near the wall base, in stiff shear wall, heavily reinforced in both longitudinal and transverse direction, and subjected to high shear.

Mode g: In this case sliding of shear wall takes place near the base, a characteristic of short wall, but it can also be observed in case of moderate slender wall. This type is prominent in walls that have improper vertical reinforcement distribution, poor concrete quality subjected to week normal loads.

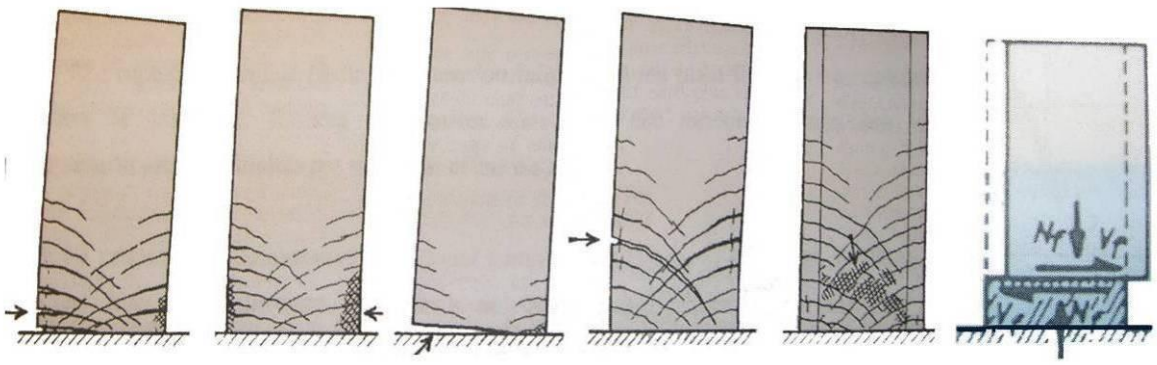

Figure 2.8: Failure modes of Slender Shear wall (Fouré 1993; Nicolae 2000)

2.4.2.2 Short wall

Short shear wall failure modes are depicted in Figure 2.9. Each failure mode is discussed briefly in the following text.

Mode T1: In this case shear sliding failure occurs due to gradual plastic yielding of vertical reinforcement. It is accompanied by significant sliding causing reduction in the stiffness and energy dissipation. It happens in shear wall having insufficient reinforcement distribution.

Mode T2: It occurs by diagonal tension failure with plastic yielding of reinforcement along the diagonal crack. It takes place in shear wall having moderate reinforcement subjected to weak normal loads.

Mode T3: It occurs by concrete crushing at the base, as at the soul of wall the reinforcement transmits compressive stresses. It is characteristic of the shear wall heavily reinforced.

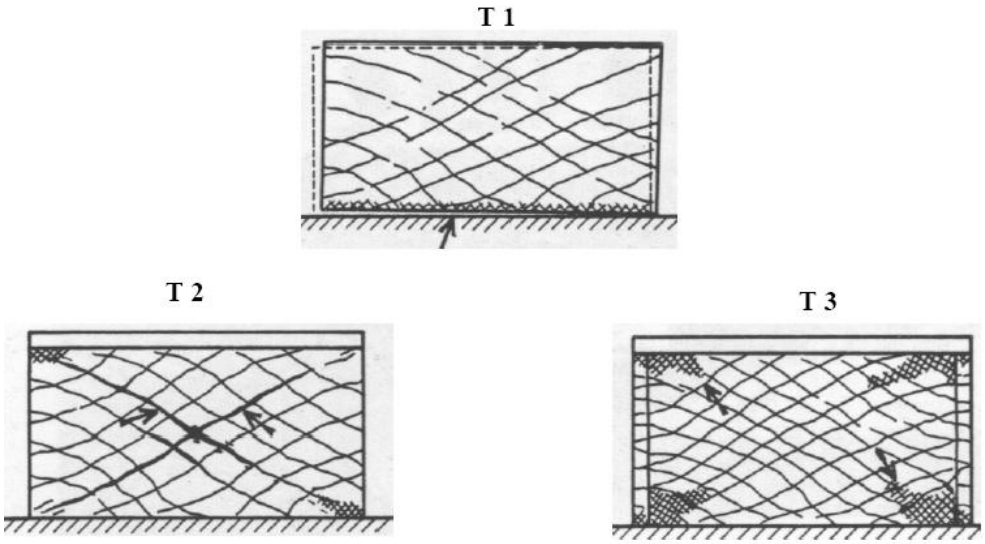

Figure 2.9: Failure Modes in Short Shear wall (Fouré 1993; Nicolae 2000)

3 Seismic Retrofit/Strengthening

3.1 Introduction

Seismic retrofit is the modification of existing structures to upgrade their performance level so that it fulfill the minimum requirements up to the current building codes and to avoid severe damage and collapse during a seismic event. The primary purpose of retrofit is to increase the strength and ductility of the structure separately or in combination, depending on structure the type and its future use. The more the structure elements are ductile the more they will dissipate the seismic induced energy. Figure 3.1 depicts the goal of retrofit in graphical format. The seismic retrofit proves to be a better option in regard to the economic consideration as its justification is to have an overall cost less than 25% of the replacement cost.

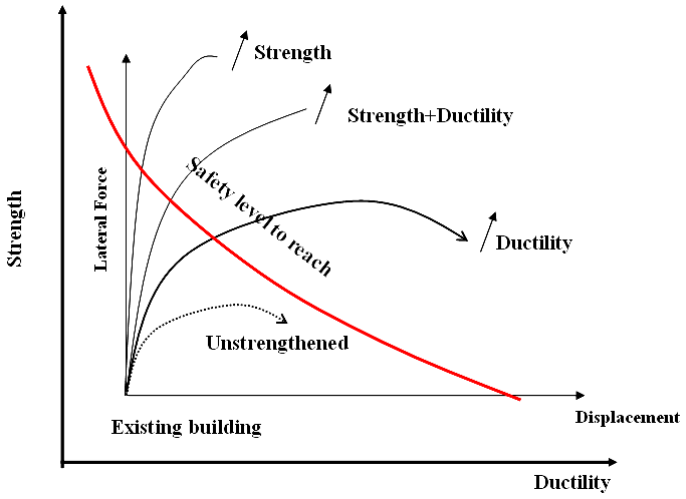

Figure 3.1: Different strategies of Strengthening / Retrofitting (Davidovici 1999)

3.2 Conventional Retrofit Technique

Building structures need strengthening due to excessive loading (change in use), modification in design code and exposure to environmental effects such as corrosion, seismic activity etc (Elmaaddawy and K. Soudki 2008). To account these issues, several strengthening techniques have been developed and utilized in the filed recently. These are classified in to two major types, global/structural level and local/member level retrofit.

3.2.1 Global method

These retrofit techniques are commonly used to enhance the lateral resistance of structures as a whole. Common global retrofit techniques include the addition of shear walls, steel braces, post tensioned cables and base isolators. These are described briefly in the following paragraphs.

3.2.1.1 Additional Shear wall

The most common strengthening method for the existing frame structures is adding shear walls. This in turn controls the structure global lateral drifts and reduces the damage in frame members. They are in use for over half a century in seismic retrofits. To reduce the lateral drift they are placed at the outer corners and to increase the strength and stiffness they are placed in the central bays of RC frame structures. Generally they are made of steel plates or of RC and in the later case to reduce time and cost, shortcrete or precast panels are used. They are connected to the existing frame structure columns and beams through dowels. The research works (Altin et al. 1992; Inukai and Kaminosono 2000; Lombard et al. 2000; Pincheira and J.O. Jirsa 1995) shows that the infilling process plays an important role in the overall response of the structure. It tends to stiffen the structure such that the base shear can increase. But the main disadvantage is that as the overturning effect and base shear are concentrated at the stiffer infill location, the strengthening of foundation is required at these locations. They are heavy and create an additional dead load in structure which can affect the structure behavior. They also overload the connected structure elements and therefore it is compulsory to analyze and strengthen them if required.

3.2.1.2 Steel bracing

The addition of steel bracing to the existing structures is effective in improving their strength, stiffness and resistance, to story drifts (Figure 3.2). This method has been practiced in Japan for over half a century. The research (Abou-Elfath and Ghobarah 2000; Badoux and J.O. Jirsa 1990; Bush et al. 1991; Teran-Gilmore et al. 1995) shows that this system is effective and it improves the ductility of the frame structure. The total strength attained by steel bracing to RC frame is more than that of the sum of the RC frame system plus the steel system. The advantages of this system are the possibility of accommodating openings, small weight addition and lesser disturbance in comparison to shear wall addition. The main disadvantages are its initial cost and maintenance cost especially when exposed to weather.

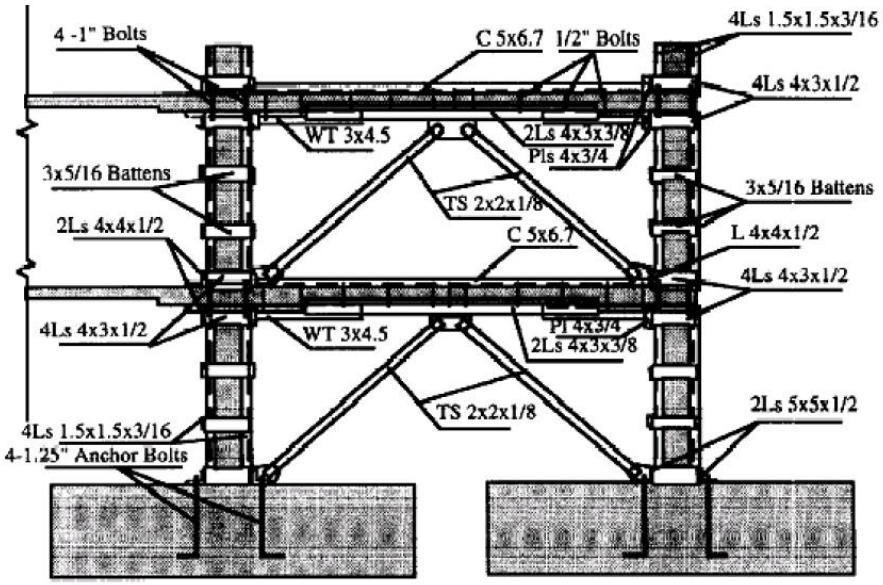

Figure 3.2: Braced system layout (Goel and Masri 1996)

3.2.1.3 Base Isolation

The base isolation technique consists of placement of flexible isolation system in between the foundation and superstructure. The installed isolation system due to its flexibility and energy absorption capability, reflect and absorb part of the earthquake induced energy before it is fully transmitted to the superstructure, reduce the energy dissipation demand on superstructure (Gates et al. 1990; Tena-Colunga et al. 1997). Base isolation system increases the natural time period of the structure and the displacement across the isolation level which in turn reduces the acceleration and displacement in the superstructure during seismic activity. However this technique is applicable only at low to mid rise structures (up to 10-12 floors) as it cannot solve the overturning effect produced due to large vertical loads (Komodromos 2000). It also require a clear area around the building at the isolation level (digging a moat around the structure) to accommodate large displacement without causing damage. This technique is not feasible in regions where lower frequency earthquakes occur or on soft soil where the amplification of low earthquake frequencies may occur.

3.2.1.4 Energy Dissipation

The most commonly used approaches to add energy dissipation to a structure, are installing frictional, hysteretic, or visco-elastic dampers as components of the braced frames. They are connected to the structural frame through column-beam joints. Friction damper consists of specially coated steel plates bolted together. They absorb the earthquake induced energy when the steel plates slide against each other at predetermined slip load and convert the induced energy in to heat energy, generated by friction. They increase the seismic load carrying capacity of the structure. The function of viscous damper is similar to friction damper. The viscous damper provides the maximum damping effect when the lateral movement of the structural system is at its highest velocity, i.e. in passing through the gravity or initial state.

3.2.2 Local method

In this approach the ductility of structural elements is increased to satisfy their specific limit states by addition of concrete, steel or FRP jackets. The conventional local retrofit techniques are discussed briefly in the following paragraphs.

3.2.2.1 RC Jacket

The section enlargement of structure elements by placing additional RC around them to improve their seismic resistance is called RC jacketing (Figure 3.3). The typical applications of this technique are column wrapping, foundation strengthening and addition of gravity forces in case of dame. Research (Rodriguez and R. Park 1994; Forrest et al. 1995; David I. McLean and M. Lee Marsh 1999) shows that this technique is fruitful in improving performance of column, foundation and dame. In case of column it is used to overcome strong beam weak column failure phenomenon. In case of foundation, addition of RC at the top increases its shear strength and elongation of foundation area limit overturning effect. In dame it is used to increase the gravity forces to improve the lateral stability.

The disadvantage of this technique in case of columns is that it increases the structure dead load, reduces space and compromises the aesthetic sense. It also requires formwork and causes disturbance to inhabitants for a long period of time.

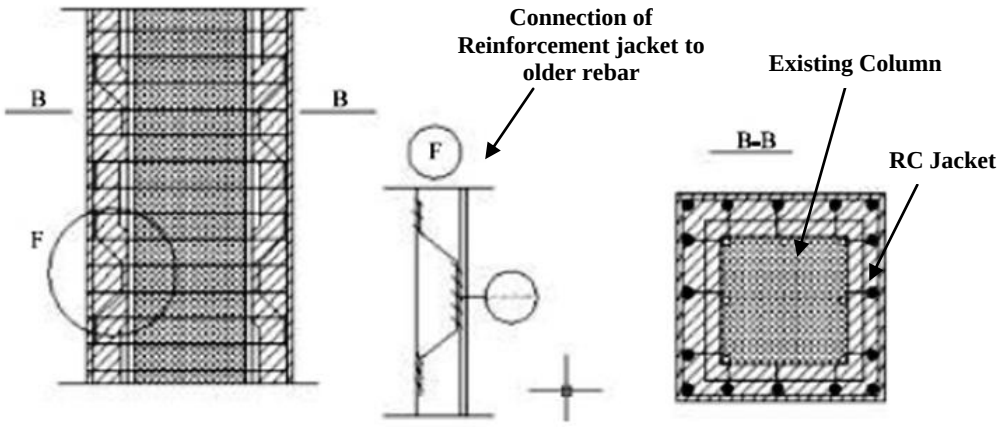

Figure 3.3: R.C jacket to old Column (Rahaee and Nemati 2004)

3.2.2.2 Steel Jacket

This technique requires lesser space and time as compared to concrete jacketing. In general it is an assembly of longitudinal angle sections and steel stirrups (Figure 3.4). To reduce the gap in between jacket and RC member the stirrups are often laterally stressed either by a special wrench or by preheating to a temperature of about 200-400°C before welding. The gap left is, later on, filled with a non-shrink mortar. In case of column the steel jacket consists of two thin plate half shells of either circular or rectangular shape. They are placed around the column with a minimum clearance of about 10-25 mm and welded. The gap left is afterward filled with a non-shrink mortar. A space of about 50 mm is left in between jacket and the supporting member (foundation) to avoid direct load transfer from jacket that may cause local buckling in it at higher drifts angles (Hiroshi Fukuyama and Sugano 2000; Giorgio Monti 2003).

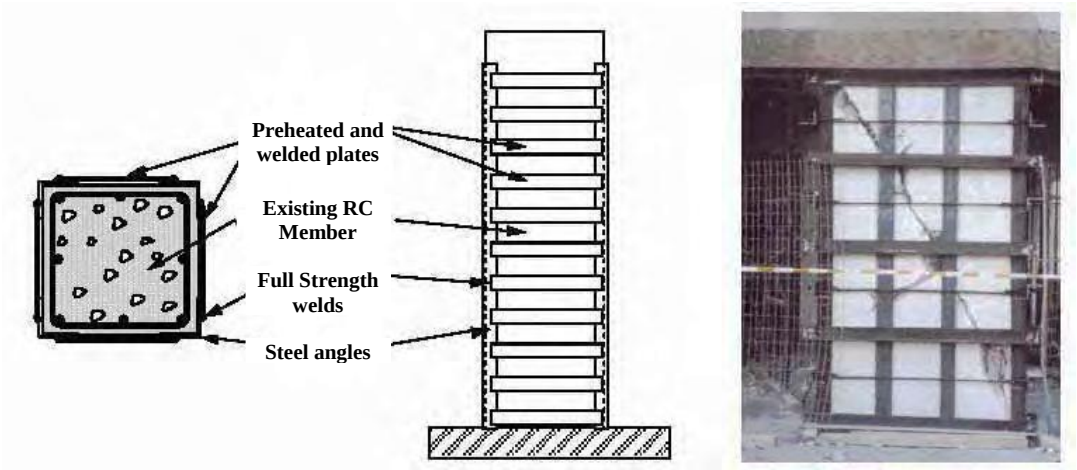

Figure 3.4: Steel jacketing (caging) of a flat column (Monti 2003)

The major disadvantages of this technique are relatively its high cost, difficulty in the transportation, requirement of a skilled workforce, difficulty in placement, welding and the problem of corrosion.

3.2.2.3 Steel plate

It is applied to beams and slabs by bonding steel elements at their lower surface with an epoxy to improve their flexural and shear strength. The steel elements used are steel plates, angles and channels. Steel elements of thickness 3-5 mm are used (Calgaro and Lacroix 1997; Guoqiang et al. 2003) and if higher thickness is required then a series of thin plates are to be bonded (Thermou and a S. Elnashai 2006). Figure 3.5 shows the steel plate arrangement made by Elnashai (A. S. Elnashai and Salama 1992) to improve stiffness, strength and ductility separately.

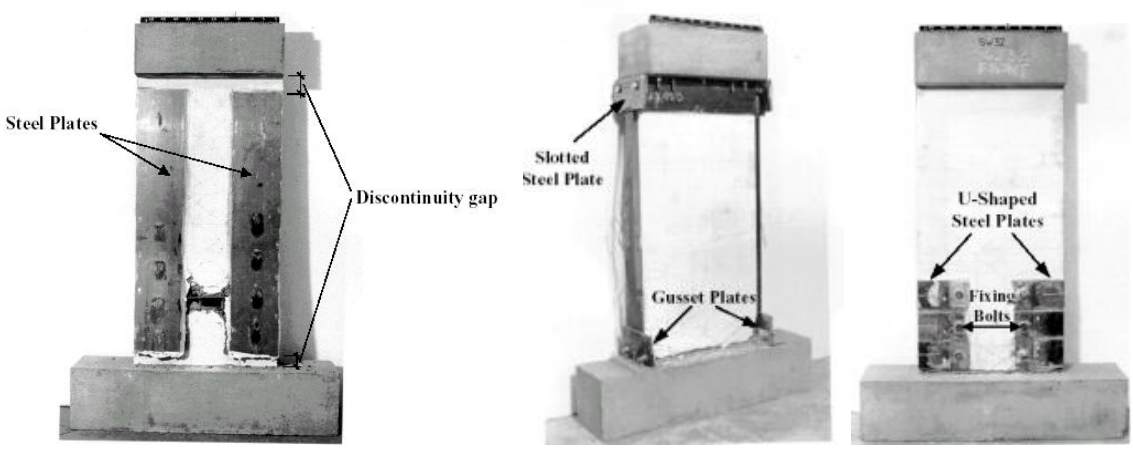

Figure 3.5: Steel plate bonding (a) Stiffness-only (b) strength-only (c) ductility-only Intervention

The main disadvantages are the steel plates debonding and corrosion. To overcome debonding problem additional metal anchor arrangement is required. A pressure of 4 kPa is required on plates during epoxy setting. It is vulnerable to fire and shocks. Transportation and placement is difficult especially in case of higher length elements

3.2.2.4 Steel cable

Steel cables are used either to prevent the structure from moving away from their support or as an external reinforcement. In case of the frame structures, cables are placed at hinges to control the horizontal displacement so that the column head displacements are limited. In this case the seismic induced effects are absorbed by steel cables. They are also used to induce pre compression forces in under-reinforced structure elements. So that development of tensile stress is limited to some extent by capitalizing concrete high compression strength.

The major drawbacks of this technique are steel cable corrosion and anchorage system arrangements.

3.3 FRP Retrofit

Fiber reinforced polymer composite retrofitting techniques have rapidly replaced the conventional retrofit techniques, because the FRP composite materials as compared to concrete and steel are lightweight, easy to transport and implement, resistance to corrosion and need low maintenance.

3.3.1 FRP composite

The FRP composite is defined as a polymer matrix reinforced with fibers. It is an anisotropic as its mechanical properties are apparent in the applied load direction and are significant in the direction of its fiber orientation. It is beneficial because of its light weight, high strength to weight ratio, directional strength, low maintenance, and resistnce to weather and corrosion. It is composed of resins (polymer), reinforcement (fibers), fillers and additives. The resin is glue that holds the composite together and influences its physical properties. The reinforcement provides mechanical strength. The fillers and additives are used to impart special properties to the final product. The FRP composite mechanical property depends on its composition and manufacturing process. The important aspects for composite design are the type of fiber reinforcement, fiber % or fiber volume, orientation of fibers (0°, ± 45° and 90°) and resin type.

3.3.1.1 Resins

The resins play a vital role in composite performance. The major functions of resins are:

- FRP adherence to concrete
- Fiber inter-adherence
- Stability of FRP dimensions and fiber orientation
- Resistance to shocks and aggressive agents
- Transfer of stress from concrete to fiber and within fibers

Resins are classified into two groups known as thermoset and thermoplastic. Thermoset resins are usually liquids and low melting point solids in their initial form. These are cured by the use of a catalyst, heat or combination of two and are irreversible chemically. The most commonly used thermoset resins are unsaturated polyester, epoxies, vinyl esters and phenolics. Among these, epoxy is the most widely utilized in composites for concrete structure repair because it exhibit good behavior in tension flexion and compression (The Japan BDPA 1999). The major advantages of epoxy are:

- Lower shrinkage
- Resistance to corrosive liquid and environment
- Good performance at elevated temperature
- Good adhesion to all types of supports
- Lesser odor
- Relatively neutral to organisms
- Good resistance towards heat

The major disadvantage is its lower resistance to shock. The mechanical characteristics of epoxy are tabulated in Table 3.1. The thermoset resins soften when subjected to high temperature. The heat distortion temperature (HDT) and the glass transition temperature (Tg) methods are used to measure the approximate temperature where the cured

resin will soften significantly to yield under load. The glass transition temperature for polymerized epoxy ranges from 30°-80°C.

Table 3.1: Epoxy resin Properties.

Tensile strength	50 – 80 MPa
Tensile modulus	3 – 10 GPa
Elongation at break	1 - 1.5 %
Compressive strength	140 – 150 MPa
Shock Resistance	7 - 10 MPa

The thermoplastic resins are not used in composite for structure strengthening, as their mechanical properties are inferior to thermosetting resins, and they melt and flow instead of softening at high temperature.

3.3.1.2 Fiber

A fiber (fiber tow or roving) is a group of filaments gathered together without twisting. It is common for fibers used in FRP reinforcements to include up to 60,000 filaments per tow, each one have a diameter between 5 and 15 micrometers, produced by textile machines. Its primary function in composite is to carry load along its length to provide stiffness and strength. The material used as reinforcing fibers can be natural, such as cellulose in wood or synthetic e.g., carbon, glass and aramid. The selection of fiber for composite depends on its intended use. The glass fibers are used in composite for reinforcement of brick or stone masonry structures due to its deformation compatibility with these structures. Carbon fiber composite are used for strengthening of reinforced concrete structure because of its higher stiffness and strength. The aramid fiber composites are used where the primary aim is an increase in the resistance to shock, impact and explosion because of its high shear strength, resistance to abrasion and good performance at higher energy levels. Table 3.2 lists the mechanical properties of mostly used fibers.

Table 3.2: Most often used Fiber Mechanical Properties.

Filament	**Dia. (µm)**	**Density (g/m^3)**	**Tension (MPa)**	**Modulus (GPa)**	**Elongation (%)**	**Fusion (°C)**
Glass E	3-30	2.54	3400	73	4.5	850
Glass D	3-30	2.14	2500	55	4.5	-
Glass R	3-30	2.48	4400	86	5.2	990
Carbon HR	8	1.78	3500	200	1	2500
Carbon HM	8	1.8	2200	400	0.5	2500
Aramid HR	12	1.45	3100	70	4	480
Aramid HM	12	1.45	3100	130	2	480

The fibers can be used simply as a unidirectional reinforcement straps or used in the form of mesh or fabric after weaving. On the basis of fiber orientation the woven fabrics are classified as unidirectional in which all the fibers are oriented in a single direction and bidirectional in which the fibers are oriented in two directions (0°, ± 45° and 90°). Generally the unidirectional composites are used in the reinforcement. As in case of bidirectional fabric only the fibers oriented along the longitudinal axis, play their role in reinforcement while the

transverse fibers helps in keeping the fibers intact and ease in implementation. The FRP composites supplied as reinforcement include fiber tow, milled fiber, fabric, rowing, continuous or chopped mat.

3.3.2 FRP Strengthening Techniques

Since 1980s the externally bonded FRP systems are used to strengthen and retrofit structural elements which include columns, beams, slabs, walls, joints, domes, tunnels, pipes and trusses (ACI 440.2R-08). In 1978 it was first used in Germany for retrofitting concrete structures (Wolf and Miessler 1989). In Japan in the year of 1980, it was first utilized on columns to provide additional confinement (Fardis and Khalili 1981; Katsumata et al. 1988). The FRP external bonded system for flexural strengthening of concrete columns was first applied in Switzerland in 1987 (Meier U 1987; Rostasy 1987).

The systems, on the basis of their delivery at site and installation technique are classified in to four forms, which are wet lay-up, prepreg, precured and near surface mounted systems. The most frequently used are wet lay-up and precured systems. The FRP material used in wet lay-up system are (a) dry unidirectional fiber sheets (b) multidirectional fiber sheet or fabrics, where the fibers are oriented in at least two directions and (c) dry fiber tows. These are impregnated with a saturating resin on site, thus in this sense they are analogous to cast in place concrete. In precured system, the composite shapes are prepared in an industry which is analogues to precast concrete. In both systems, the concrete surface is first coated with a resin and then FRP material is bonded over it either in dry or resin saturated form. In the wet lay-up technique the dry FRP fabric applied is afterward made saturated by a second resin coat.

The external FRP system, on the basis of its strengthening application, can be classified in two types.

3.3.2.1 FRP Jacketing

The FRP jacketing is applied mostly to RC columns and walls for the remedy of inadequate reinforcement arrangements, such as short splices at the base, wide tie spacing in case of column and insufficient lateral reinforcement in case of wall (Antoniades et al. 2004; Breña et al. 2007; Harajli 2008; Paterson and Mechanics 2001). In first case the retrofit procedure is applied at the column base and in second case along the entire height with or without intermediate spacing, depending on the required task. Both active and passive confinements are possible with composite wrapping (Demers and Neale 1999). Active confinement is accomplished by pressure grouting in between the inner FRP composite layer and retrofitted surface. It induces pre-stress in the FRP which leads to a significant increase in the structure elements' strength and ductility. The passive confinement, without grouting will develop a confining pressure only after concrete expansion. In case of the rectangular section, the FRP jacket confining action is less effective as compared to the circular section. To improve it either the corners are rounded or the section is inscribed with an elliptical cast in concrete prior to FRP bonding (Giorgio Monti 2003; Wu et al. 2008).

The reinforcement is applied by use of FRP shell elements, sheets, strips and filaments.

a) FRP shell

The FRP shells are generally used for the local retrofit of column base section. It is a precured system. The FRP shells either consist of two half shells of rectangular or circular shape or a circular shell with a vertical slit that can be opened to fix it around the column (Figure 3.6). The gap in between the FRP shell and column surface is filled with resin.

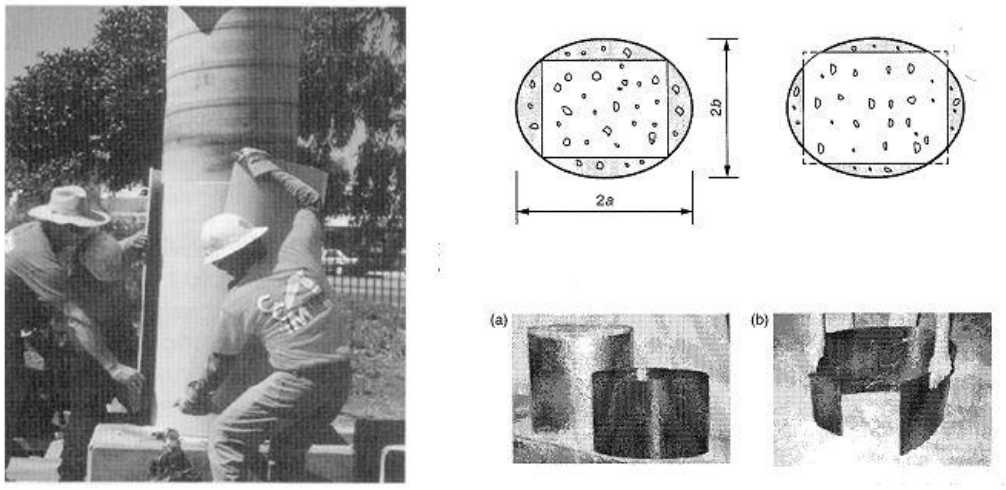

Figure 3.6: Jacketing by use of FRP shell element (Monti 2003; Teng et al. 2002)

b) FRP Strips/Sheet

FRP sheets/strips are used for jacketing of columns (rectangular or circular shape) and shear wall. The structural element surface is first resin coated then an FRP sheet is wrapped around it, either in dry or resin saturated state. In case of RC column and shear wall the jacket is generally applied at the bottom section in order to increase ductility and limit the sliding shear and steel buckling problems, caused by seismic activity induced higher drifts (Antoniades et al. 2004; Nathalie et al. 2009; Paterson and Mechanics 2001). While in case of masonry wall the FRP jacket is applied to the entire height by use of a single sheet or a series of strips. In the case of unidirectional strips, the orientation of longitudinal fibers is maintained along the circumferential direction (Harajli 2008; Cem Yalcin et al. 2008). The overlap is also made in hoop direction to avoid localized failure at the fabric ends (Breña et al. 2007).

James Paterson (Paterson and Mechanics 2001) conducted some retrofit techniques on the reinforced concrete shear wall to overcome the non-ductile seismic response. This problem exists due to the poor reinforcement details which include lap splices in the longitudinal reinforcement in the regions where flexural yielding is expected, inadequate confinement of the boundary regions, and inadequate anchorage of the transverse reinforcement. The proposed seismic retrofit involved the use of headed reinforcement and carbon fiber wrap, with or without reinforced concrete collars at the base of the wall. The retrofit schemes are shown in Figure 3.7 and Figure 3.8. It was concluded that the reinforced concrete collar was effective in strengthening the lap splice region and moving the plastic hinge to the top of the collar (Figure 3.7). It increased the ductility ratio from 1.5 to 3.8 and the retrofit specimen absorbed energy seven times more than un-retrofitted Wall. While the second strengthening technique (Figure 3.8), increased the wall ductility ratio from 4.0 to 6.3 and increased energy absorption capacity three times as compared to the non-retrofitted specimen.

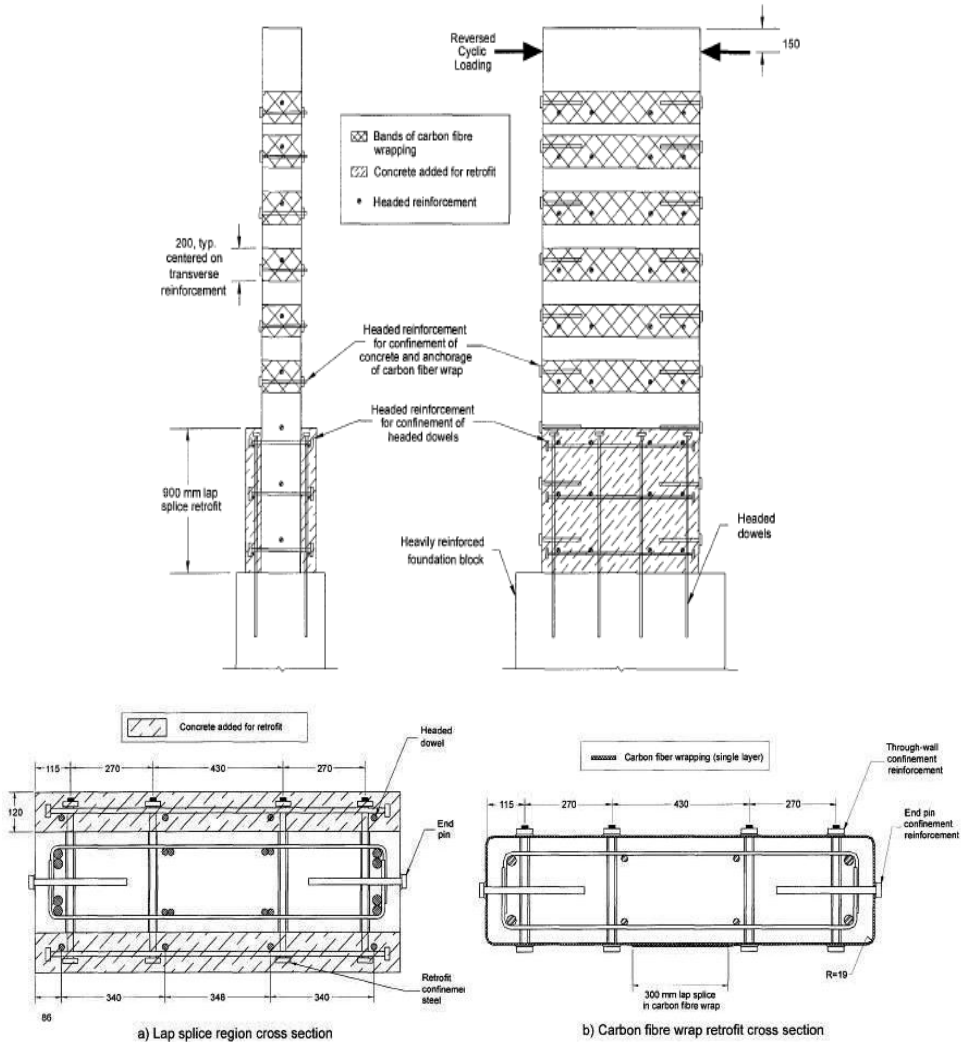

Figure 3.7: Seismic Retrofit with Reinforced Concrete Collars + FRP (Paterson and Mechanics 2001)

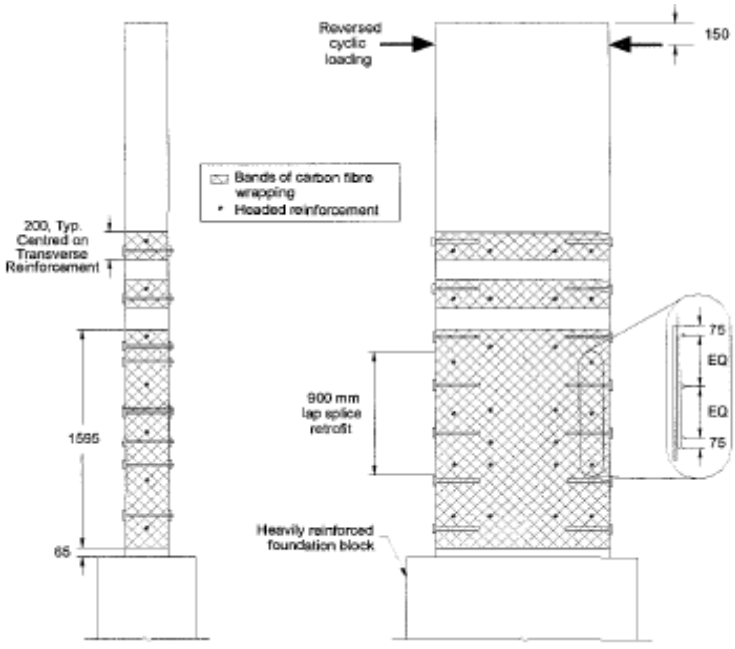

Figure 3.8: Seismic Retrofit with FRP only (Paterson and Mechanics 2001)

Konstantinos K.A. et al. (Antoniades et al. 2004) proposed a new technique of the repair and strengthening of low-slenderness reinforced concrete (RC) walls, designed according to modern design code. These were initially subjected to cyclic loading till failure, and subsequently repaired conventionally and strengthened by using Fiber-reinforced polymer (FRP) jackets. Repair work involved replacement of the damaged concrete by a high-strength mortar and lap-welding of fractured reinforcement in the plastic hinge region. The strengthening involved wrapping of the walls with FRP jackets, as well as the addition of FRP strips at the wall edges in order to enhance both flexural and shear capacity. In addition to different arrangements of steel and FRP reinforcement in the walls, the most important was the manner in which carbon FRP (CFRP) strips added for flexural strengthening, were anchored. The combinations of glass FRP (GFRP) anchors and anchoring strips, as well as anchoring steel plates, were used. Test results have shown that the addition of steel plates to the GFRP anchors and strips leads to a more effective anchorage. The strength increases up to 30% with respect to a conventionally repaired specimen when properly anchored FRP strips were used. However, the energy dissipation capacity of the original walls (designed to modern code provisions) could not be fully restored. Figure 3.9 shows a detail description of the retrofitting arrangements.

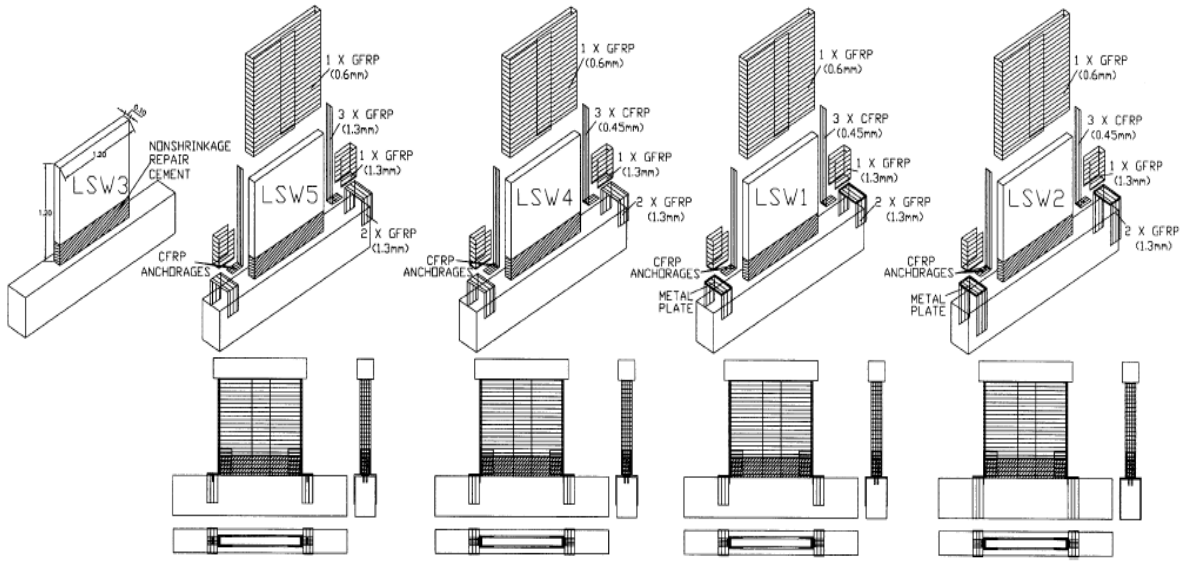

Figure 3.9: Repair and strengthening procedures applied to each specimen (Antoniades et al. 2004)

It was concluded that with respect to the strength of the anchorage systems tested, the most efficient was the combination of GFRP inverted U-sections, GFRP anchors, and 20 mm thick steel plate used to strengthen the horizontal leg of the U-section.

c) Fiber tows

In case of circular piers or column an automated fiber wrapping system is used to wind fibers around them. Figure 3.10 shows machine setup around the column. The machine first saturates the fibers with resin and then wound them around the column. It is the most efficient technique as the winding angle, fiber volume fraction and its thickness are fully controlled by the computer. The major disadvantage of this instrument is that it can be applied only to a circular section.

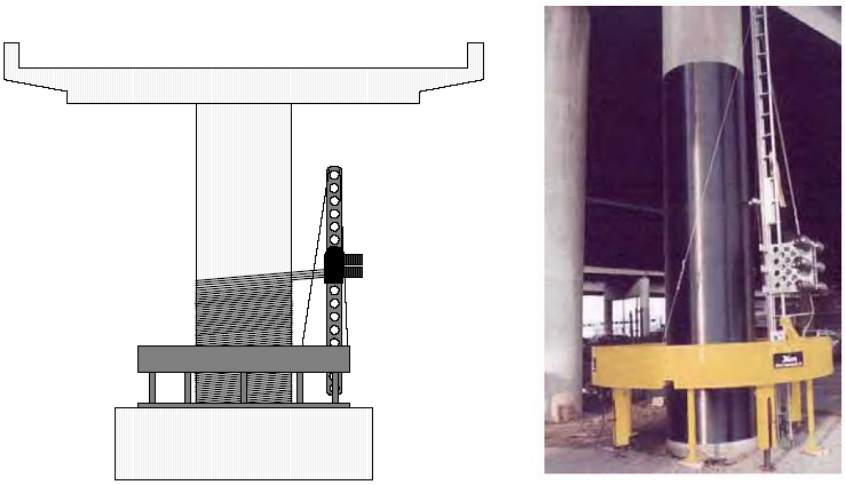

Figure 3.10: Automated Fiber wrapping system

K. Kobayashi (Kobayashi 2005) developed an innovative strengthening and repairing technique for RC shear wall. The aim was to cross the cracks in wall with aramid fibers, to control its expansion and to transfer the tensile force over cracks. The retrofitting technique adopted was: (a) drilling small holes at the grid intersection on the concrete wall panel (b) sewing in a diagonal sewing path by a bundle of ten aramid fiber tows, passed through the resin filled holes. The properties of aramid strand used were 12 µm diameter filaments, density 6000dn, tensile strength 3430 MPa and young modulus 72.5 GPa, while the concrete compressive strength was 40.2 MPa. Figure 3.11 shows the specimen internal rebar and external reinforcement detail. The retrofitting arrangement confined the concrete wall panel into a net made of aramid sewing bands. The test specimens were subjected to quasi-static cyclic load and no additional vertical load was imposed. In case of strengthened wall, the shear capacity increased by more than 25%. The failure pattern observed was: generation of shear cracks at column top (because the horizontal load was concentrated at it and also it was not retrofitted) followed by partial crushing of wall panel with a gradual decrease in bearing capacity. However, the aramid sewing bands worked as confinement to the concrete crushed part, it controlled the crack opening and thus avoided concrete peeling off. Afterwards the RC frame was redesigned by addition of four ø6 mm longitudinal bars in each column and beam width was increased from 100 to 190 mm, while the concrete compression strength was equal to 26 MPa. A total of four specimens were fabricated with this configuration. Three specimens, No 2 to No 4 were strengthened with sewing bands of 3, 6 and 12 strands. Table 3.3 shows that the shear capacity and the deformability increased in proportion to the number of strands in a sewing band.

Table 3.3: Test result of aramid sewed RC wall.

Specimen	Number of strand	Maximum load (kN)	Capacity gain (kN)	Deformation capacity* (mm)
No.1	0	193.0	-	2.9
No.2	3	209.4	16.4	4.2
No.3	6	213.5	20.5	4.6
No.4	12	240.2	47.2	5.3

* It is defined as the horizontal displacement where the bearing force decreased by 15% from the maximum

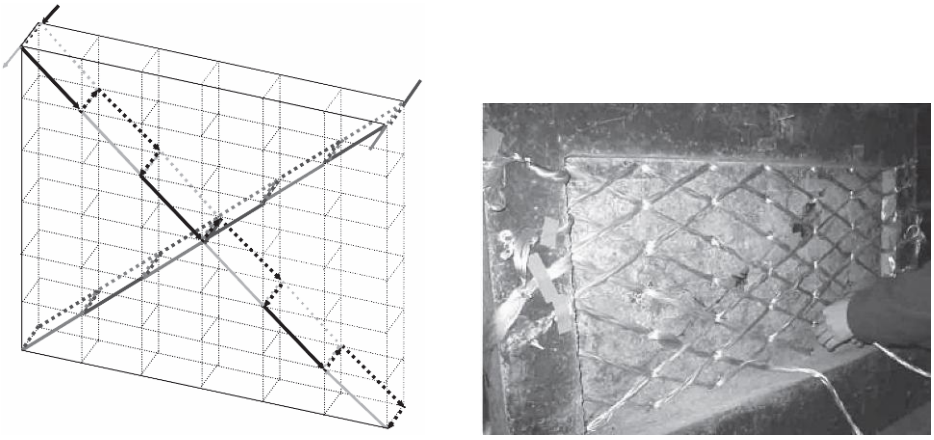

(a) Diagonal sewing path

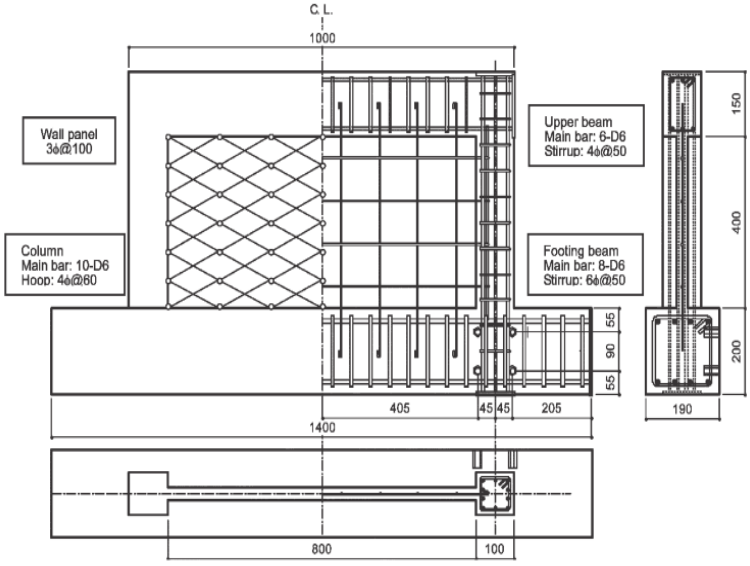

(c) Specimen detail

Figure 3.11: Dimensions and reinforcing arrangement of the test specimen (Kobayashi 2005)

3.3.2.2 FRP Bonding

This technique is generally applied to the structure elements like slabs, beams, beam column joints and walls. In case of slabs, the FRP sheet strips are bonded either over it upper surface to improve its punching shear capacity or at lower surface to improve its flexural performance (Figure 3.12).

In case of beams to improve its flexural performance, the FRP strips are bonded at its tensile stressed face in the longitudinal direction (Francesca Ceroni and Pecce 2009; Ekenel and Myers 2007; Gao et al. 2005; S. Matthys 2000). Figure 3.13 shows a typical CFRP external reinforcement arrangement applied on RC beam. To prevent the CFRP strips debonding, U-shaped or L-shaped strips are bonded over it (F Ceroni 2010; Kotynia et al. 2008). This additional arrangement also improves beam shear capacity.

Figure 3.12: Strengthening of a concrete deck on bottom and top using CFRP (Yalcin et al. 2008)

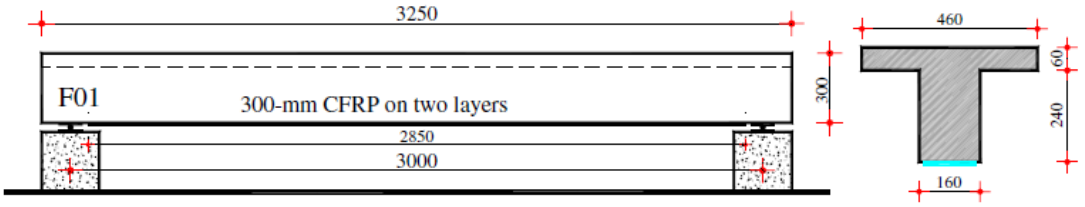

Figure 3.13: External CFRP Flexural strengthening of a RC beam (Hosny et al. 2006)

For shear strengthening, the fiber orientation is kept tilted to minimize the shear crack opening by capitalizing FRP tensile strength (Figure 3.14).

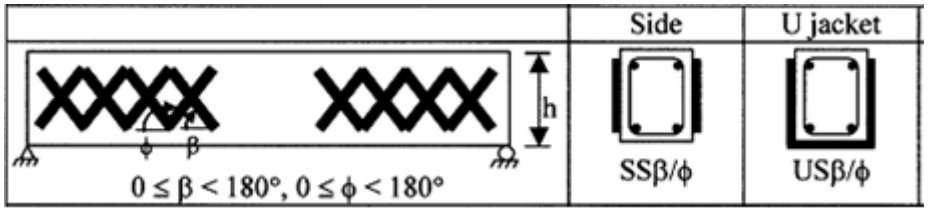

Figure 3.14: FRP Shear strengthening scheme (Chen and Teng 2003)

In case of URM walls, the FRP sheets are bonded over the entire wall surface, either on a single face or both, to keep the blocks intact. Figure 3.15 shows a URM wall retrofitted by GFRP fabric with additional CFRP strips, which were anchored with the help of an assembly of steel plates and threaded bolts.

M. Saatcioglu et al. (Saatcioglu et al. 2005) applied CFRP external bonded sheets at in-fill masonry wall with the objective to resist wall diagonal tension. The RC frame was designed according to ACI 318-1963. The infill wall retrofitting technique included bonding of one sheet per face parallel to each of the two diagonals, resulting in two sheets per wall face, while to limit its debonding CFRP anchors were used. The anchors were made by

twisting strips of CFRP sheets and folding into two. Its one end was inserted in holes drilled in RC frame and the other splayed over CFRP sheet. The specimen was tested under a constant gravity load and incrementally increasing lateral load in deformation control mode. Three cycles of lateral displacements were applied at each deformation level until failure. The retrofitted specimen, as compared to non-retrofitted one, showed an overall increase in the strength and elastic rigidity. It showed three times improvement in the peak load. Its initial stiffness was higher and remained at un-cracked stiffness value, up to its peak resistance.

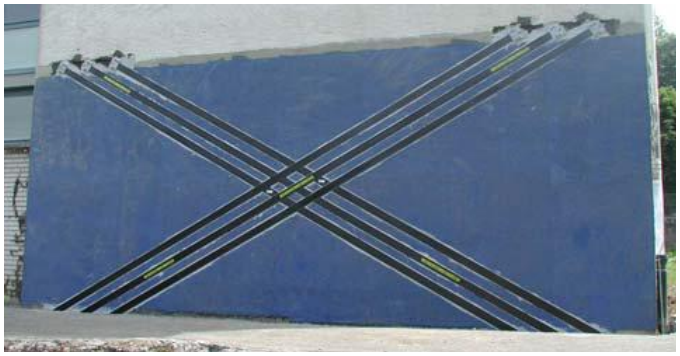

Figure 3.15: FRP retrofitted URM wall (Yalcin et al. 2008)

E. Yuksel et al. (Yuksel et al. 2010) investigated CFRP retrofitted infill masonry wall within RC frames subjected to unidirectional lateral cyclic loading with a constant normal load of 40 kN. A total of six specimens were fabricated at a 1/3 scale. These were designed according to pre-seismic codes. Figure 3.16 shows the schematic drawings of CFRP reinforcement arrangement made on four specimens. The CFRP material used was unidirectional sheets of 150 mm width. The fiber density, tensile strength, modulus of elasticity and ultimate elongation capacity were 1.79 gm/cm^3, 3900 MPa, 230 GPa, 1.5% respectively. Prior CFRP sheets bonding, the surface was prepared with an epoxy coat. The bonded sheets were afterward impregnated with another epoxy coat. To control CFRP sheet debonding FRP sheet anchors were installed in holes drilled in infill wall with 300 mm spacing. Each, retrofitted specimen showed an increase in the strength and rigidity as compared to control specimen. However, the cross diamond braced system performance was best as it exhibited less damage and had a considerable energy dissipation capacity.

In the case of RC wall a number of FRP strips are bonded on either one face or both. Some portion of the wall face is left uncovered in order to use concrete cracking for energy dissipation as in the case of columns. The various FRP bonding arrangement made on the wall are described briefly in the following paragraphs.

A. Ghobarah and A.A. khalil (Ghobarah and Khalil 2004) developed rehabilitation techniques for the concrete wall with end columns, designed according to 1963 ACI and CSA code provision. It was weak in shear strength and ductility according to the modern age requirements. For the shear improvement, two layers of bidirectional carbon fabric of 0.864 mm thickness, woven at ± 45°, were wrapped around each wall (Figure 3.17). Each layer had an overlap of 150 mm. For the ductility enhancement, the end columns were partially confined by bonding U shaped sheets of 0.89 mm thick carbon fabric. Each sheet consisted of three layers of unidirectional carbon fibers. To limit the U Shaped sheets debonding, its legs length was kept equal to 300m and FRP anchors were introduced. The anchors were made up

by wrapping 110 mm wide unidirectional sheets, were soaked in epoxy and inserted in drilled holes. The length of the anchor was 220 mm and 50 mm on each side was splayed over U shaped sheets. In the second case, the FRP anchors were replaced with steel anchors and additional four were introduced with in wall panel. The steel anchor assembly was consisted of threaded rods of 16 mm diameter, circular washer plates of 60 mm diameter and 18 mm thickness. The proposed rehabilitation techniques were effective in eliminating the premature shear failure mode, in improving wall ductility and formation of plastic hinge at wall base for energy dissipation. The shear failure mode was eliminated as the carbon fibers aligned at 45° were effective in limiting the diagonal shear cracks. The increased confinement by U shaped sheets improved ductility by delaying concrete compression crushing at high compression strains and utilizing the longitudinal steel tensile strength to a greater extent. The FRP anchors did not provide better confinement as compared to the steel anchors. It failed in shear. The retrofitting arrangement shifted the critical region to wall foundation joint.

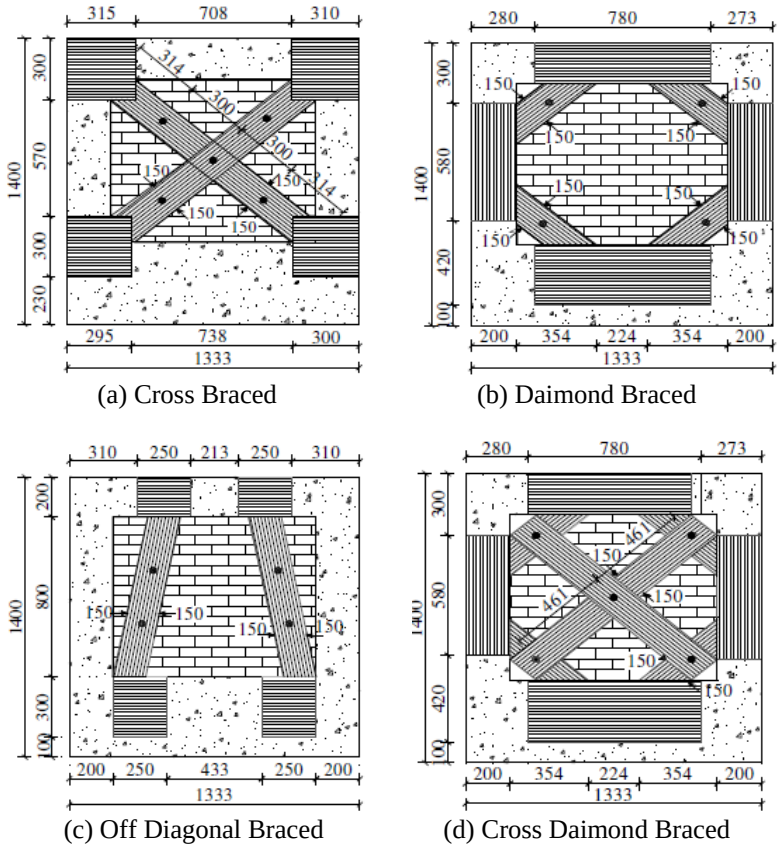

Figure 3.16: Infill Masonry wall retrofitting pattern (Yuksel et al. 2010)

Josh Lombard et al. (Lombard et al. 2000) analyzed the effectiveness of using external bonded CFRP tow sheets for the seismic strengthening and repair of RC shear walls. A total of four shear walls were fabricated with height, length and thickness equals to 1795 mm, 1500 mm and 100 mm respectively. The wall panel vertical and horizontal reinforcement ratio was maintained as 0.8% and 0.5%. Two out of four specimens were strengthened with the CFRP external reinforcement. To improve their in-plane flexural strength and stiffness, the carbon fiber tow sheets were applied on both faces, with the fibers oriented in a vertical direction. The first RC wall was reinforced by a single vertical layer of CFRP applied on each face

while the second one was strengthened with one horizontal and two vertical layers on each face. To restrict CFRP sheet debonding and transfer load from sheets to the supporting foundation block, a steel anchorage system was used. It was comprised of L shaped angles, threaded bolts and nuts. The CFRP sheets used had an elastic tensile modulus of 230 GPa, with strength and failure strain, 3480 MPa and 1.5%, respectively. The samples were subjected to in-plane quasi static cyclic lateral loading, applied at head beam and the foundation block fixed to a reaction wall floor by means of threaded rod assembly. The application of CFRP sheets increased its cracking strength up to 82% (110kN as compared to the control wall 55kN). By comparing the two strengthened walls, it was observed that the additional CFRP sheets application in case of second wall had no effect on its cracking strength, and the cracking pattern remains similar to the first one. However, it improved the specimens' yield and ultimate strength. The first CFRP strengthened specimen demonstrated an overall increase of 25% in its yield strength and 46% in the ultimate strength as compared to the control specimen. The second strengthened wall exhibited an overall increase of 39% in its yield and 132% in the ultimate strength. The failure mode in the two walls was noticed by first crushing of compression toe, followed by fracture of extreme vertical rebar and in the final stage tearing of sheets at the wall base.

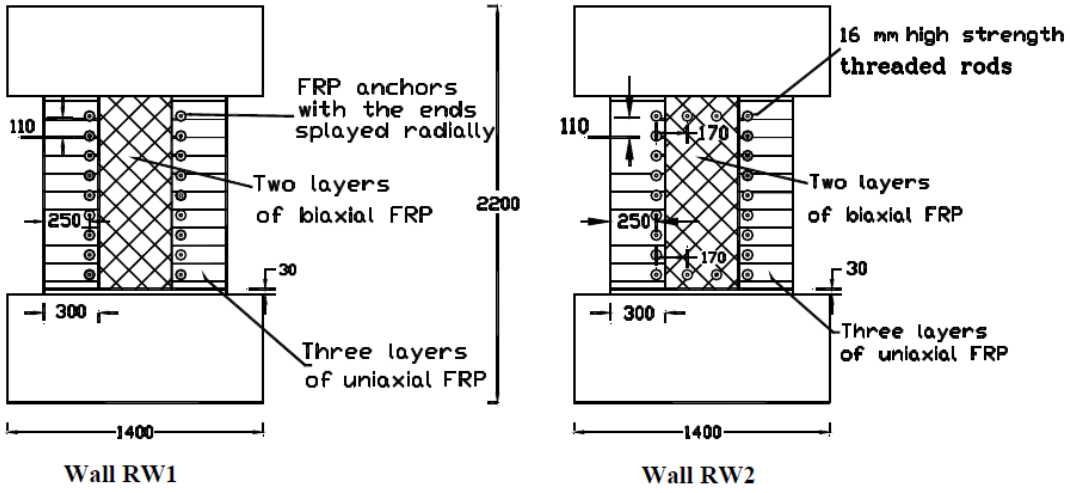

Figure 3.17: Rehabilitation scheme for RW1 and RW2 (Ghobarah and Khalil 2004)

3.4 Anchorage System

Recent seismic studies has highlighted a shortcoming in the external FRP strengthening technique that is occurrence of a premature failure as a result of the cracks formation or FRP strips debonding at joint (column/beam joint) separately or a combination of the two (Francesca Ceroni et al. 2008; El Maaddawy and Khaled Soudki 2008). Consequently, it reduces the effectiveness of the technique as the FRP materials are not stressed to their full capacity and debonding occur, due to bond failure at the concrete/FRP strip interface. Therefore it is important to develop an anchorage system to facilitate load transfer at the joint and utilize the FRP strength with its full capacity. To redress the issues, considerable efforts were made by developing different anchoring techniques, such as provision of local reinforcement in the form of small CFRP anchors (Huang and Chen 2005; Matsuzaki et al. 2001), mechanical fixing of FRP strips by FRP/steel plates glued or bolted (Francesca Ceroni et al. 2008) , wrapping of FRP lamina with FRP fan shaped anchor (Jinno et al. 2001), spike

anchors (Karantzikis et al. 2005), U-shaped anchors (Khalifa et al. 1999), and FRP sheet anchor system (Niemitz et al. 2010). These anchorage systems facilitated an overall increase in the stress development within the CFRP material during loading and to some extent behaved as an additional local reinforcement.

3.4.1 Rod Anchorage Systems

The section provides a preview of conventional rod anchorage systems for the steel pre-stressing reinforcement. They possessed hardened teeth which bite into the reinforcement to enhance the transfer of stress. With FRP reinforcement, the teeth bring about premature failure of it at the grip location. Different anchorage systems were applied with FRP tendons such as, clamp, plug and cone, resin sleeve, resin potted, metal overlay and split wedge anchorages, as shown in Figure 3.18 (*ACI 440R-07*). These anchorage systems and their gripping mechanisms can be briefly discussed as:

***a*) Clamp anchorage** - A clamp anchorage consists of two or four grooved steel plates sandwiching the FRP tendon and are held together by prestressed bolts and springs. The force is transferred by a shear-friction mechanism (Malvar L.J. & Bish 1995).

b) Plug and cone anchorage - The plug and cone (or barrel and spike) anchorage system is made of a socket housing and a conical spike (Burgoyne C.J. 1992). Such a system is suited to anchor Parafil ropes where the fibers are not encased in a resin media but are held by an outer protection sheath.

c) Resin sleeve anchorage - In this system, the FRP tendon is embedded in a resin filled in a metallic housing such as, a steel or copper tube. The resin used ranges from non-shrink cement with or without sand to epoxy-based material. The load transfer mechanism depends completely on the bonding and interlocking between the anchorage components.

d) Resin potted anchorage - The potted anchorage varies depending on the internal configuration of the socket: straight, linearly tapered, or parabolically tapered. The load transfer mechanism from the tendon to the sleeve is by interfacial shear stress that is a function of bonding and normal stress produced by the variation of the resin profile (P. Kim and Meier 1991). The practical drawbacks are pre-cutting the tendons to length and the curing time for the resin or grout.

e) Metal overlaying - The die-cast wedge system for the carbon fiber composite cable (CFCC) requires that the tendon length be predefined so that metal can be cast onto the tendon during fabrication with the result that adjustment on site is not possible. The tendon and the metal material are compressed by a typical wedge anchorage similar to those used on steel tendons. The load transfer of this anchorage is achieved by shear friction, which is a function of compressive stress and friction at the contact surfaces.

f) Split wedge anchorage - Split wedge anchorages are generally preferred because of their compactness, ease of assembly, reusability, and reliability. The wedge system is widely used in anchoring steel tendons. The anchorages are modified for use with FRP tendons by increasing their length and placing a soft metal sleeve around the tendon to prevent notching.

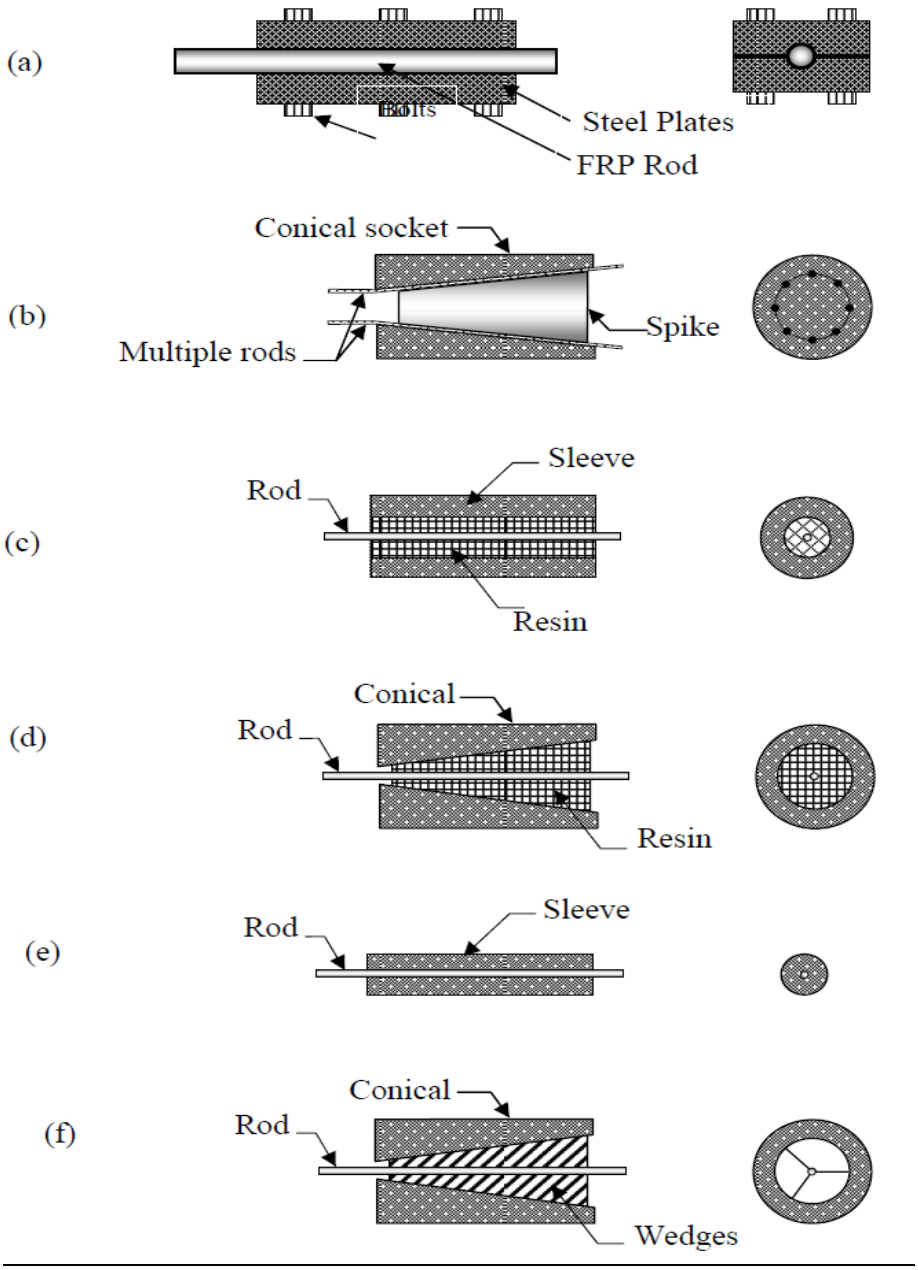

(a) Clamp; (b) plug and cone; (c) resin sleeve; (d) resin potted; (e) metal overlay; and (f) split wedge anchorage systems (ACI 440R-07)

Figure 3.18: Rod Anchoring System Description.

3.4.2 Steel Plate/Angles Anchoring System

Antoniades et al. (Antoniades et al. 2005) proposed an anchorage system in which steel plates or steel angles were used at the wall base to counter pealing apart of FRP stirrups from concrete. Figure 3.19 shows the schematic view of these systems. The specimens were strengthened using FRP sheets and strips, to increase its flexural as well as shear strength and ductility. Anchors used to prevent carbon-FRP strips from debonding were, steel plates and steel angles. Steel plates were anchored using U-shaped glass-FRP (GFRP) strips or bonded metal anchors. Authors concluded that "from the anchorage systems tested, metal plates

combined with FRP "brackets" (cut from the same fabric as the sheets), appear to be quite efficient. The effectiveness of bonded anchors used, was generally less than that of the combination of plates and FRP brackets".

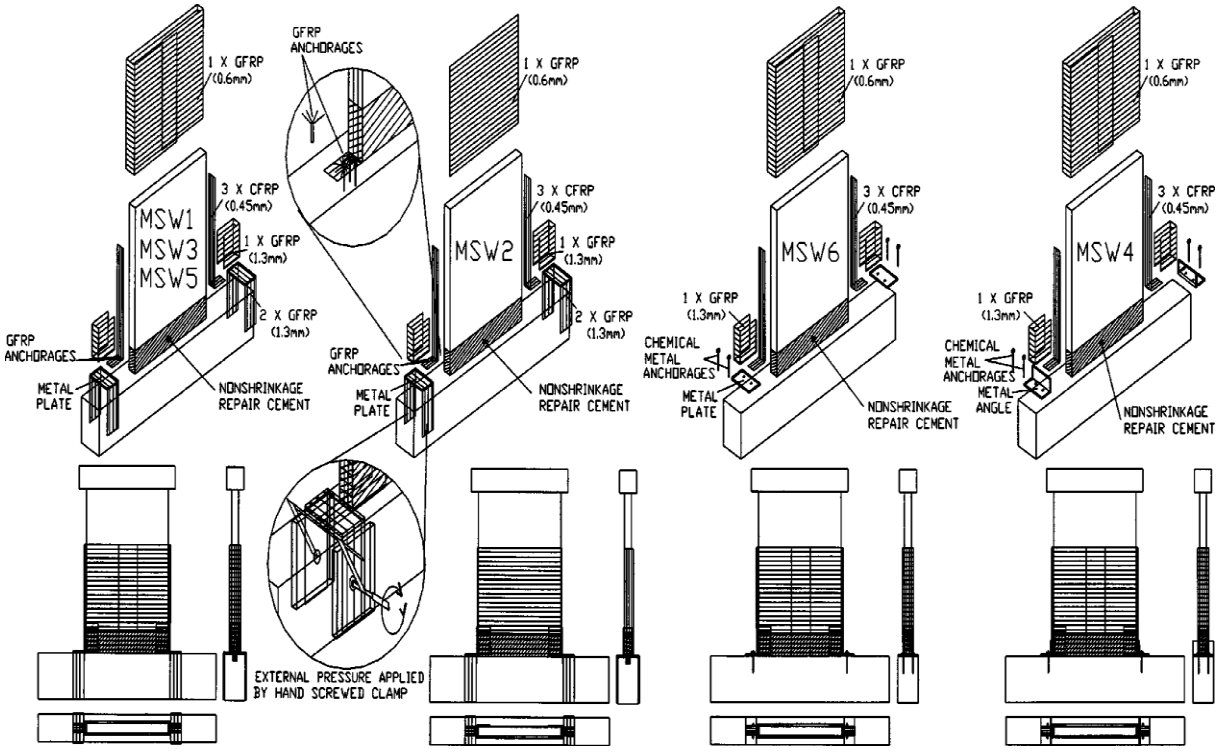

Figure 3.19: Repair and strengthening procedures applied to each specimen (Antoniades et al. 2005)

3.4.3 FRP Anchorage Systems

Among the anchorage techniques, the CFRP mesh anchors are used to prevent the CFRP from debonding and improve its efficiency in load transfer. The anchor consists of two parts: dowel that is inserted in the hole drilled in the concrete and the fan part which is splayed over the bonded CFRP strip/sheet (Figure 3.20 and Figure 3.21). The anchors can be prepared from strips cut from CFRP sheets. The recommended depth of a mesh anchor in the concrete is from 13 to 15 cm to inhibit the rupture of the concrete surface layer (Orton et al. 2008). During the installation of the wick, fibers are stamped by the whip laminated on the layer (PRF formed on the basis of tissue) in place.

In certain cases, the anchor portion to be placed in the concrete is rigid as the fibers are embedded in a cured matrix, e.g., the drilled anchor of TFC Freyssinet (CSTB 2008).
The installation procedure involve:-

- drilling holes (diameter 16 mm, a depth of 15 cm),
- bonding of first layer made of TFC fabric
- removing the fibers of the fabric and placing anchor in a drilled hole, filled with epoxy resin
- splaying and bonding the anchors' outer portion over the bonded TFC layer
- Applying a second layer of TFC, if desired.

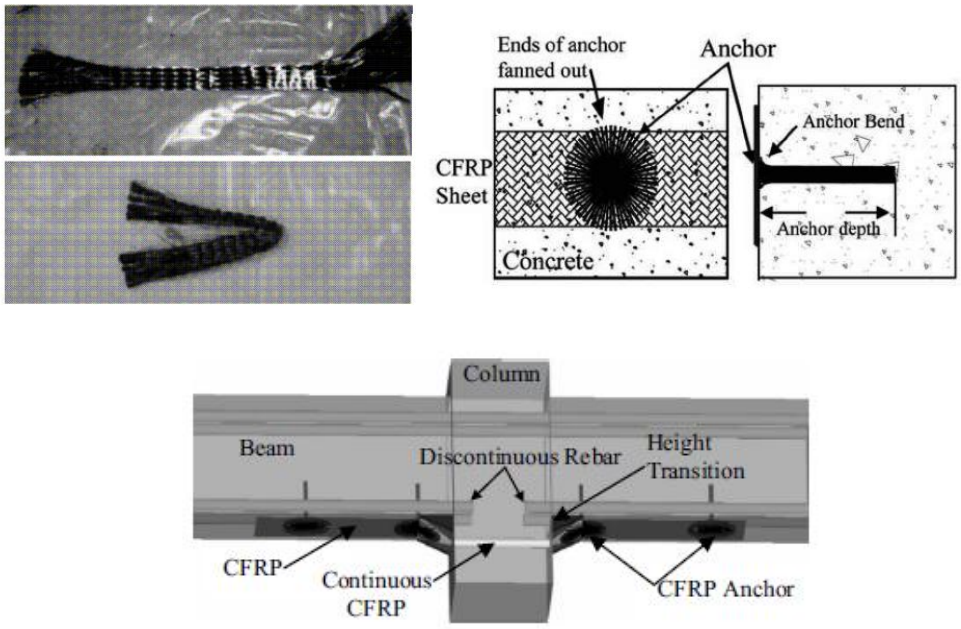

Figure 3.20: Preparation of anchor from CFRP strip and its installation procedure (Orton et al. 2008)

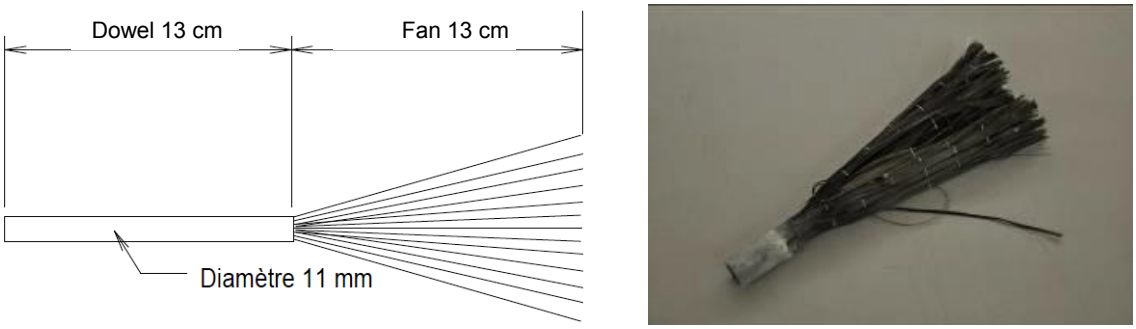

(a) (b)

Figure 3.21: (a) Description of Carbon mesh anchor of TFC (CSTB 2008) (b) Impregnated CFRP anchor (Orton et al. 2008)

This mesh anchorage technique increases the FRP strip load capacity. Numerous research have shown that its use increase the resistance capacity of the strengthened element.

Kobayashi et al. (Kobayashi et al. 2001) utilized this system by sealing the mesh anchors in an element associated to a reinforced member where the wrapping of CFRP around RC member was not possible e.g., a wall connected to the columns prevents its jacketing with CFRP sheets (Figure 3.22). The tests showed the effectiveness of the anchors, which have increased deformability and strength of the element.

The flexural retrofitting of square/rectangular RC columns by jacketing is much less effective due to the poor confinement of concrete in the middle of the column sides, especially for large columns (Wu et al. 2006). To overcome this issue Okan Ozcana and al. (Ozcan et al. 2008) used the CFRP anchor to hold back the CFRP sheet from debonding at the middle of rectangular or square column sides (Figure 3.23). They rounded column corners, drilled holes in all the four sides of the column, prepared the surface with a thin undercoat, applied epoxy based mortar and wrapped the FRP sheet around the column. Finally they placed the CFRP anchors dowels in already drilled holes and splayed the fan portion on the bonded CFRP sheet. The CFRP anchors were formed from carbon fiber strips, rolled in the fiber direction and tied with a string as shown in Figure 3.23(b).

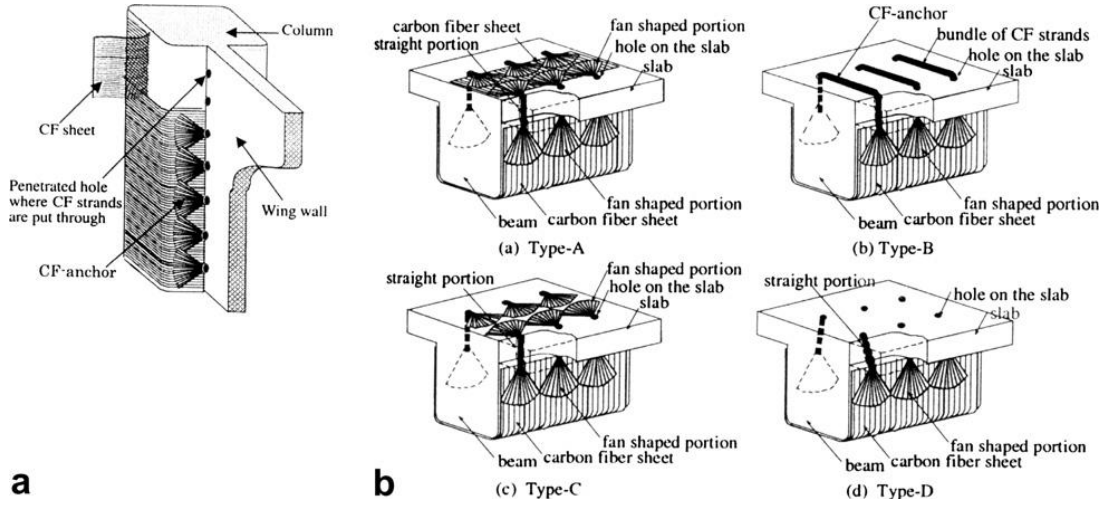

Figure 3.22: Anchorage system for interconnected RC structural elements (Kobayashi et al. 2001)

Togay Ozbakkaloglu et al. (Ozbakkaloglu et al. 2009) used an inclined drilled hole for the anchor installation (Figure 3.24). A hole of 25-100 mm length with angle of inclination 15-45° was drilled in the specimen. The mesh anchors were prepared from a fiber strip cut from fiber sheet, rolled and folded into two at its mid-length similar to the anchor shown in

Figure 3.24(a). The hole was cleaned by compressed air, filled with epoxy and then anchor was inserted in the hole. The author concluded that the pullout capacity of anchors decreases with an increasing angle of inclination.

M. Saatcioglu et al. (M Saatcioglu et al. 2005) used an identical system to anchor CFRP strips bonded over the infill masonry wall to RC frame. The anchor was made by twisting CFRP sheet and folding in half. The holes of dia 12 mm and 50 mm deep were drilled in RC frame, inclined at 45° towards the centre of frame elements. One end of the anchor was dipped in epoxy filled hole and the other end was splayed over bonded CFRP sheets.

A. Khalifa et al. (Khalifa et al. 1999) utilized an anchor by embedding a bent portion of the end (or near the end) of the FRP reinforcement into a preformed groove in the concrete/masonry (Figure 3.25). The groove was filled with a viscous paste, including a FRP bar or not. The U-anchor is compatible with any external FRP strengthening system and avoids high stress concentration and durability concerns. It can be used with sheets and pre-cured laminates that are unbonded or fully bonded to concrete. Laboratory testing confirmed

the excellent performance of the U-anchor system as it increased the shear capacity of the member and prevented FRP debonding.

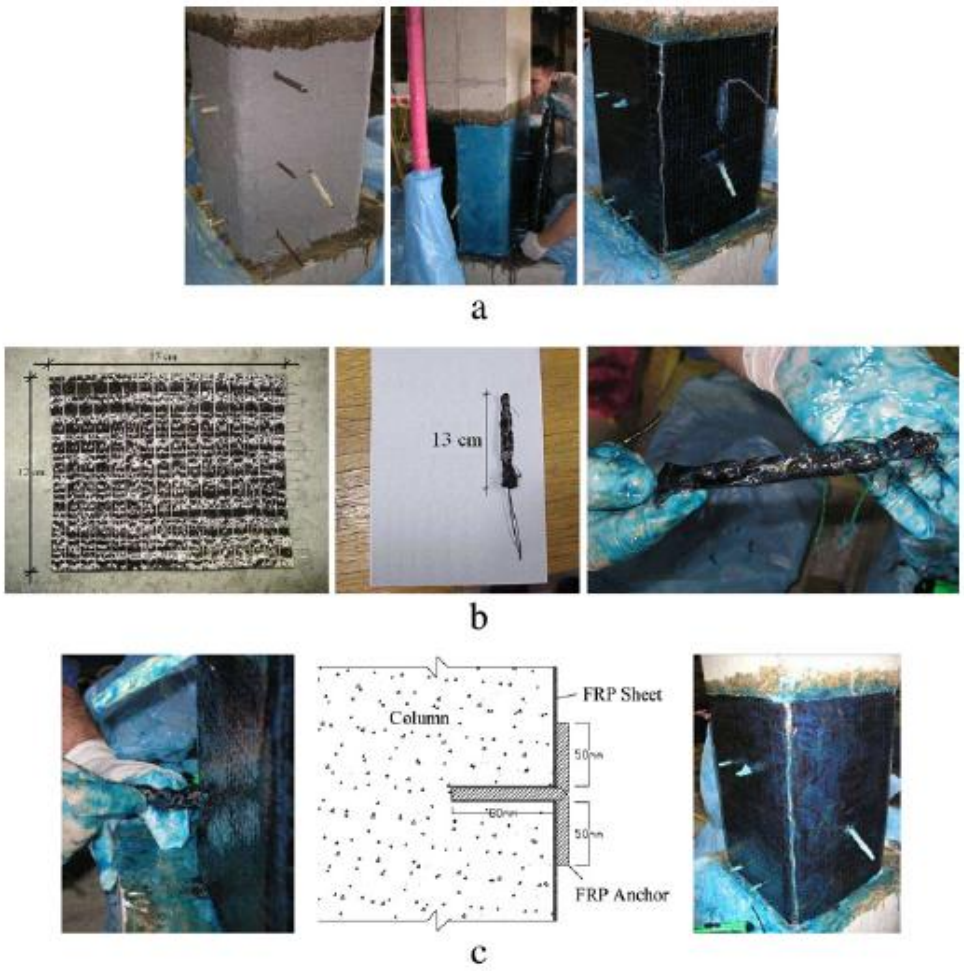

Figure 3.23: CFRP application: (a) Rounding off corners, undercoat application and CFRP wrapping, (b) CFRP anchor dowels and final shape of an anchor dowel tied with a string, (c) Anchor dowel insertion and final curing (Ozcan et al. 2008)

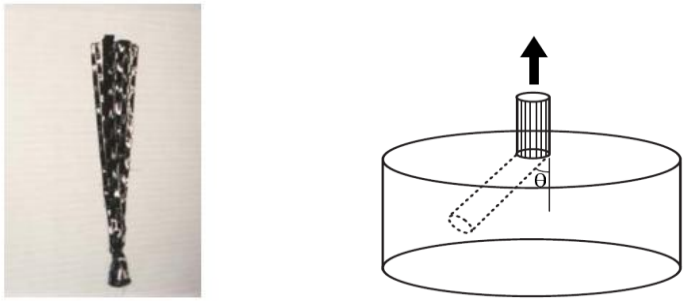

(a) Anchor (b) Inclined anchor system

Figure 3.24: Inclined Anchoring system description (Ozbakkaloglu et al. 2009)

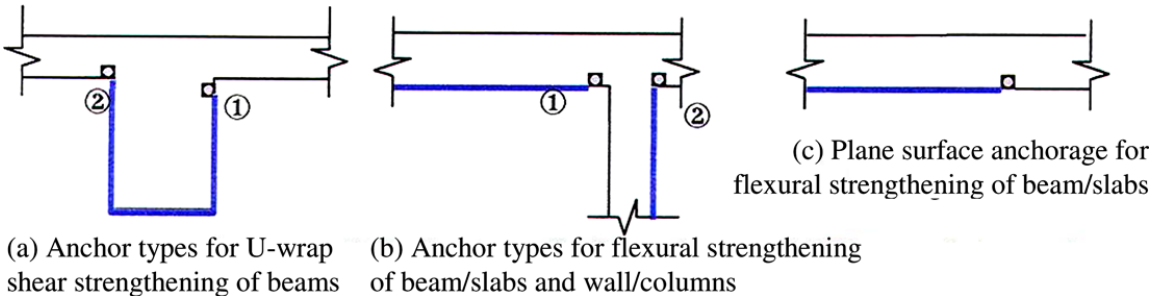

(a) Anchor types for U-wrap shear strengthening of beams

(b) Anchor types for flexural strengthening of beam/slabs and wall/columns

(c) Plane surface anchorage for flexural strengthening of beam/slabs

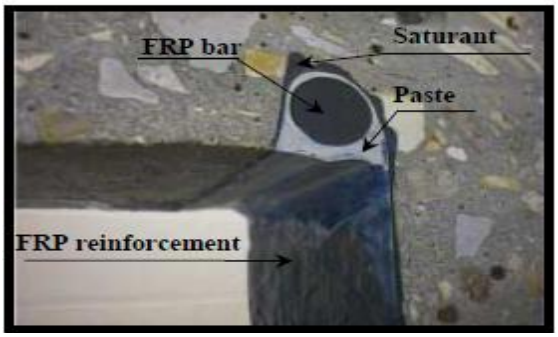

(d) Beam Cross-section showing details of the U-anchor

Figure 3.25: U-anchor detail (Khalifa et al. 1999)

Mike Beigay et al. (Beigay et al. 2003) tested a new composite anchorage system on unreinforced concrete masonry walls. The details are given in Figure 3.26. The system provides high-capacity load transfer between the fiber reinforced polymer (FRP) laminate retrofitted wall and the foundation. The retrofitted specimen investigated, showed about 300% increase in the lateral force resistance, promoting elastic response to the earthquake loads as a seismic retrofit strategy.

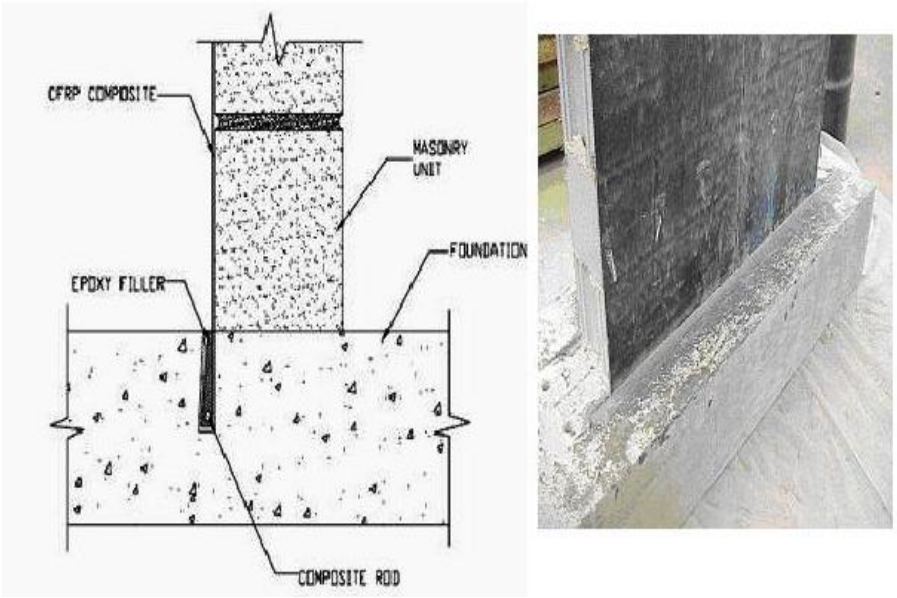

Figure 3.26: (a) Details of Composite anchor (b) Composite anchor into wall foundation

Ceroni et al. (Francesca Ceroni et al. 2008) tested and compared the performance of different anchorage systems applied on fourteen T-shaped specimens simulating the column-beam joints (Figure 3.27). The different tested configurations are shown in

Figure 3.28. On the two opposite sides of the specimen a carbon sheet was applied with a width of 100 mm, and the six specimens were provided with the CFRP only along the web (Figure 3.27a), while for the other eight specimens, fibers were extended on the flange of the T-section (Figure 3.27b). The 90° angle of the concrete block was rounded by an epoxy filling with a curvature radius of 25 mm. The anchors tested were as follow:-

- CFRP plates glued
- Steel plates glued or bolted
- FRP bars (near surface mounted bars technique).

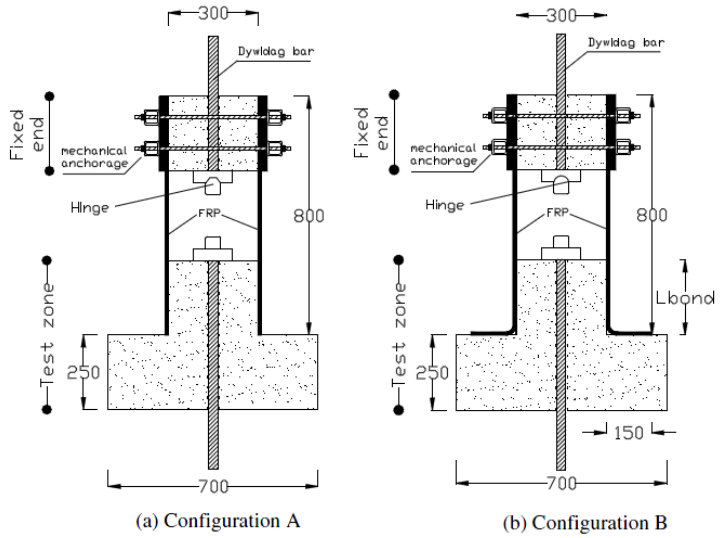

Figure 3.27: Specimen configuration (Francesca Ceroni et al. 2008)

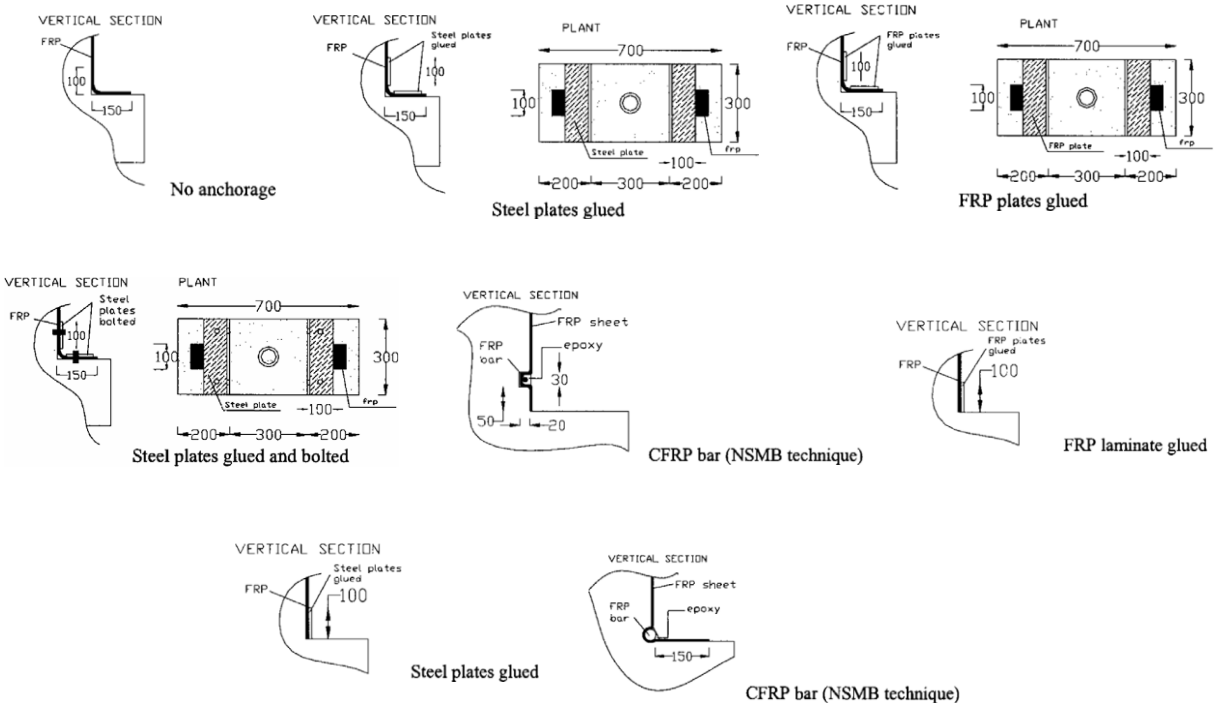

Figure 3.28: Characteristics of anchorage systems (Francesca Ceroni et al. 2008)

The rupture observed, in the majority of cases, was FRP debonding with detachment of a very thin layer of concrete and for some cases it was failure of fibers in tension. The test results showed that the application of bolts on steel plates caused stress concentration with consequent premature debonding, while NSM bar resulted in local rupture phenomenon. The performance of type A configuration was better than that of type B (Figure 3.27). This concluded that extending the reinforcement on an orthogonal surface can produce negative effect, even if the available bonded length is increased. Comparatively, the additional anchorage provided by a transverse plate bonding (CFRP or steel) in configuration A was very effective as it increased the failure load up to 55-56% as compared to the reference specimen.

Nagy Gyorgy et al. (Nagy-Gyorgy et al. 2005) developed an anchorage system to avoid CFRP debonding and improve its performance in seismic strengthening of RC walls. The anchorage system was realized by turning the fibers at the base of walls and fixing by steel L profiles bolted in the foundation slab of the wall (Figure 3.29). The arrangement proved successful in improving the wall load bearing capacity and ductility.

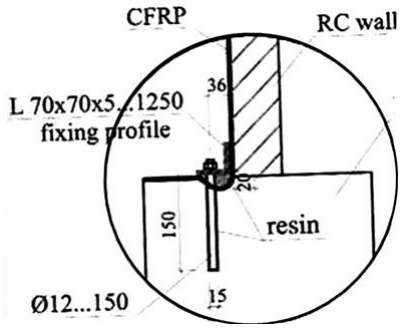

Figure 3.29: Anchorage system at footing zone (Nagy-Gyorgy et al. 2005)

4 Conclusion

This chapter intends to review the state of the art related to the scope of this research. Recent earthquakes in urban areas have repeatedly demonstrated the vulnerabilities of older reinforced concrete structural elements to seismic deformation demands. Seismic studies revealed that heir failure occurred due to occurrence of unpredictable high seismic activity, improper designing and construction flaws.

Reports from earthquake reconnaissance missions highlight that there is only a limited number of total collapses of shear wall buildings. It was highlighted that though they are used in building to dissipate seismic induced energy they too are vulnerable to seismic damage. To understand well the load response behavior of RC wall a database of wall tests is established. The dissipation capacity of RC wall depends directly on its transverse dimension i.e. doubling RC wall thickness doubles its energy absorption capacity. RC wall load response behavior depends to a great extent on its shear span to length ratio. Short wall endure high shear stress as compared to slender wall. The failure modes of short wall are sliding apart of wall from it supporting foundation, diagonal shear cracks development within wall and concrete crushing at wall toe. Slender walls are sensitive to bending loads and encounter failure either by concrete toe crushing or yielding of vertical reinforcement or a combination of both and in some cases shear slipping of wall relative to its foundation occurs. The failure mode depends on the restraint of the wall top. In addition, the loading can influence the failure mode. Although sliding shear was not reported in dynamic tests, it is observed under static-cyclic loading. A database of wall tests is established.

The strengthening of reinforced concrete (RC) structures is frequently required because of excessive loading as a result of changes in use, modifications to design codes, improper maintenance or exposure to environmental effects, such as corrosion and seismic activity. Various strengthening techniques have been developed and implemented in recent years with some success. These are: steel-plate bonding, pre-stressing, reinforced concrete jacketing and fibre-reinforced polymer (FRP) reinforcement. Among these techniques, the FRP strengthening technique is the most popular because of its light weight, easy implementation and high resistance to corrosion. The FRP strengthening technique involves the external bonding of FRP material in the form of strips or laminate to the tensioned surface of the RC structural element with the help of an adhesive (epoxy). Seismic studies have shown that whenever this technique was applied to RC structures, specimen failure occurred, either by concrete cracking or FRP strips debonding from the concrete face in the vicinity of L-shaped joints, such as a column-beam joint or both at once. The effectiveness of this technique is thus limited, as debonding occurs due to the concentration of stress at the concrete/FRP strip interface, and the FRP strips are not stressed to their full capacity. To remedy this problem research is ongoing and considerable efforts have been made to find a solution, such as the provision of local reinforcement in the form of small CFRP anchors, the mechanical fixing of FRP strips using glued or bolted FRP/steel plates, the wrapping of FRP lamina around the structural members and fixing it with an FRP fan-shaped anchor, the use of spike anchors to increase the bond contact area, the use of U-shaped anchors for tensile stressed faces such as the lower faces of slabs and beams, and the use of the FRP sheet anchor system. These anchorage systems have proved to be capable in facilitating higher stress development in CFRP material during loading and in turn augmented the acceptance of use of external CFRP reinforcement.

Part II: Experimental Work

5 Experimental Program

5.1 Introduction

The goal of experimental work is to highlight the significance of the external Carbon Fiber Reinforced Polymers (CFRP) reinforcement in improving the seismic behavior of Reinforced Concrete (RC) walls, short and slender wall, that were built prior to the introduction of earthquake resistant design recommendations into the building codes (1960-70).

The experimental program consisted of the seismic response analysis of twelve shear walls, initially not designed for earthquake action, strengthened externally with the help of CFRP strips and mesh anchors. The test specimens were subjected to quasi static and static cyclic load tests. The prime purpose was to investigate the effect of CFRP external reinforcement in improving the shear walls' ultimate load capacity, elastic and dissipated energy, and deformation capacity. Parameters applied were slenderness ratios and external CFRP reinforcement; variation in CFRP strips' arrangement and mesh anchors' placement.

The wall specimens' geometry and reinforcement detail was based on the evaluation of the earlier research work (as mentioned in sections 2.4.1 & 5.2). The shear wall load response behavior depends largely on its slenderness ratio (section 2.4.2) e.g., shear failure is dominant in the case of short wall ($h/l < 2$) and flexure failure in the case of slender wall ($h/l > 2$) therefore both slender and short walls were fabricated and analyzed. A total of twelve specimens were fabricated, six short walls and six slender walls. As rectangular shaped walls are commonly used in Europe and especially in France thus all the specimens were fabricated with rectangular cross section.

Four out of the twelve specimens, consisting two short and two slender walls, were subjected to quasi-static load test. One out of each type of specimen was strengthened with an external CFRP reinforcement. The remaining eight specimens were subjected to displacement controlled static cyclic load tests. The objective of the static tests was to find out the specimens' load displacement relationship, for use in the displacement controlled static cyclic load test, and observe the influence of CFRP reinforcement on the specimens' ultimate load capacity, ductility, wall foundation slip and stiffness.

5.2 Shear wall Test History

The specimens' geometry and loading arrangements are based on the review of the previous work done in the field of reinforced concrete shear wall. The most relevant work related in this field is presented in the following paragraphs.

- **Lopes (2000)**

The objective of the research work was to study the seismic performance of the reinforced concrete walls under extreme condition leading to shear failure. In all specimens the wall panel dimensions were kept equal to 855×450×45 mm^3. The different parameters used in this program were the amount and detailing of transverse reinforcement. With the exception of the wall SW18, all specimens had the same amount of flexural reinforcement and were designed to yield in flexure prior to achieving the ultimate load. Figure 5.1 shows the reinforcement detail of all the four types of specimens tested. In all these, the vertical reinforcement was concentrated at the wall edges. They were subjected to the displacement controlled cyclic load test in order to assess their structural characteristics beyond their strength limits. Three cycles were implemented at each load level with a maximum increment up to 0.8 mm. The specimens were subjected to loading as long as either a sudden loss in load carrying capacity

occurred or at the point at which the load carrying capacity dropped to 80 % of the ultimate load.

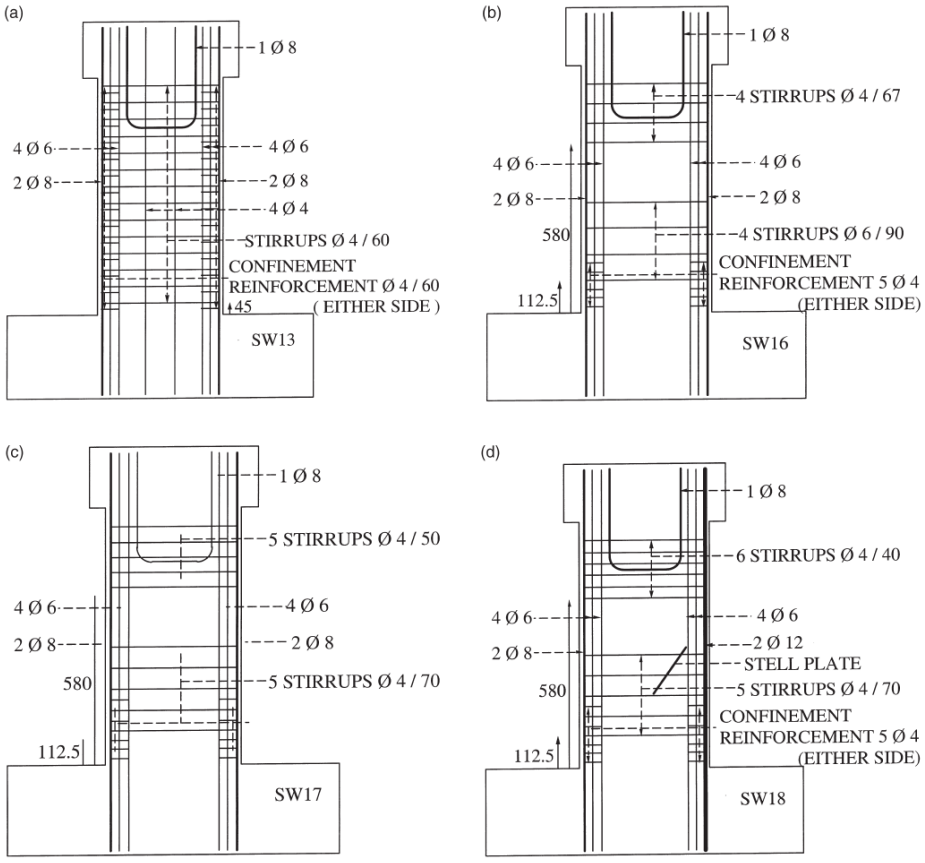

Figure 5.1: Reinforcement details of the specimens. (a) Wall SW13. (b) Wall SW16. (c) Wall SW17. (d) Wall SW18.

- **Young-Hun Oh et al. (Oh et al. 2002)**

The research objective was to investigate the effect of the boundary element details of the structural walls on their deformation capacities. For this purpose a total of four specimens (h = 3000 mm and l = 1500 mm) were fabricated, consisting of one wall with a barbell shaped cross section (t = 125 mm) and the other three with rectangular cross section (t = 200 mm). The h/l ratio of all the specimens' wall panel was kept equal to 1.3. In case of rectangular cross sectional walls, changes were made in the transverse reinforcement content (ρ_s equal to 0.99, 1.97 and 0) at the wall boundaries. Figure 5.3 shows the specimens' geometrical detail along with the reinforcement arrangements made in all four specimens.

The test specimens were subjected to a cyclic displacement controlled lateral load, in combination with a constant vertical load of $0.1 f_c^{/} A_g$. The lateral cyclic displacement, applied at the head beam, was repeated three times at each level of the drift ratios. The drift ratios were take equivalent to 1/600, 1/400, 1/300, 1/200, 1/150, 1/100, 1/75, 1/50, and 1/33. The foundation block was bolted to the reaction wall floor, to negate the foundation block slipping during the test. Figure 5.3 shows the test setup.

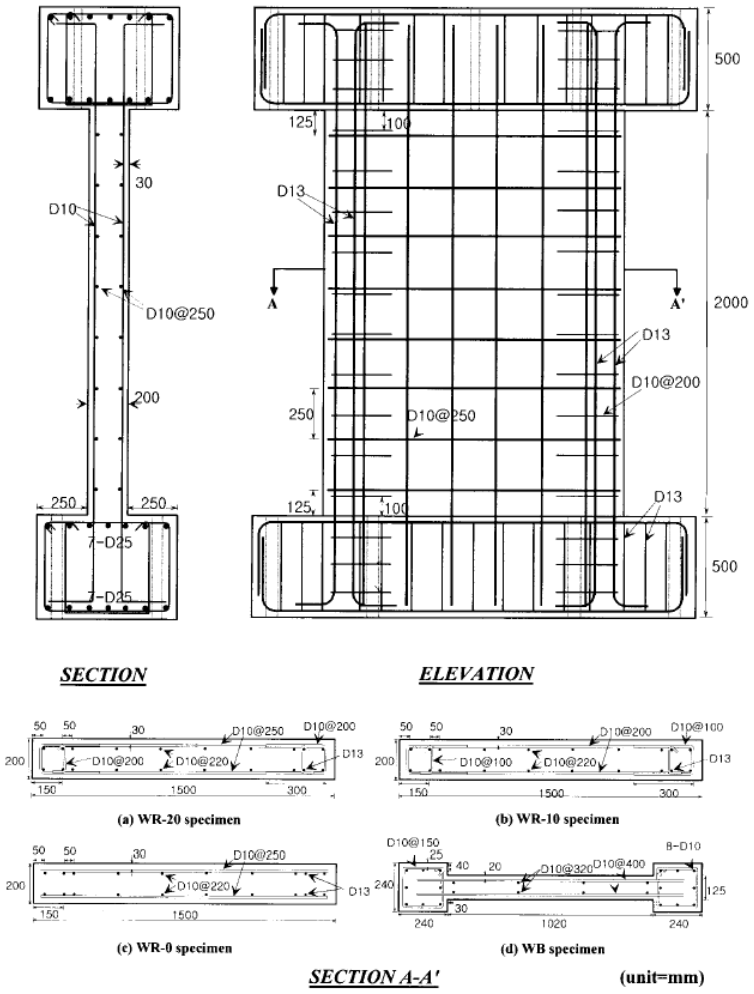

Figure 5.2: Elevations and cross-sections of the specimens.

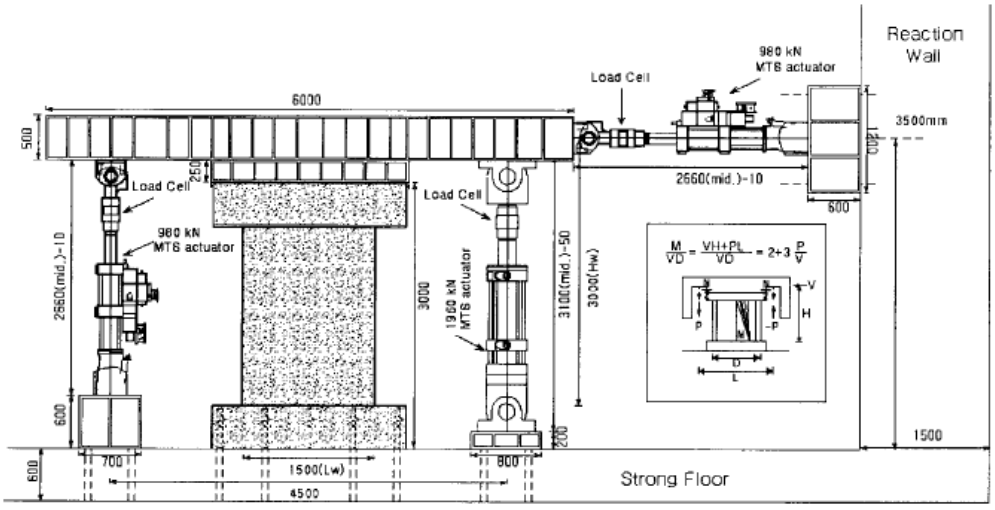

Figure 5.3: Test setup.

- **Greinfenhagen (Greifenhagen and Lestuzzi 2005)**

The specimens were fabricated on the basis of the previous work (Peter). In has been reported in the article that the existing buildings in Switzerland has a typical shear wall of 4-9m length and 0.18-0.25m in thickness with the characteristic distributed horizontal and vertical reinforcement of 0.2-0.8 %. The test specimens were prepared at a 1:3 scale with respect to the lower part of a shear wall of an existing building. Figure 5.4 indicates the specimens' geometrical detail, reinforcement arrangement and test setup.

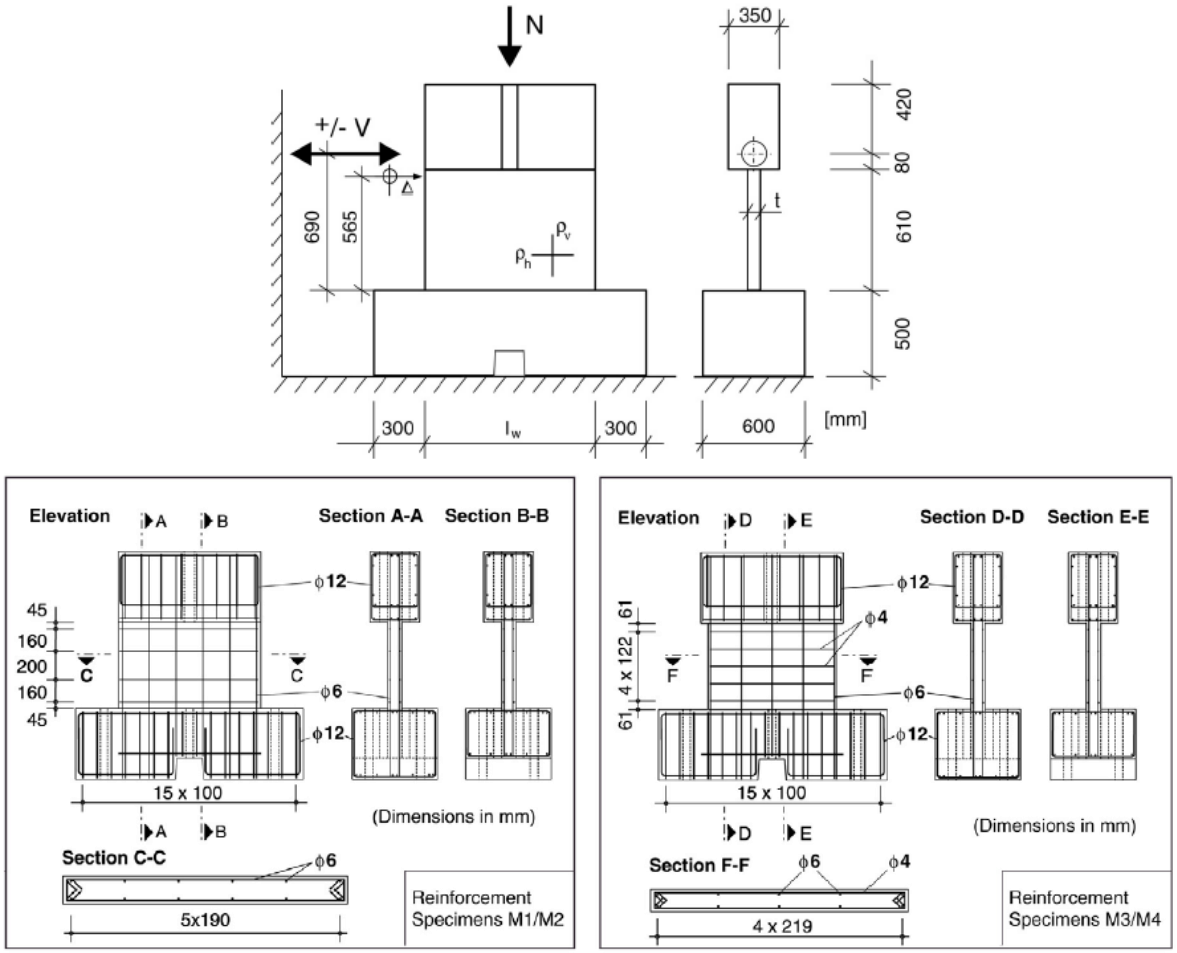

Figure 5.4: Specimen detail, test setup and reinforcement detail.

The head beam, panel and footing were cast together in the form of a slab using a single framework. The specimens were produced horizontally to facilitate fabrication. Mild steel rebar of 6 mm diameter form the vertical reinforcement for all specimens and rebar of 4 mm diameter were used for the horizontal reinforcement of M1, M3 and M4 specimens, while for specimen M2 no horizontal reinforcement was provided. Rebar of 12 mm diameter were used for the reinforcement of the head beam and the footing.

Force and displacement controlled loading histories were utilized in order to simulate seismic actions by reversed cyclic loading. Two cycles were applied at each level of base shear. The lateral cyclic load was applied by pushing the head beam with two actuators (Load capacity of 200 kN each) operated alternately. Figure 5.5 shows the loading history of all four test specimens (where N denotes the vertical load value).

Two post-tensioning bars of 12 mm diameter were provided for the axial loading. The bars were placed at mid-length of the specimens on both sides of the panel. Circular ducts of

50 mm diameter at the footing and head beam prevented contributions of these bars to the lateral stiffness of the specimen. Anchoring was provided to the post-tensioning bars by screws and washers that were placed in a recess of the footing and above the head beam.

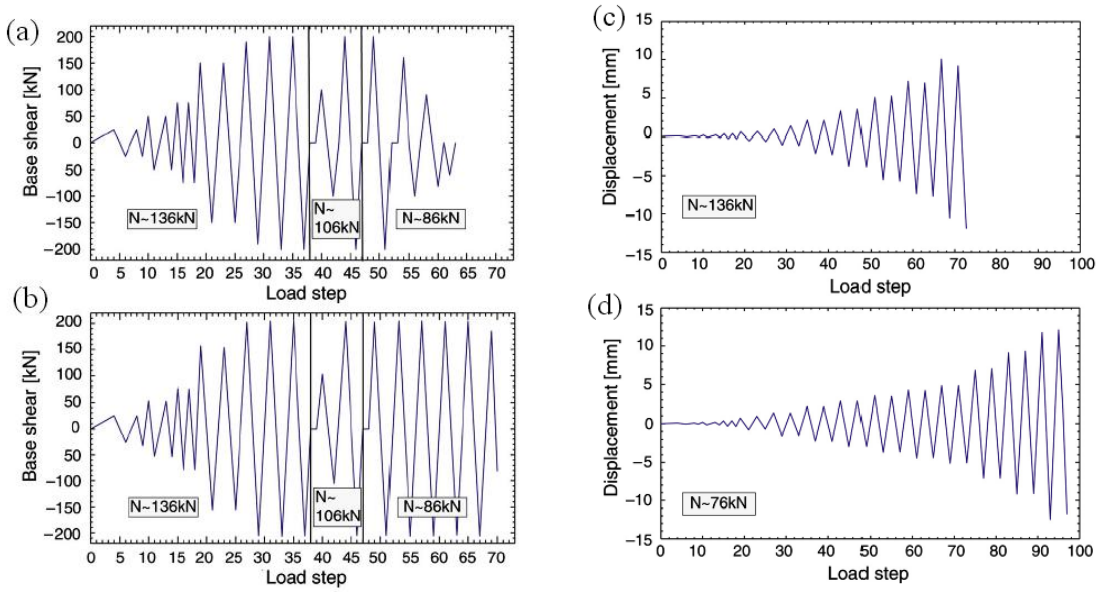

Figure 5.5: Loading history of specimens (a) M1 (b) M2 (c) M3 and (d) M4.

5.3 Materials

The materials used for the specimen construction and strengthening purpose are concrete, steel rebar, CFRP strips, CFRP anchors and epoxy.

5.3.1 Concrete

Table 5.1 lists the concrete mix used. The compressive strength of each concrete batch used was evaluated by a concrete cylinder of type 16×32 fabricated according to NF EN 12390-1 standard. The compression test was carried out according to the NF EN 12390-4 standard. Table 5.2 lists the observed concrete compressive strength. The average observed value for compression was 35 MPa. However, the concrete compressive strength utilized was 30 MPa. This was calculated with the help of correction coefficient λs.

Table 5.1: Concrete mix

Material	Cement CEM I 52.5 N	Sand 0/5	Gravel 10/25	Water
Quantity (kg/m^3)	350	850	1020	192

Table 5.2: Concrete compressive strength

Specimen	1	2	3	4	Avg.
fc (MPa)	35.35	33.95	35.95	35.9	35.3

5.3.2 Steel Rebar

The steel rebar of ø 4.5 mm, 6 mm and 12 mm has been used. Figure 5.6 depicts the stress strain curves of tested steel rebar (ø 4.5 mm and 6 mm used within wall panel). Its observed yield strengths are listed in Table 5.3. The rebar average yield strength, ultimate strength, and modulus of elasticity were evaluated to be equivalent to 500 MPa, 570 MPa, and 200 GPa, respectively.

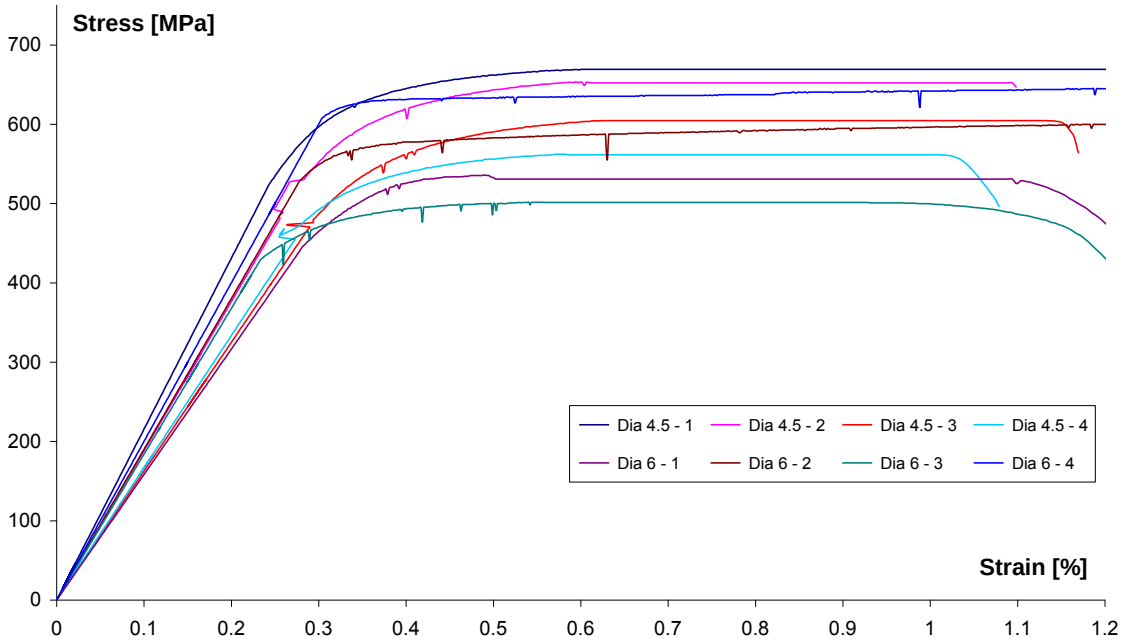

Figure 5.6: Steel rebar tensile test.

Table 5.3: Steel rebar yield strength

Rebar Dia (mm)	4.5	4.5	4.5	4.5	6	6	6	6
Yield Strength (MPa)	669	652	604	561	530	598	501	641

5.3.3 Epoxy

The commercial name of the epoxy used in this research is “l’EPONAL TFC” (Table 5.4).

Table 5.4: Epoxy Eponal TFC detail

Components	EPONAL RESIN	EPONAL HARDENER
Aspect	Thick beige color liquid	Thick amber color liquid
Density	1.32 -1.36	1.00 -1.04
Mixing ratio by mass	100	40
Mixing ratio by vol.	2	1

The specimen of epoxy (Eponal TFC) was fabricated according to the ISO 178 standards, while tensile test was executed according to ISO 527-2 standard. Figure 5.7 gives a schematic view of the specimen geometry. The observed values for the ultimate tensile strength, strain elongation and elastic modulus were 24 ± 1.5 MPa, 1 ± 0.3 %, 1961 ± 120 MPa, respectively.

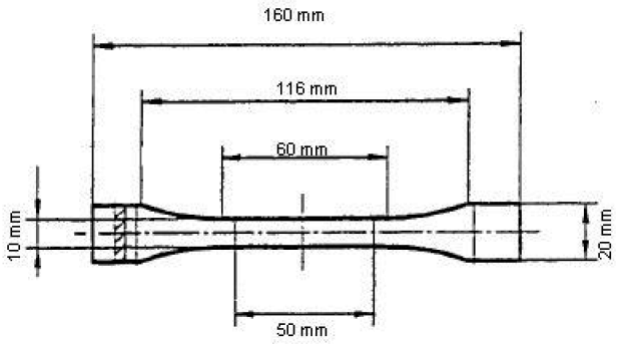

Figure 5.7: Epoxy specimen for tensile test.

5.3.4 Carbon Fiber fabric

Two types of CFRP fabric were used (a) bidirectional: Fiber tows oriented parallel and perpendicular to the strip longitudinal axis (b) unidirectional: Fiber tows oriented along the strip longitudinal axis (Figure 5.8). The fibers oriented in a transverse direction do not contribute any strength but provides ease in handling. The CFRP strip width was equal to 50 or 75 mm. Its tensile properties were evaluated by adopting the AFGC section 1.7 recommendations made for the specimen fabrication and test procedure. The stress strain curves for the tested CFRP strips are shown in Figure 5.9. The CFRP tow used in fabric manufacturing consisted of 12000 fibers each.

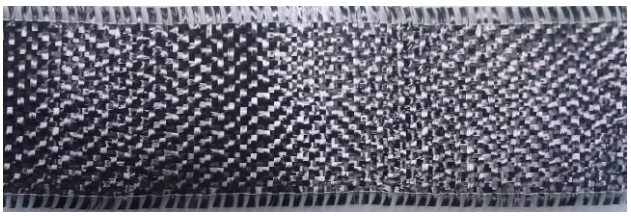

(a)

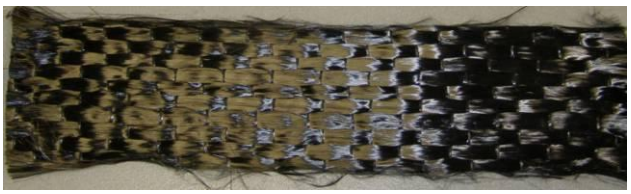

(b)

Figure 5.8: CFRP strip: (a) bidirectional (b) unidirectional

The characteristics properties of CFRP strips were:

Density: 350g/m^2
Thickness: 0.48 mm
Tensile strength: 1300 MPa
Elastic Modulus: 105 GPa

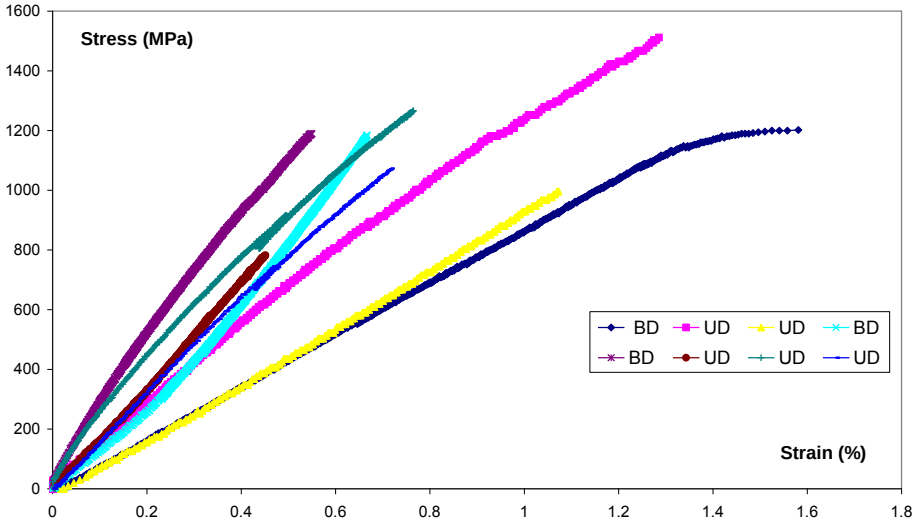

Figure 5.9: Tensile stress strain curve of CFRP strip.

5.4 Short wall specimen

A total of six RC short wall specimens were fabricated, four out of these were strengthened by the application of CFRP material. On the basis of their geometry, external reinforcement and load test, they were labeled as S1, SR2, S3, SR4, SR5 and SR6.
Where: S → Short wall
R → Re-strengthened by CFRP

5.4.1 RC Design

Figure 5.10 shows the geometric detail of the short wall specimen. The wall panel geometry details were derived from the earlier work of Greinfenhagen (2005), representing the lower part of an existing building shear wall in Switzerland at a 1:3 scale.

The slenderness ratio (h/l) of the wall panel is equal to 0.678 < 2, with a height and length of 610 mm and 900mm, respectively. The geometry details adopted were according to Eurocode ENV 1992-1-1.

$$l_w \geq 4 * t \qquad \text{[Ref. 5.4.7.1]}$$

Where $l_w \rightarrow length$ & $t \rightarrow thickness$ of the wall

The wall reinforcement is finalized by reviewing the Eurocode ENV 1992-1-1. The equations mentioned in the code for wall design are as below.

a) $|0.004A_c| \leq$ Vertical Reinforcement $\leq |0.04A_c|$ [Ref. 5.4.7.2.1]
Where $A_c \rightarrow$ Concrete cross sectional area.

b) Half of the vertical reinforcement should be located at each face of the wall panel. [Ref. 5.4.7.2.2]

c) Centre to centre distance in between two adjacent bars should not exceed either of two
(I) 2 × t (II) 300 mm [Ref. 5.4.7.2.3]

d) Horizontal reinforcement should be greater or equal to half of the vertical reinforcement, half of which to be located at each face. [Ref. 5.4.7.2.4]

According to Ref. 5.4.7.2.1, the vertical reinforcement range in the short shear wall should be

$A_c = 900 * 80 = \boldsymbol{72000mm^2} = 111.6in^2$
$|0.004A_c| = \boldsymbol{288mm^2} = 0.4464in^2$
$|0.04A_c| = \boldsymbol{2880mm^2} = 4.464in^2$

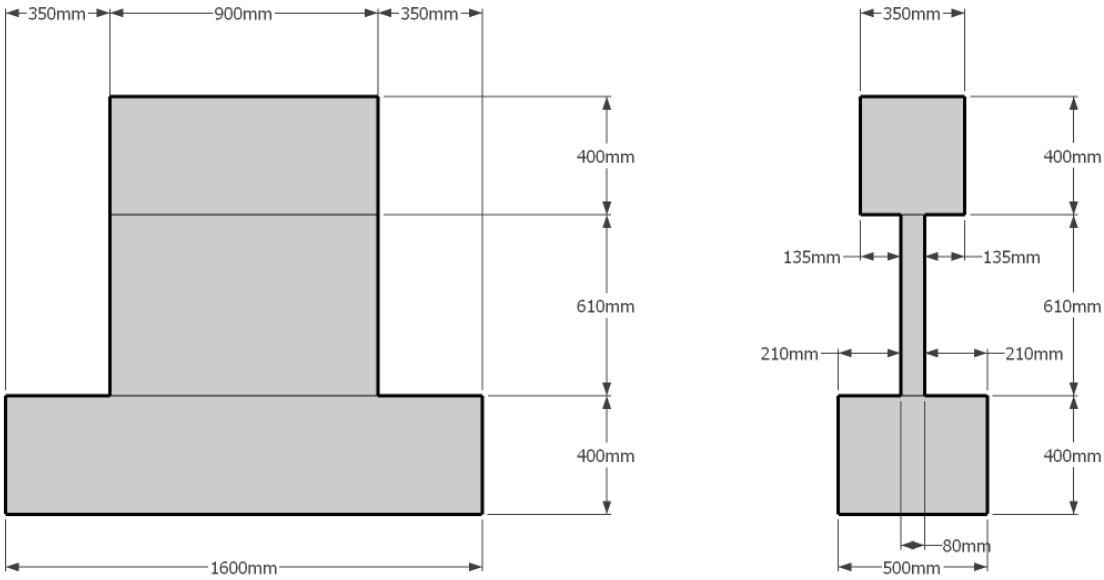

Figure 5.10: Short wall Geometry.

The objective of the research work was to strengthen under-reinforced wall with the help of CFRP laminate and to find out its significance in the strengthening of the existing structure designed, irrespective of the Eurocode recommendations. Therefore the vertical reinforcement provided was kept below the lower limit, by placing two $\phi 6$ mm and four $\phi 4.5$ mm rebar at each face of the wall (Figure 5.11) with a total vertical reinforcement equivalent to 240.28 mm^2, well below the recommended lower limit of 288 mm^2.

i.e. Cross section-Area of $\phi 4.5 = 15.9$ mm^2, Cross section -Area of $\phi 6 = 28.27$ mm^2

$\Rightarrow 2*(4*15.9+2*28.7) = 240.28 mm^2$

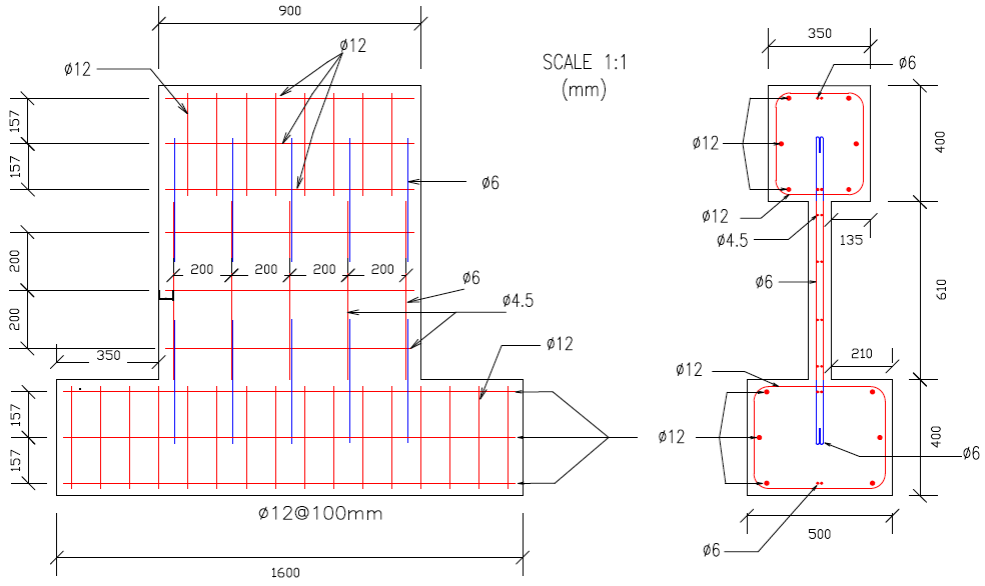

Figure 5.11: Short wall Reinforcement Detail.

The specimen foundation block and head beam strength were fabricated by using rebar of $\phi 12\,mm$ for longitudinal and shear reinforcement to make it stronger compared to the wall panel. The wall horizontal reinforcement according to Ref. 5.4.7.2.1 & Ref. 5.4.7.2.2 should be at least equal to $0.5*|0.004A_c| = 144\ \text{mm}^2 (0.2232in^2)$. But as shear failure phenomenon was required in the case of non-strengthened (no CFRP reinforcement) wall therefore the horizontal reinforcement amount was lowered by placement of $4\phi 4.5$@ c/c spacing of 200 mm, on each face of the wall, and thus getting a total horizontal reinforcement of 127.2 mm^2. *i.e.* $2*(4*15.9) = 127.2mm^2$

5.4.2 Construction

Non monolithic specimens were constructed in order to consider the influence of the construction joint (wall slab and wall foundation joints) on the wall behavior. The specimens were prepared in two stages. The wall specimens' head beam and foundation block were built and to facilitate wall formwork alignment in next stage, arrangements were made within wall head and foundation blocks formwork to prepare wall projections to the height of 3 cm (1.18 in.) simultaneously. Figure 5.12 shows the arrangements made within head beam formwork before concrete poring. The design strength of wall head beam and foundation blocks was kept higher than that of wall. The longitudinal reinforcement and shear stirrups consisted of ø 12 mm rebar. The test specimen head and foundation blocks were fabricated from two concrete batches with identical concrete mix parameters. The concrete compressive strength was 40.6 ± 0.4 MPa (5.888 ± .058 ksi). Four threaded steel rods were placed within the head beam formwork and projected out of it. For this purpose four holes were by drilled within formwork, through which rods were inserted and afterwards bolted on both sides to fix their position as shown in Figure 5.12. These rods were meant to assemble the head beam with the reaction wall hydraulic gauge to induce horizontal displacement with in wall specimen.

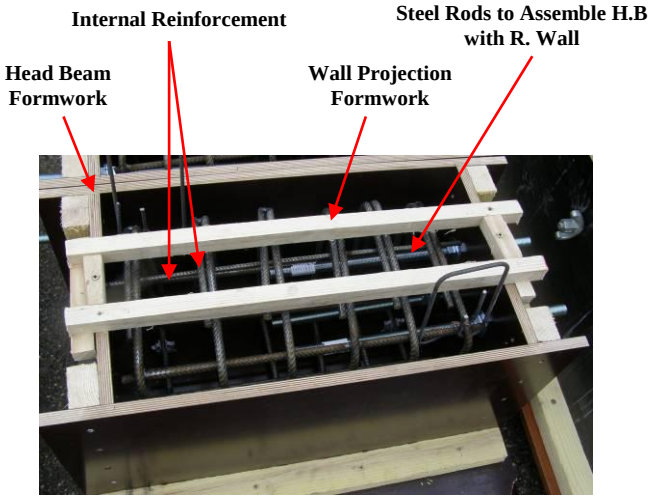

Figure 5.12: Head beam detail.

Before concrete pouring, lap spliced rebar of ø 6 mm were placed in the head beam and foundation block molds (Figure 5.13). The spliced rebar up to 250 mm length was anchored in head beam and foundation block and 180 mm length was left to be anchored in

wall panel. The 180° bent portion was inserted in the RC blocks (Head beam and Foundation) and within wall panel non contact lap spliced technique was adopted. This arrangement was made to make the RC specimen vulnerable in this critical zone and allow wall/foundation relative sliding to some extent. In second stage, after curing wall head and foundation blocks for 28 days, the wall head and foundation blocks were rested at their edges and leveled to align wall formworks in between them with the help of wall projections made in the first stage as shown in Figure 5.14. Horizontal casting of walls facilitated the concrete pouring, reduced segregation of aggregates and allowed good vibration. After curing the specimen for 28 days, specimen was turned over to rest on their foundation block with great care in order to avoid any serious damage to it. After this both faces of the specimen were made smooth by sandblasting and finally FRP strengthening was applied.

Figure 5.13: Head beam and Foundation block.

Figure 5.14: Specimen alignment for wall panel fabrication and internal rebar placement.

5.4.3 External CFRP Reinforcement

To improve the specimen performance i.e. its ductility and strength, an external bonded CFRP reinforcement arrangement was made. It was consisted of a combination CFRP strips and mesh anchors. The FRP system adopted in this study was wet lay-up system. The CFRP strips were bonded over the wall panel to improve its load response behavior and limit cracks propagation. Alterations were made in CFRP strips alignment to find out the most suitable reinforcement configuration. The mesh anchors are used to achieve two purposes (a) Mesh

anchor wall-foundation: to transfer load from the wall panel and bonded CFRP strips to the supporting foundation to limit sliding failure and CFRP debonding in joint area (b) Mesh anchor wall: to prevent the CFRP debonding from wall panel concrete surface. The CFRP retrofitting schema is shown in Table 5.5. Figure 5.15 shows the work flow of CFRP reinforcement.

Table 5.5: CFRP reinforcement schema for short wall

• To obtain uniform bond in between the CFRP strips and concrete, the wall surface was prepared (smoothened) with abrasive paper. • Each face was marked for CFRP strips bonding • Holes (ø 1.5 cm, length 15 cm and angle of inclination 45°) were drilled in wall foundation block , on each side, for mesh anchor installation	
• To get a tight bond in between the mesh anchor and concrete within the holes, they were cleaned by pressurized air to remove any debris. • Prior CFRP bonding, resin coated surface was prepared. • To saturate the bonded strips with resin, a second epoxy coat was applied over it.	
• Drilled holes were filled with Sikadur by use of a pressurized gun.	
• To obtain a uniform bond with in drilled hole the mesh anchor was impregnated with epoxy.	

• Mesh anchors were installed in drilled hole with the help of a CFRP rigid rod attached to its folded end.	
• Anchor free end was splayed and bonded over the vertically bonded CFRP strip.	
• Second strip of 25 cm length was bonded vertically over the splayed anchor to limit anchor/strip slip.	
• CFRP strips along the wall longitudinal axis were bonded.	

Mesh anchor

They are made up of CFRP fiber tow, by winding it around two nails, fixed apart a distance equal to four times the required anchor length (Figure 5.16). The winded fiber tow is afterward released from the nails and folded in the middle. At folded end a CFRP rod or a steel wire is attached to ease mesh anchor insertion in the hole. At the non folded end, the fiber tows' looped portion is cut, to splay this end. The tensile strength of a mesh anchor of 26 fiber tows was equivalent to 22 kN. The mesh anchors selected are based on the research

work conducted on asymmetric beam specimen that represented the L shape joint. Details are given in the Appendix A.

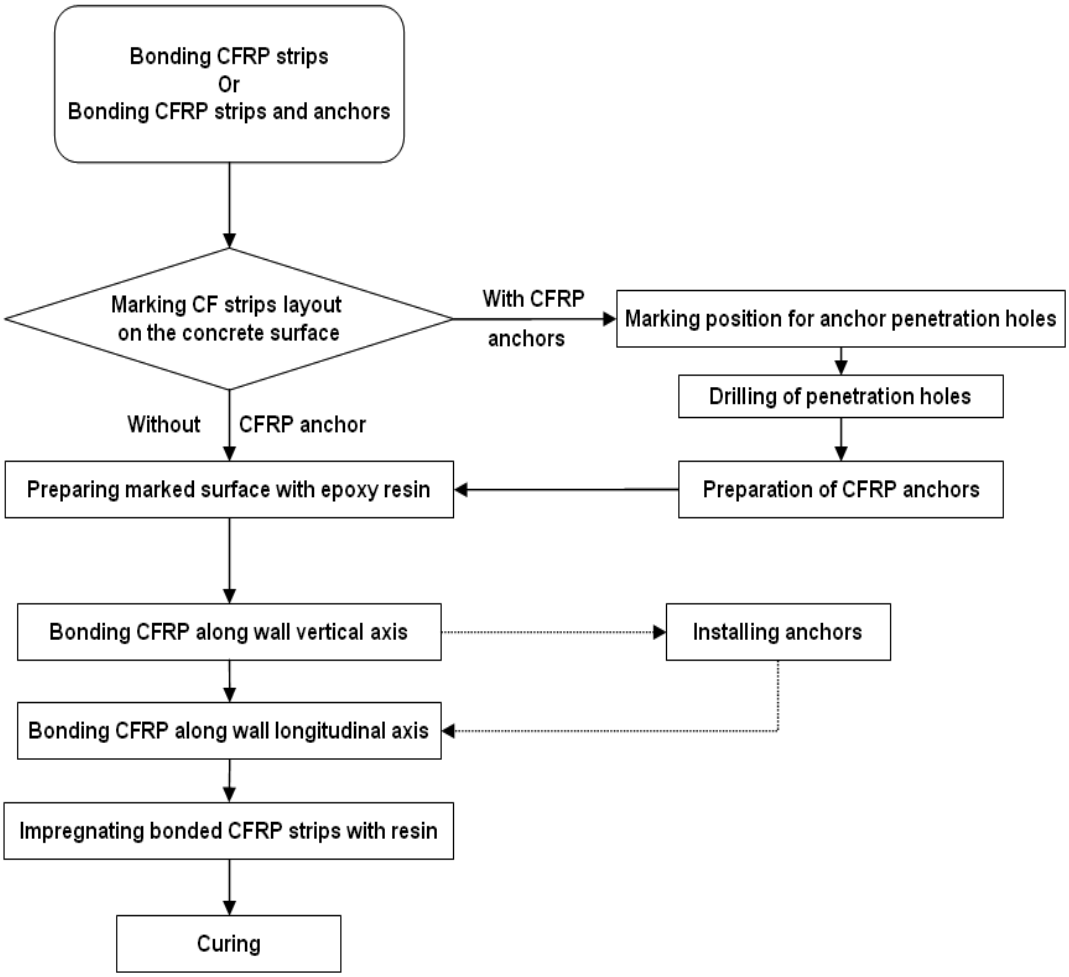

Figure 5.15: Work flow diagram of CF sheet installation

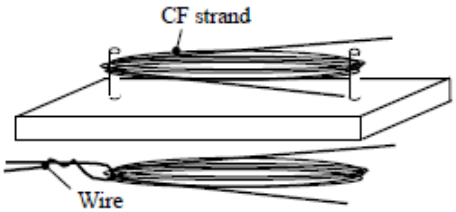

Figure 5.16: Anchor preparation.

Four types of mesh anchor were used (Figure 5.17). Anchor labeled as M1 and M3 were prepared as explained above, while M2 and M4 are commercially available. The M1 anchor had fibre tows in range of 26 to 60 while M3 had four CFRP tows. The mesh anchor M2 consisted of 44 fiber tows and had diameter equivalent to 11 mm at its portion provided with GFRP braided cover. The anchor labeled as M4 had a 5 mm diameter and was comprised

of 75 fiber tows. The mesh anchor M1 and M2 were used at wall foundation joint to limit CFRP debonding in that region, while mesh anchor M3 and M4 were used within wall panel to limit intermediate crack debonding.

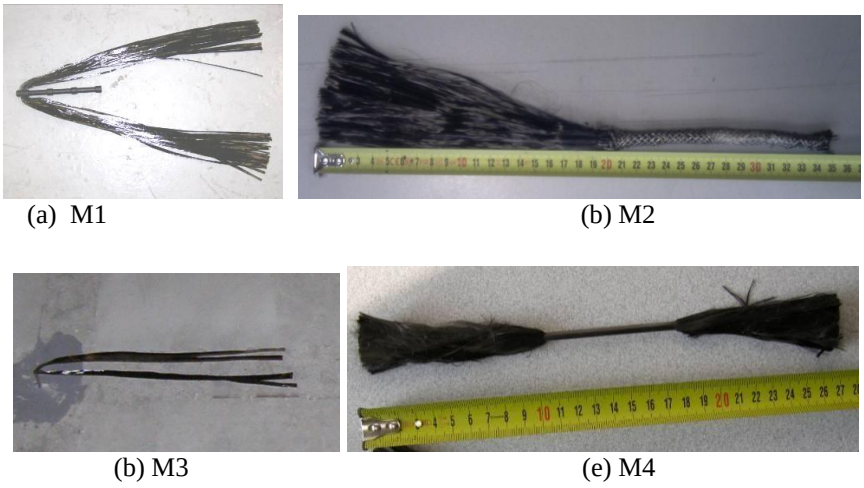

(a) M1 (b) M2

(b) M3 (e) M4

Figure 5.17: Anchor used at wall base: (a) M1 (b) M2, Anchor used within wall panel: (c) M3 (d) M4.

5.4.4 Specimen configurations

Four out of the six specimens were retrofitted by use of CFRP material. The reinforcement configuration opted for each short wall is briefly discussed in the following section.

5.4.4.1 Wall S1

The first specimen subjected to monotonic load test was not retrofitted. It was tested as a control specimen and used to observe RC wall failure mode.

5.4.4.2 Wall SR2

The second short wall specimen labeled as SR2 was retrofitted by bonding eight CFRP strips on each wall face, in order to improve its shear strength and control cracking with in wall panel (Figure 5.18). On each face, four strips were bonded along the wall vertical axis and four in the transverse direction. The CFRP strips used had the width equivalent to 50 mm. A total of four mesh anchors were installed in the vicinity of wall foundation joint on each side. The mesh anchor M1 used had an overall length of 40 cm and consisted of 26 fiber tows.

5.4.4.3 Wall S3

The wall S3 was without CFRP reinforcement. It was subjected to the quasi-static cyclic load test to observe its behavior under seismic load condition and compare its behavior with retrofitted specimens.

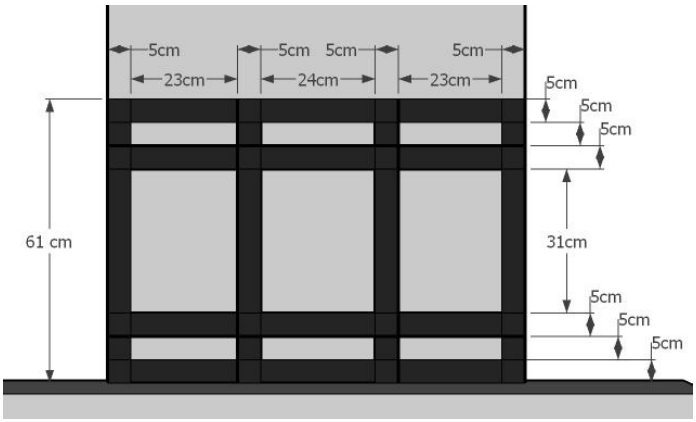

Figure 5.18: SR2: CFRP reinforcement detail

5.4.4.4 Wall SR4

A total of nine CFRP bidirectional fabric strips of width 50 mm were bonded to each face of the wall. Four out of nine, were bonded in a direction parallel to the wall vertical axis and the remaining five in a perpendicular direction. The modifications made in the external reinforcement configuration were based on the specimens S1 and SR2 observed failure modes. The vertically bonded strips at wall mid face were moved closer to the one bonded at extremity and one additional CFRP strip was bonded horizontally at mid-height of the wall (Figure 5.19). The purpose of this variation was to limit cracking in these zones, as observed in the specimen SR2.

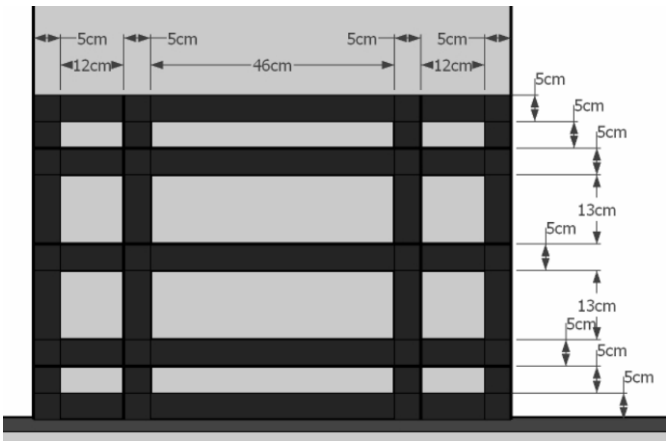

Figure 5.19: SR4: CFRP reinforcement detail

5.4.4.5 Wall SR5

In the SR5 specimen, the external CFRP reinforcement pattern was completely modified. Figure 5.20 shows the CFRP strips bonding arrangement. It was carried out by bonding three strips along wall height and another four strips bonded parallel to wall diagonals. In this case five mesh anchors M1 were installed at wall base, on each face. Three out of five were aligned with vertically bonded strips, while for the remaining two; four shorter length vertical strips were bonded on each face. This was done to increase concrete CFRP bond area in order

to control anchor slip due to high stress concentration. In this case unidirectional CFRP strips were used. To control CFRP intermediate crack debonding with in wall panel mesh anchor M3 were used at CFRP strip intersection points. Mesh anchor M1 installed at wall base had 44 fibre tows.

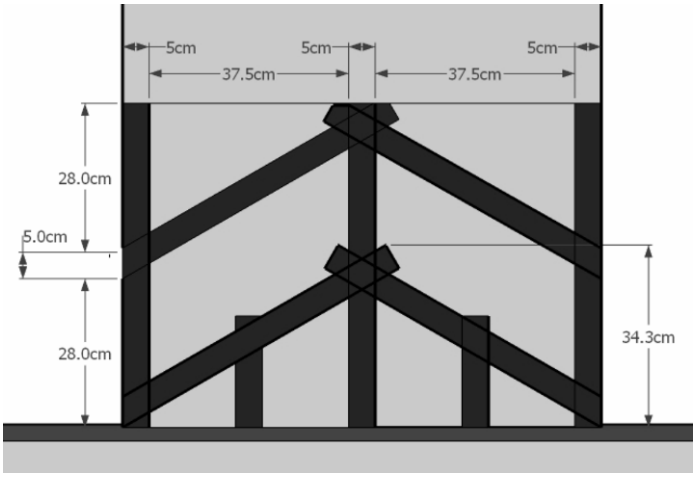

Figure 5.20: SR5: CFRP reinforcement detail

5.4.4.6 Wall SR6

In this case the CFRP strip bonding pattern adopted was kept identical to that of SR5. The modification done in this case was utilization of mesh anchor M2 instead of M1 at wall base and mesh anchor M4 within wall instead of M3.

The CFRP external reinforcement configuration details of all six short wall specimens are listed in Table 5.6.

Table 5.6: Short wall External retrofitting detail.

Specimen	CFRP Strip			Anchor fiber tows number		
	Type	Width (mm)		Wall Foundation		Wall Panel
		Centre	Exterior	Centre	Exterior	
S1	-	-	-	-	-	-
SR2	Bidirectional	50	50	26	26	-
S3	-	-	-	-	-	-
SR4	Bidirectional	50	50	44	44	-
SR5	Unidirectional	50	50	44	44	4
SR6	Unidirectional	50	50	44	44	12

5.5 Slender wall specimen

A total of six RC slender wall specimens were prepared with identical internal reinforcement configurations. Four out of these six were retrofitted by CFRP material. On the basis of their geometry, external reinforcement and load test these are labeled as SL1, SLR2, SL3, SLR4, SLR5 and SLR6. (SL → Slender wall, R → Re-strengthened by CFRP)

.

5.5.1 RC Design

The slender wall specimen geometry detail is given in Figure 5.21. The wall panel had a 1500 mm height (as an outcome of the height limit of reaction wall) and 600 mm length. In this case the slenderness (h/l) ratio was equal to 2.5.

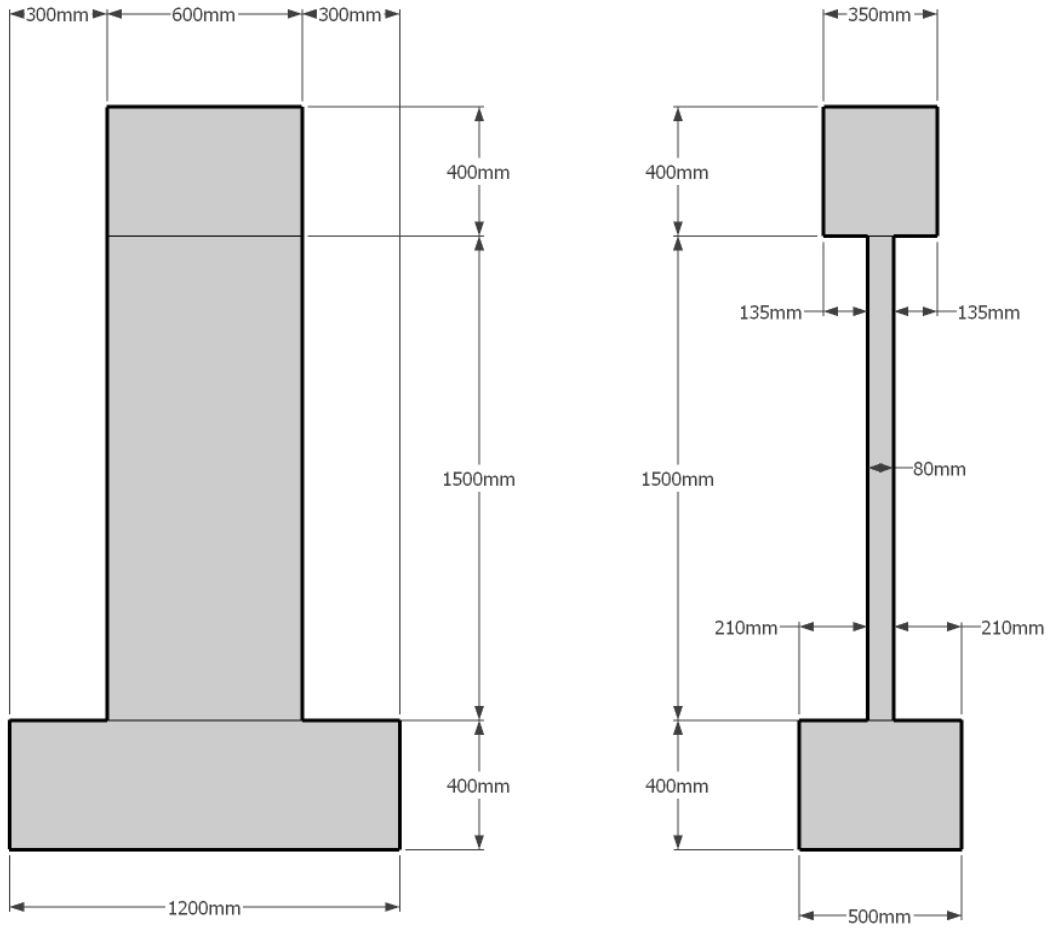

Figure 5.21: Slender wall Geometry.

$A_c = 600 * 80 = \boldsymbol{48000\ mm^2} = 74.4 in^2$

$|0.004 A_c| = \boldsymbol{192\ mm^2} = 0.2976 in^2$

$|0.04 A_c| = \boldsymbol{1920\ mm^2} = 2.976 in^2$

In this case, the aim was to strengthen under-reinforced wall with the help of CFRP laminate and find out its significance in the strengthening of existing walls vulnerable to the flexural failure, designed irrespective of the Eurocode recommendation. Thus the reinforcement provided was kept below the lower limit, by placement of $2\phi 6$ mm and $4\phi 4.5$ mm rebar at each face of the wall, with a total vertical reinforcement cross-sectional area equal to 178.4 mm^2. Figure 5.22 depicts the reinforcement arrangement made in the case of slender wall specimen.

i.e. X-Area of $\phi 4.5$ mm bar = 15.9 mm^2, X-Area of $\phi 6$ mm bar = 28.27 mm^2

$\Rightarrow 2*(2*15.9+2*28.7)=178.4mm^2$

The horizontal reinforcement arrangement made consisted of $8\phi 4.5$ rebar @ c/c spacing of 200 mm making the total horizontal reinforcement cross-sectional area equal to 254.4 mm^2. In this case the horizontal reinforcement value was kept greater than the value required according to Ref. 5.4.7.2.1 & Ref. 5.4.7.2.2.

i.e. $0.5*|0.004A_c| =$ 96 mm^2 $(0.1488in^2)$

The primary objective of this arrangement was to prevent shear cracks development within the wall web and force the flexural failure phenomenon to occur.

5.5.2 Construction

The construction procedure for RC slender wall specimens was similar to that of short wall (section 5.4.2). A total of six specimens were fabricated from the two concrete batches, two specimens (SL1 & SLR2) from one concrete batch and four from the second batch. In all specimens, the internal steel reinforcement detail was kept identical (Figure 5.22).

5.5.3 External CFRP Reinforcement

The CFRP external strengthening procedure was applied on the four out of six slender wall specimens. The purpose of restrengthening was to improve the performance within the wall panel and at wall foundation joint. The strengthening material used consisted of CFRP strips and mesh anchors.

The CFRP strips used were either uni- or bi-directional (fiber orientation) and had a width equal to 50 or 75 mm. In this case (slender wall), CFRP strips were bonded at the wall panel in a direction parallel and perpendicular to its longitudinal axis. The purpose of strips bonded along the wall height was to improve the wall panel flexural performance while the one bonded in the transverse direction were destined to limit vertically bonded strips debonding. The mesh anchors were provided to limit the CFRP strip debonding from concrete and control wall/foundation relative slipping. They were installed in vicinity of wall-foundation joint with in drilled holes (ø 12 mm, length 15 cm and angle of inclination 45°).

Procedure

In order to obtain a uniform bonding in between CFRP strips and concrete surface, the wall faces were smoothed. Each one was marked for CFRP strips placement. At wall foundation joint, three holes along each face of the wall were drilled (length 15 cm, angle of inclination 45°). These holes were cleaned by pressurized air to remove any debris. Before CFRP strips bonding, the marked area of each face was coated with epoxy resin. Then a single layer of CFRP strips, in a direction parallel to the wall longitudinal axis, were bonded over it. To saturate the strips with resin, a second epoxy coat was applied over it. After that the drilled

holes were filled with a resin sikkadure by a pressurized gun and folded end of epoxy saturated mesh anchors were placed in. To ease the mesh anchor insertion in hole, a CFRP rod was attached to the folded end. The outer portion of mesh anchors were splayed over the CFRP strips already bonded and overlapped by a single layer of vertically bonded CFRP strips of length 25 cm. Finally a total number of seven strips were bonded over the wall in a direction perpendicular to its vertical axis. The CFRP retrofitting scheme is shown in Figure 5.23.

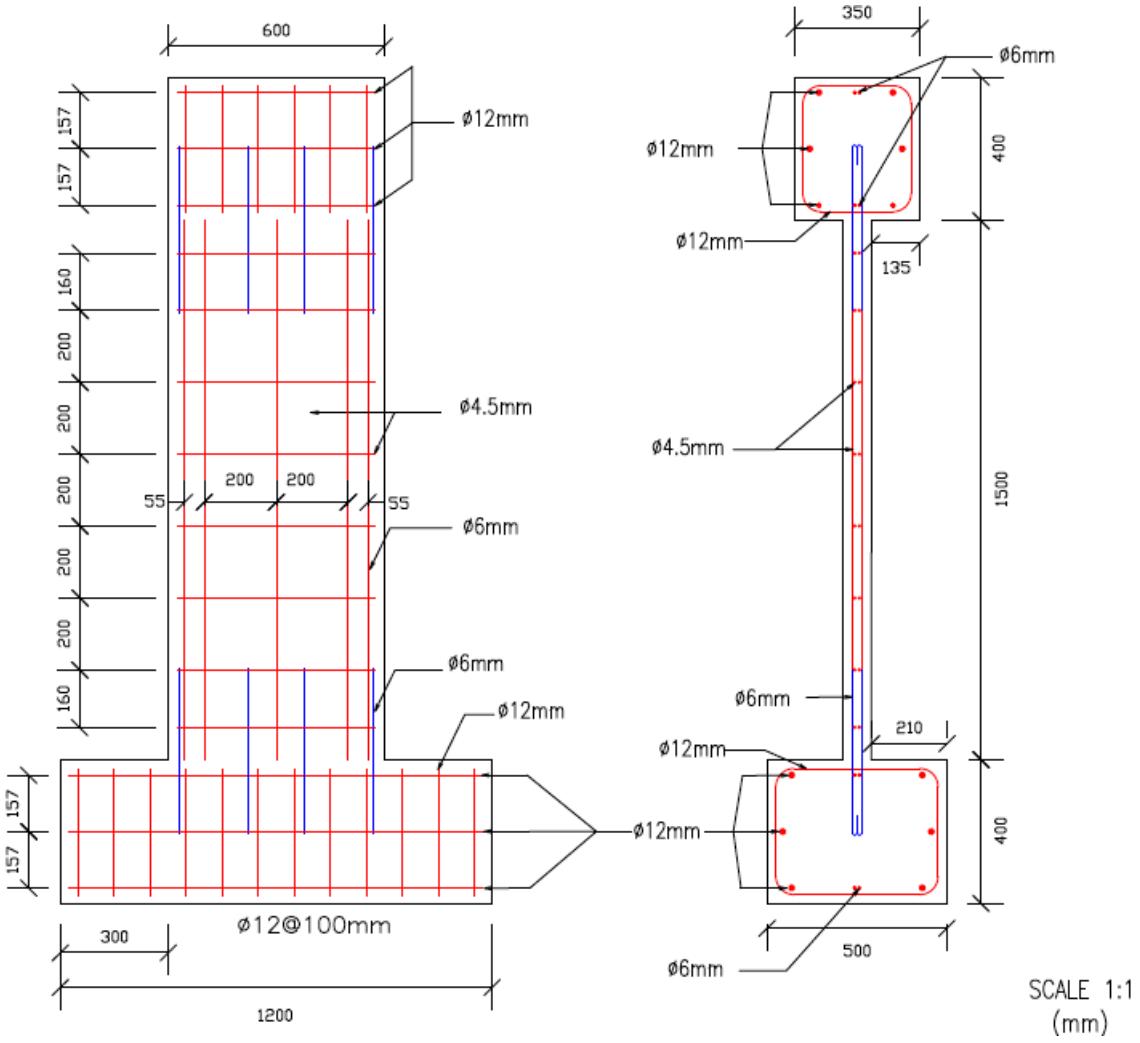

Figure 5.22: Slender wall Reinforcement Detail.

(a) (b) (c) (d)

(e) (f) (g)

(h) (i) (j)

(k)

Figure 5.23: CFRP reinforcement schema.

5.5.4 Specimen configurations

This section highlights the external CFRP reinforcement arrangements made for each specimen.

5.5.4.1 Wall SL1

One slender wall specimen was not retrofitted with CFRP material. It was subjected to quasi static load test, to determine its capacity and failure mode.

5.5.4.2 Wall SLR2

It was retrofitted with bi-directional CFRP strips of 50 mm width. The mesh anchors had 40 cm length and had 26 fiber tows. In this case 20 CFRP strips, 10 on each face, were bonded externally to the wall panel with the help of an epoxy resin (Figure 5.24). Out of these three strips were bonded along wall panel height and seven in transverse direction. Three mesh anchors were placed along each face.

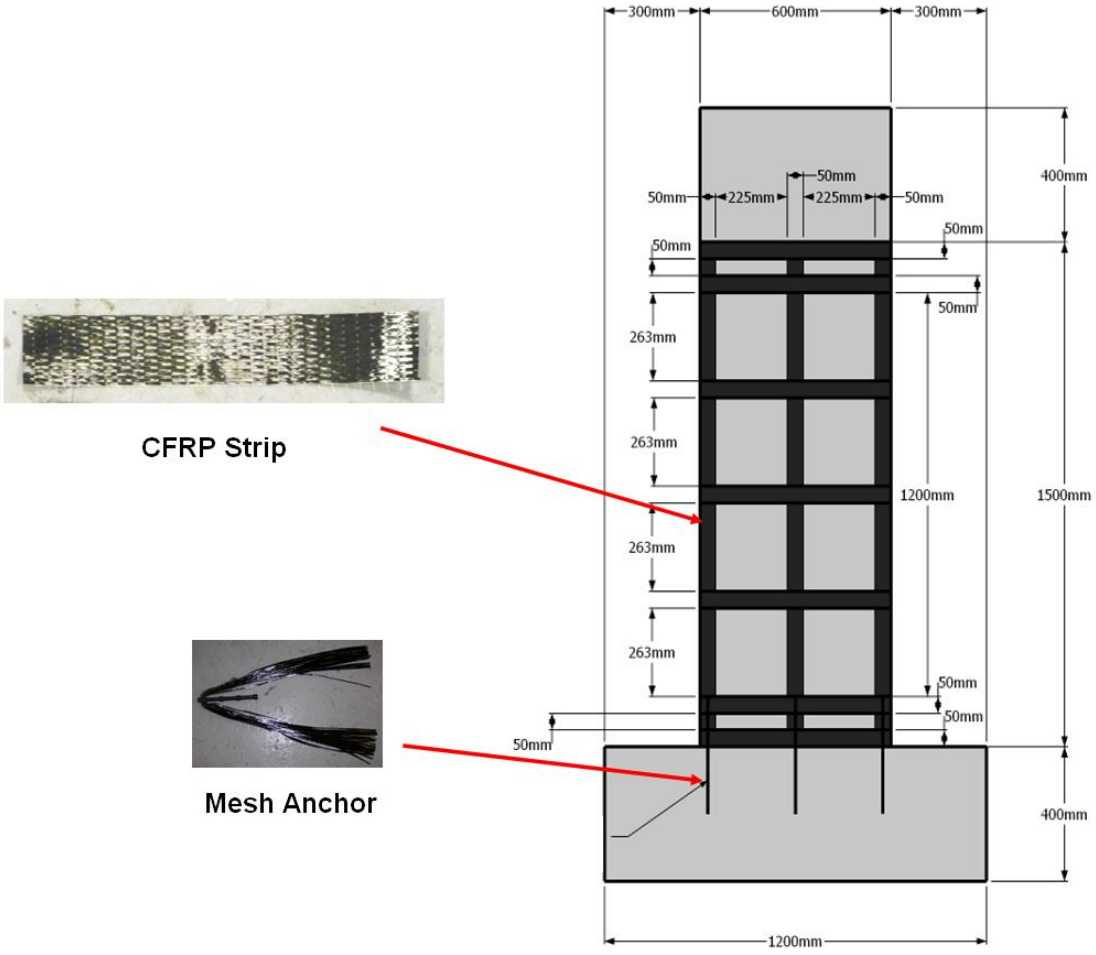

Figure 5.24: SLR2: CFRP reinforcement detail

5.5.4.3 Wall SL3

No CFRP reinforcement was applied on SL3. It was subjected to a reversed cyclic load test to compare its results with the retrofitted specimens subjected to cyclic load test in order to evaluate CFRP reinforcement contribution under seismic conditions.

5.5.4.4 Wall SLR4

The CFRP reinforcement pattern was identical to the specimen SLR2. However the changes made were: (a) width of the vertically bonded strips at the wall edges was increased from 50 to 75mm (both shorter and longer strips) (b) mesh anchors installed at wall ends had 37 cm length and consisted of 44 fiber tows.

5.5.4.5 Wall SLR5

To prevent the CFRP strips debonding within wall panel, transverse mesh anchors were introduced in the specimen. These wall panel mesh anchors were placed at the CFRP strips intersection points. Each anchor had 37 cm length and was comprised of four CFRP tows. They were constructed by winding a CFRP fiber tow around fixed nail (placed 74 cm apart) to form two loops. The loops were then folded at its mid-length and a wire was tied to it to make its insertion ease in the holes drilled within the wall panel (Figure 5.25). After the CFRP strips were bonded on wall the panel along its vertical axis, anchors were inserted in resin filled holes. After insertion, the two ends of the anchors were cut and splayed over the bonded strips, one on each face in a direction perpendicular to the bonded strips. The rest of CFRP strengthening procedure adopted similar to that of SLR4.

5.5.4.6 Wall SLR6

Based on the test observation of specimen SLR5, the wall panel mesh anchor system was modified. As CFRP strip debonding was observed too in specimen SLR5 therefore the wall mesh anchor was replaced by stronger CFRP anchors. The mesh anchors used in the SLR6 was factory built. The mesh anchor had a 5 mm diameter and was comprised of 75 fiber tows. Figure 5.25 shows the wall panel mesh-anchors arrangement. The two important variation made are (a) the CFRP strips used in this case were made of unidirectional fabric and (b) the wall foundation anchor at the wall ends, on both faces, had a total number of 60 fiber tows instead of 44 in case of SLR5 and SLR3. The rest of retrofitting configuration was kept identical to that of SLR5.

Table 5.7 summarizes the CFRP material arrangement of slender wall specimen tested in this research work.

Table 5.7: Slender wall External retrofitting detail.

Specimen	CFRP Strip			Anchor fiber tows number		
	Type	Width (mm)		Wall Foundation		Wall Panel
		Centre	Exterior	Centre	Exterior	
SL1	-	-	-	-	-	-
SLR2	Bidirectional	50	50	26	26	-
SL3	-	-	-	-	-	-
SLR4	Bidirectional	50	50	44	44	-
SLR5	Bidirectional	50	75	44	44	4
SLR6	Unidirectional	50	75	44	60	4 & 12

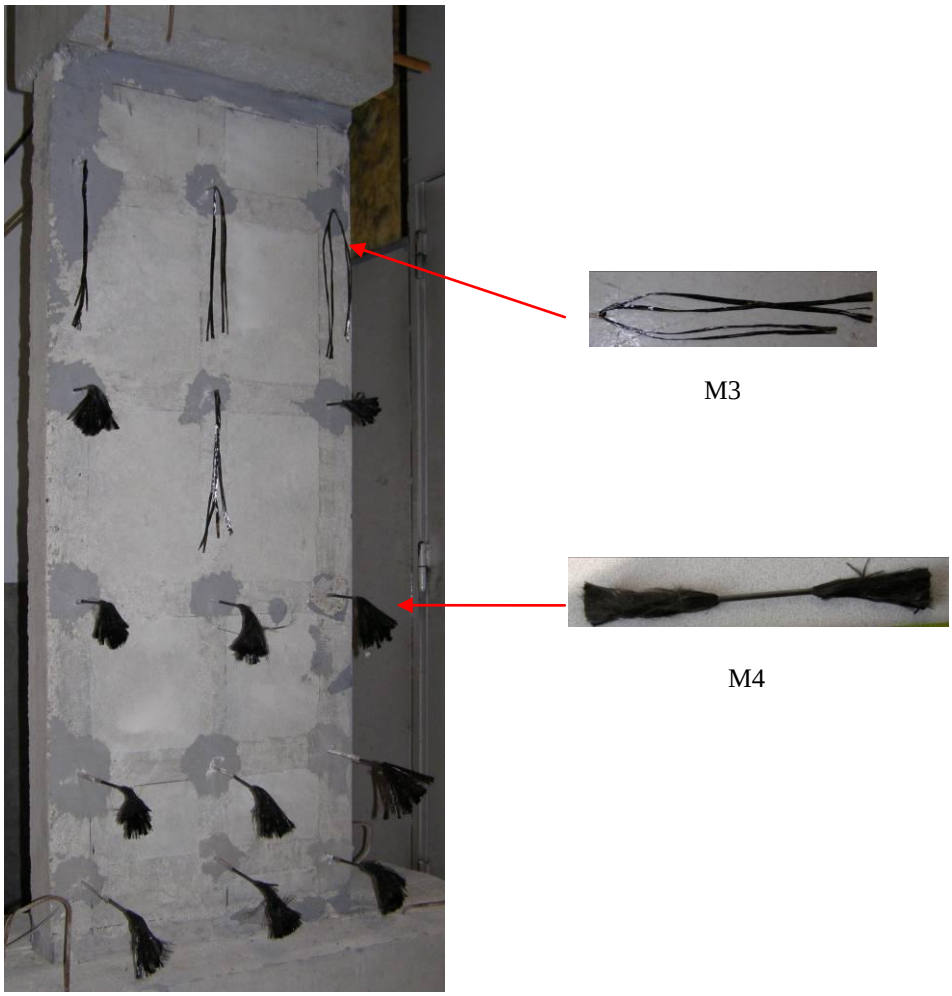

Figure 5.25: Wall panel Mesh anchor detail and location in specimen SLR6.

5.6 Test procedure

The specimens were tested as cantilevers and were subjected to both normal and lateral forces. The arrangement was based on the findings of the previous research work that a simple cantilever subjected to a constant normal and static cyclic lateral load can simulate shear wall behavior, under seismic activity (Greifenhagen and Pierino Lestuzzi 2005). A constant vertical load of 90kN was applied over the specimens' head beam, provided by two post-tensioning rods, one on its each side (Figure 5.26). The lower ends of the rods were fixed to the reaction wall floor and at the top a spreader beam was attached in order to uniformly distribute the vertical load in the two rods. The rods were post-tensioned by an actuator mounted in between the head beam and spreader beam (Figure 5.26). The lateral load was applied with the help of a hydraulic jack (load and displacement capacity of 500 kN and 2 m) connected to the specimen head beam and reaction wall (Figure 5.27).

The test specimens were consisted of three parts (a) Head beam through which load was induced into the panel (b) Panel simulated a shear wall and (c) the foundation block used to anchor the specimen to reaction wall floor. These were fabricated non-monolithically to take into account the joints that exist in real buildings in between the slabs and walls.

Figure 5.26: Vertical load setup

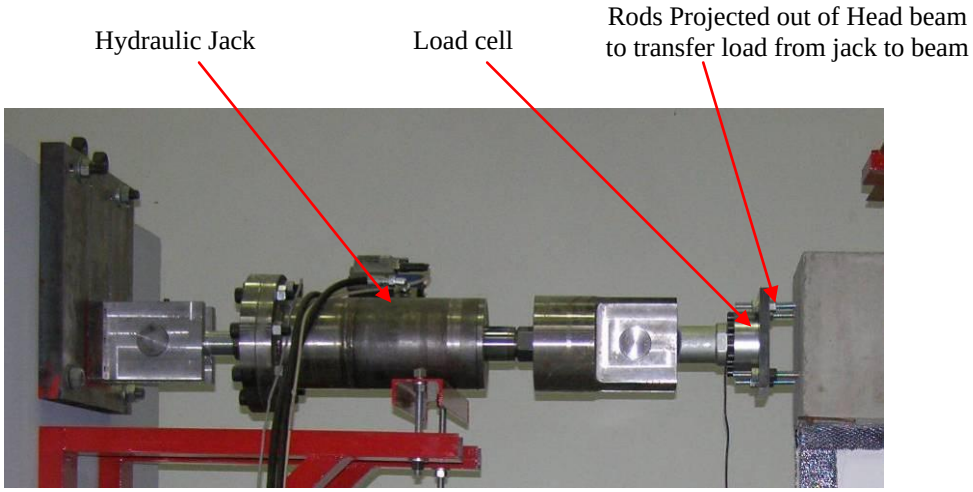

Figure 5.27: Induced lateral displacement setup

To avoid slipping and overturning during the loading, the foundation block was fixed over the reaction wall floor with the help of a combination of threaded rods, steel beams, plates, nuts and bolts. To prevent slipping, one steel wedge was placed at each edge of foundation block, fixed to the reaction wall floor with the help of threaded bolts. To overcome the overturning problem, vertical compressive load was induced on foundation block with the help of an assembly of steel beams and pre-stressed rods as shown in Figure 5.28. In the case of short wall two steel beams were fixed over each end of the foundation while for slender wall one at each end. Figure 5.29 shows a full sketch of the above mentioned arrangements in a single snapshot.

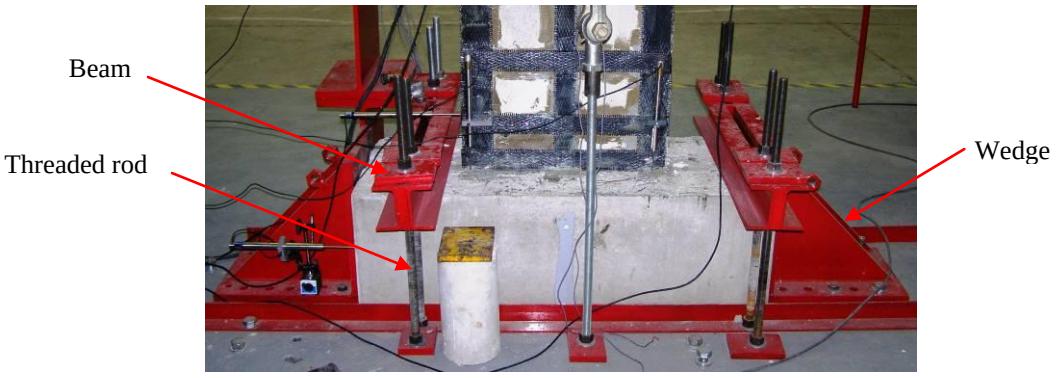

Figure 5.28: Arrangements to block Foundation block slip and overturning

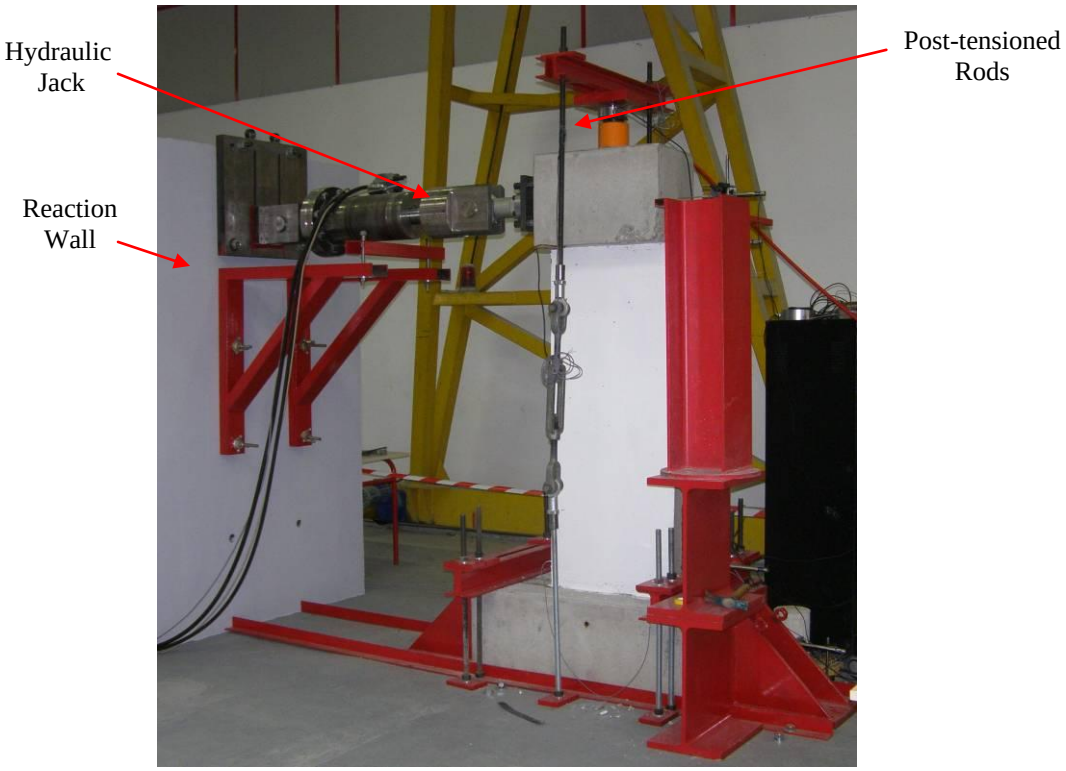

Figure 5.29: Slender wall test setup

5.6.1 Instrumentation

Load cells, strain gauges and linear voltage differential transducers (LVDTs) were used to monitor the specimens' reaction. The data was collected by software "Strain Smart". The dissimilarity present in the instrumental configurations in the two type of specimens i.e. Short and slender wall, are described briefly accompanying with sketches.

5.6.1.1 Load Cells

Two load cells were mounted to the head beam to record the induced load values (Figure 5.30). A load cell of capacity of 200 kN was placed over the head beam to record the axial compression load value and its possible variation due to lateral cyclic loading. The second one

of *500 kN* was connected to the head beam and hydraulic jack for recording the load value generated as a result of the induced lateral drift.

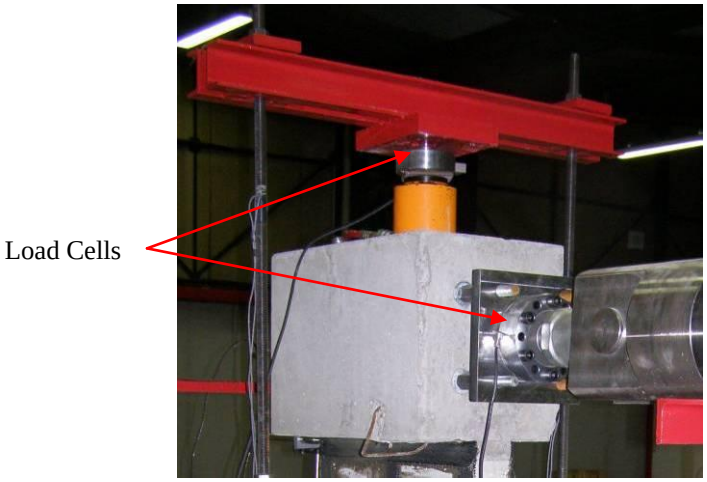

Figure 5.30: Load cell locations

5.6.1.2 LVDT

A total of six LVDTs were used to monitor the specimen deflection. Four of these were positioned at specimen free end as shown in Figure 5.31. LVDT 1 was set to record induced deflection in the head beam at its mid-point. LVDT 2 and 3 were located at the wall top and bottom to assess the wall deflection behavior under seismic condition. LVDT 4 was located at the foundation block to examine its slip. LVDT 5 and 6 were used to determine the vertical deformation at the wall bottom, caused by a combination of induced vertical compression load and lateral displacement.

5.6.1.3 Strain gauges on internal rebar

In all specimens, two strain gauges were bonded on internal rebar before concreting (Figure 5.32). These were bonded to the starter rebar, at wall edges, projecting from the foundation block in the lap splice region. These were intended to measure the load transfer from the wall longitudinal bars to lap spliced bars.

5.6.1.4 Strain gauges on CFRP strips

In retrofitted wall specimens, nine strain gauges (S.G.) were bonded on the CFRP strip to monitor the stresses developed within the mesh and strips. In slender wall specimens, three gauges were bonded over each vertical strip (Figure 5.33). The first gauge was bonded in vicinity of joint to monitor stress developed, in mesh anchor. The second one was bonded over the horizontally bonded strips (15 cm height) to find out the stress pattern in this area. Third one was bonded to vertical strip to examine the same. To avoid mesh anchor response in gauge reading, the S.G was bonded at a height of 39 cm from the foundation block, wide apart from mesh anchor splayed portion of 25 cm length.

In the short wall specimens, due to large scale variation made in the external CFRP strip bonding pattern, the strain gauge arrangement was a little bit different.

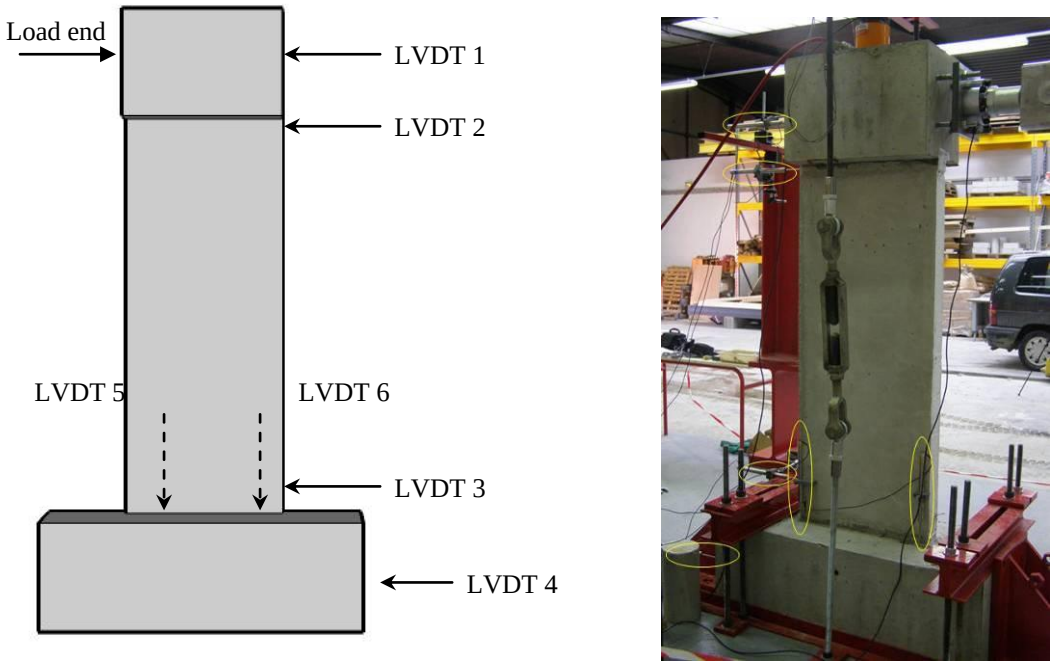

Figure 5.31: LVDT's Locations

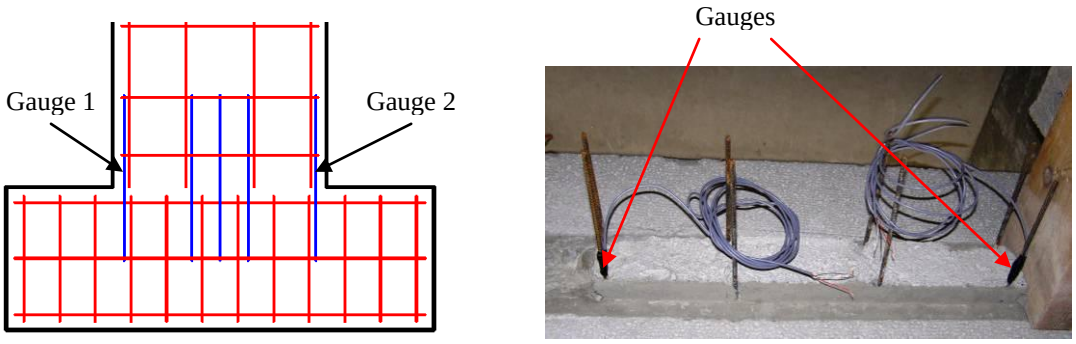

Figure 5.32: Strain gauge position on internal rebar

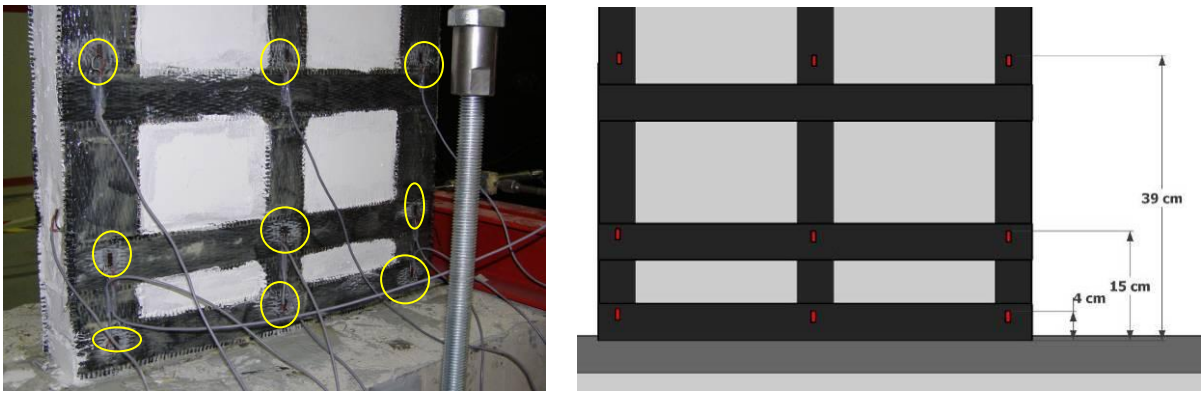

Figure 5.33: Strain gauge locations on retrofitted slender wall specimen

5.6.2 Loading histories

Test specimens were subjected to displacement control lateral loading, with the wall acting as cantilevers. In all specimens a constant axial compression load was applied over the head beam. The axial load ratio: ratio of applied axial load to axial load capacity at concrete section has a significant influence on shear wall performance, deformability and failure modes (Lefas et al. 1990; Su and Wong 2007). The axial load ratio used in previous research work for wall test was, based on specimen model and material properties, in range of 0.03 to 0.85 (Pierino Lestuzzi and Hugo Bachmann 2007; Oh et al. 2002; T.N. Salonikios et al. 2000; Su and Wong 2007). The axial load sustained on the head beam was equal to 90 kN $(0.075 * f_c^{'} * A_g)$ for slender wall and 110 kN $(0.06 * f_c^{'} * l_w * t_w)$ for short wall.

With reference to lateral loading, two specimens of each type (SL1, SLR2, S1 and SR2) were subjected to quasi static loading to determine their performance. In this case the lateral displacement was provided at a speed of 0.01 mm/sec. The rest of four specimens of each type were subjected to reversed static cyclic load test to simulate seismic actions Figure 5.34. At each load level, specimens were subjected to three full cycles as recommended by ACI (ACI T1.101, 2001). Due to changes made in the external CFRP reinforcement configurations of all specimens, the lateral displacement load levels were based on drift instead of ductility, to make an easy comparison. The drifts were 0.1%, 0.2%, 0.3%… 0.8%, 1%… 1.8%. As the speed limit of hydraulic actuator was 180 mm/min therefore these drifts were assigned at a relative speed of 10, 20… 80, 100… 180 mm/min so that the time period for each cycle was equal to 19.5 seconds.

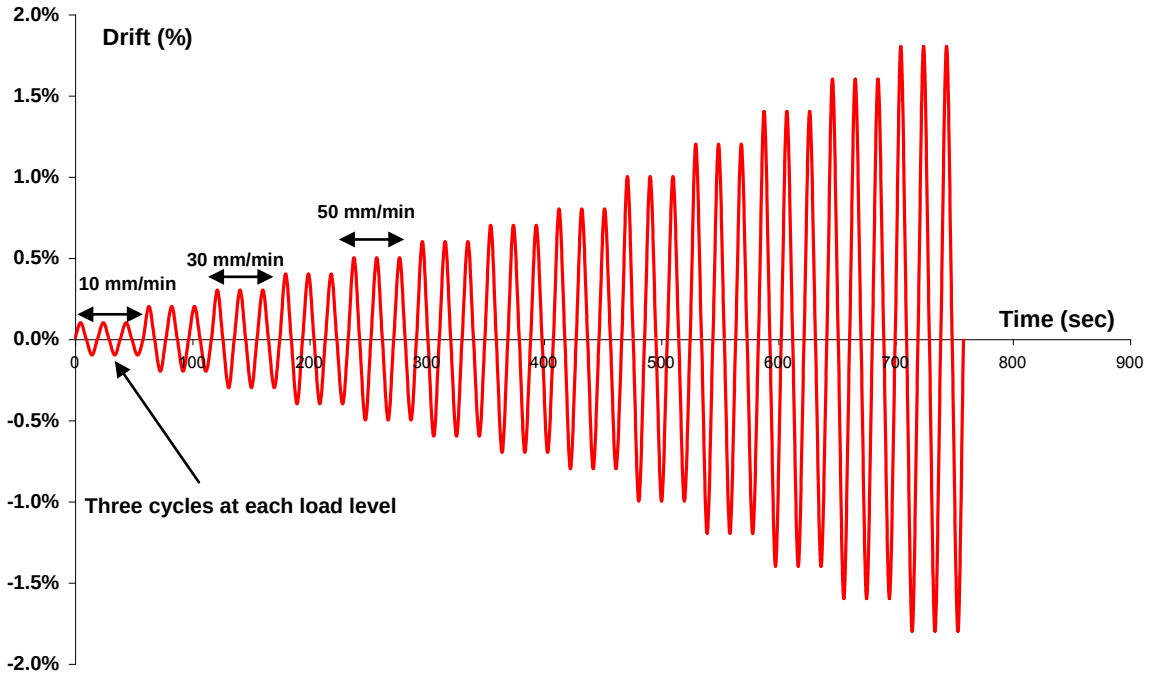

Figure 5.34: Induced lateral displacement load history

6 Test Results and Analysis

6.1 Static Load Test

Two out of six specimens of both short and slender wall were subjected to static load test to observe their load response behavior and failure modes. A lateral displacement load at a speed of 0.01 mm/sec was induced at the specimen head beam in combination with a constant overhead vertical compression.

6.1.1 Short wall

Short wall specimens labeled as S1 and SR2 were subjected to quasi static unidirectional lateral load test with a constant vertical load of 110 kN, applied at head beam. Their load response behavior is briefly discussed in the following sections.

6.1.1.1 Load- Displacement Curve

Figure 6.1 shows the load displacement curve of specimens S1 and SR2. The initial stiffness of the two is almost identical because the CFRP reinforcement initiates load contribution with concrete cracking or rebar yields. Therefore the two specimens exhibited alike behavior up to the load level of 105 kN and 0.8 mm lateral displacement. Beyond it the CFRP reinforcement contribution is evident in the load displacement curve of the two specimens. S1 exhibits plastic deformation as it exceeds the 3 mm limit while specimen SR2 shows non linear elastic behavior till failure. At plastic yield point of specimen S1, the load sustained by it and SR2 were 150 kN and 174 kN. The increase in strength of 24 kN is due to the CFRP external reinforcement.

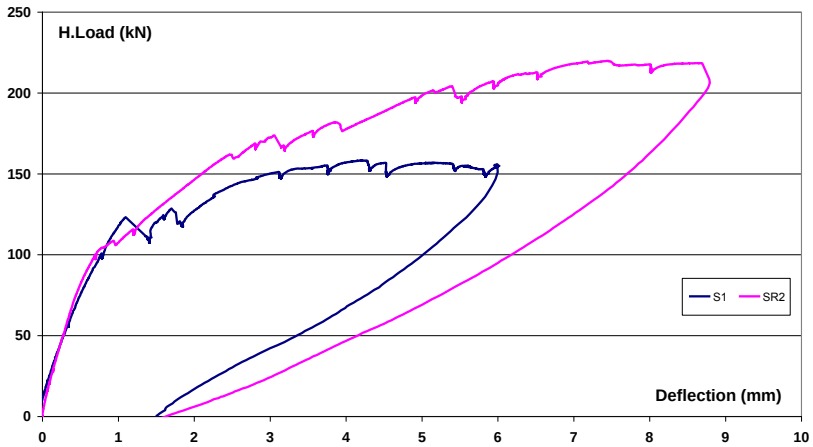

Figure 6.1: Load Displacement curve of specimen S1 & SR2

The specimen S1 demonstrated an ultimate strength of 158 kN at induced displacement level of 4.2 mm while SR2 showed an overall improvement in its strength and ductility by exhibiting an ultimate strength of 219 kN at a displacement load level of 7.43 mm. Thus CFRP external reinforcement improved RC short wall specimens' strength and ultimate displacement by 38% and 55%, respectively.

6.1.1.2 Deflected shapes

Figure 6.2 shows the deflection pattern of specimen S1 with respect to the induced load levels till its ultimate capacity. The deflection is more or less linear i.e., highest at the top and reduces with relative decrease in height. The zero value at the height of 200 mm (LVDT located at the centre of foundation block) was achieved by negating the effect of the foundation slipping. The shift in the deflection pattern, as the induced load level exceeds the yield strength of specimen S1 (110 kN), occur due to the plastic deformation in the lap splice region. The observed deflection at wall top at yield load (110 kN) and ultimate load level (150 kN) were around 1 mm and 3 mm, respectively. The specimen S1 exhibited ductility (μ) equal to 2.9.

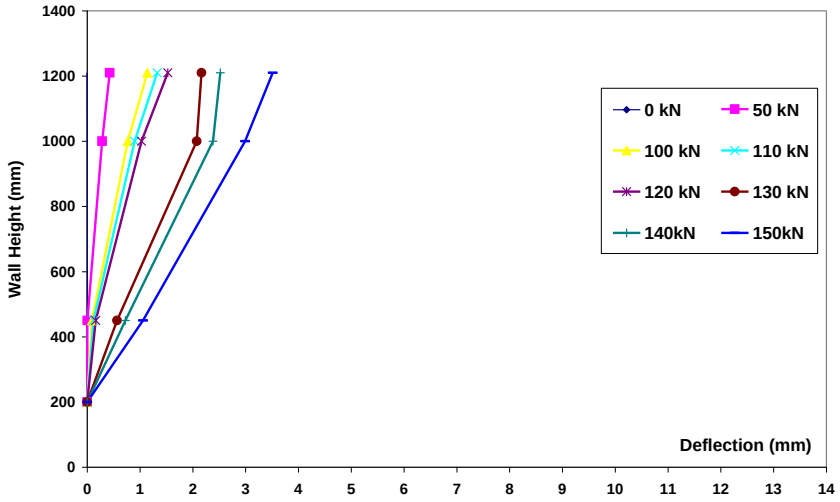

Figure 6.2: Specimen S1 Deflected shape

The deflected shapes of specimen SR2 are shown in Figure 6.3. Though, it exhibited an overall improvement in both the strength and ductility but it also depicts a nonlinear deflection pattern. This non linearity is more prominent at the initial stages because the concrete area at the joints were reduced due to drilling and also the CFRP anchors didn't initiated their contribution that resulted in relative slipping. However, the nonlinearity decreases as the load level is increased due to anchor load distribution across the joints. The observed deflection at the wall top, at yield load of 120 kN was 1.03 mm and at ultimate load of 220 kN was 7.45 mm. The specimen S1 exhibited ductility (μ) equal to 7.23 and the relative ductility index (μ_R) of SR2 with respect to S1 was 2.49, evaluated by dividing the ultimate displacement of specimen SR2 by that of S1. The calculated ductility indexes of specimen S1 and SR2 are given in Table 6.1.

Table 6.1: Short wall ductility index

Wall	Displacement Elastic (mm)	Displacement Ultimate(mm)	μ	μ_R
S1	1.03	2.99	2.9	1
SR2	1.03	7.45	7.23	2.49

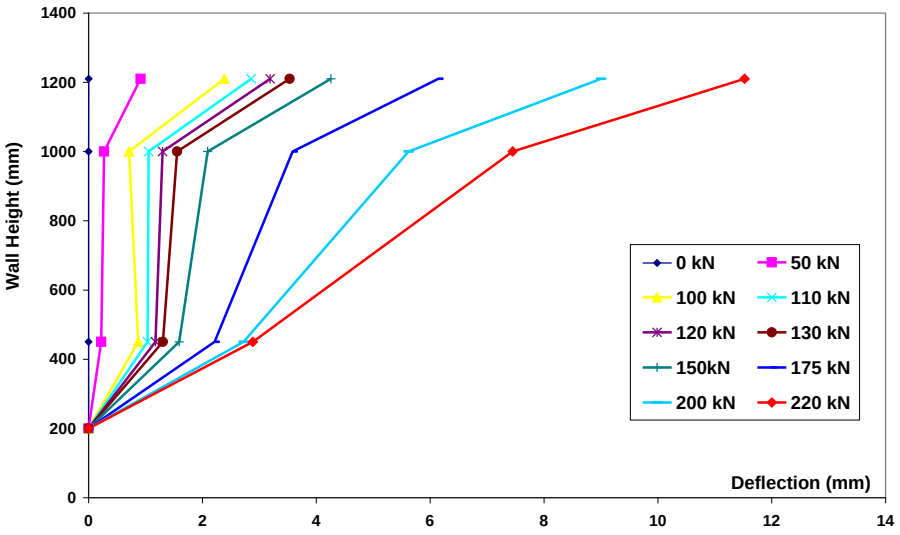

Figure 6.3: Specimen SR2 Deflected shape

6.1.1.3 Failure modes

The S1 specimen showed a typical under-reinforced RC short wall failure mode. The failure occurred due to development of diagonal cracks within the wall panel, wall foundation relative slip and extreme rebar yield. It is important to note that sliding failure occurred at the construction joint. Figure 6.4 shows the failure pattern of specimen S1. At induced lateral displacement of 1.03 mm, with a corresponding resistant load of 120 kN, three cracks developed within the wall panel, at its load end. The cracks initiated in vicinity of construction joints, at the height of 31 mm and 580 mm. The crack that developed at the wall bottom propagated in horizontal direction with a total length of 122 mm. The longer crack at the wall top first spread in horizontal direction up to 344 mm and then declined at an angle of 48° towards the wall free end, lower corner. At its mid-length third crack was located that first dipped down vertically up to length of 71 mm and then oriented diagonally towards wall free end. At induced deflection of 1.1 mm the lower diagonal crack (3^{rd}) propagated further 20.2 cm. As the induced deflection level reached a level of 3.76 mm the third crack spread 30.6 cm towards the wall (load end) lower corner. It was accompanied with a fourth crack that initiated at the wall height of 22 cm and reached to its bottom by making an angle of decline of 27°. As the induced displacement incremented to 4.2 mm the third crack reached the wall lower end and a number of cracks generated within the wall panel. At this moment the flat crack at the wall bottom almost reached the far end and extreme rebar at load end ruptured. After this a rapid decline in sustained load was observed with an increase in the displacement, therefore the test was stopped. It is important to note that these cracks were not superficial as they developed on both faces of the wall simultaneously.

The specimen SR2 retrofitted with CFRP, not only exhibited an increase in strength and ductility, but also limited crack propagation within the wall panel and wall/foundation relative sliding (Figure 6.5). At the wall foundation joint, the bonded CFRP strips hindered the visualization of crack propagation. The first diagonal crack observed in SR2, developed at the wall loaded end at a height of 29 cm. It developed at an induced displacement load level of 1.21 mm. It touched the horizontal strip (bonded at a height of 12.5 cm) and had length and angle of decline of 18.4 cm and 37°, respectively. At that moment it did not spread across the width of bonded strip. As the induced displacement incremented to a level of 2.8 mm a

second diagonal crack originated at the wall face mid section in between the two horizontal CFRP strips bonded at the wall bottom. When the load level increased to 3.06 mm the two cracks developed across the CFRP bonded strips. The test was stopped when the cracks spread across two third of the wall length.

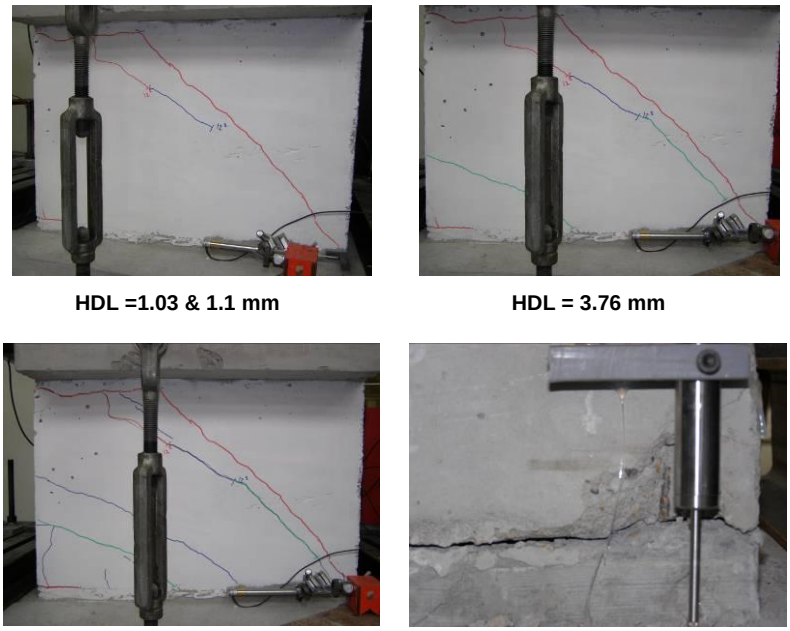

Figure 6.4: Specimen S1 Failure pattern

Figure 6.5: Specimen SR2 Failure cracking pattern

6.1.1.4 Strain distribution within bonded CFRP strip

To highlight the CFRP external reinforcement contribution in the specimen SR2 load distribution, the stain distribution curves of CFRP strips, bonded at the wall panel two extremities and along the wall length, are described briefly. Figure 6.6 shows the strain gauge arrangement made on the specimen SR2 CFRP reinforcement.

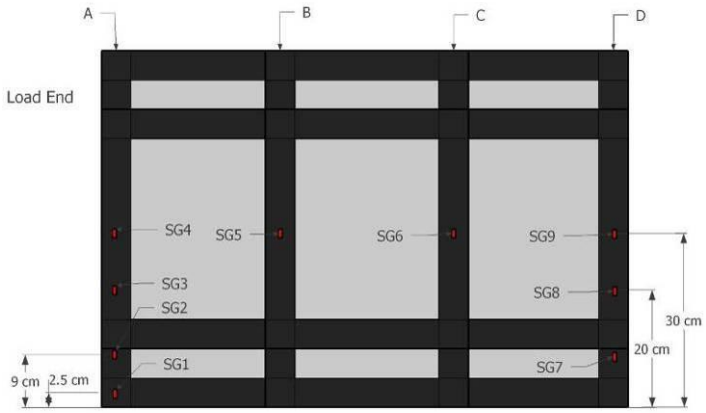

Figure 6.6: Specimen SR2 Strain gauge detail

Figure 6.7 shows the longitudinal strain distribution in the CFRP strip bonded vertically to the wall panel extremity, at its loaded end. Four strain gauges SG 1, 2, 3 & 4 were bonded over it to record its strain pattern. Initially the four gauges depict an identical strain pattern. However, as the induced load exceeded the 110 kN limit a sudden increase in SG 4 value was observed which continued to increase with increase in induced load. At wall height of up to 25 cm there were three CFRP layers: (a) a CFRP strip, 25 cm long, bonded vertically to the wall surface (b) a mesh anchor free end splayed (c) a vertically bonded CFRP strip, while above this height only one CFRP strip was bonded to the concrete surface. Therefore the wall portion above 25 cm height was relatively weak and cracks developed there. The CFRP strip bonded in that region tended to bridge the cracks by capitalizing its tensile strength and in turn experienced strain. The SR2 cracking pattern confirmed the phenomenon (Figure 6.5).

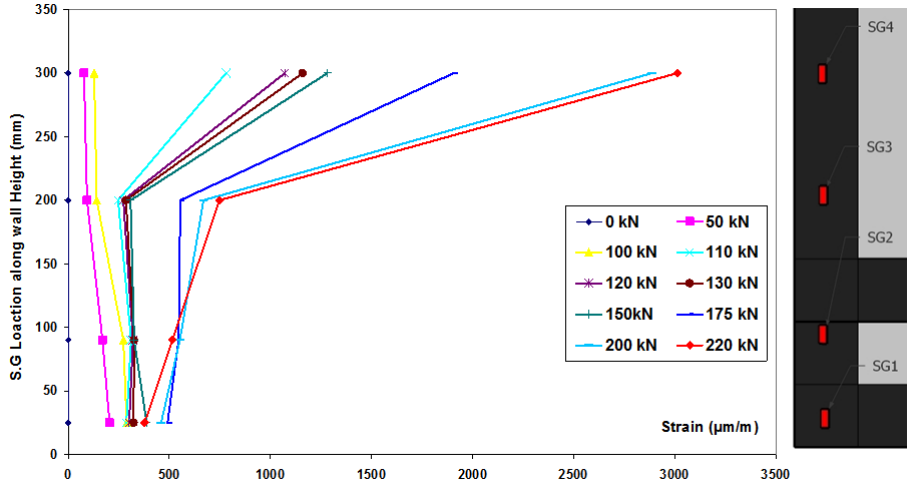

Figure 6.7: Strain distribution in vertical CFRP strip bonded at wall load end extremity

The longitudinal strain distribution in the CFRP strip bonded vertically to wall panel free end is shown in Figure 6.8. The data comprised of strain gauges SG7, 8 & 9 recorded values. The LSD curves sketched in the second quadrant signify compressive strain

development within the strip. The highest compressive strains are observed in SG 7 due to the wall toe crushing (concrete) and CFRP strip local buckling.

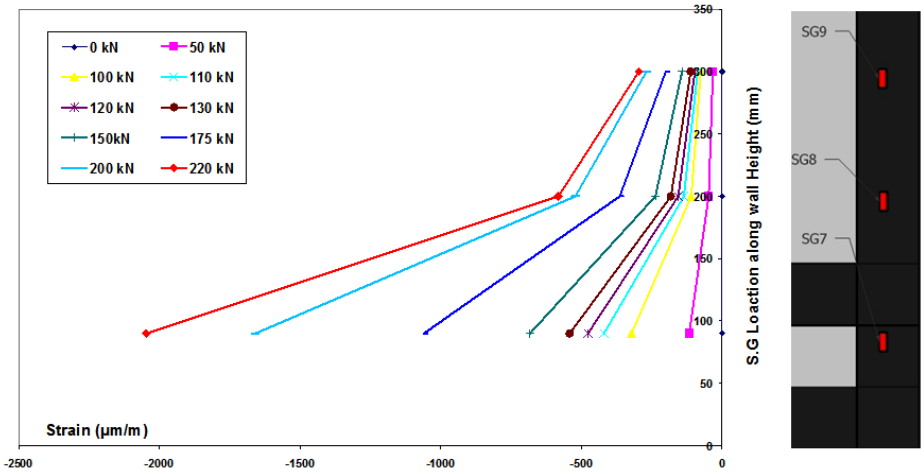

Figure 6.8: Strain distribution in vertical CFRP strip bonded at wall free end extremity

Figure 6.9 shows the strain values recorded in four vertically bonded CFRP strips at 30 cm wall height in the form of curves. Each curve represents a load level and is comprised of strain gauge SG 4, 5, 6 & 9 recorded data. The observed strain pattern is consistent with the induced load set up i.e. tensile strain developed at the load end and compressive strain at the free end. There was an abrupt increase in SG 5 recorded value as the induced load level exceeded 175 kN, it highlights sliding in the CFRP strip labeled A and cracks development across CFRP strip B. At the ultimate load level, development of tensile strain within the CFRP strip labeled C, exhibits propagation of cracks up to ¾ of the wall length.

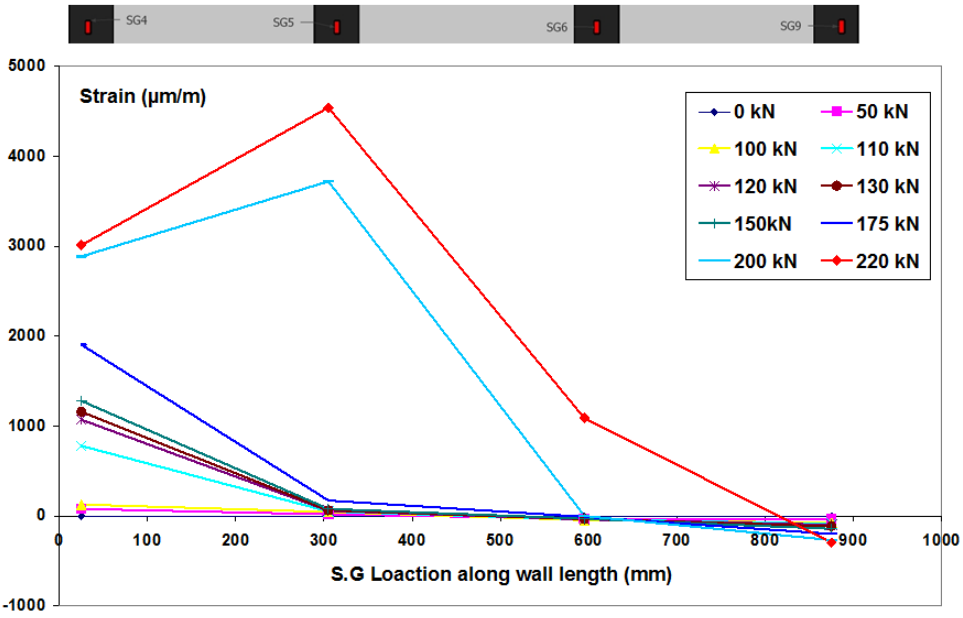

Figure 6.9: Strain distribution in CFRP strips along wall length

The difference in the behavior of CFRP reinforcement at the wall load and free end is depicted in Figure 6.10. The higher compressive strain values recorded by SG7 with increase in induced load depict the compression in wall toe at free end. The lower tensile strain recorded by SG2 is due to development of cracks in region above this zone and contribution of mesh anchor in vicinity.

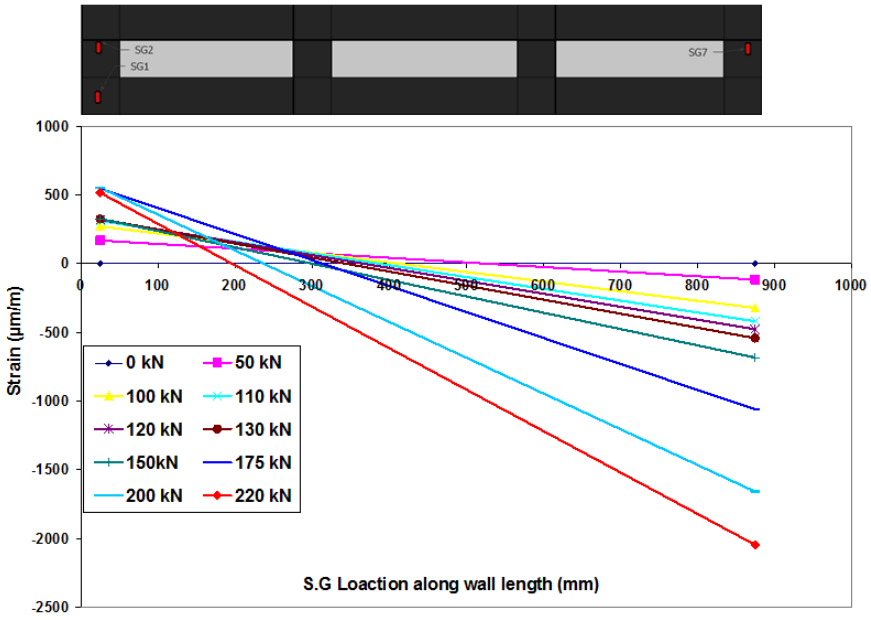

Figure 6.10: Strain recorded by SG2 & SG7

To better understand the contribution of CFRP external reinforcement on global scale, test results are further analyzed with deformability indicators.

6.1.1.5 Deformability Index

Under monotonic load the RC elements exhibits an elastic plastic response where as the one strengthened with FRP exhibit yielding but the yielding plateau is not perfectly plastic as in former. Consequently the conventional ductility index (μ) which depends on the specimen response at yield and ultimate displacement (Eq. 6.1) cannot be used to evaluate FRP contribution. Researchers such as Abdelrahman (Abdelrahman 1995), Mufti (Mufti A.A., Newhook J.P. 1996) and Zou (Zou 2003) considered deformability index to quantify the ductility of FRP strengthened specimens.

$$\mu = \left(\frac{\Delta_u}{\Delta_y} \right) \qquad \text{Eq. 6.1}$$

Naaman and Jeong (Naaman and Jeong 1995) proposed an energy based approach to define ductility. For an elastic-perfectly plastic behavior, the conventional ductility index (μ), defined as ratio of ultimate deflection (Δu) to yield deflection (Δy) shown in Eq. 6.1, can be transformed into an equivalent form expressed in terms of energies, Eq. 6.2. The total energy, E_{tot}, can be computed as the area under the load deflection curve up to the load defined as the

failure load while the elastic energy, E_{ela}, can be estimated from unloading testes. Even though Eq. (5) was developed based on an elastic perfectly plastic load deflection response, the model has been widely used to predict the ductility of FRP concrete and FRP RC beams (Alsayed and Alhozaimy 1999; Grace et al. 1998; Liang 2004; Orozco and Maji 2004; Orozco 2001; H. Wang and Belarbi 2011; Zou 2003).

$$\mu_n = 0.5 \times \left(\frac{E_{tot}}{E_{ela}} + 1 \right) \qquad \text{Eq. 6.2}$$

Table 6.2 lists the short wall test results along with the evaluated deformation factor, μ_n. Though the CFRP configuration increased the specimen lateral drift and ultimate moment capacity, but the negligible difference in μ_n values, for the two specimens indicates that the additional CFRP arrangement did not improved specimen dissipation capacity and instead resulted in diminution of about 2 %.

Table 6.2: Monotonic load test results for short shear wall

Wall	V_c (kN)	Δ_c (mm)	V_u (kN)	Δ_u (mm)	M_c (kN-m)	M_u (kN-m)	E_{tot} (kJ)	E_{ela} (kJ)	μ_n
S1	104.25	0.81	154.69	5.99	84.44	125.3	799	271	1.97
SR2	104.25	0.81	218.31	8.69	84.44	176.8	1528	538	1.92

The μ_n index indicates that the CFRP arrangement did not modify the ratio in between elastic and total energy. Because the CFRP reinforcement due to its characteristic feature improves the specimen stiffness and decreases the crack widening, but in turn, reduces its energy dissipation capacity.

6.1.2 Slender wall

Slender wall specimens, SL1 and SLR2 were subjected to quasi static load test with a constant axial compression load of 90 kN. The tests results are discussed briefly in the following sections.

6.1.2.1 Load- Displacement Curve

Specimen SL1 and SLR2 load response behavior is depicted in terms of load deflection curve in Figure 6.11. The ordinate and abscissa values are load sustained and wall top deflection as a result of induced displacement at the head beam. The CFRP strengthening technique applied on SLR2 proved to be fruitful for an increase in the strength and ductility. The specimen SL1 test was stopped when the crack at wall foundation joint area spread up to 53 cm of total wall length of 60 cm. On the other hand for SLR2, test was put to an end when the sustained load value dropped up to 20% of its ultimate value, in order to avoid any accident to occur. The pragmatic ultimate strength of specimen SL1 and SLR2 were 24.12 kN and 40.44 kN respectively, at a respective wall top deflection of 5.87 mm and 11.75 mm. The two curves are almost identical up to the induced displacement of 2.02 mm, beyond it the SLR2 behaved

differently from SL1 due to the CFRP contribution. The CFRP external reinforcement enhanced the specimen strength by almost 60%.

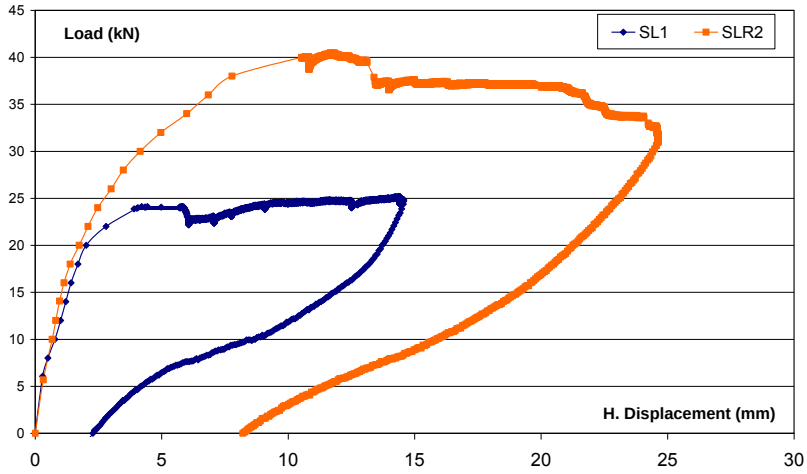

Figure 6.11: Load Displacement curve of specimen SL1 & SLR2

6.1.2.2 Deflected shapes

The deflection pattern of slender wall specimen SL1 and SLR2 are shown in Figure 6.12 & Figure 6.13, respectively. The head beam deflection in the case of specimen SL1 is non-coherent with the wall deflection. It occurred, because the load was applied at the head beam and the reinforcement arrangement at the beam/wall joint was unsuitable. The yield load observed was 20 kN, while the wall top deflection at specimen yield point and ultimate load level were 2 and 4.06 mm, respectively.

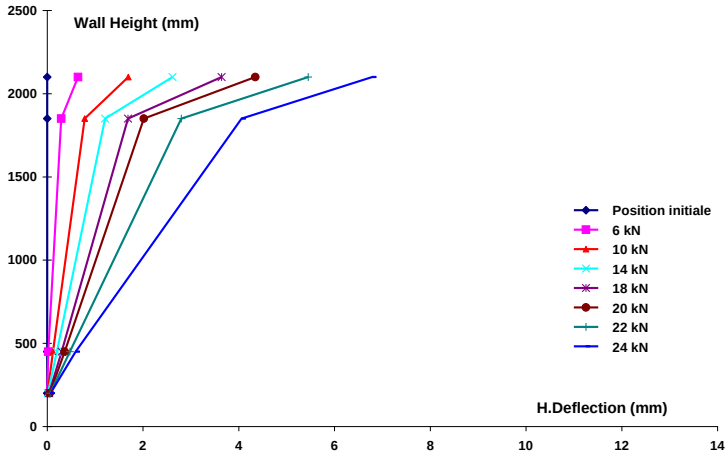

Figure 6.12: Specimens deflected shapes SL1

The specimen SLR2 deflection curve indicated a linear pattern at the initial load level, because the CFRP anchors contributed in the load distribution and reduced the beam/wall relative slip. However, near to failure, the specimen exhibited relatively higher amount of deflection at the head beam. It occurred due to mesh anchor slip as the load demand on anchor increased with an increase in the induced load level. The specimen SLR2 exhibited an overall improvement in its initial stiffness, strength and ductility in comparison to SL1. The increase

in its initial stiffness is obvious as comparatively lesser amount of deflection occurred at the same load level in specimen SLR2 with respect to SL1. The wall top deflection observed at specimen yield (20 kN) and ultimate (40 kN) load levels are 2.02 and 11.88 mm. Its ductility was equal to 5.88 and had relative ductility index (μ_R) of 2.83, as compared to SL1 (Table 6.3).

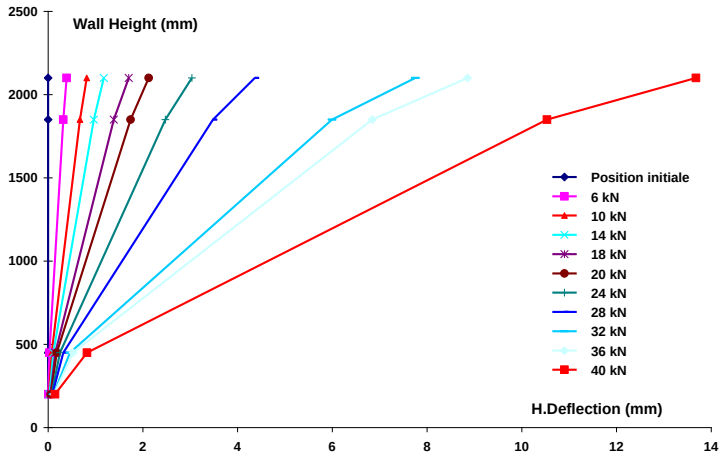

Figure 6.13: Specimens deflected shapes SLR2

Table 6.3: Slender wall ductility index

Wall	Displacement Elastic (mm)	Displacement Ultimate(mm)	μ	μ_R
SL1	2.02	4.21	2.08	1
SLR2	2.02	11.88	5.88	2.83

6.1.2.3 Failure modes

The specimen SL1 exhibited a failure mode characteristic of an under-reinforced slender wall with insufficient reinforcement at the wall foundation joint area. During the load test, horizontal cracks formed with in wall panel load end bottom section and a much wider crack formed at the joint area, spread about the entire wall length. At the induced load level of 1.2 mm, first three horizontal cracks formed within the wall panel at a height of 14.6, 37 and 53.3 cm. The respective lengths of these cracks were 30, 22 and 20 cm and they further elongated with increase in the induced displacement up to 2.02 mm, with the respective increase in the cracks length of 8.25, 18 and 5.22 cm. Beside it two more cracks (fourth and fifth) formed in vicinity of the wall-foundation joint area, fourth at the wall height of 4.6 cm and spreading up to 27 cm in a direction parallel to the wall length, and fifth developed at wall height of 10 cm which joined the first one at a distance of 5.4 cm from the wall edge. First and second horizontal cracks stretched out further with an increase in the induced load up to 7.09 mm. Later on only the first and fourth crack continued to propagate. As the induced displacement load reached the 14.2 mm level these two cracks spread almost to 53 cm, more than 3/4 of the wall length, and a number of cracks in a vertical direction formed within the wall panel load end, bottom section.

The CFRP retrofitting arrangement made on specimen SLR2 did changed the specimen crack pattern. The CFRP strips bonded at the wall bottom hindered the visibility of crack formation in this area. The first crack appeared at the wall height of 25 cm, when the induced displacement reached a level of 1.74 mm. The initial length of the crack after the CFRP strip was 16.6 cm, and continued to spread towards the vertical strip, bonded at the middle of the wall, with increase in the induced load and touched it at induced load level of 3 mm. No further propagation was observed in the crack thus the CFRP strip limited the crack propagation. As the induced load incremented to 3.5 mm, two cracks formed at the respective wall height of 31 and 51.2 cm. The second crack (height 31 cm) had a total length and angle of decline of 8.5 cm and 22.4°, while the third one initiated at the wall height of 51.2 cm, had 17 cm length and touched the horizontally bonded strip by making 12.3° angle of decline. The second crack further prolonged with an increase in induced load. It touched the first crack line at wall height of 22 cm at induced load level of 5 mm.

Figure 6.14: Specimen SL1 Failure pattern

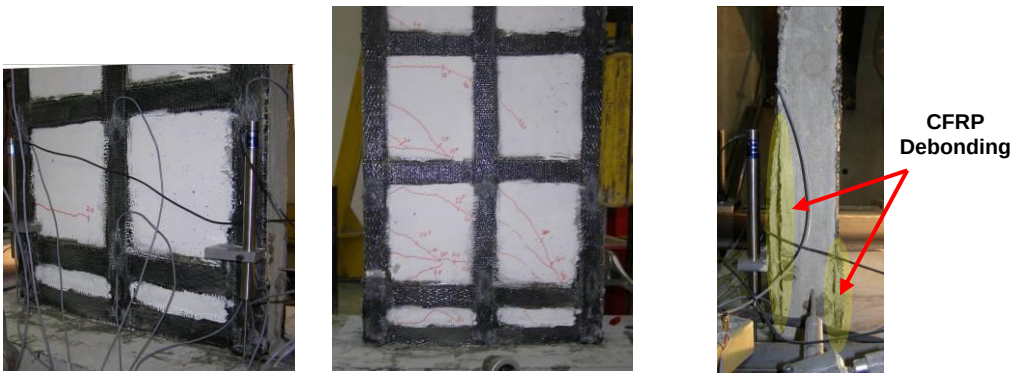

Figure 6.15: Specimen SLR2 Failure pattern

6.1.2.4 Strain distribution within bonded CFRP strip

The strain measurement arrangement made on specimen SLR2 CFRP reinforcement is depicted in Figure 6.16. The letter symbols A, B and C is used to distinguish in between the vertically bonded CFRP strips and SG represent strain gauges.

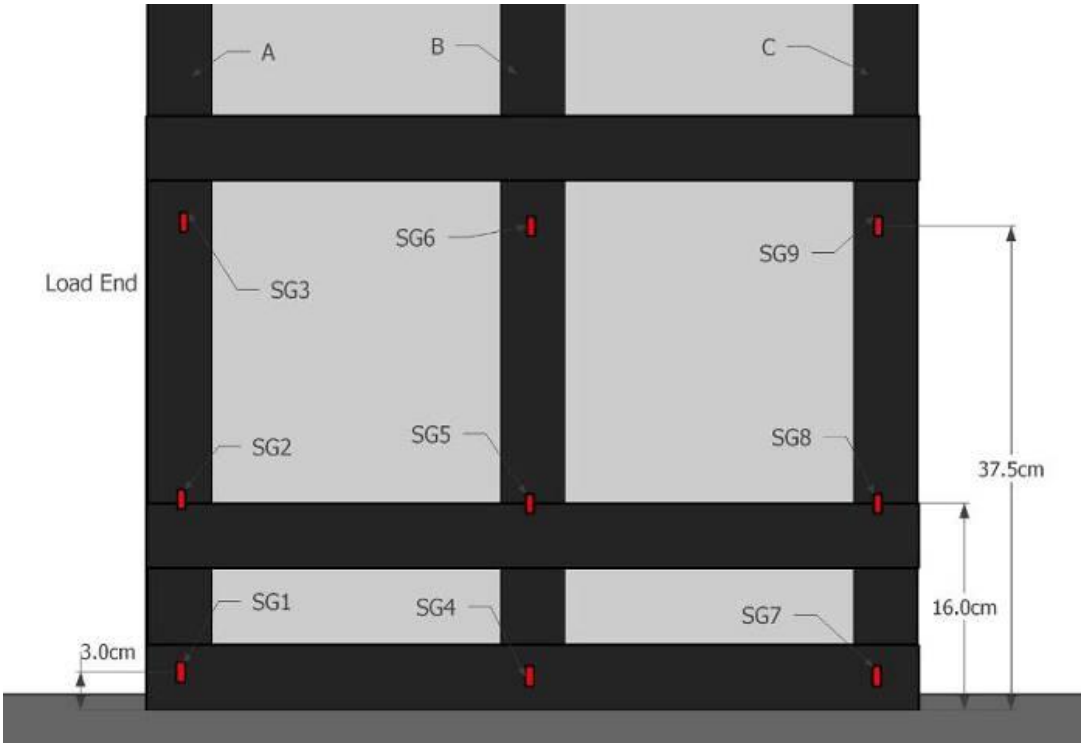

Figure 6.16: Specimen SLR2 Strain gauge detail

Figure 6.17 shows the longitudinal strain distribution (LSD) curves of CFRP strip labeled as A. Each curve represents a load level and is prepared by capitalizing strain gauges SG1, 2 & 3 recorded data. The slightly negative strain values observed in LSD curve representing 6 kN load level occurred under the effect of a vertical compression load induced over the head beam. Up to load level of 24 kN the maximum strain was recorded by SG1, as the flexural load effect is highest at the wall base. However, as the induced load exceeds the 24 kN threshold level, the strain in SG1 increase but maximum strain is then observed in SG3. This shift in maximum strain location occurred, because when the induced load exceeded 27 kN level, crack developed in the wall panel at 31 cm height. The CFRP strip across the crack tended to bridge it and in turn experienced strain. Also the mesh anchor arrangements made in this case were kept almost identical to that of SR2. Therefore above the wall height of 25 cm the CFRP reinforcement had only one layer instead of three layers. This resulted in a higher strain development in SG3 as the thickness of CFRP reinforcement was thin. On the other hand the gradual increase in recorded data of SG1 & 2 signifies the profitable contribution of mesh anchor arrangement made at the wall foundation joint.

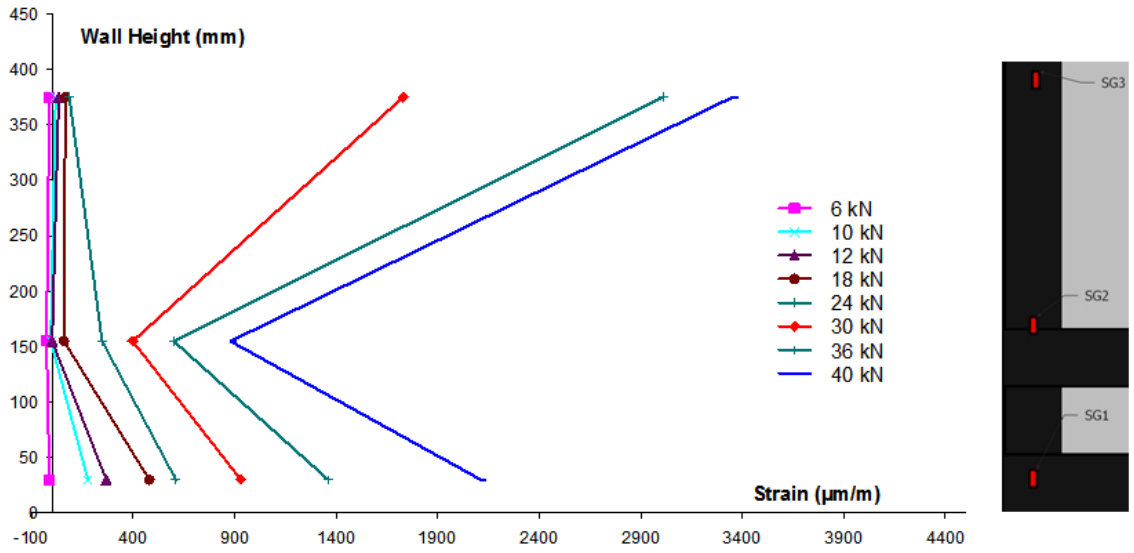

Figure 6.17: Longitudinal strain distribution in CFRP strip A

To analyze compression load effect on the CFRP reinforcement, the LSD curves of CFRP strip labeled as C are shown in Figure 6.18. Till 24 kN load level, highest strain was developed in vicinity of the wall bottom. After that the LSD curve pattern changes as the maximum strain was recorded by SG8. This variation is attributed to debonding and buckling of CFRP strip as shown in
Figure 6.15.

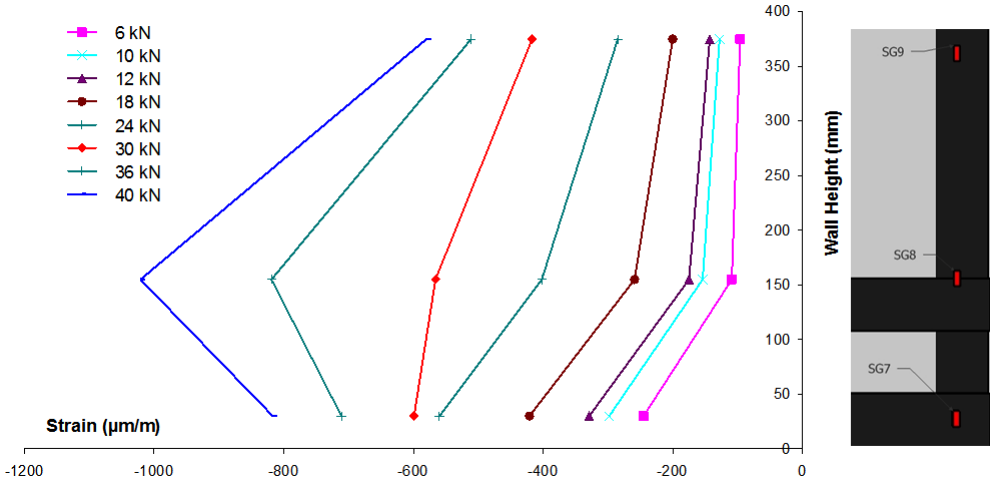

Figure 6.18: Longitudinal strain distribution in CFRP strip C

Figure 6.19 shows the strain pattern along the wall length starting from load end to free end. The curve data is comprised of strain gauges SG1, 4 & 7 which were bonded with orientation along the wall length. Therefore the curves depict the variation in flexural strain along the wall length. The recorded positive strain values by SG4 at the higher load level reflect the tensile cracks propagation across three fourth of the wall length at failure.

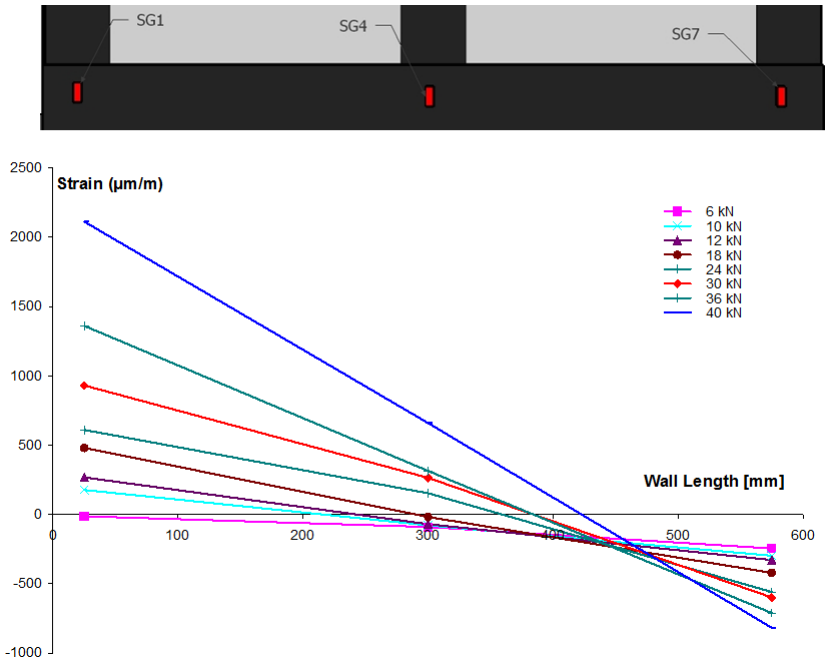

Figure 6.19: Strain distribution in CFRP strips along wall length

6.1.2.5 Deformability Index

The literature review relevant to this part has been explained in section 6.1.1.5. Table 6.4 enlists the test data of slender wall specimens SL1 and SLR2 subjected to monotonic load test. The decrease in the evaluated values of deformability index, μ_n, depicts a decrease in specimen energy dissipation capacity. In this case the reduction is about 15%. On the other hand the additional CFRP reinforcement improvement the specimen capacity in terms of lateral deflection sustained and ultimate moment capacity.

By using Eq. 6.2

SL1

$$\mu_n = 0.5 \times \left(\frac{E_{tot}}{E_{ela}} + 1 \right) = 0.5 \times \left(\frac{323}{128} + 1 \right) = 1.762$$

SLR2

$$\mu_n = 0.5 \times \left(\frac{834.27}{418.03} + 1 \right) = 1.498$$

Table 6.4: Monotonic load test results for slender shear wall

Wall	V_c (kN)	Δ_c (mm)	V_u (kN)	Δ_u (mm)	M_c (kN-m)	M_u (kN-m)	E_{tot} (kJ)	E_{ela} (kJ)	μ_n
SL1	14	1.208	25.06	14.427	23.8	42.6	323	128	1.762
SLR2	20	1.742	40.43	11.832	34	68.73	834	418	1.498

6.2 Cyclic load test

Four specimens of each of short and slender wall were subjected to quasi-static cyclic load test accompanied with a constant overhead compression load.

6.2.1 Short wall

During the load test, all specimens were subjected to lateral displacement induced at head beam level, accompanied with a constant over head load of 110 kN. The applied lateral displacement load levels were maintained at drift levels of 0.1, 0.2… 0.8, 1… 1.8 with a speed of 10, 20… 80,100,120 .180 mm/min, respectively.

6.2.1.1 Failure modes

Figure 6.20 shows a picture of the failed specimen S3. At test end a flat crack developed along the construction joint, which covered the entire wall length. This was accompanied with concrete crushing and lap splice rebar buckling at wall toe, at both ends.

Figure 6.20: Specimen S3 Failure pattern

Figure 6.21 show photos of failed specimen SLR4. In this case diagonal cracks developed at wall free end. Initially a crack developed in the wall, at one fourth of its height, at induced displacement of 6.48 mm and load of 170.5 kN. Another crack developed diagonally at the wall mid height at induced displacement of 8.1 mm and load of 150 kN. Both cracks spread towards the wall foundation joint and were not superficial as they developed at both wall faces including wall end. The cracks formed at wall free end because the test was initiated with pushing therefore at each load level the wall free end first experienced compression and then tension. This initial compression initiated CFRP debonding and buckling at free end as it cannot withstand compression load. This in turn resulted in tensile cracks initiation at the wall free end during pulling as the RC section could not sustained higher tensile stresses. The CFRP debonding is shown in second photo (Figure 6.21). The test was stopped at displacement load level of 9.72 mm due to formation of flat crack at the wall foundation joint and reduction in sustained load up to 30 %. The flat crack at wall foundation joint originated at wall free end and surpassed at half length of the wall. At the final stage of test, toe crushing and rebar yield at the wall free end was observed.

The failure pattern observed in specimen SR5 is depicted in Figure 6.22. The crack pattern observed in this case was almost alike at both ends of the wall. In this case first a diagonal crack developed at the wall free end in vicinity of the wall foundation joint, at induced displacement of 6.48 mm with a load level of 181.4 kN. At this stage no CFRP strip debonding was observed. However, at induced displacement level of 8.1 mm two diagonal cracks developed at wall mid-height at its both ends, which spread across the diagonally bonded CFRP strips and touch the wall bottom. This crack propagation across the bonded CFRP strips depicts their inability in limiting cracks. At induced displacement load level of 9.72 mm a wide range of CFRP strips delamination was observed especially in the lower half section and at CFRP strips intersection points. The specimen suffered abrupt shear failure due to Concrete/CFRP bond shear failure. Near test end a flat crack developed at wall toes accompanied with the lap splice rebar yielding. It is important to note that for the safety measure the induced load level was not increased above 9.72 mm and the test specimen were subjected to a total of four cycles at this level.

Figure 6.21: Specimen SR4 Failure pattern

Figure 6.22: Specimen SR5 Failure pattern

Though specimen SR6 showed an overall improvement in ductility and strength as compared to SR5, yet the wall panel crack pattern was almost identical in the two. Figure 6.23

depicts specimen SR6 failure pattern. At induced load level of 8.1 mm two diagonal cracks, one at each end appeared at the wall panel lower half. These cracks propagated across the diagonally bonded CFRP strip and touched the wall bottom in vicinity of its mid-length. However the diagonally bonded strips reduced the crack widening to a certain extent. Afterwards a number of diagonal cracks developed within wall panel lower half middle portion accompanied with another diagonal crack along wall free end upper diagonal while touching the CFRP strip bonded in the same direction. At test end, debonding was observed in the CFRP strips located within the wall lower half. It included debonding of strips along the wall diagonals and the interior vertical strips. On the other hand in wall upper half portion, the vertically bonded strip located at wall mid–length, ruptured beneath the intersection point of diagonally bonded CFRP. In this case the CFRP debonding was not severe as in case of SR5 due to the improvement made in the transverse mesh anchors introduced at CFRP strip intersection points.

Figure 6.23: Specimen SR6 Failure pattern

6.2.1.2 Hysteresis Curve

The hysteresis curves shown in Figure 6.24 depict the variation in the cyclic load response behavior of all the specimens (S3, SR4 & SR6). The observed max load sustained by S3, SR4 and SR6 is 138.69, 170.53 and 169.44 kN respectively. The hysteresis curves indicate an increase in the initial stiffness in specimens SR4 and SR6 as compared to S3. The relatively higher initial stiffness of SR6 in comparison to SR4 is owed to the additional transverse mesh anchor arrangement made within the wall panel. The pinching of hysteresis curve of specimen SR4 and SR6 as compare to S3 at identical load level, after the crack initiation, point out that the additional CFRP external reinforcement depreciate the dissipation capacity of the RC wall. The comparative analysis of SR4 and SR6 indicates a relatively smooth decline in the sustained load of SR6 after exceeding their ultimate capacity. This difference in behaviors is owed to transverse mesh anchor which retained the CFRP intact with concrete surface and thus avoided abrupt failure on a large scale.

The hysteresis envelopes of specimens S3, SR4 and SR6 are shown in Figure 6.25. The ultimate displacements observed in these specimens were 7.43, 9.81 and -12.1 mm, respectively. The relative increase in initial stiffness due to introduction of CFRP reinforcement in SR3 and afterward additional improvement owed to transverse mesh anchor within SR6 wall panel is well depicted by envelope curves relative incline in initial slope.

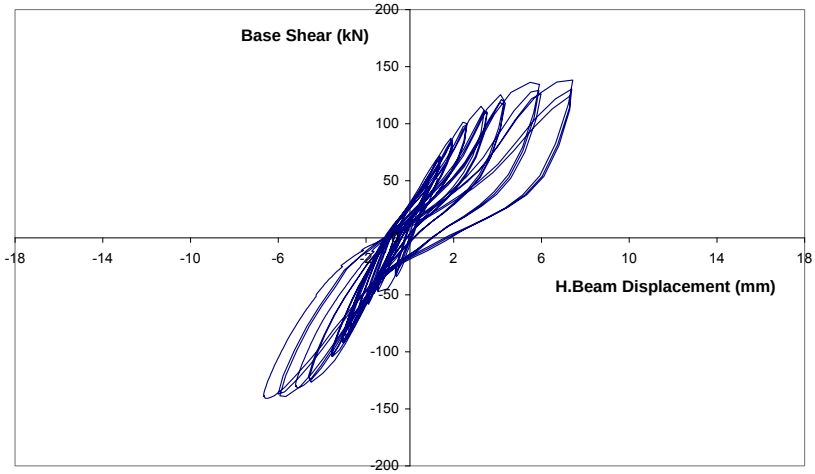

(a) S3

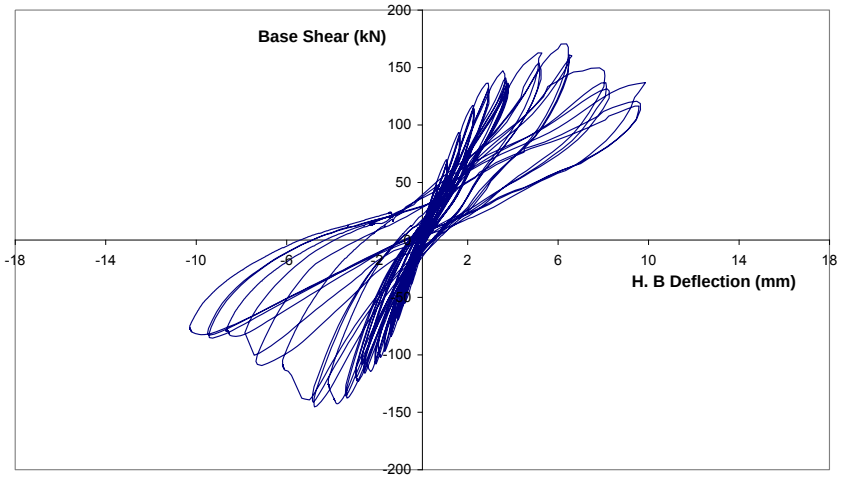

(b) SR4

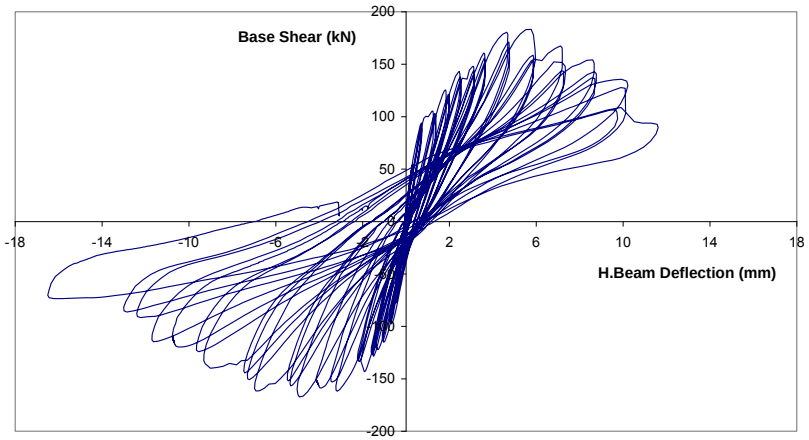

(c) SR6

Figure 6.24: Hysteresis curve

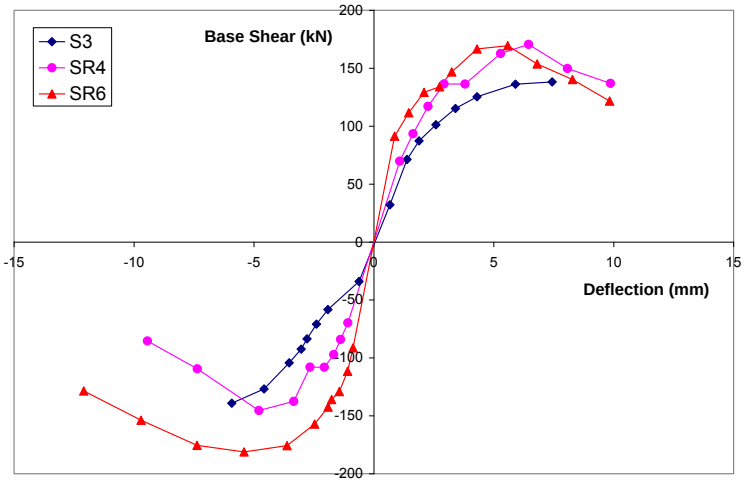

Figure 6.25: Load displacement envelopes

6.2.1.3 Degradation in restoring force

Figure 6.26 shows the degradation in the restoring force of specimens S3, SR4 and SR6. The ordinate consists of the restoring force ratio, which is defined as the ratio of maximum base shear observed in third cycle to first cycle at each drift level. The base shear values correspond to the initial half cycles i.e. comprising: push and relaxation only.

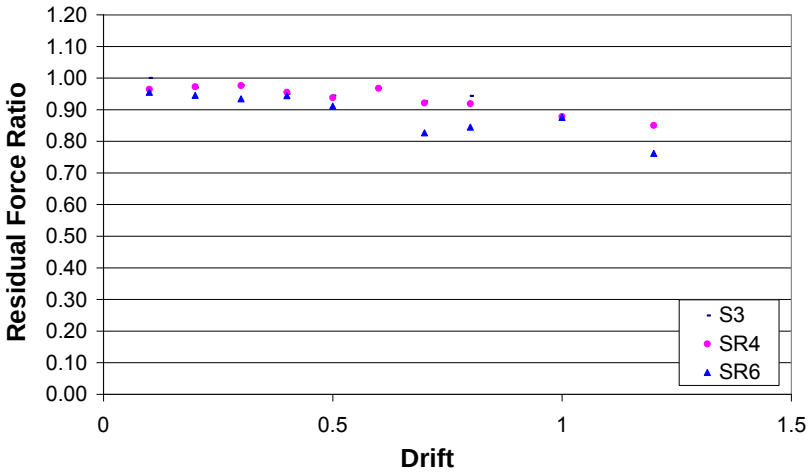

Figure 6.26: Decay in restoring force, Specimen S3, SR4 & SR6.

Walraven (Walraven 1994) reported the cyclic behavior of an aggregate interlock as a partial cause of decay of restoring force. He pointed out that sliding is produced up to the previously achieved displacement level, after which the crack asperities lock in. Therefore, both stiffness and transmitted shear increase up to maximum load of cycle. This is due to accumulation of damage at the contact surfaces. In the subsequent cycle, the crack slip necessary to lock in the crack asperities increases and consequently the restoring force decreases.

The restoring force ratio observed in specimen S3, SR4 and SR6, at test end, were 0.94, 0.85 and 0.76, respectively. Generally, specimen failure is assumed when the restoring force falls below 0.80. However in the cases of specimen S3 and SR4 tests were put to an end due to the formation of flat horizontal crack across the entire wall length at the bottom in S3 and wide scale CFRP strips debonding in SR4.

6.2.1.4 Stiffness degradation

The hysteresis curves show a relative decline in their slope with an increase in the induced displacement load levels, that is a relative decline in their stiffness with increase in induced displacement. Figure 6.27 shows the stiffness Vs displacement curves of the specimens S3, SR4 and SR6. On the ordinate are the values of secant stiffness, equivalent to the maximum force divided by maximum displacement (Greifenhagen C. 2006; Weichen Xue et al. 2007). The values correspond to the first cycle at each load level. At initial load level, the influence of CFRP reinforcement in improving the specimen stiffness is eminent. The increase observed in the initial stiffness of specimens SR4 and SR6 as compared to specimen S3 is 12.3 % and 83% respectively. Near test end the stiffness curves of all the three specimens are almost identical because of the wide range of CFRP strips debonding from concrete surface.

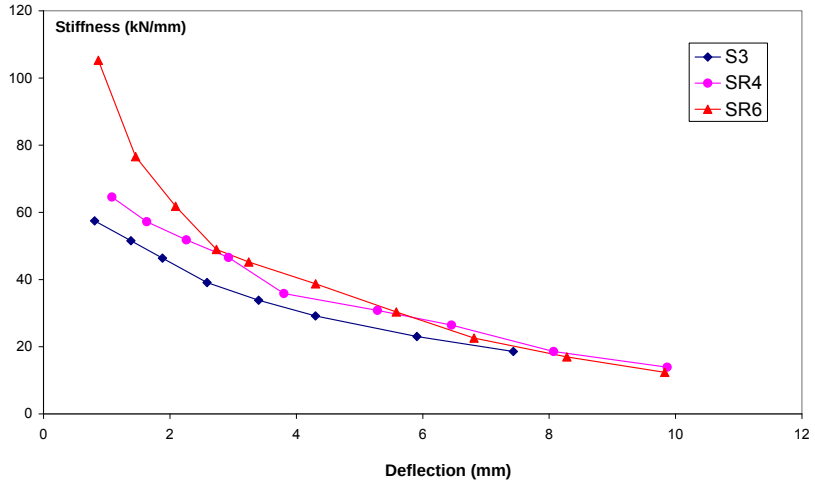

Figure 6.27: Stiffness Curves

6.2.1.5 Elastic and dissipated energy

For test specimens S3, SR4 and SR6 the total, elastic and dissipated energy values are given in Figure 6.28 in the form of bar charts. The energy values correspond to half load cycles and were evaluated by use of trapezoidal rule. The total, elastic and dissipated energy were evaluated by computing the area under the loading curve, under the un-loading curve and in between the loading and unloading curves, respectively. In all the three specimens the dissipated energy at each load level decreased with relative increase in cycle number, due to smoothening of the cracked surfaces. Specimens S3 and SR6 at their ultimate drift level (0.8 and 1.2%, respectively) exhibited higher amount of energy dissipation in comparison to their elastic energy (E.E).

Figure 6.29 shows the EE and dissipated energy (DE) curves of the three specimens. The values were obtained by summation of EE and DE for three complete cycles at each load level. The curves indicate that the CFRP reinforcement arrangement made in SR4 has

improved its elastic energy compared to S3 while on the other hand reduced its dissipation capacity. This development is attributed to the CFRP elastic nature. In specimen SR6, an additional transverse anchor arrangement made within wall panel improved both its elasticity and energy dissipation capacity as compared to SR4 and S3. At induced drift level of 0.8 %, the cumulated E.E for specimen S3, SR4 and SR6 was 1.4, 1.7 and 2.06 kJ, respectively. The SR4 and SR6 CFRP reinforcement arrangement improved specimen elasticity up to 21.4% and 47% at 0.8% drift. The cumulated D.E within specimen S3, SR4 and SR6 at 0.8 % drift was 1.59, 1.23 and 1.68 kJ, respectively. Specimen SR4 depicted a decline in DE of 22.6 % and SR6 exhibited an improvement of 5.6 % with respect to control specimen S3.

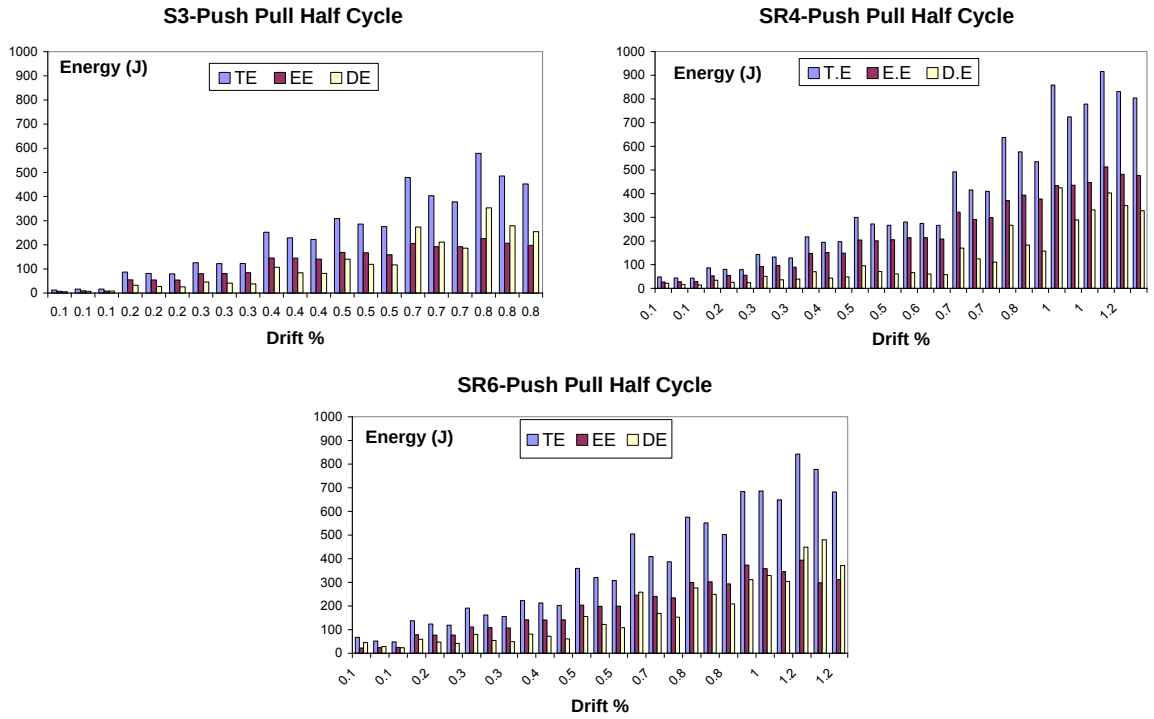

Figure 6.28: S3, SR4 and SR5 T.E, E.E and D.E bar charts

Table 6.5 lists the evaluated E.E and D.E from three complete cycles at each load level. Specimen SR6 exhibited superior performance in comparison to SR4. At drift level of 1.2 %, specimen SR6 showed a relative increase in the E.E and D.E to that of specimen SR4. These were 23% and 45 %, respectively. This improvement in behavior was attributed to the transverse mesh anchor. It kept the CFRP strip intact with concrete surface and therefore improved the wall elasticity. On the other hand the diagonally bonded CFRP strips tended to bridge the cracks developed in a direction transverse to it and reduced its widening apart. This arrangement retained the cracked surfaces in contact and dissipated the energy by friction due to relative slipping.

Table 6.5: Total E.E and D.E at each drift level

	Drift %	0.1	0.2	0.3	0.4	0.5	0.7	0.8	1	1.2
E.E (J)	S3	41	240	362	665	829	1172	1401		
	SR4	157	282	452	686	913	1356	1697	1699	1841
	SR6	158	475	663	859	1294	1653	2067	2333	2271
DE (J)	S3	39	132	195	404	563	1102	1592		
	SR4	93	142	217	289	388	761	1235	1835	1899
	SR6	145	274	313	418	864	1238	1682	2314	2759

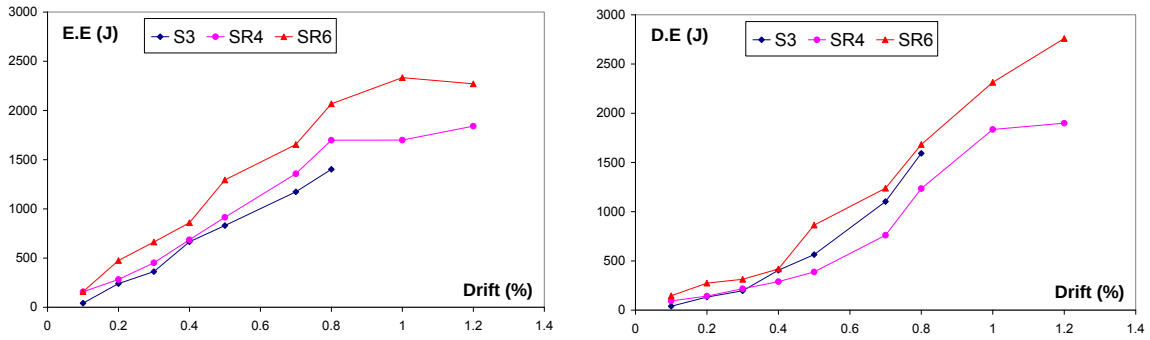

Figure 6.29: S3, SR4 and SR5 (a) E.E (b) D.E curves

6.2.1.6 Equivalent Damping

The equivalent damping is a mean to introduce the energy dissipation in a dynamic calculation (Greifenhagen 2006). The equivalent damping ratio is defined as follows.

$$\xi_{eq} = \frac{A_d}{4\pi A_i} \qquad \text{Eq. 6.3}$$

Here A_d represents the energy dissipated in one complete cycle and A_i represents potential energy (Figure 6.30(a)). The later is taken equivalent to 1/2 times product of maximum displacement to maximum base shear i.e. $0.5*V_{max}* \Delta_{max}$. Figure 6.30 depicts a schematic view of A_d and A_i on hysteresis curve and ξ_{eq} Vs Drift curves of specimen S3, SR4 and SR6.

The curve shows that in terms of equivalent damping ratio the specimen S3 performance is well compared to the specimen SR4 and SR6, due to the elastic nature of CFRP strengthening material. The CFRP reinforcement arrangement made in specimen SR6 produced better performance than SR4 CFRP reinforcement.

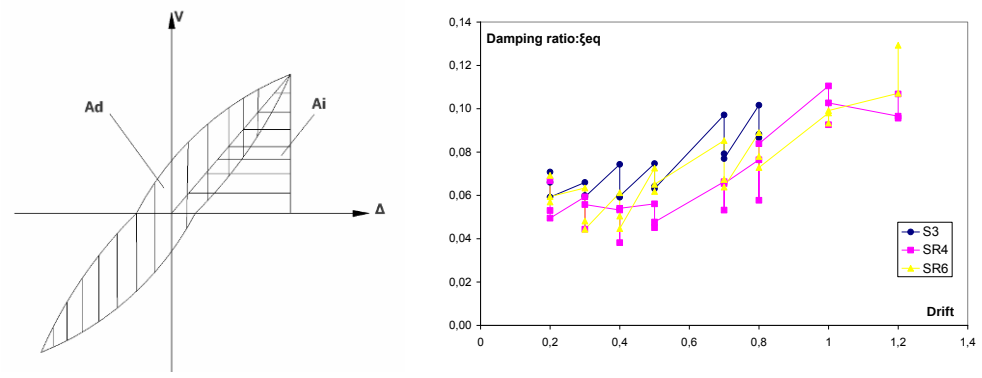

(a) (b)

Figure 6.30: (a) Equivalent damping ratio definition, (b) Equivalent damping ratio Vs Drift

6.2.1.7 Damage Index

A quantitative assessment of damage is feasible by using damage indicators (H. S. Ang et al. 1993; Izuno et al. 1993). These are usually defined in terms of ductility or energy related ratios (Rao et al. 1998). Research studies worked on the structure components showed that the damage is dependent on both permanent deformations and the energy absorbed in hysteretic cycles (Y. J. Park and A. H. S. Ang 1985). Parameters such as displacement, strength, strain, energy, rigidity and intrinsic dynamic properties are used to evaluate damage indicators, which can be categorized in two groups: cumulative and non cumulative indicators (Promis et al. 2009). The cumulative index evaluates damage dependency on loading amplitude and number of loading cycles. The final damage index is obtained by accumulation of damage indices under cyclical loads. Non cumulative indices are appraised with maximum mechanical parameters such as displacement, rotation and curvature. The numerous damage indices utilized in the earlier research work are listed below.

Ductility index: takes into account ultimate and elastic displacement (Abdelrahman 1995).

$$\mu = \frac{\delta_u}{\delta_y} \qquad \text{Eq. 6.4}$$

Relative ductility index: is used to evaluate the strengthening procedure influence on ductility (Promis et al. 2009). It is defined as the ratio of ultimate displacement of strengthened specimen to non strengthened (control) specimen.

The flexural damage ratio: points out the decrease in stiffness and is defined as the ratio of initial stiffness to final secant stiffness (Abdelrahman 1995).

$$FDR = \frac{k_o}{k_m} \qquad \text{Eq. 6.5}$$

The Modified flexural damage ratio: is used to evaluate specimens' stiffness degradation and is based on initial and ultimate stiffness (Roufaiel and C. Meyer 1987).

$$MFDR = \frac{k_f}{k_m} \times \frac{k_m - k_o}{k_f - k_o} \qquad \text{Eq. 6.6}$$

Where k_o, k_m, k_f are initial, final and ultimate stiffness, respectively (Figure 6.31).

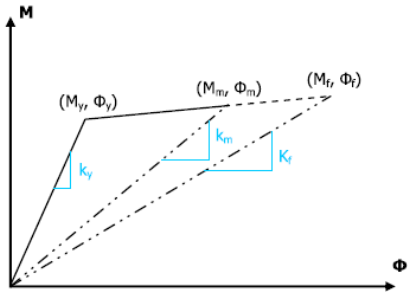

Figure 6.31: Secant stiffness definition

Index based on displacement: applied in the research work (Banon and Veneziano 1982; Stephens and Yao 1987) has two indices. The first one indicates linear accumulation of damage and second index is the sum of the ratios of plastic deformation.

$$D_1 = \frac{e^{n\beta_w} - 1}{e^n - 1} \qquad \text{Eq. 6.7}$$

$$\beta_w = c\sum_i \frac{\delta_i}{\delta_f} \qquad \text{Eq. 6.8}$$

$$D_2 = \sum_i \left(\frac{\Delta\delta_+}{\Delta\delta_f} \right)^{1.77} \qquad \text{Eq. 6.9}$$

Where δ_i stands for maximum displacement for cycle I, δ_f for displacement at failure during monotonous loading and $\Delta\delta_+$ for positive increment of plastic displacement in cyclic loading. Parameters c and n depends on specimen configurations.

Index based on energy: have been used by Meyer (I. F. Meyer 1988) and Garstka (Garstka et al. 1993). They normalized the energy dissipated during cyclic loading with the energy dissipated under monotonic loading.

$$D_Q = D_Q^+ + D_Q^- - D_Q^+ D_Q^- \qquad \text{Eq. 6.10}$$

$$D_Q = \frac{\sum E_{pi}^{\pm} + \sum E_{si}^{\pm}}{E_U^{\pm} + \sum E_{si}^{\pm}} \qquad \text{Eq. 6.11}$$

Where E_{pi}, E_{si} and E_U represents energy dissipated by primary half-cycle, energy dissipated by following half-cycle and maximum energy dissipated under monotonic load, respectively. The ± sign represents positive or negative phase of cyclic deformation. Sadeghi (Sadeghi et al. 1993) made a modification in Eq. 6.11 to reduce the overestimation of damage due to secondary cycles.

$$D_Q = \frac{\sum E_{pi}^{\pm} + \lambda_i^{\pm} \sum E_{si}^{\pm}}{E_U^{\pm}} \qquad \text{Eq. 6.12}$$

Where

$$\lambda_i^{\pm} = \frac{E_U^{\pm} - \sum E_{pi}^{\pm}}{\sum E_{si}} \qquad \text{Eq. 6.13}$$

However, all the above mentioned damage indicator equations either consider displacement or energy parameters for it solution, separately. As the reinforced concrete elements exhibit degradation in the strength and stiffness quantities under cyclic loading along with energy dissipation. To take these into account Park and Ang (Y. J. Park and A. H. S. Ang 1985) developed a damage index as follows.

$$Park'sDI = \frac{\delta_m}{\delta_u} + \frac{\beta}{\delta_u P_y}\int dE \qquad \text{Eq. 6.14}$$

Here δ_m is the maximum deformation under earthquake, δ_u is the maximum deformation under monotonic loading, P_y is the yield strength, dE is the increment in absorbed hysteretic energy and β is a constant which emphasizes the strength deterioration per cycle. The damage index is normalized to produce values between 0 and 1, where 1 signifies collapse. The parameter β gives the ratio of the incremental damage caused by an increase of the maximum response to the normalized incremental hysteretic energy (Y. J. Park et al. 1985). Based on the analysis of 260 beam and columns test data, the parameter β empirically formulated form is:

$$\beta = \left\{0.37n_o + 0.36\left(k_p - 0.2\right)^2\right\} \times 0.9\rho_w \qquad \text{Eq. 6.15}$$

Here n_o is the normalized stress, k_p is the normalized steel ratio $\left(=\rho_t f_y / 0.85 f_c^{'}\right)$, f_y is the yield stress of reinforcement and ρ_w is the confinement ratio (> 0.4%). For slightly reinforced structures β is taken equal to 0.25 (Promis et al. 2009).

Evaluated Indicators

Figure 6.32 shows the development of FDR with an increase in drift level. The disparity in curves is an outcome of diversity made in the CFRP external reinforcement arrangement. The specimen SR4 showed a decrease in FDR in comparison to that of specimen S3. At 0.8 % drift, specimen SR4 showed a decrease in FDR of 21% in comparison of S3. It shows that additional CFRP reinforcement has decreased the damage to certain extent. On the other hand at same drift level, specimen SR6 exhibited an increase in FDR of about 51%. The higher FDR index is attributed to the presence of holes within the wall panel, drilled to install wall mesh anchor to decrease CFRP strip debonding. The two CFRP strengthening technique applied resulted in the ultimate displacement increase up to 50% with respect to S3. This was accompanied with an overall increase in the FDR showing a higher level of sustained damage.

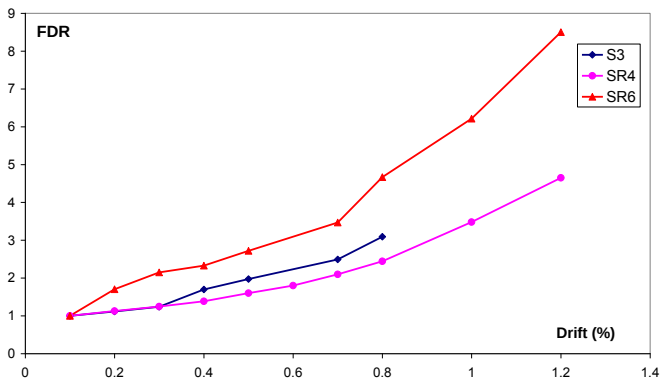

Figure 6.32: Flexural Damage Ratio S3, SR4 & SR6

The MFDR damage index presents the advantage to normalize the maximum damage up to 100%. Therefore, we can accurately quantify the rate of damage of the structural element. Thus, considering the ultimate displacement of the reinforced concrete element as a criterion dictating the behavior factor in the regulatory design, we can evaluate the performance of reinforced configurations. The plot of the evolution of the MFDR damage indicator (Figure 6.33) depicts an efficiency of the composite strengthening. The flatter curves of strengthened specimens as compared to that of non-strengthened specimens show that at same drift level, the strengthened specimens sustained lesser damage.

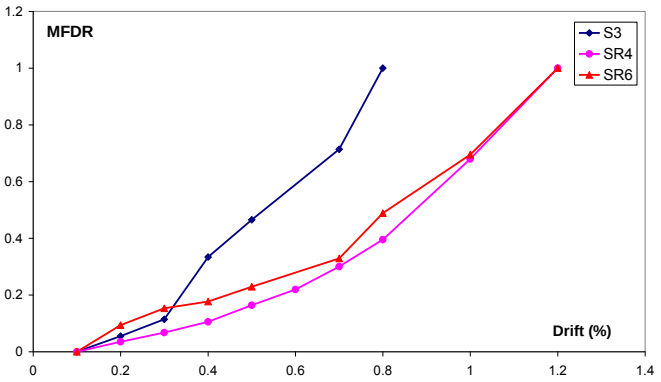

Figure 6.33: Modified Flexural Damage Ratio S3, SR4 & SR6

Figure 6.34 shows the Park's damage index Vs induced lateral deflection curves of the short shear wall specimens subjected to a seismic loading. The curve of SR6 is flatter as compared to S3 and SR4. As Parks' I is directly proportional to the dissipated energy and inversely proportional to the ultimate deflection, therefore the curves flatness exhibits a relative increase in ultimate deflection and reduction in energy dissipation capacity in specimen SR6. This phenomenon is due to elastic behavior of CFRP material. Its reinforcement increases the overall strength of RC specimen but due to its elastic behavior till failure, it does not contribute in amelioration of specimens' energy absorption capacity.

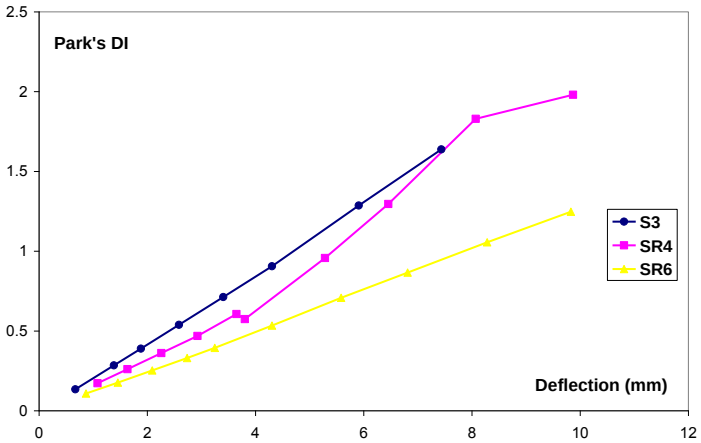

Figure 6.34: Park's Damage Index Vs Lateral Deflection

6.2.2 Slender wall

In this case the loading protocol was maintained identical to that of short wall with one modification i.e. the vertical compression load induced over the head beam was kept equal to 90 kN.

6.2.2.1 Failure modes

The pictures of specimen SL3 at failure are shown in Figure 6.35. In this case first two flat horizontal cracks appeared, at 0.3 % lateral drift with corresponding lateral load equal to 22.7 kN, at wall height of 30 mm and 180 mm. The two cracks initiated at the wall free end and propagated towards the load end, with respective length of 373 mm and 284 mm. As the drift level was incremented to 0.4 % with the corresponding load value of 25.42 kN, two new cracks developed at load end at roughly same height of the first two and joined it. At drift level of 0.6 % and loading of 27.12 kN, wall toe crushing was observed at both ends. It was accompanied with the formation of vertical cracks within the wall panel and edges at the wall bottom region. The test was ended due to the crack widening at construction joint, concrete spalling at wall edges and decline in resistive load up to 38% of its ultimate capacity (27.12 kN). The failure mode exhibited by specimen SL3 is characteristic of the walls that are under-reinforced in terms of flexure and possesses insufficient lap splice reinforcement arrangements.

Figure 6.35: Specimen SL3 Failure pattern

The external CFRP reinforcement arrangement worked out on specimen SLR4 modified its strength and ductility with reference to the control specimen SLR3. The specimen SLR4 developed its ultimate base shear of 43.44 kN at 18 mm lateral deflection. Figure 6.36 shows photos of failed specimen SLR4. The CFRP strips bonded to the wall panel hindered cracks visibility. At the induced drift level of 0.3 %, and corresponding lateral load of 30.6 kN, three flat cracks initiated at wall free end at wall height of 204, 358 and 509 mm. The lower two cracks had a length equivalent to 70 mm while the upper most crack reached

the vertical strip bonded at wall mid-length but it did not propagated across it. At the load end, three cracks developed in the first load cycle at 0.4% drift level with a corresponding lateral load equal to 34.81 kN. The cracks developed at wall height of 70, 200 and 423 mm and declined towards wall bottom. The upper most crack spread across three fourth of wall length and CFRP strips, bonded in a vertical and horizontal direction, while the lower cracks ended at the underneath horizontally bonded strips. One new flat crack developed at induced drift of 0.6 % and lateral load of 41.6 kN, at each extremity. They formed at 720 mm wall height, next to CFRP strips bonded at the extremities and almost reached the vertical strip bonded at wall panel mid-length. The CFRP strips bonded vertically at the wall extremities detached with concrete surface peeling off at the wall lower bottom at induced drift level of 1%. At this level the specimen achieved its maximum lateral load of 43.44 kN. The CFRP strips buckled out due to their inability to withstand compression and was aggravated by concrete core spalling at the wall edges. After wards the restoring force kept on decrease with increase in induced drift. The specimen failed due to wide scale CFRP strips debonding in the wall lower half and concrete spalling and crushing at bottom. At the end wide cracks developed at the wall foundation junction due to mesh anchor failure and the vertical strips bonded at the wall panel extremities, peeled off up to two third of wall height.

Figure 6.36: Specimen SLR4 Failure pattern

Figure 6.37 shows photo of specimen SLR5 at test end. In this case the specimen developed its ultimate base shear of 45.69 kN at 9.64 mm lateral deflection. The bonding of vertical CFRP strips of width 75 mm, instead of 50 mm at the wall panel extremities and transverse mesh anchor within the wall panel improved the wall shear strength and avoided CFRP strips debonding and concrete spalling at the wall edges to a greater extent. At 0.3% drift level and 39.56 kN base shear, two flat cracks developed at wall free end at 338 and 535 mm height. They appeared within the third panel in close vicinity to horizontally bonded strip. They spread horizontally from the vertical strip bonded at extremity to middle one. A number of new cracks developed at 0.6% drift and base shear equivalent to 45.63 kN at both ends. One of the cracks developed at wall free end at 440 mm height, propagated towards the load end and crossed the CFRP reinforcement at the intersection point of vertical and horizontal bonded strips. In this region the CFRP local debonding was observed at test end. It was

accompanied with concrete spalling at both ends in vicinity of construction joint. The test was ended due to reduction in the sustained load up to 48% with respect to its ultimate capacity.

Figure 6.37: Specimen SLR5 Failure pattern

Photos of failed specimen SLR6 are shown in Figure 6.38. In this case the CFRP strips utilized were made of unidirectional fabric. The specimen developed its ultimate shear capacity of 56.63 kN at 13.34 mm lateral deflection. At 0.5% drift and 49.5 kN base shear, three cracks formed at each end within the wall lower half section. The cracks were interconnected and had a more or less horizontal orientation. After it, at 0.6 % drift and 53.5 kN base shear, a pair of new cracks developed at each end in the vicinity of initial cracks. Debonding of small vertical CFRP strips, adhered to mesh anchor splayed portion at the wall extremities occurred at 0.7% drift and base shear of 56.63 kN. Later on a number of cracks appeared at the wall edges with in lap splice region and CFRP strips debonding enhanced to the lower one third of the wall height. In the same region debonding and delamination of horizontal strips occurred at the wall panel extremities.

Figure 6.38: Specimen SLR6 Failure pattern

6.2.2.2 Hysteresis Curve

Figure 6.39 shows hysteresis curves of specimens SL3, SLR4, SLR5 and SLR6. The control specimen SL3 exhibited flexure failure mode as shown in Figure 6.35 and it showed maximum base shear (27.75 kN) equivalent to base shear at its nominal flexural strength (27.84 kN). The nominal flexural strength was computed with the material properties. The assumptions made for it consisted of elastic perfectly plastic and parabolic rectangular stress strain relationship for steel and concrete, respectively. The S.G bonded to rebar in lap splice region, recorded its yielding at 23.4 kN base shear and 0.03% drift. The wide scale cracking observed in consecutive drift level can be easily depicted by the hysteresis curves tendency to lean down in the consecutive cycle at each level with respect to initial one. It is due to the formation of new crack in the first cycle and smoothing effect in the consecutive cycle. The axial load also contributes to pinching of hysteresis loops which consequently reduces energy dissipation.

The hysteresis curves of specimen SLR4 indicate an overall improvement in the strength and ductility, due to additional external CFRP reinforcement arrangements. The maximum base shear of 43.44 kN was developed at 1% drift. After which the specimen exhibited a gradual decline in base shear with respective increase in drift. The relative leaning of secondary cycles with respect to the initial one was observed in this case too. This phenomenon aggravated when specimen exceeded its ultimate capacity and in this case the third load cycle further flatten because of the continuation of CFRP strips debonding with the load reversal.

The hysteresis curves of specimen SLR5 and SLR6 shows an improvement in base shears but also show an abrupt decline in sustained load. The maximum base shear developed in specimens SLR5 and SLR6 were 45.69 kN at 0.5% drift and 56.63 kN at 0.6% drift, respectively. The improvement in strength is owed to the increase in the width of CFRP strips and introduction of transverse mesh anchor within the wall panel to hold the bonded strip firmly. However, the anchors arrangement within the wall panel also caused an abrupt decline in sustained load due to its shear failure. The improvement in ultimate base shear in specimen SLR6 with respect to specimen SLR5 was brought out by the increase made in wall anchor filament numbers only. Because in CFRP strips with bidirectional fiber orientation, the longitudinal fibers contribute in stress distribution while the fibers in the transverse direction just keep the fabric intact. The hysteresis loops, flag shape show the axial load effect.

Figure 6.40 shows the hysteresis envelope curves of all specimens. The more or less similar slope of all the curves at initial stage exhibits that in term of initial stiffness the additional CFRP reinforcement arrangement did not contributed largely. However, on the other hand it did improve its ultimate base shear. The abrupt failure of specimen SLR5 and SLR6 is well represented by their respective curves. The specimen SL3 and SLR4 curves exhibit an identical ductile failure in the two. The maximum base and corresponding drift levels are listed in Table 6.6.

Table 6.6: Slender wall maximum base shear

Speicmen	SL3	SLR4	SLR5	SLR6
Base Shear (kN)	27.75	43.44	45.69	56.63
Drift (%)	0.5	1	0.5	0.8

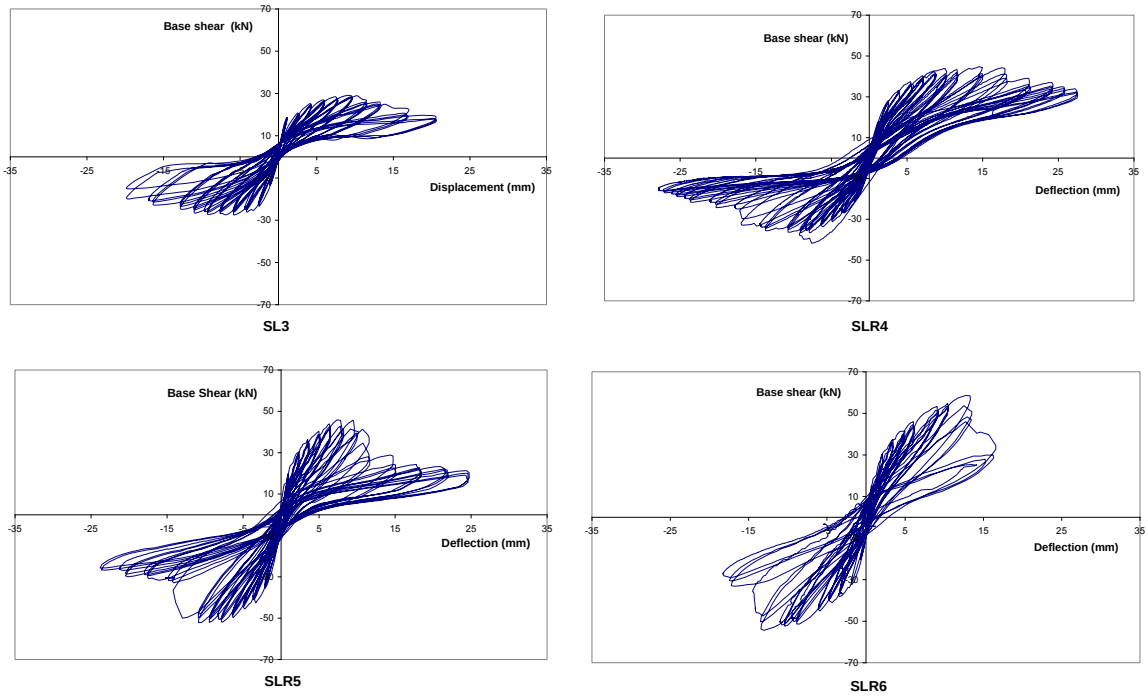

Figure 6.39: Hysteresis curves: S3, SR4, SR5 & SR6.

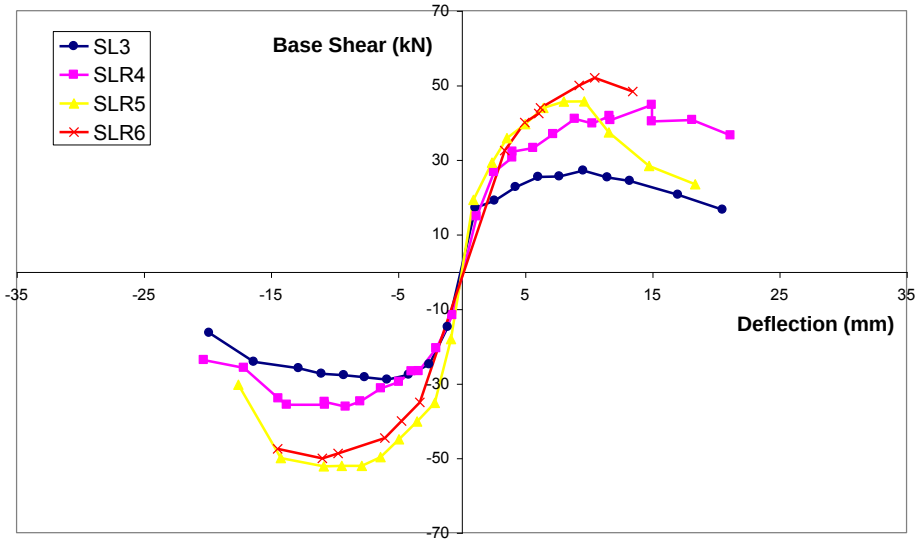

Figure 6.40: Load displacement curve

6.2.2.3 Stiffness degradation

Figure 6.41 shows the specimen SL3, SLR4, SLR5, and SLR6 secant stiffness values Vs drift curves. The secant stiffness (k) is equivalent to the ratio of average maximum base shear to average relative deflection, observed in the initial cycle at each load level. The minute gap between the specimen stiffness values at the initial stage indicates negligible contribution of CFRP reinforcement in terms of initial stiffness improvement. However the decline observed in stiffness with an increase in drift, does show a slight improvement in terms of control specimen (SL3) curve steep decline.

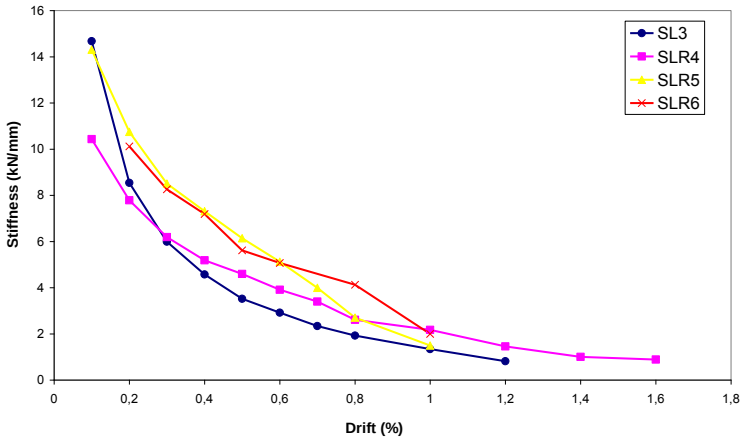

Figure 6.41: Stiffness degradation curve

6.2.2.4 Energy Dissipated

Figure 6.42 shows the energy bar charts of specimen SL3, SLR4, SlR5 and SLR6. The energy values presented here, correspond to half load cycle i.e. push and relaxation. The values are determined from hysteresis curve, as calculated in case of short wall specimens. In terms of elasticity the specimen SLR4 exhibited maximum improvement. However, in terms of energy dissipation it does not display amelioration on the same scale. In each case, the bar charts exhibit a monotonic increase in energy dissipation with an increase in the load. The energy dissipation in the secondary cycles is smaller than that the first one. On the other hand very small decrease in elastic energy in the secondary cycles is observed. Energy dissipation in slender wall is due to sliding, concrete degradation and rebar plastic straining. The cracks smoothing and widening in subsequent cycles is a major cause of drop off in energy dissipation. In terms of dissipation ratio, ratio of dissipated energy to total energy, CFRP strengthened specimen SLR5 and SLR6 exhibited good performance.

The cumulative elastic and dissipated energy at each load level are depicted in the form of curves (Figure 6.43). The ordinate values correspond to summation of energy evaluated for the three complete cycles at each load level (drift). In terms of elasticity, the positive influence of external CFRP reinforcement arrangement is represented by rise in EE Vs drift curves for re-strengthened specimens in comparison to the control specimen SL3. The DE Vs drift curves depicts well the influence of additional CFRP arrangement on amelioration of energy dissipation capacity. However, its improvement is not better than the first one.

Dazio (Dazio 2000) found energy ratios of approximately 0.60 for slender, ductile walls subjected to static-cyclic loading and displacement ductility up to 6.0. Numerical simulations for investigating the influence of axial force on the behavior of such walls provided energy ratios between 0.45 and 0.80 for axial force ratios between 0.13 and 0.035, respectively. The decrease in energy dissipation with an increase in axial force may originate from both pinching of hysteretic loops and reduction of residual displacements. Lestuzzi (P. Lestuzzi 2000) examined records of dynamic tests of slender, ductile walls for energy dissipation. It was observed that the energy ratio is insensitive to the flexural strength of the walls. The energy ratios were between 0.60 and 0.70. The energy ratio curves of the slender wall specimens tested, shown in Figure 6.44, validates the above mentioned statement.

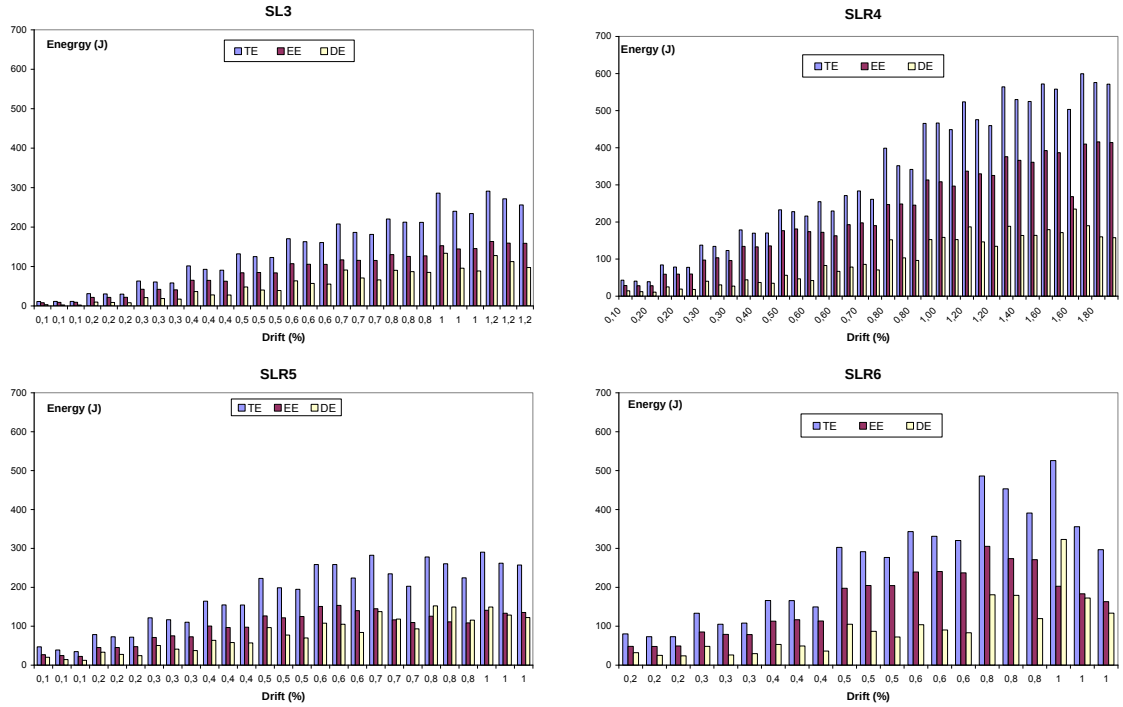

Figure 6.42: Specimen SL3, SLR4, SLR5 and SLR6 Energy bar chart

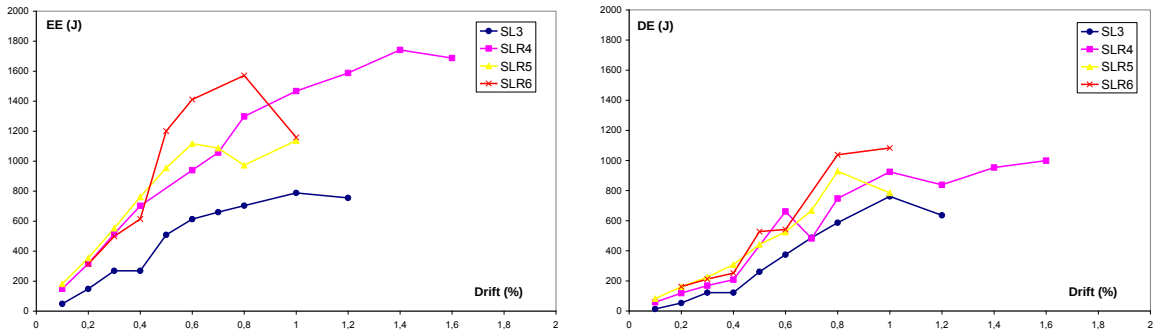

Figure 6.43: Specimen SL3, SLR4, SLR5 and SLR6 cumulative energy curves

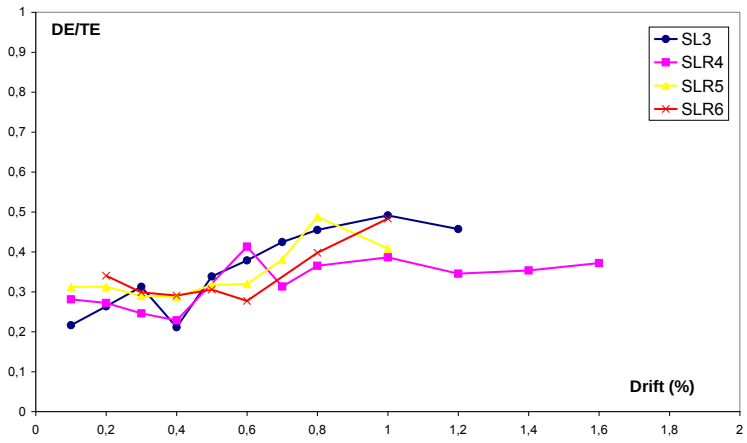

Figure 6.44: Ratio of DE to TE Vs Drift Curves

6.2.2.5 Damage Index

The bibliographic review of damage indicators has been discussed in section 6.2.1.7. Figure 6.45 shows the FDR Vs Drift curves of all slender RC walls subjected to cyclic load tests. The effect of changes made in the CFRP external reinforcement arrangement is well depicted by disparity in the curves. The relatively lower curves of retrofitted specimens as compared to that of specimen SL3 (RC wall only) highlights the positive influence of composite strengthening on limiting sustained damage. As FDR index is the ratio of the initial stiffness to final secant stiffness, therefore the smaller FDR values of retrofitted specimen represents an increase in the overall stiffness. In terms of FDR index the specimen SLR4 and SLR6 performed well. At 1% drift they exhibited a decrease in FDR up to 72% in comparison to SL3. Specimen SLR5 curve shows that its performance was first coherent with that of specimen SLR4 and SLR6 up to 0.6% drift. But latter on shows a steep incline, due to the crack concentration at hole (drilled within wall panel) and slipping of mesh anchor installed in it. In case of specimen SLR6 this was controlled by installment of a thicker mesh anchor (anchor made of 12 CFRP tows instead of 4) in wall panel.

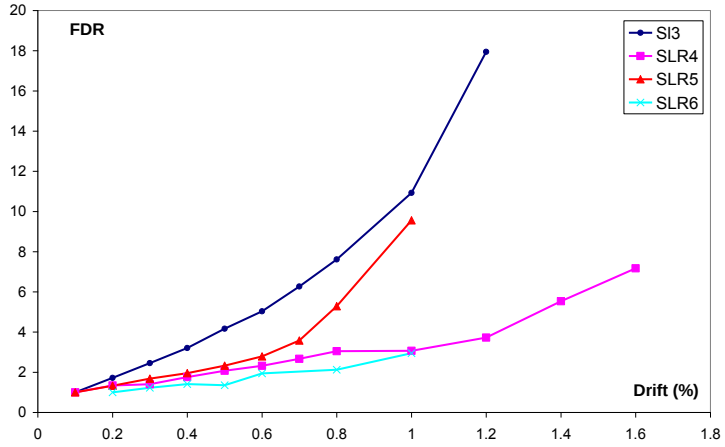

Figure 6.45: Flexural Damage Ratio SL3, SLR4, SLR5 & SR6

A plot of the evolution of the MFDR damage indicator with the passage of drift is shown in Figure 6.46. The curves of specimen SL3, SLR4 and SLR5 show an almost identical pattern till drift level of 0.7%. After which there is dissimilarity in behavior. The SLR4 curves first flatten due to slipping of CFRP strips and then incline as composite imitate to contribute in stiffness amelioration. The steeper incline observed in specimen SLR5 occurred due to placement of mesh anchors within the wall panel that controlled initial slipping of bonded CFRP strips. The higher inclination of SLR6 curve is attributed to same phenomenon and in this case the stiffness effect is higher due to installation of stronger anchors in the wall panel.

Figure 6.47 shows the Park's DI Vs deflection curves of all the four slender walls subjected to a displacement controlled cyclic load test. The curves of strengthened specimens are flatter as compared to non-strengthened specimen SL3 which depicts development of smaller displacement and lesser energy dissipation at identical load levels. This phenomenon is attributed to higher stiffness of composite reinforcement that in turn increases specimen stiffness and therefore reduces deflection and concrete crack propagation. As energy dissipation in RC structure element takes place due to friction in between concrete cracks and

rebar yielding therefore by reducing crack propagation, the specimen capacity to dissipate energy is reduced.

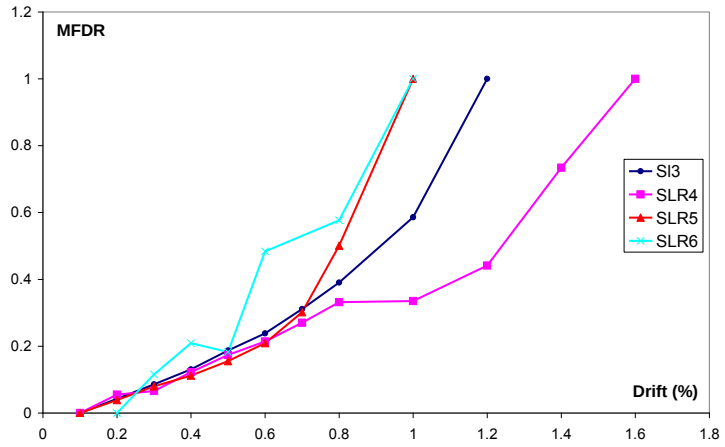

Figure 6.46: Modified Flexural Damage Ratio SL3, SLR4, SLR5 & SR6

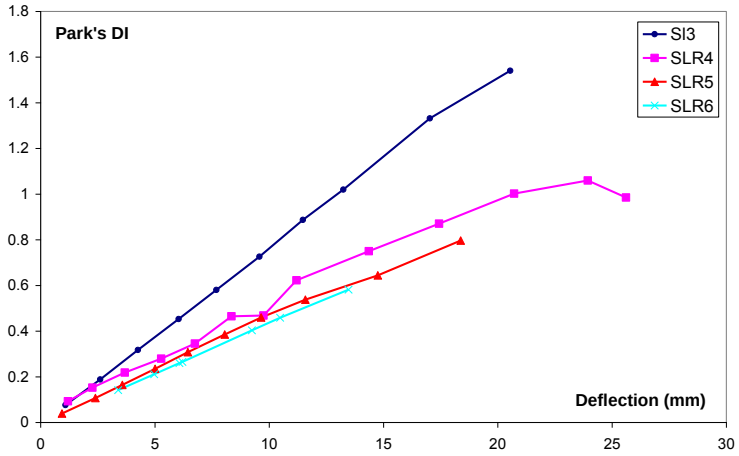

Figure 6.47: Park's Damage Index Vs Lateral Deflection

7 Conclusion

This part of thesis presents a series of monotonic and static cyclic tests of lightly reinforced shear walls strengthened with CFRP. The RC specimens used were not designed for earthquake actions and had uniformly distributed reinforcement (vertical and horizontal). The short wall specimen is the model of the bottom part of a two story building shear wall at 1:3 scale. All the specimens were tested as cantilevers with a constant axial force. The objective of the test series was to investigate the influence of external CFRP reinforcement on the load response behavior of lightly reinforced concrete walls. A total of six short and six slender RC walls were fabricated. They were under-reinforced to fail in shear and flexure, respectively. Four out of six specimens, in each case, were afterward strengthened with an external CFRP reinforcement.

The CFRP strips bonded to RC wall panel showed some improvement in the RC wall specimen ultimate load capacity, ductility, and reduced the crack propagation to a certain extent. The mesh anchor placed at the wall foundation joint inhibited the joint failure due to improper reinforcement arrangement in this region. They also reduced CFRP strips debonding problem, the major issue in external FRP reinforcement, by transfer of load effects from the bonded strips to lower foundation block. The partial FRP strengthening adopted here, proved to be successful as it did not deteriorate the RC wall energy dissipation capacity. As the RC structures dissipate energy due to concrete crack relative friction and rebar yielding. This arrangement ensured concrete cracking within the wall panel to some extent which in turn resulted in energy dissipation. Table 7.1 summarizes the test result for both monotonic and cyclic load test. The elastic energy and energy dissipated values listed in case of specimens subjected to cyclic load test is evaluated by summation of first complete cycle at each load level.

Table 7.1: Summary of test results

Specimen	Vu (kN)	Δu (mm)	EE (kJ)	ED (kJ)
S1	154.69	5.99	528.00	271.00
SR2	218.31	8.69	990.00	538.00
S3	138.69	7.43	4711.56	4027.71
SR4	170.53	9.81	9082.07	6857.37
SR5	169.44	12.10	11614.94	9860.96
SL1	25.06	14.43	195.00	128.00
SLR2	40.43	11.83	416.00	418.00
SL3	27.75	9.57	1665.00	1327.00
SLR4	43.44	14.90	4220.60	2486.22
SLR5	45.69	9.64	2433.67	1664.01
SLR6	56.63	10.48	1992.73	972.67

Part III: Numerical Analysis

8 Analysis of RC short wall

8.1 Introduction

Modeling of RC walls involves several challenges in representing the combine effects of axial load, shear forces and moment, in addition to rebar slip, buckling, damping, boundary conditions, as well as additional retrofitting/restrenthening techniques, if any (K. Galal and H. El-Sokkary 2008). In ideal case, the model should be capable to represent additional phenomenon like concrete cracking, tension stiffening, opening and closing of cracks with the recovery of stiffness, strength degradation with cyclic loading and confinement effects in compression, etc. However in majority of cases, one or more of these factors are neglected for simplicity of model, while ensuring that this approximation do not make a significant impact on model accuracy in simulating different behaviors of RC walls.

8.2 Review of RC wall analysis models

The different modeling techniques used previously by researchers for RC shear walls analysis are discussed in this section.

8.2.1 Fibre model

In this model, the member is divided longitudinally in to several segments each consisting of parallel layers representing concrete and steel material. The constitutive laws of concrete and steel materials are defined therefore the moment curvature relationship of the member at each load level can be evaluated. The model considers the axial flexure interaction and flexibility distribution along the member length. It was applied to determine the RC member behavior (Emori and Schnobrich 1981; G. Monti and Spacone 2000; R. Park et al. 1972). To simulate the behavior of RC shear wall under dynamic excitation, Kotronis et al. (Kotronis et al. 2005) used this model. The limitations in the model were: assumption of linear shear deformations, neglecting bond slip effect, and complexity of simulating the boundary conditions. Afterwards, Belmauden and Lestuzzi (Belmouden and Pierino Lestuzzi 2007) used this model to predict the non linear behavior of RC shear walls under reversed cyclic loading with consideration of the nonlinear shear behavior and effect of bar slip in analysis. Figure 8.1 shows the model used.

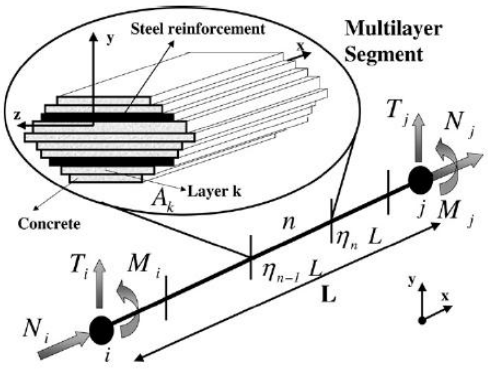

Figure 8.1: Mutli-layer finite element model (Belmouden and Pierino Lestuzzi 2007)

8.2.2 One component beam-column element

Giberson (Giberson 1967) developed an element, comprised of one linear elastic member with two nonlinear rotational springs at the two ends (Figure 8.2). The assumptions made were: lumped plasticity at the zero-length end springs, double curvature deformed shape with a fixed point of contra flexure at member middle, and the plain sections to remain plain. The model needs an appropriate hysteretic load-deformation model to be defined. This requires definition of different properties of the member's plastic hinges such as stiffness, strength, ductility, cyclic behavior, etc., which may be difficult unless some assumptions are to be considered. Recently, Tremblay et al. (Tremblay et al. 2001) and Panneton et al. (Panneton et al. 2006) used this model to examine the higher mode effects on the behavior of high-rise RC walls. They utilized the modified Takeda hysteretic model (Otani 1974) with degrading stiffness to simulate the inelastic behavior of the rotational springs, while shear deformations were assumed to be linear.

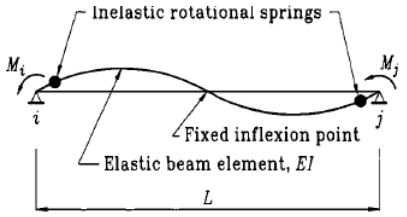

Figure 8.2: One-component element model.

8.2.3 Multiple spring model

Takayanagi and Schnobrich (Takayanagi and Schnobrich 1976) proposed a model, having a number of in elastic springs connected in series with rigid members as shown in Figure 8.3. The spring's inelastic properties varied according to the segment properties and the axial load level on that segment. The segment properties were assumed to be constant along its length. Emori and Schnobrich (Emori and Schnobrich 1981) used this model to simulate the shear wall of a 10-storey frame-wall building. It represented satisfactorily the nonlinear behavior of the structure under study. During analysis, linear shear deformations were assumed.

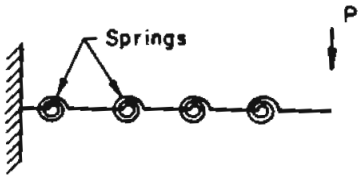

Figure 8.3: Multiple spring model (Takayanagi and Schnobrich 1976)

8.2.4 Multi axial spring (MS) model

Lai et al. (Lai et al. 1984) first proposed this model to simulate the axial-flexural relation of RC columns. It consisted of an elastic linear member with two multi axial spring elements of zero dimensions, one located at each end (Figure 8.4). The multi axial spring element was a combination of five concrete and four steel springs. Each spring was assumed to be uniaxially stressed and its behavior was governed by the hysteretic stress strain characteristics of the

material simulated i.e. concrete or steel. Galal (Galal 2008) used the canny wall element (Li 2006), which is based on MS model, to investigate the response of RC wall subjected to a lateral load. It considers the axial-flexural interaction, concrete cracking, stiffening in tension, and confinement effect in compression related to RC walls. To control the shear deformation of the wall, the model includes a non linear spring. The model depicted well the experiment results of both static and dynamic analysis.

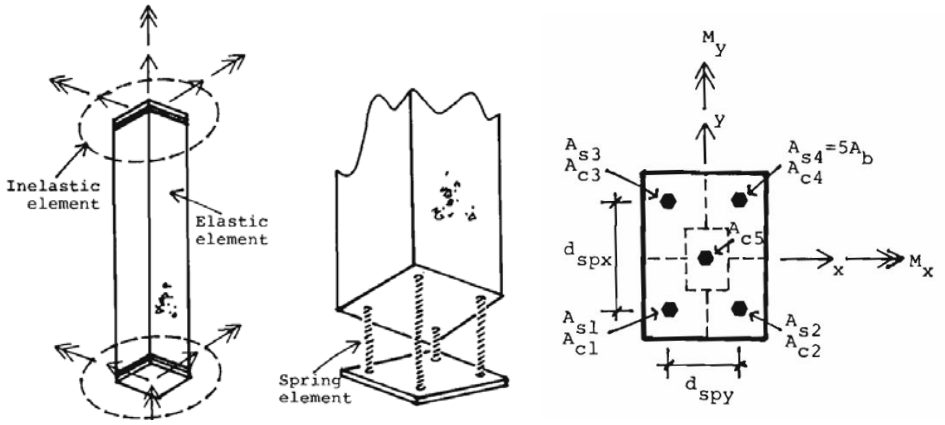

Figure 8.4: Multi-axial spring model (Lai et al. 1984): a) Member model, b) Inelastic element, c) Effective concrete and steel springs

8.2.5 Three vertical line element model

This model was developed by Kabayasawa et al. (Kabayesawa et al. 1982). It consisted of three vertical line elements, connected to two rigid bar (beams), located at the wall top and bottom. Two of the three vertical elements located at the wall extremity, consisted of one axial spring, to represent the boundary elements. A third one located at wall centre comprised of three springs to control vertical, horizontal and rotational deformations of the wall as shown in Figure 8.5(a). To overcome the issues like lack of deformation compatibility between wall and boundary elements and difficulty in defining springs properties. The model was modified later on by removing the rotational spring at the central element, and providing a coupling between the axial-flexure behaviors. To simulate the behavior of RC shear walls this modified model was used by researchers (T. Kim and Foutch 2007; Kunnath et al. 1990; Linde and H. Bachmann 1994). To reduce the complexity in defining hysteresis properties of modal spring elements, Vulcano and Bertero (Vulcano and Bertero 1986) proposed another modification in the vertical axial elements at wall extremity. The axial springs of the boundary element was replaced by two axial elements connected in series as shown in Figure 8.5(b). It is named as axial-element-in-series model (AESM). The upper one element represents the axial stiffness at boundary element where the bond between steel and concrete still exist and lower two elements where the bond is lost. Although this modified model was successful in predicting the flexure behavior of wall that showed flexural failure mode, but it could not simulate the actual shear deformation of wall that had shear deformation in dominance.

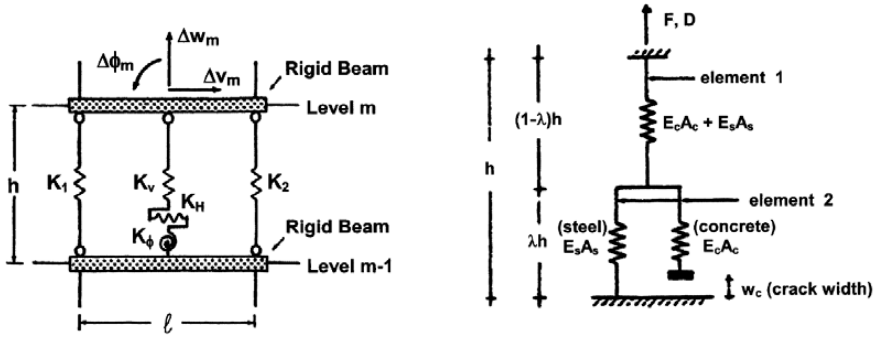

Figure 8.5: (a) Three Vertical Line Element model (b) Axial-element-in-series model

8.2.6 Multiple vertical line element model

Vulcano et al. (Vulcano et al. 1988) introduced this model to simulate wall behavior. It is consisted of a number of uniaxial elements connected in parallel by utilizing two infinitely rigid bars, one located at the wall top and other at bottom (Figure 8.6-a). The two external elements simulate the wall boundary elements while the rest of internal elements simulate the axial flexural behavior and a horizontal spring placed at the centre of model simulates wall inelastic shear behavior. The axial spring elements is a combination of two elements connected in series and each element itself is a combination of two uniaxial spring connected in parallel (Figure 8.6-b). Element 1 represents the uncracked concrete and steel behavior while element 2 represents cracked concrete and steel behavior where the bond is lost. Though the model predicted well the performance of wall in flexure but it could not couple the wall shear and flexure behavior. Researchers (Vincenzo Colotti 1993; Fischinger et al. 1990; Orakcal and Wallace 2006) have introduced some modification in the model and constitutive laws for concrete and steel to improve model efficiency in predicting RC shear wall response without compromising on accuracy.

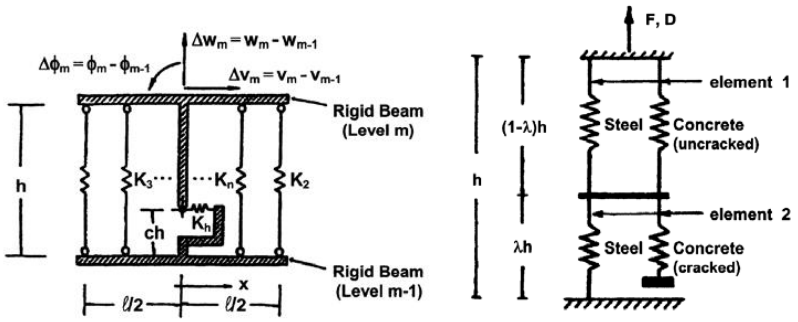

Figure 8.6: (a) Multiple vertical line element model (b) Modified axial-element-in-series Model (Vulcano et al. 1988)

8.2.7 Shear crack model

Greifenhagen (Greifenhagen C. 2006) used this model to simulate squat wall, subjected to a cyclic load test. He derived the idea from Bachmann (H. Bachmann 1967), who proposed a model for plastic hinges in support zones of continuous RC beams. In this case, wall is considered as a plastic hinge consisting of discrete cracks (inclined relative to member axis) and rigid bodies as shown in Figure 8.7. The widening of such cracks result in rotation which is assumed to be constant over the plastic hinge length. This model takes into account both

axial force and base shear. The model is based on certain assumption such as crack pattern, localization of concrete compressive strain near the wall base, bond, and strength decay. The model encompasses failure modes: concrete crushing, reinforcement rupture and shear sliding. It can predict well the wall static cyclic and shear strength envelope.

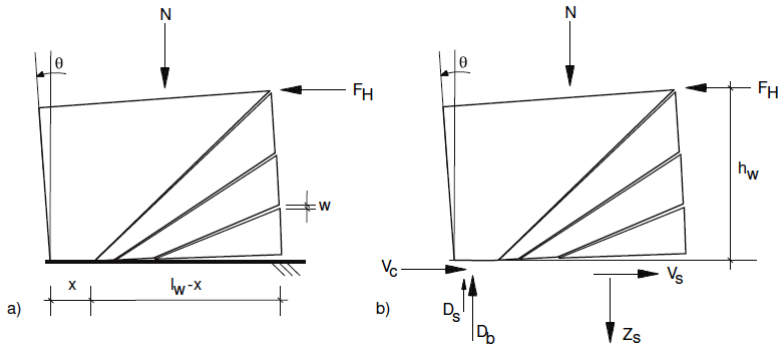

Figure 8.7: Shear crack model (a) geometry (b) Reaction forces in the base joint

8.2.8 Truss model

Oesterle at al. (Oesterle et al. 1984) used a truss model for analysis of RC wall. It consists of two vertical boundary elements to carry wall moments, diagonal compression members called struts that represent concrete and horizontal tie members representing shear steel reinforcement. The model predicts well the shear capacity of wall.

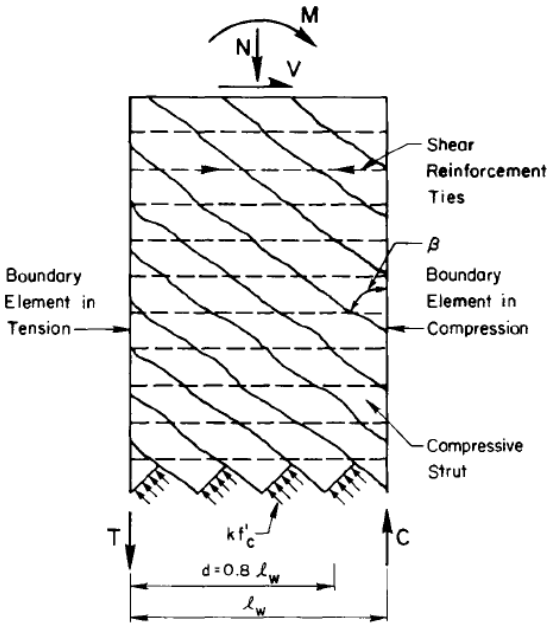

Figure 8.8: Truss model

Hwang et al. (Hwang et al. 2001) proposed a strut and tie model to evaluate the shear strength of a squat wall for diagonal compression failure. The model satisfies equilibrium, compatibility and constitutive law of cracked reinforced concrete. It is based on the assembly

of diagonal, horizontal and vertical shear resisting mechanisms for wall (Figure 8.9). The model predicts well the wall shear strength.

The depth of the diagonal strut (a_s) depends on its end condition is provided by the compression zone at the base of the wall. It is intuitively assumed that

$$a_s = a_w \qquad \text{Eq. 8.1}$$

Here a_w = depth of the compression zone at the base of the wall.

For simplicity, a_w was approximated with Paulay and Priestley's (1992) equation used to evaluate the depth of the flexural compression zone of an elastic column.

$$a_s = \left(0.25 + .85\frac{N}{A_w f_c^{'}}\right) \times l_w \qquad \text{Eq. 8.2}$$

Here: N = axial force, A_w = net area of the concrete section (wall panel), l_w = length of the wall section in the direction of the shear force and $f_c^{'}$ = compressive strength of the concrete.

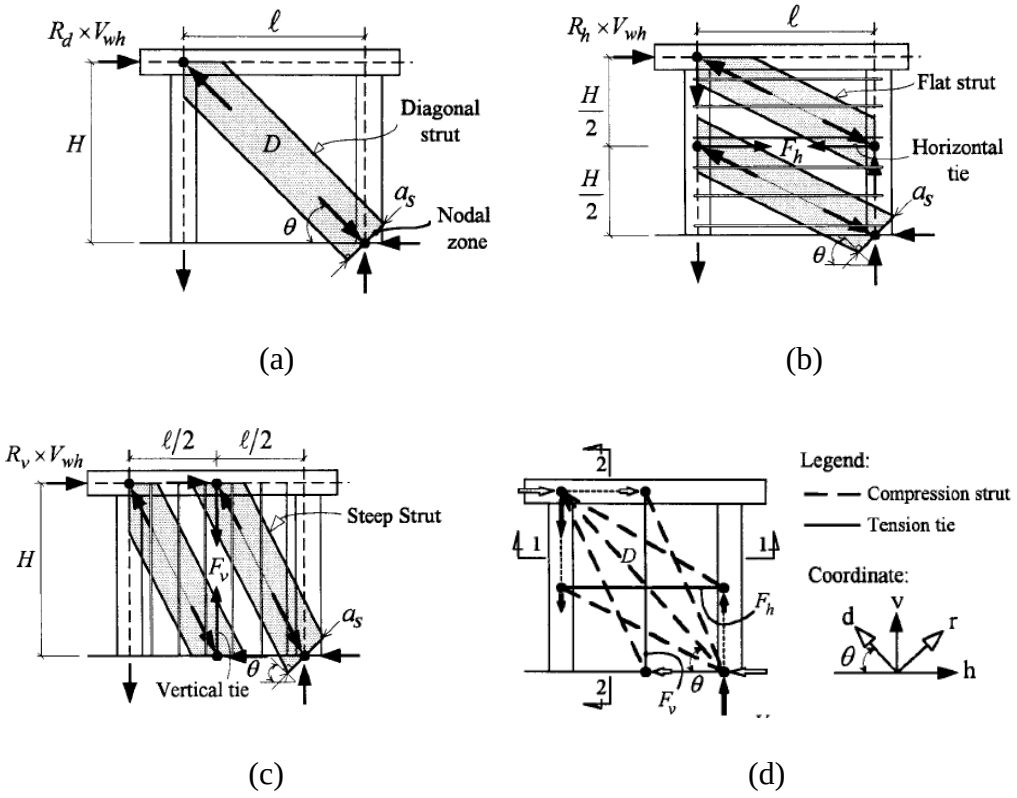

Figure 8.9: Softened-Strut-and-Tie model

Greifenhagen used the strut and tie model for the calculation of non linear response of a specimen (labeled as S4: $\rho_v = \rho_h = 1.03\%$) tested by Maier and Thürlimann (Figure 8.10). The model he used consisted of an assembly of trusses. Each truss consisted of a tie and strut. The

tie locations were based on location of vertical steel rebar location in test specimen. The analysis mechanism he adopted is shown in Figure 8.10-c.

Based on the simplicity of the truss model and its easy implementation in the commercially available structural analysis software like RSAP, SAP2000, SAFE etc, it was used to evaluate the load response analysis of wall. The truss model was mostly used successfully by researchers for evaluation of shear strength of RC short wall. It was used in design codes (*AASTHO LRFD Bridge Design Specifications, 2nd Edition* 1998; ACI Committee 318 2005; CSA Committee A23.3-94 1994; FIP-Commission 3 1996) to evaluate the reinforcement detail for the shear dominated structural members or D region of members. It has been used for analysis of deep beams (Aguilar et al. 2002; Carlos G. Quintero-Febres et al. 2006; Mitchell et al. 2002; Rogowsky et al. 1986; Uribe and Alcocer 2001). The model in detail is discussed in the following section.

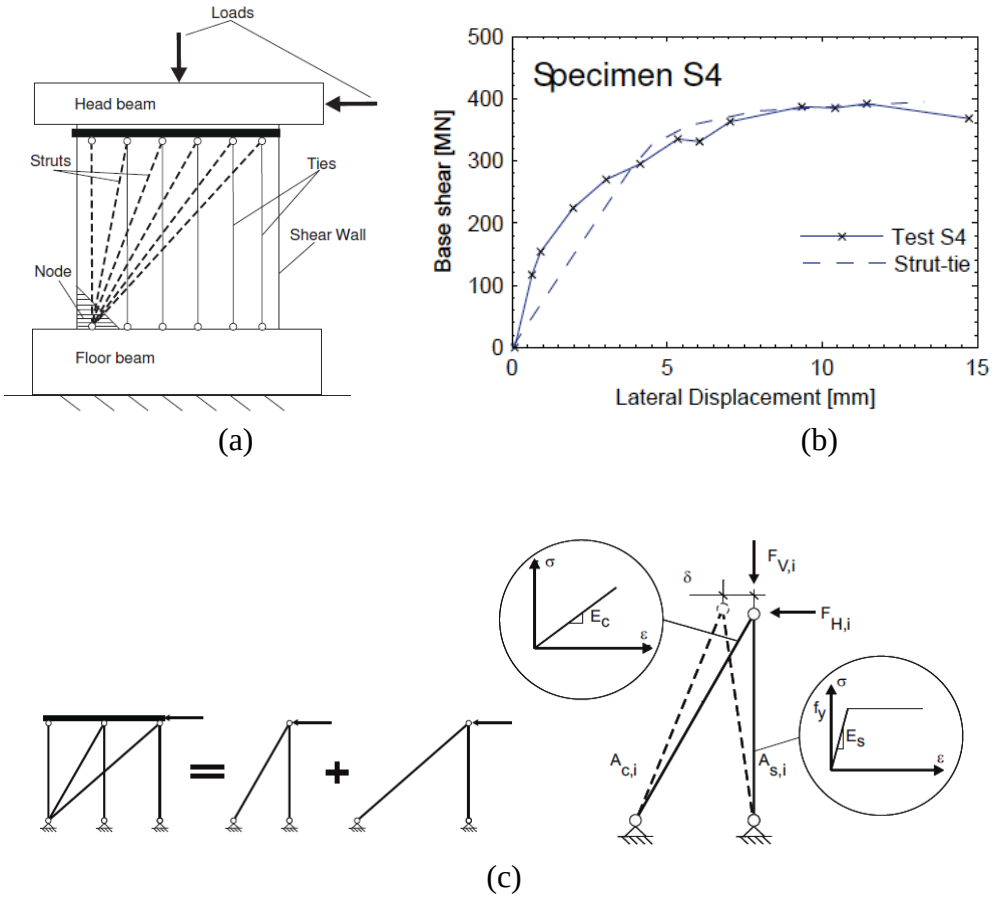

Figure 8.10: Greifenhagen Strut-and-Tie model for squat RC wall (a) model (b) results and (c) sub models and their stress strain relation ship

8.3 Strut and Tie Model in Detail

The STM is an equilibrium method of analysis and design of discontinuity regions (D-regions) in reinforced and pre-stressed concrete structures (Tjhin and Kuchma 2007). The D-regions are part of structure where strain distribution is not linear. It includes parts of structure near concentrated loads/reactions or abrupt change in geometry (holes/change in cross section) (ACI Committee 318 2005; James G. MacGregor 2002; Tjhin and Kuchma 2007).

Figure 8.11 gives a schematic view of the D regions. In these regions the traditional flexural theory and traditional design approach for shear (V_c + V_s) does not apply (James G. MacGregor 2002). The D regions are modeled by a hypothetical truss model based on assumption that major portion of load transfer occur directly to supports, by in plane compressive forces in concrete and tensile forces in reinforcement. The idea of using a truss model was first proposed by Ritter (Ritter 1899) and Mörsch (Mörsch 1909) in the early 1900's for shear design of flexural concrete members. The publications of Collins and Mitchell (Collins and Mitchell 1986) and Schlaich et al. (Schlaich et al. 1987) played a key role in wide-spread acceptance of truss model.

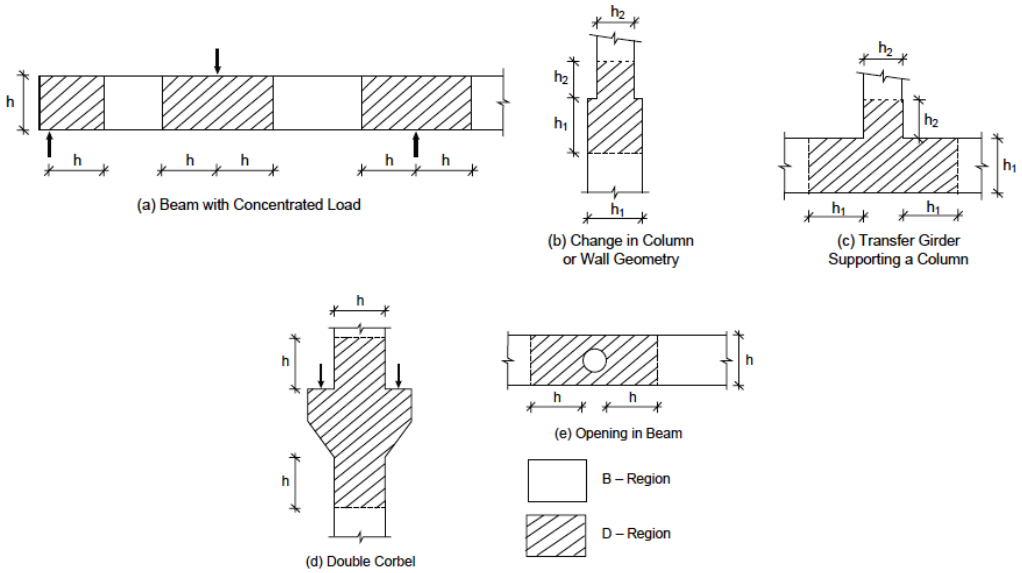

Figure 8.11: Load and Geometric Discontinuities

The truss or STM model is comprised of concrete struts stressed in compression, steel ties stressed in tension and nodes where the struts and tie joins together (Figure 8.12). The truss components are discussed one by one in the following paragraphs.

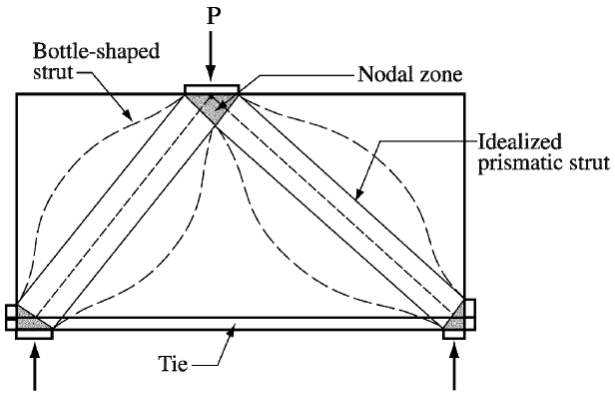

Figure 8.12: Description of strut-and-tie model.

8.3.1 Struts

Struts are the compression elements of the strut-and-tie model. They represent the resultants of a compression field and are modeled as either parallel or fan shaped (Figure 8.13). They serve as either the compression chord of the truss mechanism which resists moment or they serve as the diagonal struts which transfer shear to the supports. The struts in general has three shapes: Bottle shape, (Figure 8.12) the common one because the strut stresses wider concrete at mid length than at ends, prismatic shape, ideal for design simplification, and tapered shape when the nodal zones at two ends have different strengths (ACI Committee 318 2005).

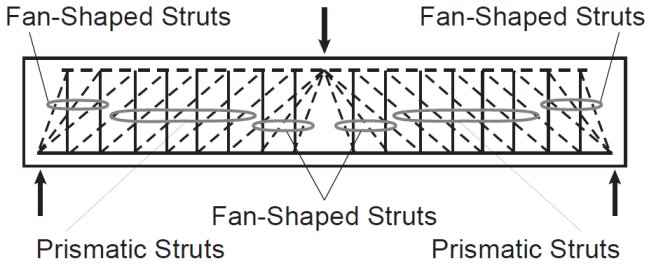

Figure 8.13: Prismatic and Fan-Shaped Struts.

The design specification, for evaluation of strut strengths, in ACI 318-05 code, AASHTO LRFD and DIN1045-1 is discussed one by one below.

8.3.1.1 ACI 318-05

The nominal compressive strength of a strut without longitudinal reinforcement is evaluated with equations Eq. 8.3 and Eq. 8.4 (ref Appendix A).

$$F_{ns} = f_{ce} A_{cs} \qquad \text{Eq. 8.3}$$

$$f_{ce} = 0.85 \beta_s f_c^{'} \qquad \text{Eq. 8.4}$$

Here A_{cs} = the cross-sectional area at the strut end and f_{ce} = the effective compressive strength of the concrete in a strut. The β_s factor accounts for the effect of cracking and possible presence of transverse reinforcement in struts. The value of β_s attributed in different cases is summarized as below:-

Struts in compression member

Prismatic: $\beta_s = 1.0$

Bottle shaped with reinforcement to resist concrete transverse splitting: $\beta_s = 0.75$

Bottle shaped without reinforcement to resist concrete transverse splitting: $\beta_s = 0.60\lambda$

$\lambda = 1.0$ for normal weight concrete

$\lambda = 0.85$ for sand-lightweight concrete

$\lambda = 0.75$ for all lightweight concrete

Strut intersecting cracks in tensile zone: $\beta_s = 0.40$

All other cases: $\beta_s = 0.60$
To use $\beta_s = 0.75$ in case of $f_c^{'} \leq 6$ ksi, the reinforcement across strut should satisfy Eq. 8.5 or else $\beta s = 0.60\lambda$ should be used.

$$\sum \frac{A_{si}}{b_s s_i} \sin \gamma_i \geq 0.003 \qquad \text{Eq. 8.5}$$

Here A_{si} is the total area of reinforcement at spacing S_i in a layer of reinforcement with bars at an angle γ_i to the axis of the strut (Figure 8.14), and b_s is the width of the strut.

In case of struts having compression reinforcement aligned parallel to its axis, the total strength of the strut can be evaluated as

$$F_{ns} = f_{ce} A_{cs} + A_s^{'} f_s^{'} \qquad \text{Eq. 8.6}$$

Here $f_s^{'}$ is the stress in the longitudinal strut reinforcement at nominal strength. In case of Grade 40 and 60 rebar $f_s^{'} = f_y$.

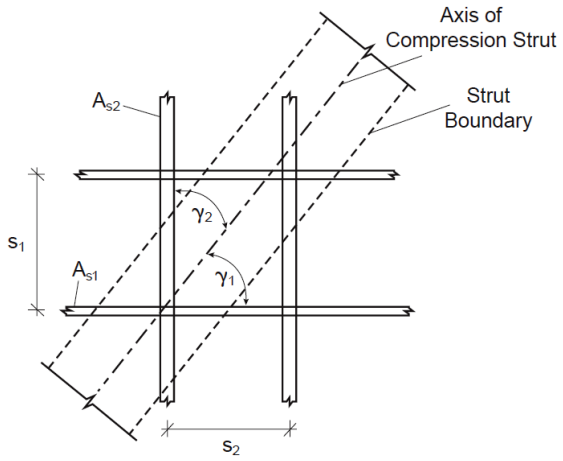

Figure 8.14: Layers of Reinforcement to Restrain Splitting Cracks of Struts.

8.3.1.2 AASHTO LRFD

The compressive strength of strut with and without reinforcement is given by equations Eq. 8.7 & Eq. 8.8, respectively (ref section 5.6).

$$P_n = 0.7 f_{cu} A_{cs} \qquad \text{Eq. 8.7}$$

$$P_n = 0.7 f_{cu} A_{cs} + f_y A_{ss} \qquad \text{Eq. 8.8}$$

$$f_{cu} = \frac{f_c^{'}}{0.8 + 170\varepsilon_1} \leq 0.85 f_c^{'} \qquad \text{Eq. 8.9}$$

$$\varepsilon_1 = \varepsilon_s + (\varepsilon_s + 0.002)\cot^2 \alpha_s \qquad \text{Eq. 8.10}$$

Here: P_n = nominal resistance of strut or tie, f_{cu} = the limiting compressive stress, A_{cs} = effective cross-sectional area of strut, A_{ss} =area of reinforcement in the strut, ε_s = the tensile strain in the concrete in the direction of the tension tie, α_s = the smallest angle between the compressive strut and adjoining tension ties.

Checking for crack control in struts includes provision of orthogonal grid of reinforcing bars near each face across struts with spacing ≤ 12.0 in and that the ratio of reinforcement in each direction must be greater than 0.003.

8.3.1.3 DIN1045-1

According to this code, the compressive strength capacity of strut without reinforcement, for uncracked concrete compressive zones and the one parallel to cracks is given by equations Eq. 8.11 & Eq. 8.12 (ref section 10.6)

$$Strength = \eta_1 f_{cd} A_{cs} \qquad \text{Eq. 8.11}$$

$$Strength = 0.75\eta_1 f_{cd} A_{cs} \qquad \text{Eq. 8.12}$$

Here:
η_1 =1 for normal concrete.
$\eta_1 = 0.4 + 0.6(\rho / 2200)$ for lightweight concrete
f_{cd} = design concrete compressive strength.

No equation is available for taking into account the reinforcement contribution in strut compression capacity. The only information given in respect of reinforcement is that the stress in reinforcement shall not exceed the steel design yield strength.

To check strut crack, the reinforcement ratio provided should satisfy that:

$$\rho_w = \frac{A_{sw}}{s_w b_w \sin\alpha} \geq \rho \qquad \text{Eq. 8.13}$$

$$\rho = 0.16\left(\frac{f_{ctm}}{f_{yk}}\right) \qquad \text{Eq. 8.14}$$

Here:
f_{ctm} = Mean axial tensile strength of concrete
f_{yk} = characteristic yield strength of reinforcing steel.

8.3.2 Ties

Ties are the tension elements of the strut-and-tie model. A tie consists of steel reinforcement (deformed bar or prestressing or both), plus a portion of surrounding concrete that is concentric with the axis of tie. The surrounding concrete is not considered in axial strength.

However, it lessens the elongation of the tie (tension stiffening, in particular, especially under service load. It also defines the zone in which the forces in struts and ties are to be anchored (ref. ACI 318-05 Appendix A.1).

The design specifications for tie available in codes such as ACI 318-05, AASHTO LRFD and DIN1045-1 are discussed one by one below.

8.3.2.1 ACI 318-05

In this case the tie nominal strength is evaluated as the summation of steel rebar yield strength and force in prestressing steel.

$$F_{nt} = A_{ts} f_y + A_{tp}(f_{se} + \Delta f_p) \qquad \text{Eq. 8.15}$$

where: $f_{se} + \Delta f_p \leq f_{py}$

Here: A_{ts} is the non prestressed reinforcement in tie, A_{tp} is the prestressed reinforcement in tie, f_y is the reinforcement yield strength, f_{se} is the effective stress in prestressing steel, Δf_p is the stress increase in prestressing steel due to factored load, f_{py} is the yield strength for prestressed steel.

The axis of tie assumed in model should coincide with the centroidal axis of reinforcement because tie represents tension element in truss.

8.3.2.2 AASHTO LRFD

Reinforcement must be proportioned to resist the tie forces in the strut-and-tie model, must be placed to coincide with the location of the ties, and must be appropriately anchored. The nominal resistance of a tension tie shall be taken as:

$$P_n = f_y A_{st} + A_{ps}(f_{pe} + f_y) \qquad \text{Eq. 8.16}$$

Here: f_y = yield strength of mild steel longitudinal reinforcement, A_{st} = total area of longitudinal mild steel reinforcement in the tie, A_{ps} = area of prestressing steel, and f_{pe} =stress in prestressing steel due to prestress after losses.

8.3.2.3 DIN1045-1

The tie strength in this case is equivalent to design yield strength of tie rebar and for prestressed steel it is considered equivalent to

$$f_{p0.1k}/\gamma_s$$

Here:
$f_{p0.1k}$ = Characteristic 0.1% proof stress of prestressing steel
γ_s = Reinforcement partial safety factor =1.15

8.3.3 Nodes

Nodes are the intersection points of the axes of the struts, ties and concentrated loads. To maintain equilibrium at node, at least three forces should act on it. On the basis of the type of forces acting on node (with three forces on it) they are labeled as CCC, CCT, CTT and TTT (Figure 8.15). Here C stands for compression and T for tension.

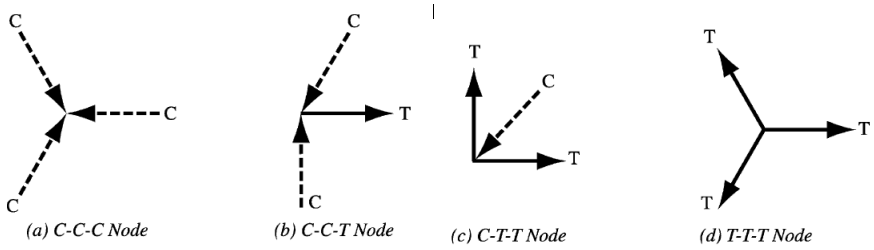

Figure 8.15: Classification of nodes.

A nodal zone is defined as the concrete volume that is assumed to transfers the strut and tie forces through node. Generally the nodal zone has three planes. The one that has equivalent stresses on all its in-plane sides is called the hydrostatic nodal zone (Figure 8.16). Its loaded faces are perpendicular to the axes of the applied forces, struts and ties. In this case the ratio of stresses is proportional to the ratio of the length of nodal zone sides.

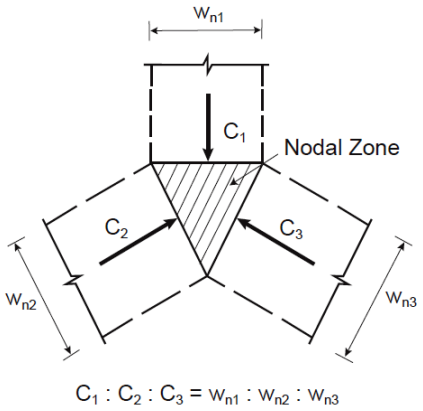

Figure 8.16: Hydrostatic nodal zone

8.3.3.1 ACI 318-05

The nominal compressive strength at the face of a nodal zone according to ACI 318-05 A.5 is

$$F_{nn} = f_{ce} A_{nz} \qquad \text{Eq. 8.17}$$

$$f_{ce} = 0.85 \beta_n f_c^{'} \qquad \text{Eq. 8.18}$$

Here:

f_{ce} = Effective concrete compressive strength in the nodal zone

A_{nz} = Area of the face of nodal zone perpendicular to strut axis

β_n = Influence factor of the type of forces acting on node

β_n = 1 in nodal zones bounded by struts or bearing areas (e.g., C-C-C nodes)

β_n = 0.8 in nodal zones anchoring one tie (e.g., C-C-T nodes)

β_n = 0.6 in nodal zones anchoring two or more ties (e.g., C-T-T or T-T-T nodes)

In order to mitigate the potential cracking problems and to avoid incompatibilities due to shortening of the struts and lengthening of the tie in almost the same direction at any single node, the angle between axes of a strut and tie should not be taken less than 25 degree.

8.3.3.2 AASHTO LRFD

In this case the concrete compression stress in the nodal zone shall be

$0.85 f_c^{'}$ in case of CCC node

$0.75 f_c^{'}$ in case of CCT node

$0.65 f_c^{'}$ in case of CTT node

In this case there is no limit for the angle in between strut and tie at as single node.

8.3.3.3 DIN1045-1

The nominal compressive stress for nodal zone in this case is

For CCC node

$$1.1\eta_1 f_{cd}$$

For CCT and CCT node, such that angle in between strut and tie great or equal to 45 degree

$$0.75\eta_1 f_{cd}$$

Here:

η_1 =1 for normal concrete.

$\eta_1 = 0.4 + 0.6(\rho / 2200)$ for lightweight concrete

f_{cd} = design concrete compressive strength.

In this case the angle in between strut and tie axes at a single node should not be less than 45 degree.

The ACI 318-05 design guidelines for strut and tie model were used in this research. It was chosen on the basis of its comprehensiveness and simplicity in design equation.

8.4 Modeling

The modeling of RC wall and RC wall plus CFRP, subjected to monotonic load test were conducted by using commercially available software named Autodesk Robot Structural Analysis Professional (RSAP) 2012. This software was used due to its easy implementation and flexibility in modeling to some extent.

8.4.1 Model geometry

The RC wall was simulated as a two dimensional strut and tie model, shown in Figure 8.17. The dotted lines represent struts, comprised of concrete only, solid vertical lines represent ties consisted of steel rebar and a horizontal solid line at the top represents a rigid bar. The most crucial step in strut and tie modeling is the decision of load path and arrangement of struts and ties. The strut and tie pattern used here is based on: vertical rebar location in the test specimen and static load induced at wall top (load end). To make the model as simple as possible: (a) the concrete cover around the tie was not considered, because tie concrete cover do not contribute in resistance, and is provided mainly for tension stiffening particularly under service loads (ACI Committee 318 2005), (b) horizontal reinforcement was replaced by fixing ties at the lower end, and (c) vertical load induced on test specimen was taken into account in modeling while defining concrete strut dimension only. In case of RC wall strengthened with external CFRP bonding, the tie bar was used as a steel CFRP composite bar or replacing tie bars after steel yield with composite bar that had cross sectional area equivalent to CFRP band used.

The struts width was taken equivalent to the width of wall panel (*AASTHO LRFD Bridge Design Specifications, 2nd Edition* 1998; ACI Committee 318 2005; Hwang et al. 2001) and its breadth equivalent to the depth of compression zone at the base of wall (Hwang et al. 2001) (Eq. 8.2). The struts were shaped as prismatic; therefore the concrete strength was taken equivalent to $0.85\beta_s f_c^{'} = 0.85*1* f_c^{'}$ (According to ACI Code 318-05).

Tie bar diameter was taken equivalent to two times the diameter of rebar, used in the test specimen. In place of horizontal tie bars in the model, vertical tie bars were fixed at the bottom.

The node width was taken equivalent to wall panel width. In plane dimension of node at wall free end bottom i.e., node length and height was taken equivalent to a_s. The node used was a CCC type therefore the concrete strength was equivalent to $0.85\beta_n f_c^{'} = 0.85*1* f_c^{'}$ (According to ACI Code 318-05). Figure 8.18 and Figure 8.19 shows the analysis pattern adopted in detail.

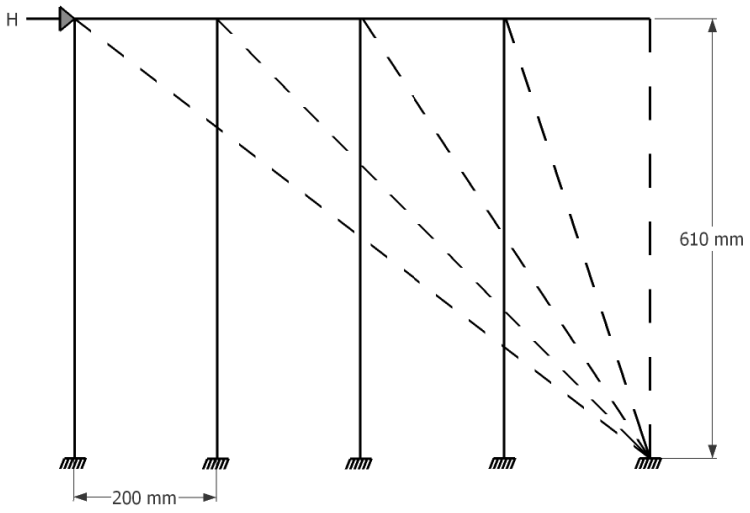

Figure 8.17: Strut and tie arrangement of RC short wall model

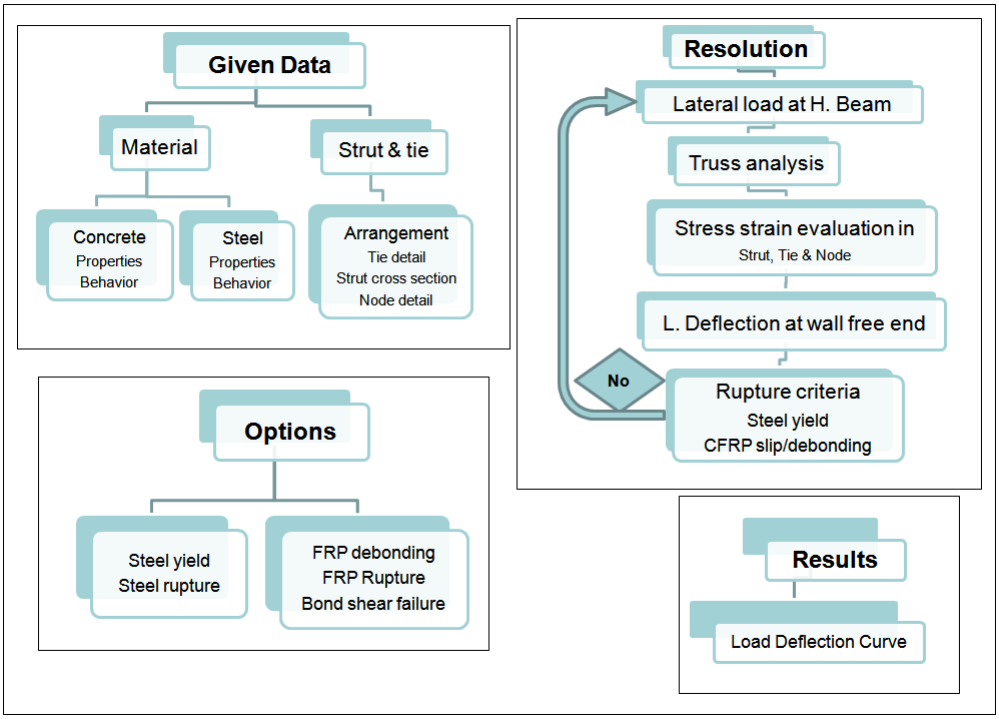

Figure 8.18: Software analysis pattern

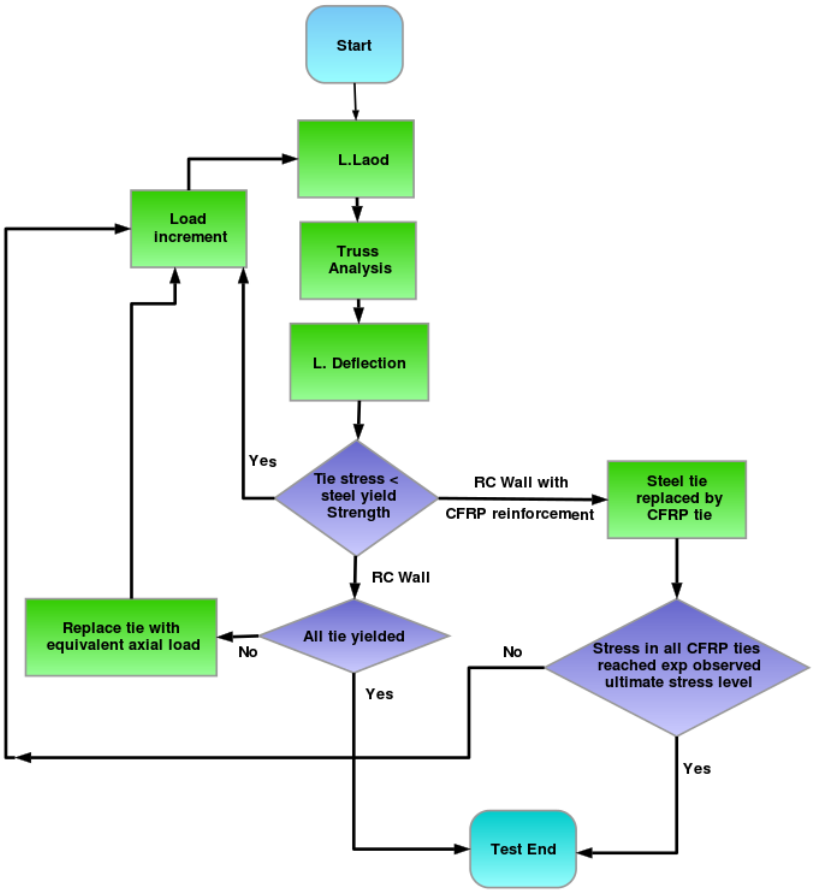

Figure 8.19: Strut and tie analysis flow chart

8.4.2 Material characteristics

Concrete:

Strength in compression: 30 MPa

Steel:

Number of steel ties: 4
Yield strength: 500 MPa
Elastic modulus: 210000 MPa

Composite:

Thickness of composite on lateral face: 0.48 mm
Length of composite band: 610 mm
Width of composite band: 50 mm
Pre-stress force on composite: 0 N
Ultimate stress: 1 400 MPa
Young Modulus: 105 000 MPa

8.4.3 Laws of behavior

The selection of compression and tension behavior of materials is an important step in designing as it significantly influence the stress distribution in the section and hence the values of internal forces and specimen global load displacement behavior.

8.4.3.1 Concrete behavior in compression

The concrete behavior in compression is defined by Sargin law (Figure 8.20).

$$\frac{\sigma_b}{f_{cj}} = \frac{k\left(\frac{\varepsilon_b}{\varepsilon_{bo}}\right) + (k^{'} - 1)\left(\frac{\varepsilon_b}{\varepsilon_{bo}}\right)^2}{1 + (k-2)\left(\frac{\varepsilon_b}{\varepsilon_{bo}}\right) + k^{'}\left(\frac{\varepsilon_b}{\varepsilon_{bo}}\right)^2} \qquad \text{Eq. 8.19}$$

$$k = \frac{E_{ij}\varepsilon_{bo}}{f_{cj}} \;\&\; k^{'} = k - 1$$

Where ε_{bo}: concrete deformation in compression corresponding to σ_b/f_{cj}, ε_b: concrete ultimate deformation and E_{bj}: initial tangent modulus.

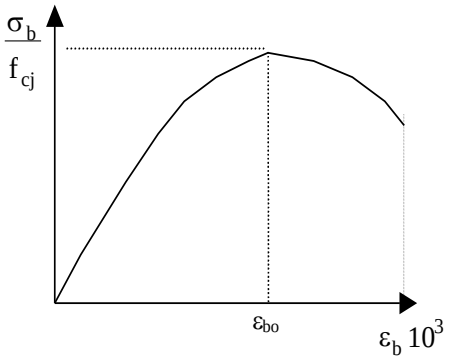

Figure 8.20: Law of concrete behavior in compression

8.4.3.2 Law of steel behavior

The steel behavior is considered as elastic-plastic, neglecting steel hardening as illustrated by the simplified bilinear curve represented in Figure 8.21. The parameters used here are modulus of elasticity (E_s) and the design yield strength of reinforcement (f_{yd}). In addition the steel strain is considered unlimited as shown in the figure in accordance with the French annex to Eurocode 2 (Eurocode 2 2005).

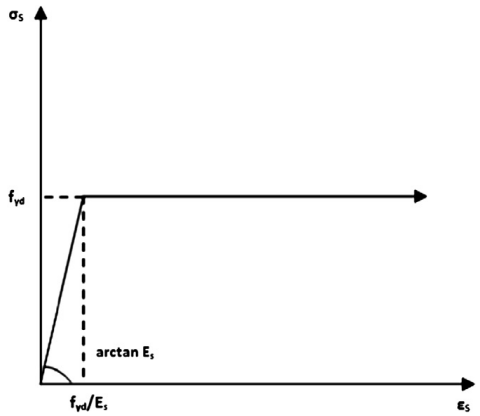

Figure 8.21: Law of steel tensile behavior

8.4.3.3 Law of composite behavior

The behavior of the composite plate is considered as elastic linear till failure (Figure 8.22). In this case, the parameters to be determined are the modulus of elasticity (E_c) and rupture stress (f_c).

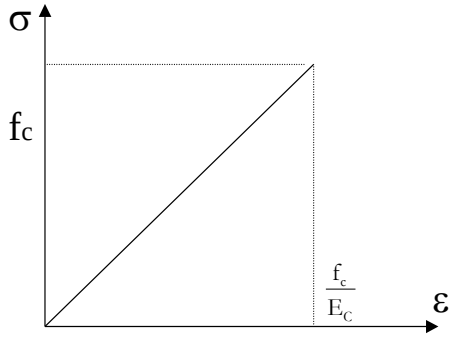

Figure 8.22: Law of composite behavior

8.4.4 Results

Figure 8.23 shows the specimen S1 load displacement curves: (a) based on observed test data, (b) evaluated with strut and tie model. The model represents the load displacement behavior of the tested specimen well to a certain extent, based on the use of a simplified model. The model predicted well the specimen yielding and its ultimate capacity. However, it did not forecast well the specimen initial stiffness and deformability. The model behavior was controlled by tie bar behavior, as the strut dimensions taken were larger and therefore the compressive stresses in strut were well below than its strength. The strut and tie model predicted ultimate capacity for specimen S1 was 148.8 kN while the actual was 157.8 kN.

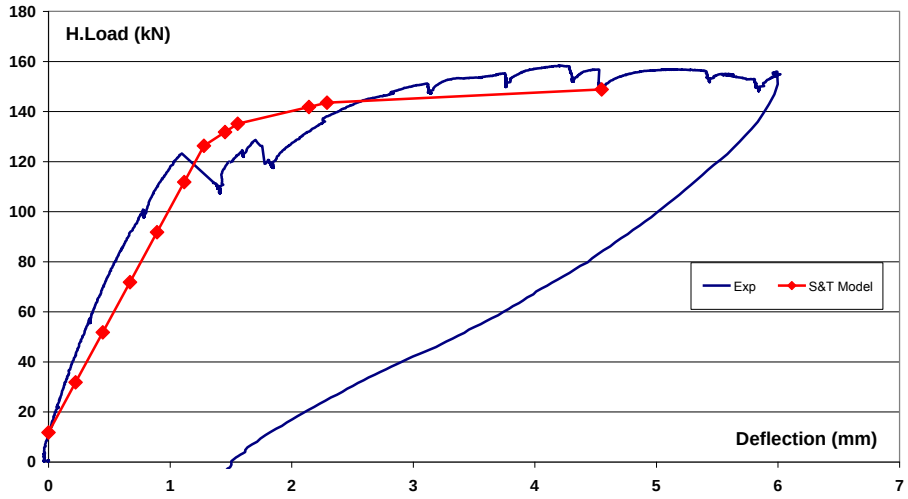

Figure 8.23: Specimen S1 loads Displacement curves: experimental and strut and tie model

Figure 8.24 depicts the specimen SR2 load displacement curves: (a) based on measured test data, (b) evaluated with strut and tie model with difference in tie bar used. To evaluate the contribution of external CFRP reinforcement, tie bars with different configuration were used in this model. In the case depicted by blue line curve, first tie that represented steel rebar as used in case of specimen S1 modeling were used and then as steel yielded they were replaced with the one that represented composite material. The CFRP tie area was taken equivalent to the two CFRP strips bonded vertically on wall two faces. In this case the evaluated curve showed coherence particularly in an interval of 110-160 kN but afterward deviated from the experimentally observed curve. In the model the observed CFRP slip during experiment was negated and the ties were assumed to capitalize CFRP full strength. In the third case, described by green line curve, the CFRP slip phenomenon neglected in the second case was considered and the maximum stress observed in CFRP strip during experiment was taken as its ultimate capacity (316 Mpa). In this case the evaluated curve was coherent to the experimental curve for the most part and depicted well the test specimen deformability. However, the ultimate load value was 185 kN as against the experimental 218 kN value.

Figure 8.25 shows the load displacement curves of FRP reinforcement arrangement other than evaluated experimentally to find out their contribution in improving short wall performance. Table 5.7 lists the dimension and properties of the FRP reinforcement material used along with evaluated load capacity of the strengthened specimens.

Table 8.1: Numerous FRP arrangement configuration plus ultimate load of strengthened wall.

Strengthening System	Ef (Mpa)	bf (mm)	Strength (kN)
RC + GFRP Strip	40000	50	167,64
RC + CFRP Strip	105000	50	184,75
RC + CFRP Strip	105000	100	235
RC + CFRP HR Laminate	160000	50	182,45
RC + CFRP HR Laminate	160000	100	233,4
RC + CFRP HM Laminate	350000	100	250

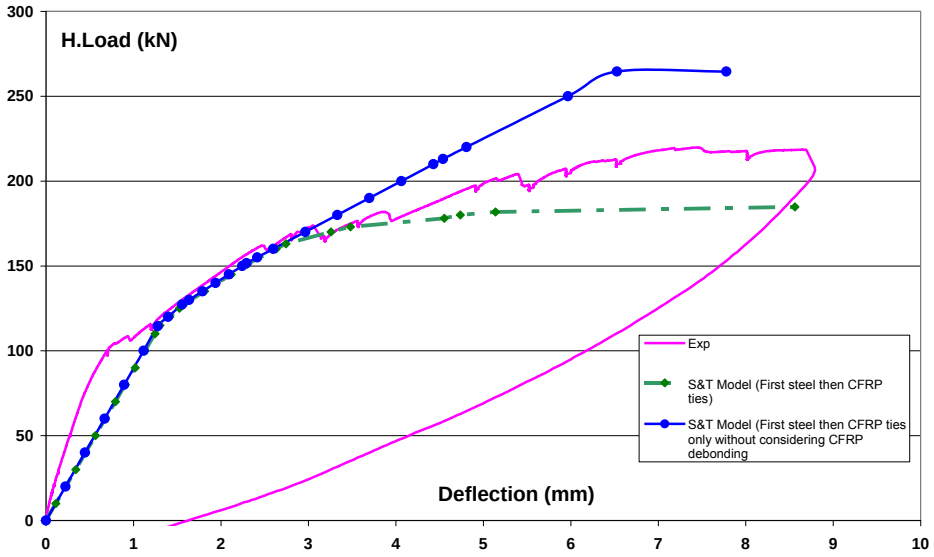

Figure 8.24: Specimen S2R loads displacement curves: experimental and strut and tie model

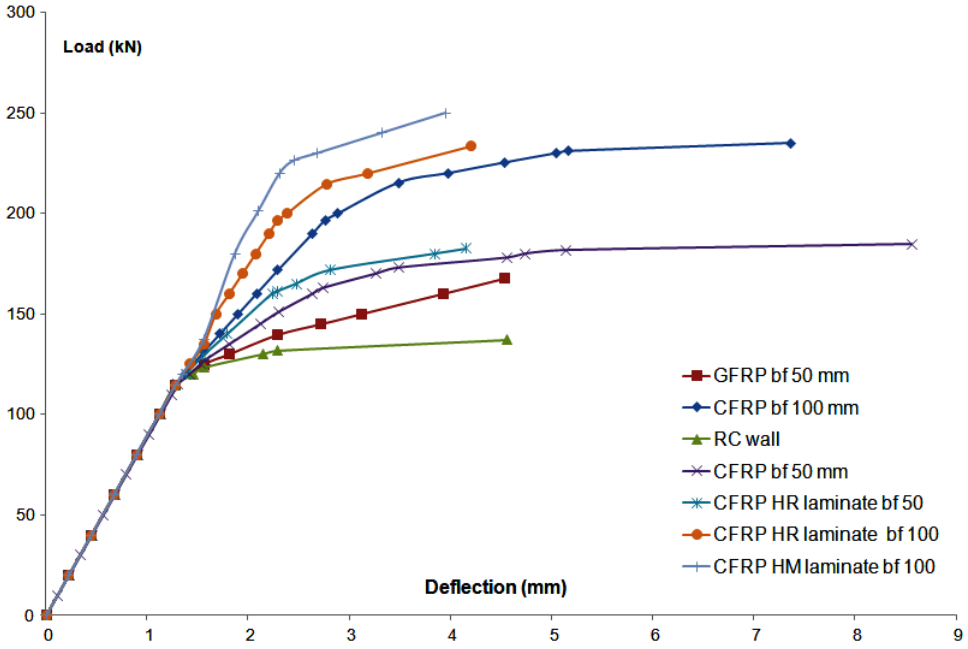

Figure 8.25: Load Displacement curve of different strengthening arrangement

8.5 Conclusion

The proposed simplified strut and tie model successfully predicted the load response behavior of short wall specimens: reinforced concrete and reinforced concrete strengthened with carbon fiber reinforced polymer. The crucial step in this model is depiction of the load path and assumption of strut and tie pattern. During study a simplified version of strut and tie model was used. The struts positions were based on the lateral load applied at wall top and the vertical induced load contribution was considered in finalizing strut dimension. The specimens' vertical reinforcement was modeled as vertical ties and horizontal rebar effect was

taken in to account by fixing the lower end of each tie. In specimen strengthened with CFRP, the tie bars were first consisted of steel rebar, similar to RC wall specimen and as the stress in tie bar reached the rebar yield strength value, steel tie was replaced with CFRP tie. This arrangement was based on the assumption that CFRP reinforcement initiates its contribution after steel rebar yield and concrete starts cracking. The evaluated load displacement curve was similar to the experimentally measured curve in both cases. However, in case of CFRP strengthened specimen, the curve showed coherence with experimentally observed data when the ultimate capacity was reduced to the experimentally observed maximum stress observed in CFRP strip. The difference in the ultimate load capacity depicted by model in comparison to experimentally observed was 5.7% in specimen S1 and 15 % in SR2.

9 Slender wall modeling

9.1 Software utilized

The analytical modeling of slender wall specimen subjected to static load test was done with the help of Beam compo software, developed in LGCIE. The software as its name suggest was basically developed to assess the behavior of beam. Due to its ability of nonlinear analysis while taking in to account the characteristics behavior of materials and interface, it can evaluate the mechanical behavior of reinforced concrete beams that includes pre-stressed and the one strengthened with composites (Nasseri and Hamelin 1998; Varastehpour and Hamelin 1996). The software analysis procedure is depicted in the form of flow chart in Figure 9.1.

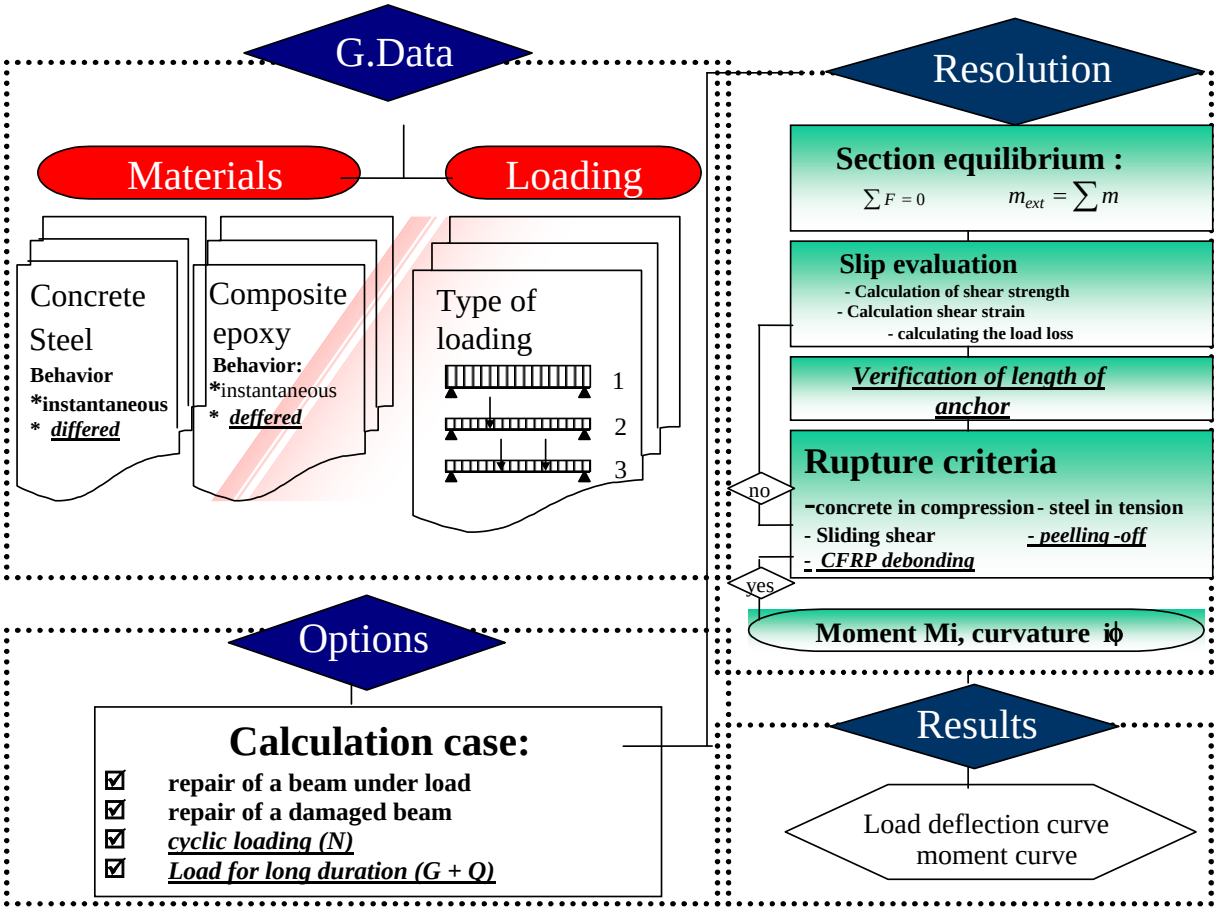

Figure 9.1 : Software analysis pattern

The software analysis procedure can be classified into four main modules:

⇒ Given data: data input by user to define specimen geometry, materials composition and test load type.

⇒ Options: choices available in software for user to define specimen initial condition and load duration.

⇒ Resolution: stress and strain evaluation procedure and failure criteria.

⇒ Results: output in the form of moment curvature curves and computation of the load displacement curves by finite difference method.

The slender shear wall specimen modeled in this software was considered as a cantilever beam. The behavior of each material was considered multi-linear which permit to approximate the nonlinear behavior of specimen through iteration.

9.2 Laws of behavior

The selection of compression and tension behavior of materials is an important step in designing. In continuity with the kinematics fields of displacements and deformations of structural behavior, they significantly influence the stress distribution within the section and hence the values of internal forces.

9.2.1 Laws of concrete behavior

9.2.1.1 Concrete in compression

The concrete behavior in compression is defined by Sargin law (Figure 9.2).

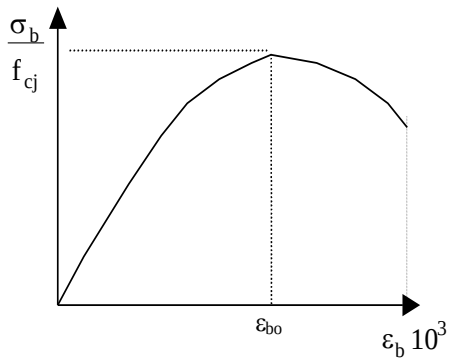

Figure 9.2: Law of concrete behavior in compression

$$\frac{\sigma_b}{f_{cj}} = \frac{k\left(\frac{\varepsilon_b}{\varepsilon_{bo}}\right) + (k^{'} - 1)\left(\frac{\varepsilon_b}{\varepsilon_{bo}}\right)^2}{1 + (k-2)\left(\frac{\varepsilon_b}{\varepsilon_{bo}}\right) + k^{'}\left(\frac{\varepsilon_b}{\varepsilon_{bo}}\right)^2} \qquad \text{Eq. 9.1}$$

Where $$k = \frac{E_{ij}\varepsilon_{bo}}{f_{cj}} \;\&\; k^{'} = k - 1$$

Here ε_{bo}: concrete deformation in compression corresponding to δ_b/f_{cj}, ε_b: concrete ultimate deformation and E_{bj}: initial tangent modulus.

9.2.1.2 Concrete in tension

The concrete tensile behavior is considered elastic bilinear while taking into account the post-resistance phenomenon (Figure 9.3).

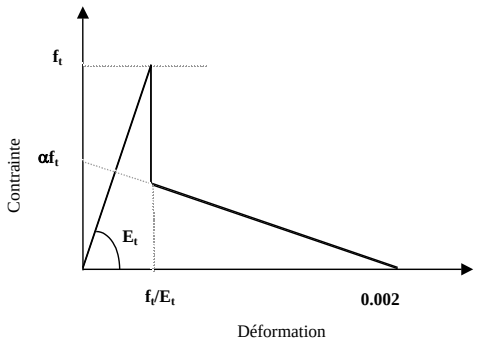

Figure 9.3 : Law of concrete behavior in tension

$$f_t = 0.06 \cdot f_{c28} + 0.6 \qquad \text{Eq. 9.2}$$

Here: f_{c28} is concrete compressive strength after 28 days of molding and f_t is concrete tensile strength.

9.2.2 Law of steel behavior

The steel behavior is considered as elastic-plastic with or without steel hardening (Figure 9.4). The parameters used here are modulus of elasticity (E_s), yield point (f_e), and strain hardening point (f_u).

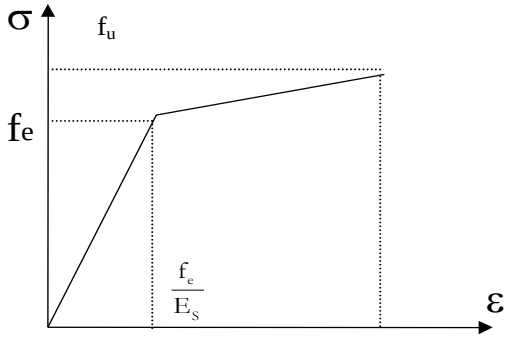

Figure 9.4 : Law of steel tensile behavior

9.2.3 Law of composite behavior

The behavior of the composite strip is considered to be elastic linear till failure (Figure 9.5). In this case, the parameters to be determined are the modulus of elasticity and rupture stress.

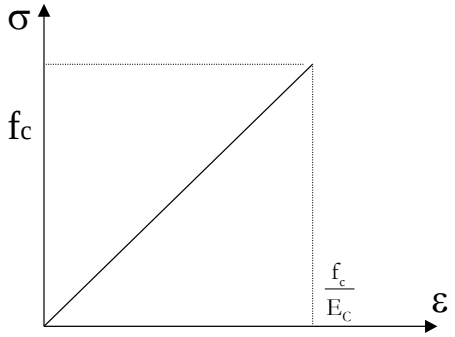

Figure 9.5 : Law of composite behavior

9.2.4 Law of behavior of concrete-composite interface

The bilinear shear-slip behavior is utilized (Figure 9.6). The elastic plastic law is defined by the shear modulus of rigidity of bonded joint and plasticity threshold.

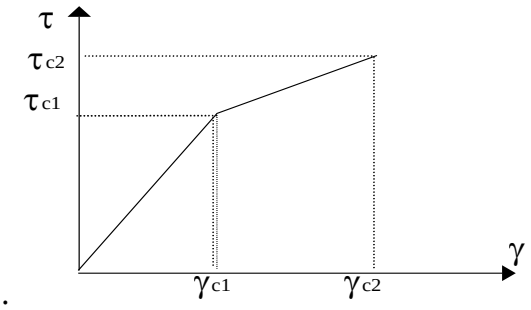

Figure 9.6 : Law of shear behavior at interface

$$\text{if } \tau_{moy} < \tau_{c1} \text{ then } \gamma_{c1} = \frac{\tau_{c1}}{G_1}$$

$$\& \text{ if } \tau_{moy} > \tau_{c1} \text{ then } \gamma_{c2} = \frac{\tau_{c2}}{G_2}$$

Here: γ_{c1}, γ_{c2}: elastic and plastic shear deformation; τ_{c1} et τ_{c2}: elastic and plastic shear stress, G_1, G_2: shear modulus.

9.3 Non linear method for flexural analysis

9.3.1 Evaluation of moment curvature relationship

Beam Compo software (BCS) evaluates the moment-curvature curves of beams: reinforced concrete or pre-stressed concrete, according to the design rules. The initial concrete deformation at the time of composite bonding can be evaluated by negating the composite reinforcement. This case is predominant in the repair of pre-stressed concrete *(H. Nasseri, 1998, [11])*. The comprehension of material behavior laws permits to evaluate the stress distribution with in a beam cross section (Figure 9.7) with the help of observed deformation by iterative calculation:

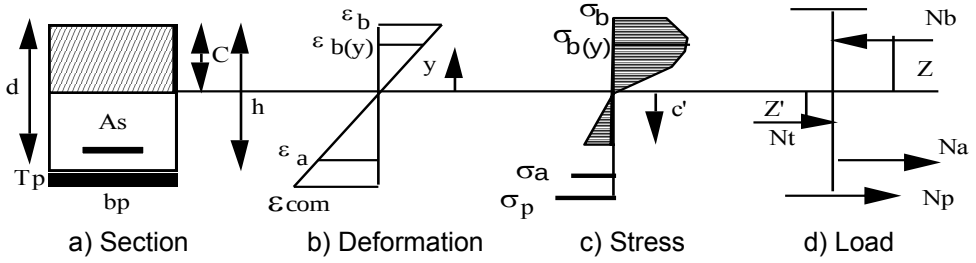

Figure 9.7 : Cross sectional analysis of R.C. beam with composite strip at bottom

The equilibrium equations at cross section are:

$$\sum F_x = 0 \Rightarrow N_a + N_b + N_t + N_p = 0 \Rightarrow N_b = \int \sigma_b dA_b$$

$$\sum M = 0 \Rightarrow M_a + M_b + M_t + M_p = 0 \Rightarrow M_b = \int \sigma_b Y dA_b$$

To obtain the moment curvature curves, the general characteristic formulation that define the reinforced concrete behavior are utilized with some modification to take in to account the sliding phenomenon at the interface (concrete/composite). The moment-curvature curves till rupture can be constructed by iterative calculations (Figure 9.8), by initializing, at first time, the concrete deformation and, afterwards, recalculation of neutral axis position while taking into account the loss of stress in composite strip due to its sliding (Figure 9.9). The stresses are calculated at each point of the cross section by utilizing the material behavior laws. When the condition of equilibrium between the internal forces is satisfied, the values of moment and curvature are then evaluated.

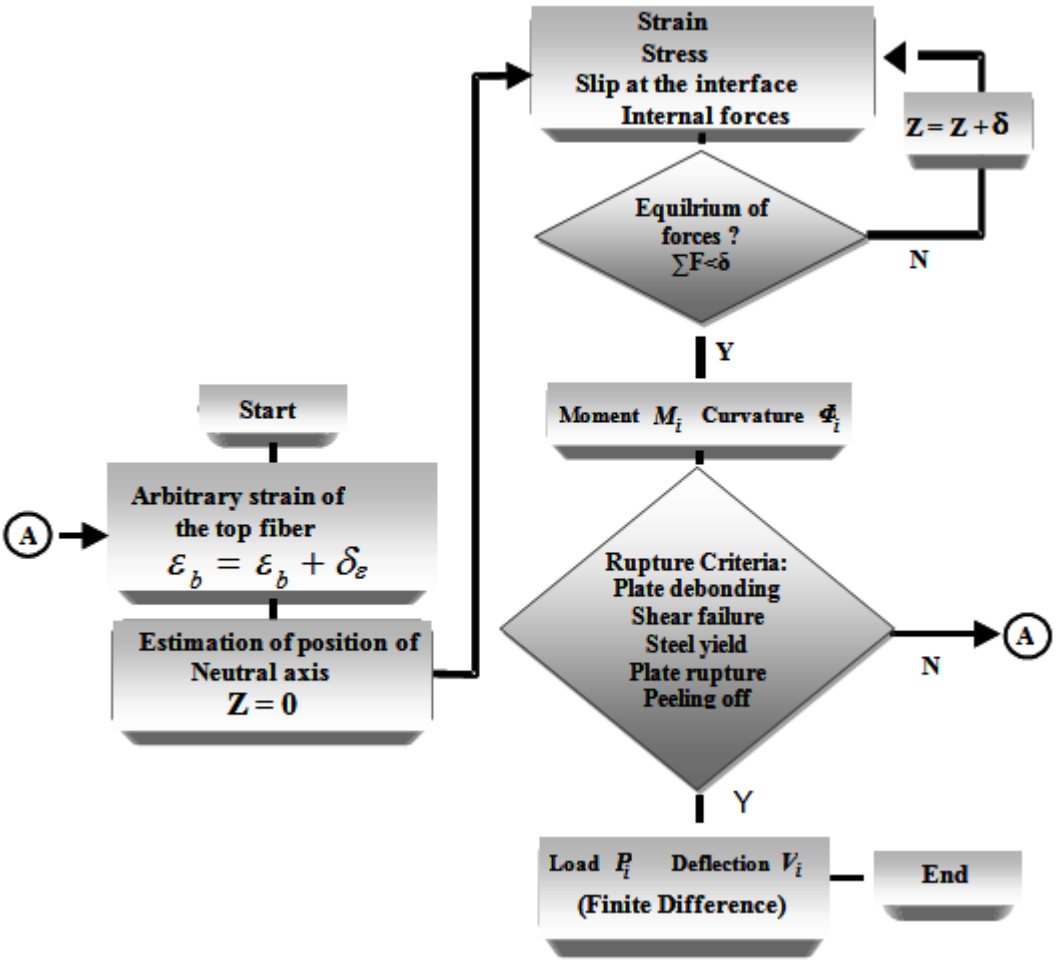

Figure 9.8 : Analysis flow chart (H. Nasseri, 1998, [11])

The effect of the sliding of the bonded CFRP over concrete surface in the analysis of reinforced concrete beams proposed by H. Varastehpour is shown in Figure 9.10.

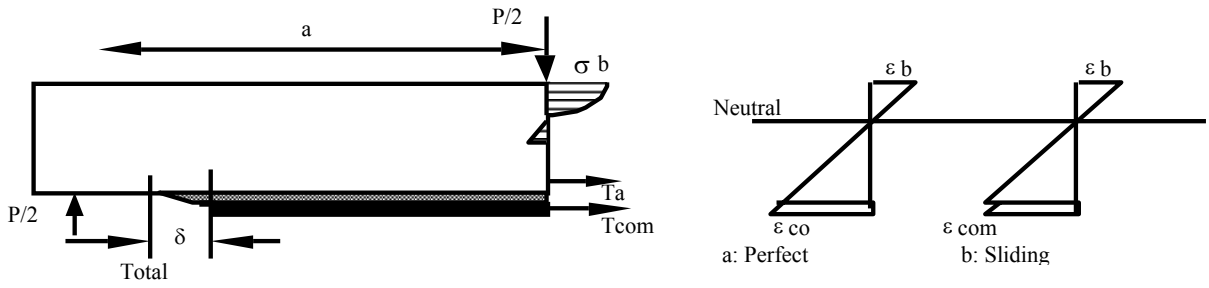

Figure 9.9 : Diagram of the deformation influenced by the sliding

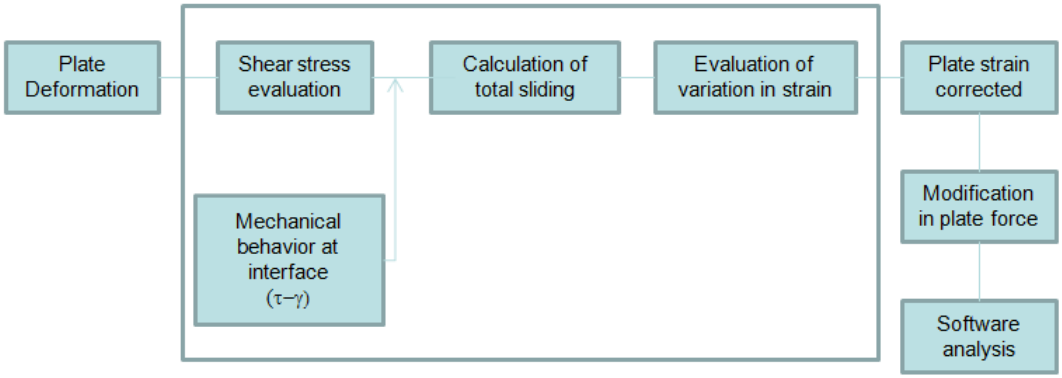

Figure 9.10 : Flowchart of calculation of sliding effect in the composite strip

9.3.2 Rupture criteria

Beams strengthened with composite plate/strips exhibit a number of failure modes:

- concrete compression rupture,
- tensile rupture of internal rebar,
- tensile rupture of composite,
- concrete shear rupture due to shear,
- composite strip detachment,
- peeling-off.

The different rupture modes observed, due to the failure of steel, concrete and composite materials can be evaluated by the following equations:

- Steel rupture as a result of internal stress exceeding the steel rebar ultimate strain limit ε_{ult},

$$\varepsilon_a > \varepsilon_{ult} \;\&\; \varepsilon_a = 0.01$$

- Composite strip rupture due to development of tensile stress higher than its ultimate tensile strength,

$$\varepsilon_{com} > \varepsilon_{ucom} \;\&\; \varepsilon_{ucom} = \frac{\sigma_{up}}{\mathrm{E}_p}$$

- Concrete failure in compression as a result of compressive strain exceeding over its ultimate compression strain limit,

$$\varepsilon_b > \varepsilon_{ub} \;\&\; \varepsilon_{ub} = f(f'_{c28})$$

In case of concrete in tension, Rankine failure criteria can be used:

$$\sigma_I = R$$

$$\sigma_{II} = R$$

Where R defines concrete tensile strength

For compression failure, another criterion proposed by Drucker Prager is:

$$f(\sigma) = \sqrt{3 \cdot J_2} + A \cdot I_1 \leq C \qquad \text{Eq. 9.3}$$

The variables I_1 and J_2 denote the first and second invariant of stress deviator, respectively, and C denotes concrete compressive strength.

Apart from this other specific failure modes exists such as rupture due to shear load, concrete/composite bond failure, rupture of concrete layer in between steel and composite. Their causes and associated criteria are described below:

- Rupture due to induced shear load is a stress criterion. At each iteration, it is verified that the shear stress induced in the specimen by external shear load is sustained by concrete, internal rebar and composite strip bonded at extremity.

$$V_{acier} + V_{béton} + V_{composite} < V_{ultime}$$

- Rupture at the concrete/FRP interface can occur as an in plane crack within adhesive bond due to the combine effect of induced shear and normal stress.

At the moment of strip detachment, the rupture can be expressed by a modified Mohr-Coulomb law *(H. Varastehpour, P. Hamelin, (1998, [9])*, which can be expressed by the following equation

$$\tau_{int} + \sigma_n \cdot tg\phi = C \qquad \text{Eq. 9.4}$$

The variable τ_{int} stands for shear stress at interface, C for cohesion, σ_n for normal stress with in the bond plan and ϕ for angle of internal friction. The values of C and ϕ are dependent on: surface preparation, properties of concrete and adhesive. The normal stress at the extremities of strip can be calculated by:

$$\sigma_n = K \cdot \tau_{int} \qquad \text{Eq. 9.5}$$

In this equation, K is the parameter that establishes a direct relation in between shear and normal stress at strip extremity; it depends on the physical and mechanical properties of strip and adhesive *(T.M. Roberts, 1989, [10]).*

$$K = 1.31 \cdot \left(\frac{T_p \cdot E_a}{T_a \cdot E_p} \right)^{\frac{1}{4}} \qquad \text{Eq. 9.6}$$

Here Ea & Ep → Modulus of elasticity of adhesive and strip.

To determine the friction angle ϕ, different specimens strengthened with composites strips are to be tested till flexural failure. By using the shear and normal stress relationship equation and Mohr-Coulomb equation, the average value of ϕ obtained is 33 °.

$$\tau_{adm} = \frac{5.41}{1 + K * tg * 33} \qquad \text{Eq. 9.7}$$

It is evident that to predict the strip detachment, it is necessary to determine the shear stress distribution at the interface during loading.

- Rupture by peeling-off of concrete situated in between steel rebar and composite strip i.e. clear cover can be determined by the following equation.

$$\tau_{\text{int}} = \frac{0.1 f_c^{'} b I_p}{6 b_p d^{'}} \qquad \text{Eq. 9.8}$$

Here $d^{'} = (h - d) + T_c + {}^{T_p}\!/_{2}$

All of the above mentioned rupture criteria are listed in Table 9.1 along with sketches to depict the corresponding beam rupture mode.

The software considers the failure criteria at each stage of calculation by comparing each material sustained deformation to their respective maximum deformation limit defined by user.

9.3.3 Beam shear strength evaluation

In case of reinforced concrete beams, the resultant of the forces acting on the beam shear critical area develops tensile stress in concrete. This tend to initiate tensile cracks in concrete (Figure 9.11) but this phenomenon is reduced to some extent by provision of shear stirrups.

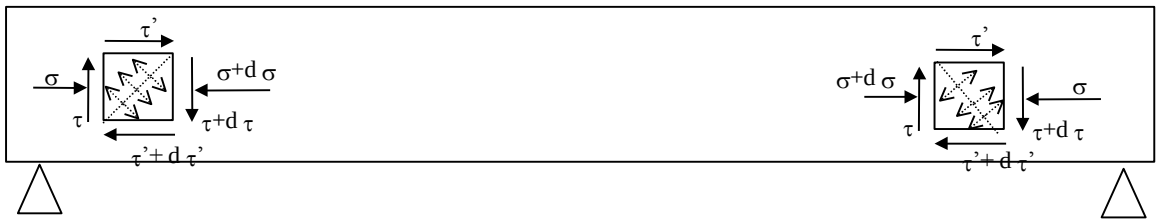

Figure 9.11 : Shear critical regions in a rectangular element

Table 9.1: Different rupture modes (H. Nasseri, 1998)

Rupture modes	Formulation
(a) Steel rupture 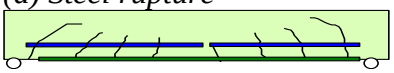	$\varepsilon_a > \varepsilon_{ult}$ & $\varepsilon_a = 0.01$
(b) Composite rupture 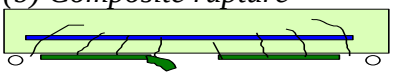	$\varepsilon_{com} > \varepsilon_{ucom}$ & $\varepsilon_{ucom} = \frac{\sigma_{up}}{E_p}$
(c) Concrete compression rupture 	$\varepsilon_b > \varepsilon_{ub}$ & $\varepsilon_{ub} = f(f'_{c28})$
(d) Shear failure 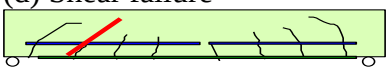	$V_{acier} + V_{béton} + V_{composite} < V_{ultime}$
(e) Detachment 	$\tau_{adm} = \frac{5.41}{1 + K * tg * 33}$ $K = 1.31 \cdot \left(\frac{T_p \cdot E_a}{T_a \cdot E_p} \right)^{\frac{1}{4}}$
(f) Peeling-off 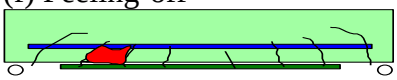	$\tau_{int} = \frac{0.1 f'_c b I_p}{6 b_p d'}$ $d' = (h - d) + T_c + T_p/2$

To avoid shear failure, the beam lateral faces must be strengthened. The additional lateral composite reinforcement is provided as an external framework and can be dimensioned with use of a simplified formula. The shear resistance is the summation of the contribution offered by concrete, steel and composite. This formulation of the shear failure criterion is explained by many authors including P. Lamothe (Lamothe 1999) such as:

$$V_r = V_c + V_s + V_p \qquad \text{Eq. 9.9}$$

Here V_r: shear resistance of section, V_c: shear resistance offered by concrete, V_s: shear resistance offered by stirrups, V_p: shear resistance offered by composite strips

$$V_c = 0.2 \cdot \lambda \cdot \phi_c \sqrt{f'_c \cdot b_w \cdot d} \qquad \text{Eq. 9.10}$$

$$V_s = \frac{\phi_s \cdot A_{vv} \cdot f_y \cdot d}{s} \qquad \text{Eq. 9.11}$$

$$V_p = \frac{\phi_p \cdot A_{vp} \cdot E_p \cdot \varepsilon_p \cdot d}{s_p} \qquad \text{Eq. 9.12}$$

Here $A_{vp} = 2 \cdot b_p \cdot t_p$

Here: b_p and t_p denotes width and thickness of composite stirrup; b_w represents beam width ; λ is a coefficient dependant on concrete density; ϕ_s, ϕ_c, ϕ_p :are the reduction coefficients; $f_c^{/}$: concrete compressive strength; f_y : steel yield strength; d : beam effective depth ; s : steel stirrup spacing ; E_p : modulus of composite ; ε_p : composite strain ; s_p : composite stirrup spacing.

These equations do not tack in to account the inclination of composite reinforcement. Indeed, in the case where the composite reinforcement is arranged vertically, the fiber orientation is at 45 ° with respect to the shear crack developed (Figure 9.12). Vecchio and Collins proposed a modification in above mentioned equations to take into consideration this phenomenon in evaluating the specimen shear capacity:

$$V_{cg} = 1.3 \cdot \lambda \cdot \phi_c \cdot \beta \cdot \sqrt{f'_c \cdot b_w} \cdot d_{ve} \qquad \text{Eq. 9.13}$$

$$V_{sg} = \frac{\phi_s \cdot A_v \cdot f_y \cdot d_{ve} \cdot \cot\theta}{s} \qquad \text{Eq. 9.14}$$

For composite stirrups bonded in direction orthogonal to beam longitudinal axis, the composite shear contribution (V_{pg}) can be calculated by Eq. 9.15 and for the one bonded at an angle other then that can be calculated by Eq. 9.16.

$$V_{pg} = \frac{\phi_p \cdot A_{vp} \cdot f_p \cdot d_{ve} \cdot \cot\theta}{s_p} \qquad \text{Eq. 9.15}$$

$$V_{pg} = \frac{\phi_p \cdot A_{vp} \cdot E_p \cdot d_{ve\cdot} \cdot (\cot\theta + \cot\alpha) \cdot \sin\alpha}{s_p} \qquad \text{Eq. 9.16}$$

These modified equations of Vecchio and Collins are utilized in beam campo software.

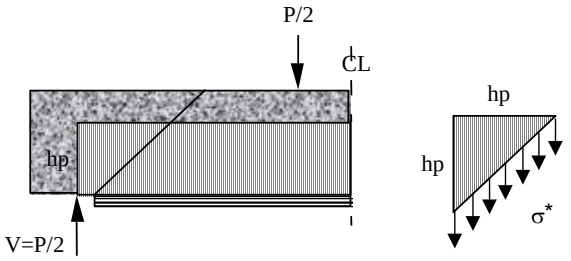

Figure 9.12 : Diagonal crack and stress distribution

9.4 Beam Compo Design software pre-dimensioning potential

This analysis software was developed and validated through two doctoral research works (H. Varastehpour and H. Nasseri). The analysis results obtained in the form of load deflection curves and moment curvature curves were compared with curves based on experimental results of the tests conducted on large scale beams of reinforced and pre-stressed concrete. The validation of resemblance in the two curves gives the proof that the stiffness of beams: non-strengthened or strengthened with composite, can be approximated with reasonable accuracy. Similarly, the ultimate moment can be calculated with good approximation. An example of analysis and its comparison with experimentally obtained curves is shown in Figure 9.13. The software was validated with additional tests by using various composite materials.

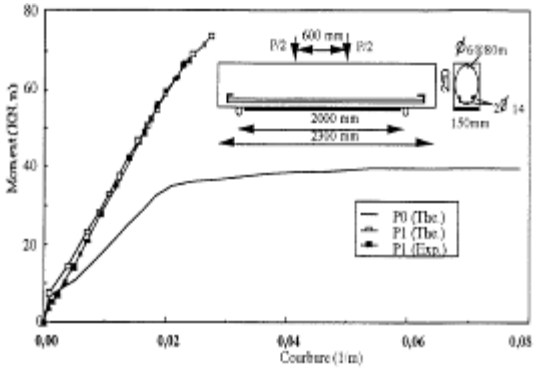

(a) Validation of R.C. (H. Varastehpour)

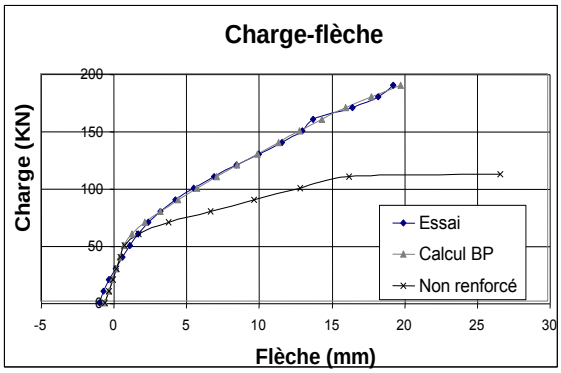

(b) Validation of prestressed concrete (H. Nasseri)

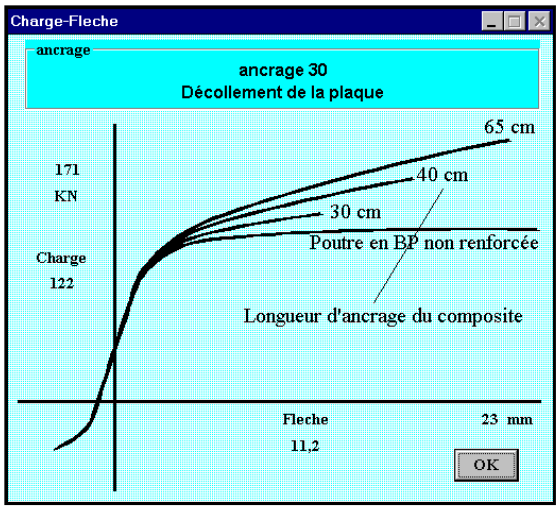

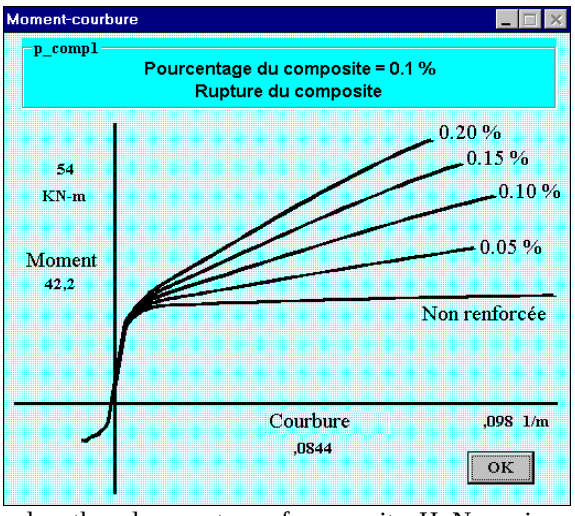

(c) Parametric study, the influence of the anchorage length and percentage of composite, H. Nasseri

Figure 9.13 : Experimental and analytical analysis of reinforced concrete beam (H. Varastehpour, H. Nasseri, P. Hamelin)

The incremental iterative calculation method makes it possible to explain the nonlinear behavior of beams. It also can take in to consideration the initial deformation of concrete at the time of bonding the composite material. The FRP strengthening design for a structure can

be achieved by considering the calculations made for several sections of composite. This software can simulate eight design cases simultaneously.

9.5 Reinforcement detail

As stated in the introduction, the model parameters selected are identical to test specimen parameters. Figure 9.14 depicts the internal reinforcement configuration of test specimen. There is one critical cross section, based on the reinforcement ratio, along the wall length. This section is located in the area where the moment is maximum that is to say at the construction joint.

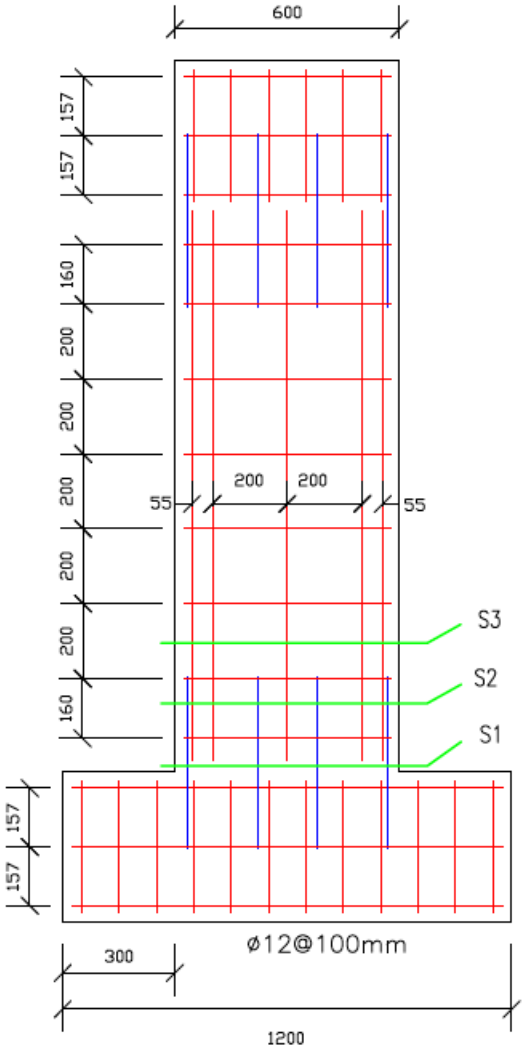

Figure 9.14 : Wall reinforcement detail and section location

The critical section S1 is located at wall height of 2 cm. Here only lap splice bar of φ6 mm are present. It was the critical wall cross-section because of lesser reinforcement ratio and higher arm of horizontal load, induced at the head beam level.

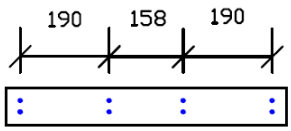

Figure 9.15*: Critical section 1*

9.6 Given data

9.6.1 Dimensions

Beam:

Beam length: 1500 mm
Load Displacement increment: 1 mm

Section:

b * h = 80 * 600 mm²

9.6.2 Materials

Concrete:

Strength in compression: 30 MPa
Time of loading: 0 hours
Number of cycles: 0

Steel:

Number of steel layers: 4 or 5
Yield stress: 500 MPa
Elastic modulus: 210000 MPa
Ultimate stress: 570 MPa
Ultimate strain: 1%
Steel layers:

Table 9.2: Section 1 reinforcement detail

Section (mm²)	Depth of the layer (mm)	Pre-stressed load (N)
56.55	31	18000
56.55	221	18000
56.55	379	18000
56.55	569	18000

Composite:

Thickness of composite on lateral face: 0.48 mm
Length of composite: 1499 mm
Pre-stress force on composite: 0 N
Ultimate stress: 1400 MPa
Young Modulus: 105000 MPa

Shear reinforcement:

Stirrups yield stress: 500 MPa
Stirrups diameter: 4.5 mm
Stirrups spacing: 200 mm
Thickness of composite bonded laterally for shear strength improvement: 0.48 mm

Interface:

Thickness of bond: 0.01 mm
Tensile modulus of elasticity of bond: 3000 MPa

Part 1:
Stiffness: 3000 MPa
Strength: 6 MPa
Part 2:
Stiffness: 3000 MPa
Strength: 6 MPa

9.6.3 Options

Consideration of composite: yes / no
Consideration of sliding: no
Increase in number of steps: yes
Initial load: 0 N

9.7 Results interpretation

The beam compo software gives results in the form of moment-curvature curves and evaluates the beam moment capacity. From which the ultimate load sustained by beam (elastic cantilever) can be evaluated by using equation below.

$$P_u = \frac{M_u}{L} \qquad \text{Eq. 9.17}$$

Here:
P_u = ultimate lateral load subjected at wall head
M_u = ultimate moment in beam
L = Lever arm
L = 1300 mm for section 1

The moment curvature relationship of a cantilever beam, shown in Figure 9.16, can be given by Eq. 9.18.

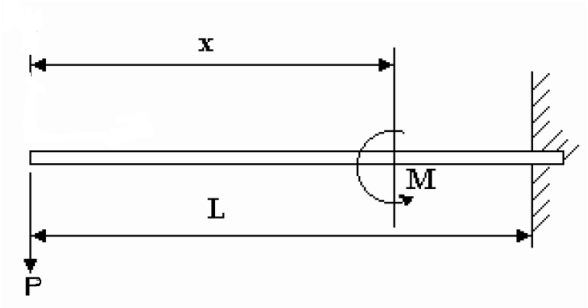

Figure 9.16*: Cantilever beam*

$$y''(x) = \frac{M}{E \times I} = \frac{P}{EI}(x) \qquad \text{Eq. 9.18}$$

By performing a double integration on this equation, we obtain an expression for deflection Eq. 9.19.

$$y(x) = \int_{x=0}^{L} y'(x)dx = \frac{Px^3}{6EI} + C_1 x + C_2 \qquad \text{Eq. 9.19}$$

The constant C_1 and C_2 depend on condition limits. For a cantilever beam the rotation and deflection at fixed end are zero.

i.e.:

$$y'(L) = 0 \;\&\; y(L) = 0$$

So:

$$C_1 = -\frac{PL^2}{2EI} \;\&\; C_2 = \frac{PL^3}{3EI}$$

Therefore:

$$y(x) = \frac{Px^3}{6EI} - \frac{PL^2 x}{2EI} + \frac{PL^3}{3EI} \qquad \text{Eq. 9.20}$$

At free end of beam, the displacement is:

$$y(0) = \frac{PL^3}{3EI} \qquad \text{Eq. 9.21}$$

The approximation of the deflection at any point of the beam is possible by the various combinations of moment and flexural stiffness data given by the software. However, in case of shear wall it does not make sense because the software does not allow modeling of a beam with variable reinforcement along its length. Thus the useful information provided by the software is the rupture moment for a section. This in turn can be used to evaluate wall top deflection with the help of above mentioned equations.

9.7.1 Reinforced concrete wall

Modeling of a R.C wall not strengthened with composite gives the result in the form of global moment curvature curve. The output is a non linear curve (Figure 9.17-a) and it depicts a failure mode which is an outcome of the internal vertical rebar yield and rupture.

9.7.2 Reinforced concrete wall strengthened with composite

In this case the specimen model depicts well the mechanical response of a shear wall strengthened with CFRP strips. The efficiency of composite reinforcement is well depicted by the increase observed in the specimens' strength and ductility. The wall shows an improvement in its behavior on global scale (Figure 9.17-b).

9.7.3 Evaluation of improvement

To highlight the significance of composite strengthening the load displacement curves of slender wall strengthened and non-strengthened with composite is shown in Figure 9.18.

At section 1, the ultimate load capacity evaluated in case of the non-strengthened wall was 27.65 kN and 39.79 kN in case of the wall strengthened with composite. The additional composite reinforcement arrangement improved the specimen strength by 44% (Table 9.3).

These results show that this section, despite of its vulnerability is capable of supporting higher load due to CFRP reinforcement contribution.

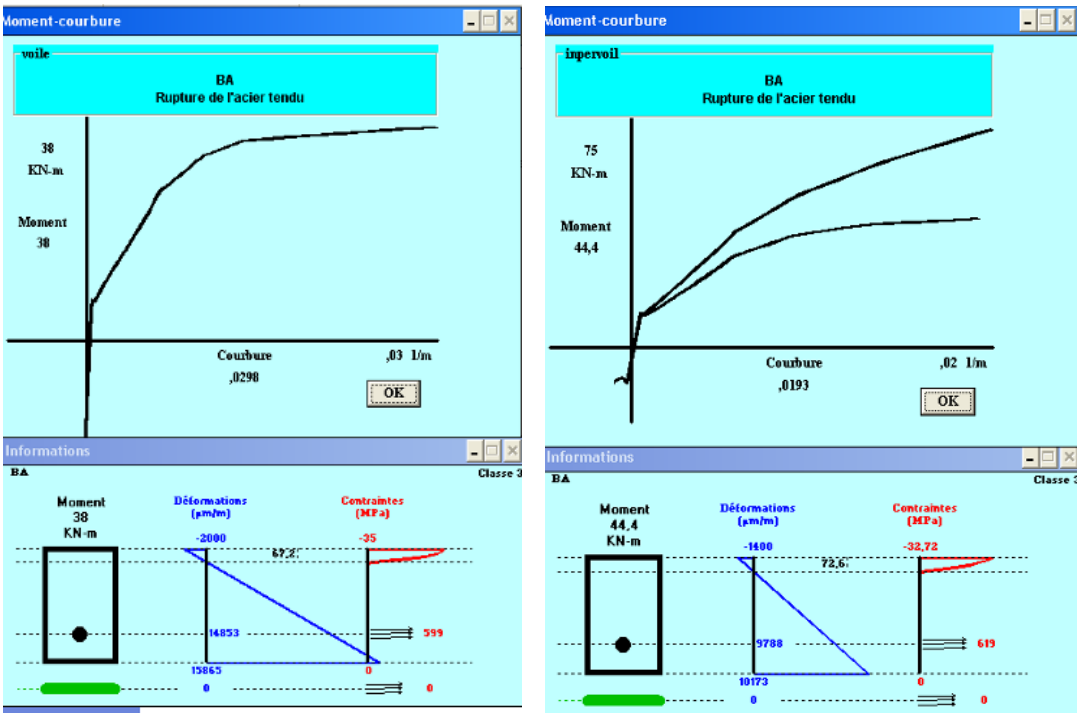

Figure 9.17 : Model of RC slender wall (a) non-strengthened (b) strengthened with composite

Table 9.3: Strength gain, section1

Specimen	RC wall	RC wall + CFRP
Ultimate load (kN)	27.65	39.79
Gain (%)	-	44

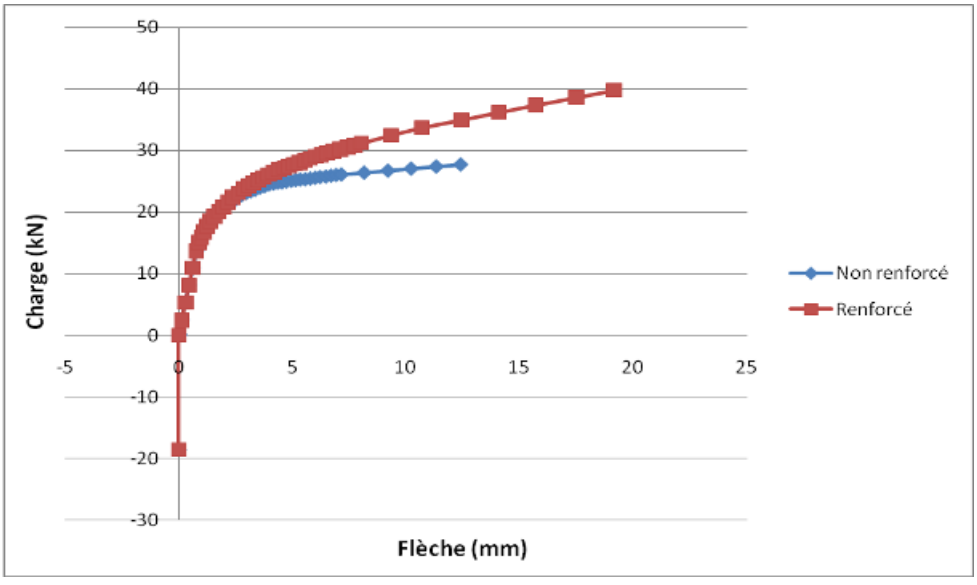

Figure 9.18 : Behavior of non strengthened and strengthened specimen at section 1

9.8 Comparison with experimental data

To confirm the validity of modeling carried out by Beam compo software, the moment curvature curves obtained by it are compared with the curves developed on experimentally observed data (Figure 9.19). The two curves are initially almost identical. However, the post-peak behavior is not modeled correctly to the extent as the software does not take into account the degradation at steel / concrete interfaces and steel buckling.

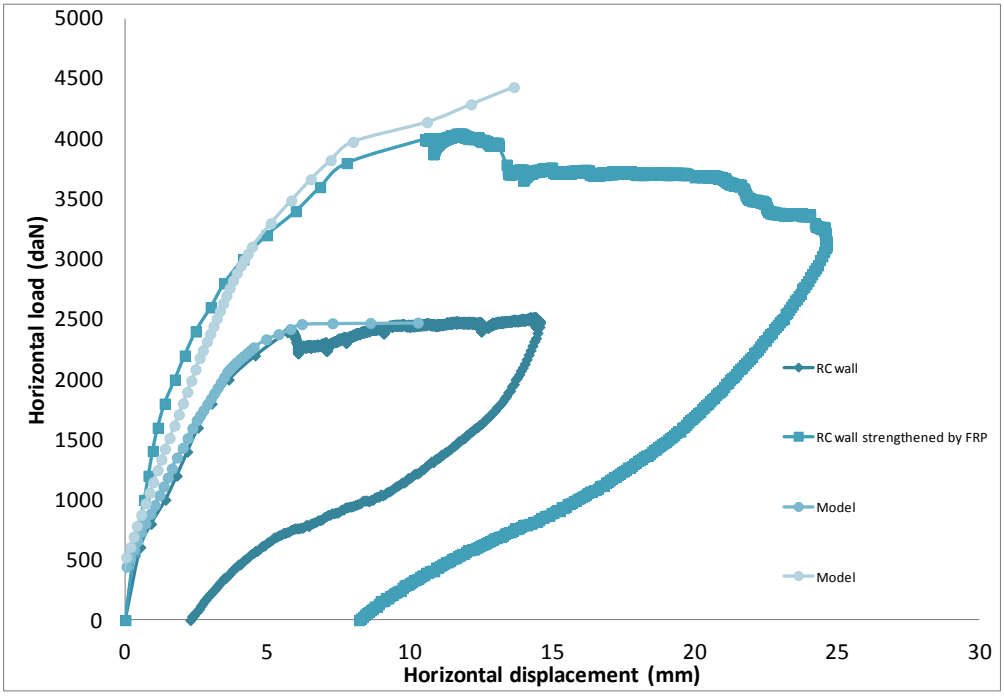

Figure 9.19 : Comparaison experimental/ modeling

Results given by software (Beam Compo) are in close proximity to the experimental results. The errors observed in case of RC wall is 4% and -5% for strengthened wall (Table 9.4). No safety factor has been used in values entered in the software in both cases. As the difference in the values evaluated by the software and the values recorded during experiment is small, therefore the proposed analysis technique used in software is favorable.

Table 9.4: Comparison of experimental and analytically evaluated ultimate load capacity

Specimen	Experiment (kN)	Analysis (kN)	Relative error (%)
RC wall	25.19	27.65	4
RC wall + CFRP	40.44	39.79	-5

In the following section the above mentioned procedure is adopted to evaluate the performance of different composite strengthening arrangement made on the RC slender wall.

9.9 Simulation with other strengthening system

In this section the influences of FRP reinforcement, other than the one applied on test specimen, are evaluated. Table 9.5: lists the details of proposed FRP reinforcement arrangements modeled in software to evaluate their influence on shear wall performance. The strengthening ratio is the axial stiffness of FRP system divided by the cross section of RC wall (Eq. 9.22).

$$E_f \times \frac{A_f}{A_c} = E_f \times \frac{2 \times b_f \times t_f}{b_w \times h} \qquad \text{Eq. 9.22}$$

Table 9.5: ***Detail of strengthening system***

Case	Strengthening system	E_f (MPa)	b_f (mm)	Strengthening ratio (MPa) $E_f \times \frac{A_f}{A_c}$
1	none	none	none	none
2	GFRP strip	40000	50	21
3	GFRP strip	40000	100	42
4	CFRP strip	105000	50	54.46
5	CFRP strip	105000	100	109.6
6	CFRP HR laminate	160000	100	333
7	CFRP HM laminate	350000	200	729

The BCS output in the form moment curvature curves is shown in Figure 9.20. Figure 9.21 shows the evaluated moment curvature curves of the different composite reinforcement configuration on RC wall. Their comparative analysis shows that the external FRP reinforcement influence on wall behavior is directly related to stiffness and width of FRP strips bonded. The wall strength augments with increase in the strip width i.e., from 50 to 100 mm and increase in changing the FRP strip from CFRP fabric to laminate.

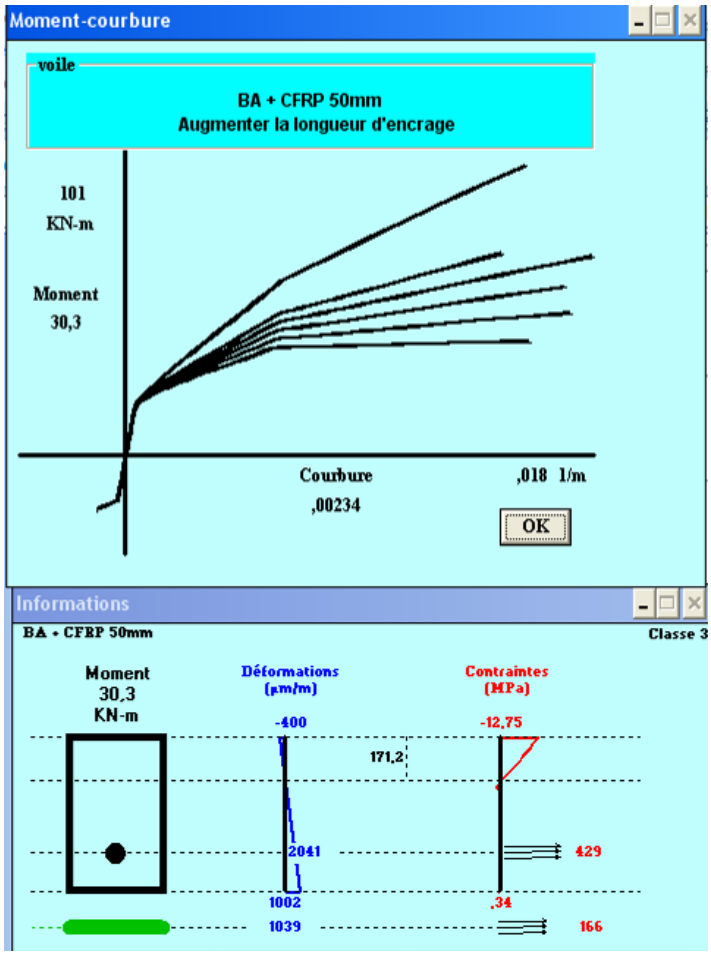

Figure 9.20 : Software output of different strengthening arrangements

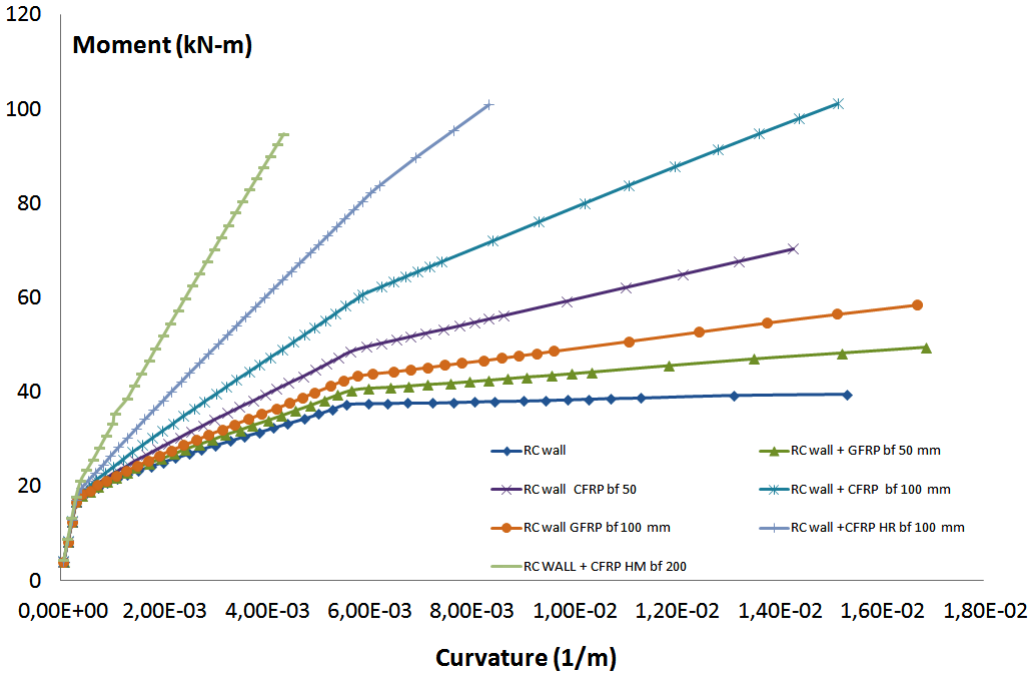

Figure 9.21 : Comparison of experimental and evaluated moment curvature curves

10 Summary

10.1 Review of thesis

Enhanced acquaintance of the seismic hazards necessitates both the modification of the design code for new construction and the re-strengthening of existing structures. The research presented herein focus on the latter task, which includes the assessment of structures that do not comply with modern safety standards and their strengthening to meet the new demands. In this context, the static cyclic behavior of lightly reinforced shear walls (short and slender) re-strengthened with CFRP is investigated. The term lightly reinforced refers to insufficiencies in the amount of reinforcement as well as to the lacking of seismic detailing compared to what is required by code specifications for new buildings. The following keywords can classify this research:

- Seismic evaluation of existing buildings
- Non-ductile response
- Reinforced concrete shear walls
- CFRP strengthened RC shear walls
- Displacement-based assessment.

Literature review, on the observed shear wall performance, revealed that despite of the improper reinforcement detailing only a limited number of total collapses of shear wall buildings were reported by the earthquake reconnaissance missions. To evaluate their performance the available experimental data on the shear walls tested has been assessed. The specific knowledge of the behavior of structures strengthened for extreme load conditions (shocks, explosions or earthquakes) remains to be established. It is necessary, even essential to formulate and calibrate the calculation methods for sizing reinforcements that are most feasible to implement. This knowledge must be based on experimental data sets, as complete as possible, in order to stay relevant to a wide range of composites, implementation techniques, reinforcement configurations, and according to the different demands on the proposed structure to be reinforced. The principal objectives of this research were:

- To provide additional experimental data on the behavior of lightly reinforced R.C. shear walls externally reinforced with CFRP under cyclic lateral loading,
- To perform/provide more realistic analytical modeling techniques for the evaluation of structures strength, deformability, and load deflection response under monotonic loading.

In this context, this thesis aimed at substantiating the displacement-based assessment of existing shear walls plus shear walls with external CFRP reinforcement.

10.2 Conclusions

10.2.1 Experimental data

The experimental work highlights the positive influence of external CFRP reinforcement on RC wall. The parameters were slenderness ratio, axial load ratio and CFRP reinforcement configuration. The CFRP strips bonded to RC wall panel did improve their ultimate load capacity, ductility, and limited the crack propagation to a certain extent. The mesh anchor placement at wall foundation joint remedied the joint failure due to improper reinforcement arrangement in this region. They also limited CFRP strips debonding, which is the major issue in use of external FRP reinforcement in vicinity of L shape Joints, by transferring load effects from the bonded strips to lower foundation block. The additional transverse anchor arrangement with in wall panel also helped in limiting the intermediate crack debonding phenomena. The partial FRP strengthening adopted here proved to be successful as it did not deteriorated the RC wall energy dissipation capacity. This arrangement ensured concrete cracking within wall panel in controlled manner that in turn resulted in energy dissipation because RC structures dissipate energy due to concrete crack relative friction and rebar yielding.

10.2.2 Modeling

It is interesting to note in this summary concerning modeling that the attempts to model the behavior of walls using techniques other than finite element method did not lead to usable results. It came out, that these methods even though potentially very interesting are not the appropriate tool. They can be used to evaluate specimen strength. However due to their shortcomings they cannot evaluate the load response behavior of RC wall plus CFRP.

For short walls an analytical model (struts and tie model) for the evaluation of the global load deflection response was proposed in section 8. To make this model easy to understand for field engineer and implement it with commercially available software (RSAP) some modifications were proposed. The model estimates the shear strength, deformability, and predicts its static-cyclic envelope curve. Evaluation, of the above mentioned parameters, achieved with this model agrees particularly well to certain extent with the aforementioned test results on RC short walls. However, the predictions for CFRP strengthened short wall specimen requires the use of maximum stress observed in CFRP strips during test to take into account the CFRP strip slipping.

For slender walls an analytical model (considering wall as cantilever beam) for the evaluation of the global load deflection response was proposed in section 9. This model estimates flexure strength, deformability and predicts the specimen load displacement response under static monotonic load test. The analysis gets conducted on a moment critical section at the wall base. Evaluation, of the above mentioned parameters, achieved with this model agrees well to a certain extent with the aforementioned test results. The errors observed in case of RC wall is 4% and -5% for strengthened wall. No safety factor has been used in the values entered in the software in both cases.

10.3 Recommendations

As the proposed model is only based on limited experimental data, there is an apparent need for additional experimental investigations. The present research emphasizes on the static-cyclic behavior of lightly reinforced concrete shear walls strengthened with CFRP. Experimental investigations were made on small-scale test units that modeled cantilever walls. Although the test series was carefully conceived in order to maximize congruence with full-size structures, it necessitated a number of limitations. Further experimental research in the field should include the following:

- Study the behavior of wall as a structural element instead of a cantilever model.
- Study the role of CFRP reinforcement detailing.
- Used of glass fiber instead of CFRP as the CFRP strength could not be capitalized fully in this research work.
- Conduct test series in possibly real scale to provide answers to the size effect.
- Numerical analysis of the behavior of wall as structural element.

APPENDIX A

Experimental Investigation of CFRP Anchorage Systems used for Strengthening RC Joints

Fibre-reinforced polymer (FRP) composite materials are widely used for strengthening existing reinforced concrete structures because of their light weight, easy implementation and high efficiency. However, recent seismic studies have revealed that FRP-strengthened specimens underperform due to the debonding of the FRP strips in the vicinity of L-shaped structural joints, resulting from the lack of an anchoring system to transfer loads from the FRP strips to the supporting structural element. To address this issue, four new anchorage techniques are presented in this paper, and experimental results for each are analysed in the form of load displacement curves and the ultimate capacity. This research results highlights the significance of carbon fiber (CF) anchor systems in enhancing the overall seismic performance of FRP-strengthened specimens.

A-1 Test description

The laboratory tests consisted of subjecting asymmetric beam test specimens to three-point flexural tests. The beam dimensions were specified according to the tensile properties of the concrete and the CFRP that were intended to be used. Their respective tensile strengths were 3 MPa and 825 MPa. Fig. A-1 shows the geometric details of the test specimen and the loading arrangements. To represent an L-shaped beam/column or wall/foundation joint, the depth of the test specimens was reduced from 140 mm to 80 mm at their mid-length. It also helped in the portrayal of the differences in the stiffness values of the connecting structural elements (beam/column or wall/foundation) at the joints. In the field, failure in L-shaped joints occurs as a result of the intermediate crack (IC) debonding, in which debonding initiates at a critical section in the high moment region. Therefore, the test specimens were subjected to three point flexural load tests with a deflection load applied at the point of asymmetry to make it vulnerable.

To limit intermediate crack (IC) debonding and facilitate load transfer at joints (column-beam or column-foundation joints), four new retrofit techniques are presented here and discussed briefly in the section “Strengthening description”. The strengthening techniques consisted of the following: (a) bonding a CFRP fabric strip to the lower tensioned face of the less stiff section of each specimen (representing a column or a wall), (b) placement of a mesh anchor in a hole drilled in the stiffer section (representing a supporting beam or foundation), (c) splaying the anchor-free end over a bonded CFRP strip and (d) bonding a second CFRP strip over it.

A-2 Strengthening description

Specimens were classified into four types depending on the CFRP reinforcement techniques used for the efficient transfer of load between the CFRP fabric and the mesh anchor. Two to three test specimens were fabricated for each type; three reference (control) specimens were also fabricated. The bi-directional CFRP fabric strip that was bonded to the lower tensile-stressed face of the specimens had a length and width of 240 mm and 65 mm. Fig.A- 2 shows the specimen configurations for all test specimens. In the reference specimens, two CFRP

strips were bonded to the specimens' less stiff section, and no mesh anchor arrangement was made. These reference specimens were used for comparison, to evaluate the efficiency level of each type of anchorage system. For Type 1 specimens, one CFRP strip was first bonded to the specimen in a manner similar to the reference specimen. Then, the folded end of mesh anchor M1 was placed in the epoxy-filled hole, and its outer portion was splayed and bonded over the previously bonded CFRP strip. A second CFRP strip was then bonded over it. For Type 2 test specimens, two transverse grooves were made on the specimens' lower surfaces to improve the concrete/CFRP bond. The grooves were made at a distance of 20 mm and 100 mm from the midsection of the specimen with respective widths of 40 mm and 25 mm. The depth of the grooves was equal to 5 mm, and the length of each groove was equivalent to the beam width. Before the first CFRP strip was bonded, the grooves were filled with polyurethane. The rest of the procedure was identical to that used for the Type 1 specimens. The variation in the specimen reinforcement configuration for Type 3 with respect to that of Type 1 involved the replacement of the mesh anchor M1 with anchor M2. The CFRP arrangement for Type 4 test specimens in comparison with Type 1 specimens involved the addition of a polyurethane strip (commercial name Polyurethane BPU) sandwiched between the inner CFRP fabric (in contact with the concrete) and the splayed portion of the mesh anchor. The retrofitted specimens were cured for 5 days at 20°C prior to the load tests. Table 1 lists the reinforcement arrangements for each type of test specimen.

A-3 Test setup

The specimens were subjected to three-point flexural tests. Displacement-controlled loading was applied with a hydraulic actuator at each specimen's midpoint (interface of two sections) to induce shear forces in this section, which represents a column-foundation joint. Tests were conducted to determine the ultimate strength, and load response of each type of test specimen by applying a displacement-controlled load at a uniform rate of 1 mm/min until specimen failure occurred.

A-4 Load-displacement analysis

The load-bearing capacities of all of the test specimens are listed in Table A-2 and, to represent their load-response behaviour, the load-displacement curve for each type of test specimen is shown in Fig. A-3. The load-response curve of the reference (control) specimen is shown in Fig. A-3; it was identical to the characteristic load-response curve for reinforced concrete. The average load-bearing capacity of the reference specimens listed in Table A-2 is 13.99 kN, which is the lowest of all the specimens. The mean value of the ultimate load-bearing capacities of the Type 1 specimens was 20.5 kN. Type 1 specimens performed well, exhibiting plastic deformation after their maximum load capacity was exceeded. The load-response curves of the Type 2 and 4 test specimens are similar in shape (Fig. A-3) though large differences exist in their load capacities. The average load capacities of Type 2 and Type 4 specimens are 43.58 kN and 31.85 kN, respectively (Table A-2). Fig. A-3 shows a rapid decline in their respective load-response curves after their respective ultimate load levels is exceeded; this trend occurred because the induced shear exceeds the bond shear strength. The additional bonding arrangements on the specimens' tensioned surfaces improved the overall strength but resulted in a more or less abrupt failure. The average maximum load-bearing capacity of the Type 3 specimens, as listed in Table A-2, is 37.51 kN, which is the second highest after Type 2. The specimens' load-response curve shows plastic deformation similar to that of Type 1 after the ultimate load capacity is exceeded. The relative improvement in the ultimate level of Type 3 in comparison with Type 1 signifies the positive effect associated with the uniform concrete-anchor bond within the hole.

Table A-1. Description of specimen types

Strengthening	Specimen Types			
	1	2	3	4
CFRP Strip	✓	✓	✓	✓
Mesh Anchor M1	✓	✓	-	✓
Mesh Anchor M2	-	-	✓	-
Polyurethane	-	✓	-	-
Polyurethane Strip	-	-	-	✓

Table A-2. Measured response and observed failure modes

Specimen	Force (KN) Max	Avg.	F(T) / F(R)	Max. Moment (KN-m)	ΔM (KN-m)	F in Mesh (KN)	Avg.F in Mesh (KN)	Detail
Reference	15.13	13.99		2.12				Flexural Crack at joint
	13.74		-	1.92				
	13.1			1.83				
Type 1	20.1	19.25	1.38	2.81	0.89	15.50	13.43	Flexural Crack at joint Plus slip in CFRP
	20.625			2.89	0.96	16.78		Strip and Anchor
	17.02			2.38	0.46	8.00		
Type 2	41.6	43.58	3.11	5.82	3.90	67.91	72.73	Flexural Crack at joint Plus shear crack
	45.55			6.38	4.45	77.54		in thin section
Type 3	41.42	37.51	2.68	5.80	3.88	67.47	57.94	Cracks at joint and in vicinty Plus Anchor
	33.6			4.70	2.78	48.41		pull out and Concrete splitting
Type 4	31.3	31.85	2.28	4.38	2.46	42.81	44.15	Flat Crack at joint Plus shear crack in
	32.4			4.54	2.61	45.49		thin section

NOTE: *Load* represents specimen ultimate sustained load, while *Max.* to denote maximum value and *Avg.* for average values.
LT /LR denotes ratio of average load values of Test specimen and reference specimen.
ΔM denotes difference in moment in between test specimen and reference specimen moment value 1.92 KN-m.
F: Axial force developed within Mesh anchor.

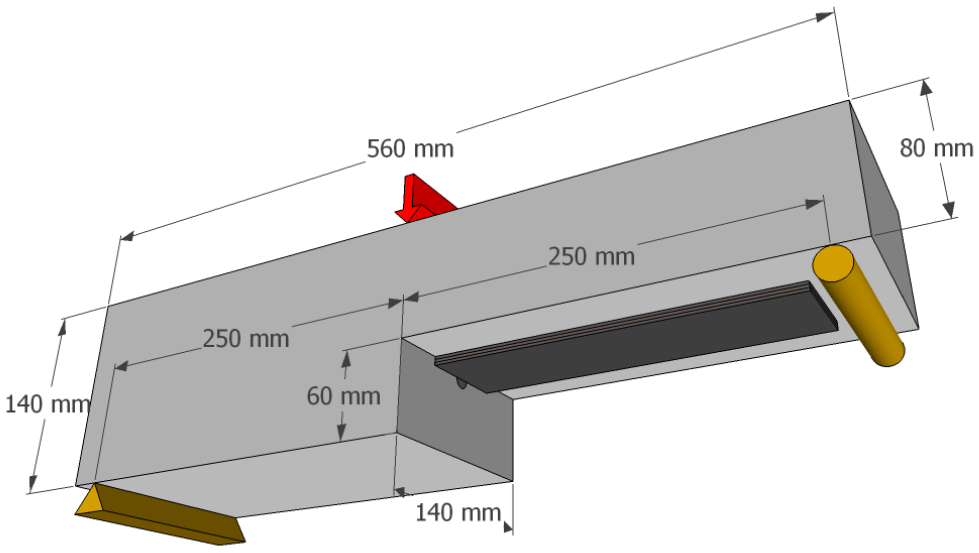

Fig. A-1. Specimen detail and loading arrangements

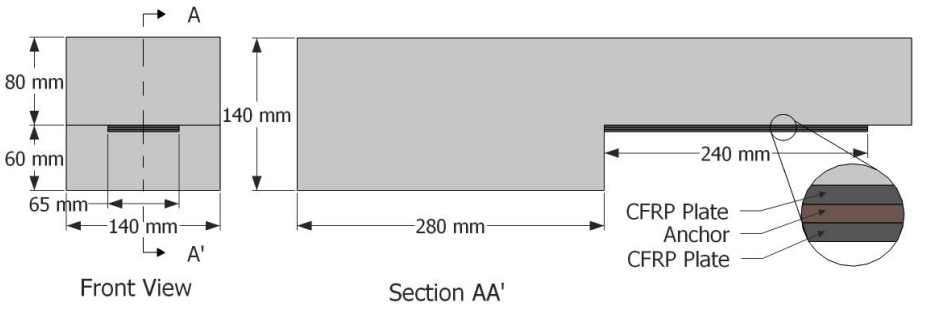

(a)

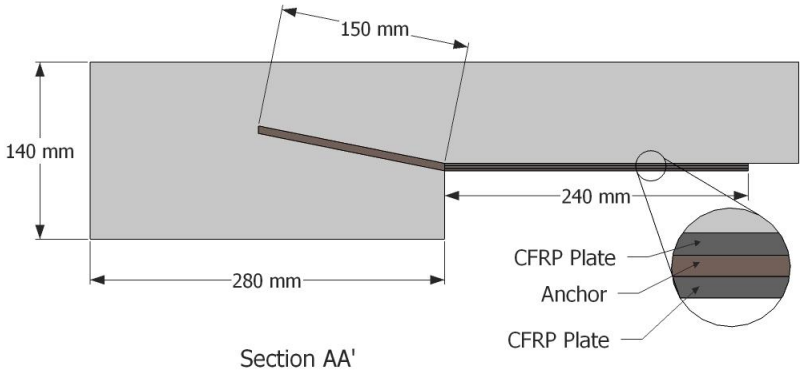

(b)

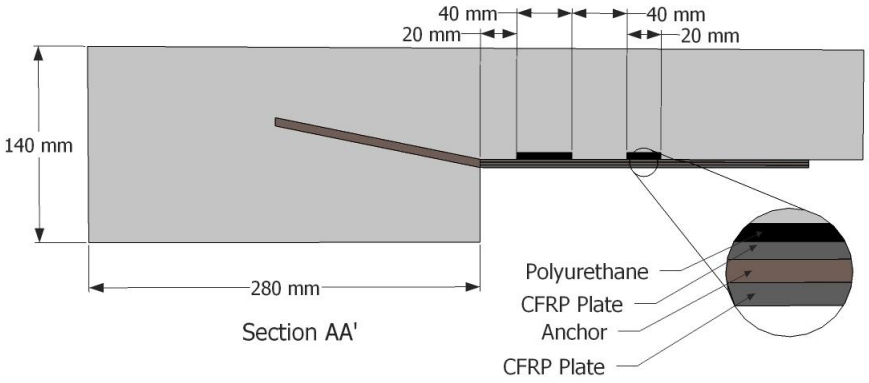

(c)

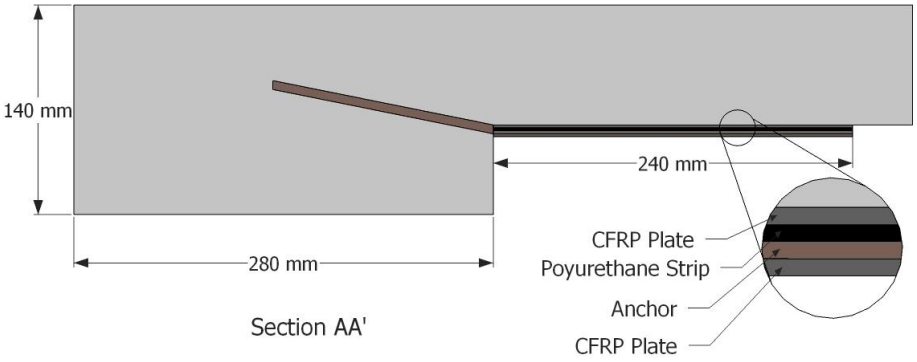

(d)

Fig. A-2. Specimen configuration: (a) Reference (b) Type 1 (c) Type 2 (d) Type 4

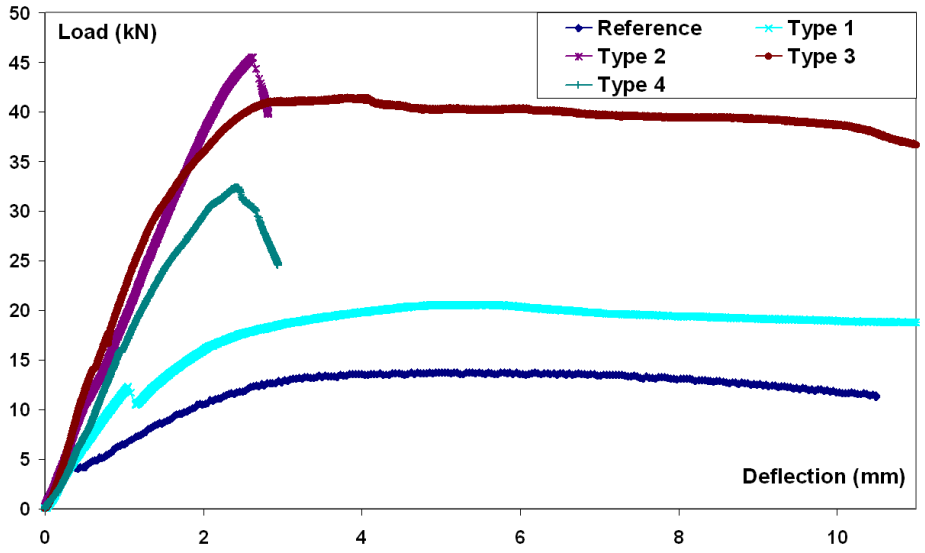

Fig. A-3. Load-deflection curves

References

AASTHO LRFD Bridge Design Specifications, 2nd Edition. (1998). Washington, DC.

ACI 440R-07:Report on Fiber-Reinforced Polymer (FRP) Reinforcement for Concrete Structures. (2007). American Concrete Institute (ACI), Farmington Hills, Michigan.

ACI Committee 318. (2005). *Building Code Requirements for Structural Concrete (ACI 318-05) and Commentary (318R-05)*. Farmington Hills, MI, 430.

Abdelrahman, A. A. (1995). "Serviceability of concrete beams prestressed by fibre reinforced plastic tendons." University of Manitoba, Canada.

Abou-Elfath, H., and Ghobarah, A. (2000). "Behaviour of reinforced concrete frames rehabilitated with concentric steel bracing." *Canadian Journal of Civil Engineering*, NRC Research Press Ottawa, Canada, 27(3), 433–444.

Aguilar, G., Matamoros, A. B., Parra-Montesinos, G. J., Ramírez, J. A., and Wight, J. K. (2002). "Experimental Evaluation of Design Procedures for Shear Strength of Deep Reinforced Concrete Beams." *ACI Structural Journal*, 99(4), 539–548.

Alsayed, S. H., and Alhozaimy, A. M. (1999). "Ductility of Concrete Beams Reinforced with FRP Bars and Steel Fibers." *Journal of Composite Materials*, 33(19), 1792–1806.

Altin, S., Ersoy, U., and Tankut, T. (1992). "Hysteretic Response of Reinforced-Concrete Infilled Frames." *Journal of Structural Engineering*, 118(8), 2133–2150.

Ambraseys N.N., and Simpson K. A. (1996). "PREDICTION OF VERTICAL RESPONSE SPECTRA IN EUROPE." *Earthquake Engineering & Structural Dynamics*, 25(4), 401–412.

Ang, H. S., Kim, W. J., and Kim, S. B. (1993). "Damage Estimation of Existing Bridge Structures." *ASCE: Structural Engineering in Natural Hazards Mitigation*, irvine california, 1137–1142.

Antoniades, K. K., Salonikios, Thomas N, and Kappos, Andreas J. (2004). "Cyclic Tests on Seismically Damaged Reinforced Concrete Walls Strengthened Using Fiber-Reinforced Polymer Reinforcement." (100).

Arslan, M. H., and Korkmaz, H. H. (2007). "What is to be learned from damage and failure of reinforced concrete structures during recent earthquakes in Turkey?" *Engineering Failure Analysis*, 14(1), 1–22.

Bachmann, H. (1967). "Zur plastizit¨atstheoretischen Berechnung statisch unbestimmter Stahlbetonbalken." ETH Z¨urich.

Badoux, M., and Jirsa, J.O. (1990). "Steel Bracing of RC Frame for Seismic Retrofitting." *Journal of Structural Engineering*, 116(1), 55–74.

Banon, H., and Veneziano, D. (1982). “Seismic safety of reinforced concrete members and structures.” *Earthquake Engineering & Structural Dynamics*, 10(2), 179–193.

Barda, F., Hanson, J. M., and Corley, W. G. (1977). “Shear Strength of Low-Rise Walls with Boundary Elements.” *ACI special publications, Reinforced Concrete in Seismic Zones*, 53(8), 149–202.

Beigay, M., Young, D. T., and Gergely, Janos. (2003). “AN IMPROVED COMPOSITE ANCHORING SYSTEM.” *Civil Engineering*, 32(9), 1701–1706.

Belmouden, Y., and Lestuzzi, Pierino. (2007). “Analytical model for predicting nonlinear reversed cyclic behaviour of reinforced concrete structural walls.” *Engineering Structures*, 29(7), 1263–1276.

Breña, S. F., Asce, M., and Schlick, B. M. (2007). “Hysteretic Behavior of Bridge Columns with FRP-Jacketed Lap Splices Designed for Moderate Ductility Enhancement.” (December), 565–574.

Building Guidance, Division, Housing Bureau, M. of C. (1999). *The Japan Building Disaster Prevention Association (1999): Seismic retrofit design and guidelines for existing RC buildings and steel encased RC buildings using continuous fiber reinforced materials*. Tokyo.

Burgoyne C.J. (1992). “Tests on beams prestressed with polyaramid tendons.” *1st Int. Conf. on Advanced Composite Materials in Bridges and Structures*, Sherbrooke, Quebec.

Bush, T. D., Jones, E. A., and Jirsa, J.O. (1991). “Behavior of RC Frame Strengthened Using Structural Steel Bracing.” *Structural Engineering*, 117(4), 1115–1126.

CSA Committee A23.3-94. (1994). *Design of Concrete Structures*. Rexdale, ON, 199.

“CSTB, 2008 - Avis technique n°3/07-540 du procédé de renforcement Foreva TFC de Freyssinet.” (n.d.). .

Calgaro, J.-A., and Lacroix, R. (1997). *Maintenance et réparation des ponts*. Presse de l’école nationale des ponts et chaussées, Paris, 666.

Cardenas, A. E., Russell, H. G., and Corley, W. G. (1980). “Strength of Low-Rise Structural Walls.” *ACI Special Publications*, 63(10), 221–241.

Carlos G. Quintero-Febres, Gustavo Parra-Montesinos, and James K. Wight. (2006). “Strength of Struts in Deep Concrete Members Designed Using Strut-and-Tie Method.” *ACI Structural Journal*, 103(4), 577–586.

Ceroni, F. (2010). “Experimental performances of RC beams strengthened with FRP materials.” *Construction and Building Materials*, Elsevier Ltd, 24(9), 1547–1559.

Ceroni, Francesca, and Pecce, M. (2009). “Design provisions for crack spacing and width in RC elements externally bonded with FRP.” *Composites Part B: Engineering*, 40(1), 17–28.

Ceroni, Francesca, Pecce, M., Matthys, Stjin, and Taerwe, L. (2008). "Debonding strength and anchorage devices for reinforced concrete elements strengthened with FRP sheets." *Composites Part B: Engineering*, 39(3), 429–441.

Choi, C. A. (2006). "Improvement of Earthquake-Resistant Performance of Squat Shear Walls under Reversed Cyclic Loads." *Key Engineering Materials*, 324-325, 535–538.

Collins, M. P., and Mitchell, D. (1986). "Rational Approach to Shear Design—The 1984 Canadian Code Provisions." *ACI Journal Proceedings*, 83(6), 925–933.

Colotti, Vincenzo. (1993). "Shear Behavior of RC Structural Walls." *Journal of Structural Engineering*, American Society of Civil Engineers, 119(3), 728–746.

David I. McLean, and M. Lee Marsh. (1999). "Seismic Retrofit of Bridge Foundation." *ACI Structural Journal*, 96(2), 174–182.

Dazio, A. (2000). "Entwurf und Bemessung von Tragwandgeb¨auden unter Erdbebeneinwirkung." ETH Z¨urich.

Demers, M., and Neale, K. W. (1999). "Confinement of reinforced concrete columns with fibre-reinforced composite sheets - an experimental study." *Canadian Journal of Civil Engineering*, NRC Research Press Ottawa, Canada, 26(2), 226–241.

Direction Générale de la Prévention des Risques (DGPR). (2009). *Plan Séisme Antilles : Note de synthèse, Bilan 2008 et perspectives 2009-2010*.

EN 1998-1: Eurocode 8- Design of structures for earthquake resistance - Part 1: General rules, seismic actions and rules for buildings. (n.d.). .

Ekenel, M., and Myers, J. J. (2007). "Durability performance of RC beams strengthened with epoxy injection and CFRP fabrics." *Construction and Building Materials*, 21(6), 1182–1190.

El Maaddawy, T., and Soudki, Khaled. (2008). "Strengthening of reinforced concrete slabs with mechanically-anchored unbonded FRP system." *Construction and Building Materials*, 22(4), 444–455.

Elmaaddawy, T., and Soudki, K. (2008). "Strengthening of reinforced concrete slabs with mechanically-anchored unbonded FRP system." *Construction and Building Materials*, 22(4), 444–455.

Elnashai, A. S., and Salama, A. I. (1992). *Selective Repair and Retrofitting Techniques for Structures in Seismic Regions*. London.

Emori, K., and Schnobrich, W. C. (1981). "Inelastic Behavior of Concrete Frame-Wall Structures." *Structural Division*, 107(1), 145–164.

Eurocode 2. (n.d.). *Calcul des structures en béton*. AFNOR, Paris, 2005.

FINTEL, M. (n.d.). “Performance of buildings with shear walls in earthquakes of the last thirty years.” *PCI journal*, Precast/Prestressed Concrete Institute, 40(3), 62–80.

FIP-Commission 3. (1996). *FIP Recommendations, Practical Design of Structural Concrete*. London, UK.

Fardis, M. N., and Khalili, H. (1981). “Concrete Encased in Fiberglass Reinforced Plastic.” *ACI Journal* , 440–446.

Fischinger, M., Vidic, T., Selih, J., Fajfar, P., Zhang, H. Y., and Damjanic, F. B. (1990). “Validation of a Macroscopic Model for Cyclic Response Prediction of RC Walls.” *Computer Aided Analysis and Design of Concrete Structures*, N. B. Bicanic and H. Mang, eds., Pineridge Press, Swansea, 1131–1142.

Forrest, M. P., Morgan, D. R., Obermeyer, J. R., Parker, P. L., and Lamoreaux, D. D. (1995). “Seismic Retrofit of the Littlerock Dam .” *ACI Concrete International*, 17(11), 30–S1.

Fouré, B. (1993). *Un programme d’essais des murs de contreventement. In: Colloquium AFPS-SECED experimental methods in earthquake engineering and structural dynamics*. Saint-Rémy-lès-Chevreuse.

Fukuyama, Hiroshi, and Sugano, S. (2000). “Japanese seismic rehabilitation of concrete buildings after the Hyogoken-Nanbu Earthquake.” *Cement and Concrete Composites*, 22(1), 59–79.

Galal, K. (2008). “Modeling of lightly reinforced concrete walls subjected to near- fault and far-field earthquake ground motions.” *The Structural Design of Tall and Special Buildings*, 17(2), 295–312.

Gao, B., Leung, C. K. Y., and Kim, J.-K. (2005). “Prediction of concrete cover separation failure for RC beams strengthened with CFRP strips.” *Engineering Structures*, 27(2), 177–189.

Garstka, B., Krätzig, W. B., and Stangenberg, F. (1993). “Damage Assessment in Cyclically Loaded Reinforced Concrete Members.” *Second EURODYN*, Trondhiem, 121–128.

Gates, W. E., Hart, G. C., and Crouse, C. B. (1990). “Vibration Studies of an Existing Building for Base Isolation Retrofit.” *4th U.S. National Conference on Earthquake Engineering*, Earthquake Engineering Research Institute (EERI), Palm Springs, California, 559–568.

Ghobarah, A., and Khalil, A. A. (2004). “SEISMIC REHABILITATION OF REINFORCED CONCRETE WALLS.” (3316).

Giberson, M. F. (1967). “The response of nonlinear multi-story structures subjected to earthquake excitation.” California Institute of Technology.

Grace, N. F., Soliman, A. K., Abdel-Sayed, G., and Saleh, K. R. (1998). “Behavior and Ductility of Simple and Continuous FRP Reinforced Beams.” *Journal of Composites for Construction*, American Society of Civil Engineers, 2(4), 186–194.

Greifenhagen C. (2006). “Sesimic behavior of lightly reinforced concrete squat shear walls.” ÉCOLE POLYTECHNIQUE FÉDÉRALE DE LAUSANNE.

Greifenhagen, C., and Lestuzzi, Pierino. (2005). “Static cyclic tests on lightly reinforced concrete shear walls.” *Engineering Structures*, 27(11), 1703–1712.

Grünthal, G. (Ed.). (1993). *European Macroseismic Scale 1992 (up-dated MSK-scale). Conseil de l’Europe, Cahiers du Centre European de Geodynamique et de Seismologie*. Luxembourg, 79.

Guoqiang, L., Scott, H., Su-Seng, P., Walid, A., John, E., and Christopher, A. (2003). “Repair of damaged RC columns using fast curing FRP composites.” *Composites Part B: Engineering*, 34(3), 261–271.

Harajli, M. H. (2008). “Seismic Behavior of RC Columns with Bond-Critical Regions: Criteria for Bond Strengthening Using External FRP Jackets.” *Journal of Composites for Construction*, American Society of Civil Engineers, 12(1), 69–79.

Hidalgo, P. A., Ledezma, C., and Jordan, R. M. (2002). “Seismic behavior of squat reinforced concrete shear walls.” *Earthquake Spectra*, 18(2), 287–308.

Huang, X., and Chen, G. (2005). “BONDING AND ANCHORING CHARACTERIZATION BETWEEN FRP SHEETS , CONCRETE , AND VISCOELASTIC LAYERS UNDER STATIC AND DYNAMIC LOADING.” *Proceedings of the International Symposium on Bond Behaviour of FRP in Structures (BBFS 2005)*, C. and Teng, ed., International Institute for FRP in Construction, Hong Kong, China, 489–494.

Hwang, S.-J., Fang, W.-H., Lee, H.-J., and Yu, H.-W. (2001). “Analytical Model for Predicting Shear Strengthof Squat Walls.” *Journal of Structural Engineering*, American Society of Civil Engineers, 127(1), 43–50.

Inukai, M., and Kaminosono, T. (2000). “Seismic Performance of an existing RC frame retrofitted by Precast Prestressed Concrete Shear Walls.” *12th World Conference on Earthquake Engineering*, Auckland, New Zeland, 2246.

Izuno, K., Iemura, H., Yamada, Y., and Fujisawa, S. (1993). *SeismicDamage Assessment of RC Structures Using Different Hysteretic Models*. Kyoto , 1–19.

JORF n°0248. (2010a). “Décret n° 2010-1254 du 22 octobre 2010 relatif à la prévention du risque sismique .” <http://www.legifrance.gouv.fr/affichTexte.do?cidTexte=JORFTEXT000022941706&dateTexte=&categorieLien=id#JORFARTI000022941709> (Oct. 24, 1BC).

JORF n°0248. (2010b). “Décret n° 2010-1255 du 22 octobre 2010 portant délimitation des zones de sismicité du territoire français .” <http://www.legifrance.gouv.fr/affichTexte.do?cidTexte=JORFTEXT000022941731&dateTexte=&categorieLien=id> (Oct. 24, 1BC).

James G. MacGregor. (2002). “Derivation of strut and tie model for the 2002 ACI code.” *ACI SP-208: Examples for the Design of Structural Concrete with Strut-and-Tie Models*, American Concrete Institute, ed., Karl Heinz Reineck, Michigan, 7–39.

Jinno, Y., Tsukagoshi, H., and Yabe, Y. (2001). “RC Beams with Slabs strengthened by CF sheets and bundles of CF strands.” *FRPRCSS International symposium*, Tomas Telford, Cambridge (UK), 981–7.

Kabayesawa, T. H., Shiohara, S., Otani, S., and Aoyama, H. (1982). “Analysis of the Full-Scale 7-Story R.C. Test Structure.” *3rd Joint Technical Coordinating Committee*, U.S. Japan Cooperative Earthquake Research Program, Building Research Institute, Tsukuba.

Kaplan, H., Bilgin, H., Yilmaz, S., Binici, H., and Oztas, A. (2010). “Structural damages of L’Aquila (Italy) earthquake.” *Natural Hazards and Earth System Science*, 10(3), 499–507.

Kara, I. F., and Dundar, C. (2009). “Prediction of deflection of reinforced concrete shear walls.” *Advances in Engineering Software*, Elsevier Ltd, 40(9), 777–785.

Karantzikis, M., Papanicolaou, C. G., Antonopoulos, C. P., and Triantafillou, T. C. (2005). “Experimental Investigation of Nonconventional Confinement for Concrete Using FRP.” *ASCE Journal of Composites for Construction*, American Society of Civil Engineers, 9(6), 480–487.

Katsumata, H., Kobatake, Y., and Takeda, T. (1988). “A Study on the Strengthening with Carbon Fiber for Earthquake-Resistant Capacity of Existing Reinforced Concrete Columns.” *Ninth World Conference on Earthquake Engineering*, Tokyo, Japan, 517–522.

Khalifa, A., Alkhrdaji, A., Nanni, A., and Lansburg, S. (1999). “Anchorage of surface Mounted FRP Reinforcement.” *Concrete International: Design and Construction*, 21(10), 49–54.

Kim, P., and Meier, U. (1991). “CFRP Cables for Large Structures.” *Advanced Composite Materials in Civil Engineering Structures Conference*, Las Vegas, Nevada.

Kim, T., and Foutch, D. A. (2007). “Application of FEMA methodology to RC shear wall buildings governed by flexure.” *Engineering Structures*, 29(10), 2514–2522.

Kobayashi, K. (n.d.). “Innovative Application of FRPs for Seismic Strengthening of RC Shear Wall.” 1269–1288.

Kobayashi, K., Fujii, S., Yabe, Y., Tukagoshi, H., and Sugiyama, T. (2001). “Advanced wrapping system with CF-anchor: stress transfer mechanism of CF-anchor.” *FRPRCS5 International symposium*, Thomas Telford, ed., Cambridge, UK.

Komodromos, P. (2000). *Seismic Isolation for Earthquake Resistant Structures (Advances in Earthquake Engineering)*. WIT Press, 201.

Kotronis, P., Ragueneau, F., and Mazars, J. (2005). "A simplified modelling strategy for R/C walls satisfying PS92 and EC8 design." *Engineering Structures*, 27(8), 1197–1208.

Kotynia, R., Abdel, B. H. ., Neale, K. W., and Ebead, U. A. (2008). "Flexural strengthening of RC beams with externally bonded CFRP systems: test results and 3-D nonlinear FE analysis." *ASCE Composite Construction* , 12(2), 190–201.

Kunnath, S. K., Reinhorn, A. M., and Park, Y. J. (1990). "Analytical Modeling of Inelastic Seismic Response of R/C Structures." *Journal of Structural Engineering*, American Society of Civil Engineers, 116(4), 996–1017.

Lai, S. S., Will, G. T., and Otani, S. (1984). "Model for Inelastic Biaxial Bending of Concrete Members." *Journal of Structural Engineering*, 110(11), 2563–2584.

Lamothe, P. (1999). "Essais de renforcement avec des matériaux composites pour des poutres de pont en béton armé." Université de Sherbrooke ISIS, Canada.

Lefas, I. D., Kotsovos, M. D., and Ambraseys, N. N. (1990). "Behavior of reinforced concrete structural walls: strength, deformation characteristics, and failure mechanisms." 87(1), 23–31.

Lestuzzi, P. (2000). "Dynamisches plastisches Verhalten von Stahlbetonw¨anden unter Erdbebeneinwirkung." ETH Z¨urich.

Lestuzzi, Pierino, and Bachmann, Hugo. (2007). "Displacement ductility and energy assessment from shaking table tests on RC structural walls." *Engineering Structures*, 29(8), 1708–1721.

Li, K. N. (2006). "Three dimensional nonlinear static and dynamic structural analysis computer program." Vancouver, Canada.

Liang, Y. (2004). "Ductility and damage evaluation of post-tensioned concrete beams with hybrid FRP tendon." University of Illinois at Chicago.

Linde, P., and Bachmann, H. (1994). "Dynamic modelling and design of earthquake-resistant walls." *Earthquake Engineering & Structural Dynamics*, 23(12), 1331–1350.

Lombard, J., Humar, J. L., and Cheung, M. S. (2000). "No Title." *12th World Conference on Earthquake Engineering*, Auckland, New zeland, 2032.

Maier, J., and Thurlimann, B. (1985). *Bruchversuche an Stahlbetonscheiben*. Zurich, 130.

Malvar, L.J., Bish, J. (1995). "Grip Effects in Tensile Testing of FRP Bars." *Second FRP International Symposium, Non-Metallic (FRP) Reinforcements for Concrete Structures*, Gent, Belgium, 108–115.

Matsuzaki, Y., Nakano, K., Fukuyama, H., and Watanabe, S. (2001). "Advanced Wrapping system with CF-Anchor, shear strengthening of RC columns with spandrel wall." *Fifth International Symposium on Fiber Reinforced Polymer Reinforcement for Reinforced Concrete Structures*, Cambridge (UK), 813–822.

Matthys, S. (2000). “Structural behaviour and design of concrete members strengthened with externally bonded FRP reinforcement.” Ghent University.

Mau, S. T., and Thomas, T. C. H. (1986). “Shear Design and Analysis of Low-Rise Structural Walls.” *ACI Journal Proceedings*, 83(2), 306–315.

Meier U. (1987). “Bridge repair with high performance composite materials.” *Material und Technik*, 4, 125–128.

Meyer, I. F. (1988). “Ein werkstoffgerechtes Schädigungsmodell und Stababschnittselement für Stahlbeton unter zyklisher nichtlinearer Beanspruchung.” Institut für Konstruktiven Ingenieurbau, Ruhr-Universität Bochum.

Mickleborough, N. C., Ning, F., and Chan, C. M. (1999). “Prediction of Stiffness of Reinforced Concrete Shearwalls under Service Loads.” *ACI Structural Journal*, 96(6), 1018–26.

Mitchell, D., Cook, W. D., Uribe, C. M., and Alcocer, S. M. (2002). “EXPERIMENTAL VERIFICATION OF STRUT-AND-TIE MODELS. IN: EXAMPLES FOR THE DESIGN OF STRUCTURAL CONCRETE WITH STRUT-AND-TIE MODELS.” *ACI Fall Convention*, American Concrete Institute, ed., Reineck, ed, Farmington Hills, MI, 41–62.

Monti, G., and Spacone, E. (2000). “Reinforced Concrete Fiber Beam Element with Bond-Slip.” *Journal of Structural Engineering*, American Society of Civil Engineers, 126(6), 654–661.

Monti, Giorgio. (2003). *SEISMIC UPGRADE OF REINFORCED CONCRETE COLUMNS WITH FRP*. Tehran, 29.

Mufti A.A., Newhook J.P., T. G. (1996). “DEFORMABILITY VERSUS DUCTILITY IN CONCRETE BEAMS WITH FRP REINFORCEMENT.” *2ND INTERNATIONAL CONFERENCE ON ADVANCED COMPOSITE MATERIALS IN BRIDGES AND STRUCTURES, ACMBS-II*, MONTREAL, 189–199.

Murty, C. V. R., Rai, D. C., Bajpai, K. K., and Jain, S. K. (2003). “Effectiveness of Reinforcement Details in Exterior Reinforced Concrete Beam-Column Joints for Earthquake Resistance.” *Structural Journal*, 100(2), 149–156.

Mörsch, E. (1909). *Concrete-Steel Construction (English Translation by E. P. Goodrich)*. McGraw Hill, New York, 368 .

Naaman, A. E., and Jeong, S. M. (1995). “Structural ductility of concrete beams prestressed with FRP tendons.” *2th International Symposium on Fiber Reinforced Polymer Reinforcement for Reinforced Concrete Structures (FRPRCS-2)*, Ghent, Belgium, 379–386.

Nagy-Gyorgy, T., Mosoarca, M., Stoian, V., Gergely, J., and Dan, D. (2005). “Retrofit of reinforced concrete shear walls with CFRP composites.” *FIB Symposium “‘Keep concrete Attractive’,”* Budapest, Hungary, 897–902.

Nasseri, H. R., and Hamelin, P. (1998). “Modélisation des ouvrages en béton précontraint renforcés par plats composites.” *11èmes Journées Nationales sur les composites*, Arcachon, 1273–1281.

Nathalie, R., Pierre, L., Jean, P., Éric, S., and Patrick, P. (2009). “FRP Wrapping of RC Structures Submitted to Seismic Loads .” *Geotechnical, Geological and Earthquake Engineering*, 10, 297–305.

Niemitz, C. W., James, R., and Breña, S. F. (2010). “Experimental Behavior of Carbon Fiber-Reinforced Polymer (CFRP) Sheets Attached to Concrete Surfaces Using CFRP Anchors.” *Journal of Composites for Construction*, American Society of Civil Engineers, 14(2), 185–194.

OPECST. (n.d.). “La France est-elle préparée à un tremblement de terre ?” *Communiqué du 28 octobre 2010*, <http://www.senat.fr/presse/cp20101028.html>.

Oesterle, R. G., Aristizabal-Ochoa, J. D., Shiu, K. N., and Corely, W. G. (1984). “Web Crushing of Reinforced Concrete Structural Walls.” *ACI journal Proceedings*, 81(3), 231–241.

Oh, Y., Han, S. W., and Lee, L. (2002). “Effect of boundary element details on the seismic deformation capacity of structural walls.” 1602(January), 1583–1602.

Orakcal, K., and Wallace, J. W. (2006). “Flexural Modeling of Reinforced Concrete Walls - Experimental Verification.” *ACI Structural Journal*, 103(2), 196–206.

Orozco, A. L. (2001). “Investigation of ductility in FRP reinforced concrete beams.” University of New Mexico.

Orozco, A. L., and Maji, A. K. (2004). “Energy Release in Fiber-Reinforced Plastic Reinforced Concrete Beams.” *Journal of Composites for Construction*, American Society of Civil Engineers, 8(1), 52–58.

Orton, S. L., Asce, A. M., Jirsa, James O, Asce, M., and Bayrak, O. (2008). “Design Considerations of Carbon Fiber Anchors.” (December), 608–616.

Otani, S. (1974). “Inelastic Analysis of R/C Frame Structures.” *Journal of the Structural Division*, 100(7), 1433–1449.

Ozbakkaloglu, T., Ph, D., and Saatcioglu, Murat. (2009). “Tensile Behavior of FRP Anchors in Concrete.” (April).

Ozcan, O., Binici, B., and Ozcebe, G. (2008). “Improving seismic performance of deficient reinforced concrete columns using carbon fiber-reinforced polymers.” *Engineering Structures*, 30(6), 1632–1646.

Panneton, M., Léger, P., and Tremblay, R. (2006). “Inelastic analysis of a reinforced concrete shear wall building according to the National Building Code of Canada 2005.” *Canadian Journal of Civil Engineering*, NRC Research Press Ottawa, Canada, 33(7), 854–871.

Papazoglou, J., and Elnashai, A. S. (1996). "ANALYTICAL AND FIELD EVIDENCE OF THE DAMAGING EFFECT OF VERTICAL EARTHQUAKE GROUND MOTION." *Earthquake engineering and structural dynamics*, 25, 1109–1137.

Park, R., Kent, D. C., and Sampson, R. A. (1972). "Reinforced Concrete Members with Cyclic Loading." *Structural Division*, 98(7), 1341–1360.

Park, Robert, and Paulay, Thomas. (1975). *Reinforced Concrete Structures*. John Wiley & Sons, Newyork, 800.

Park, Y. J., and Ang, A. H. S. (1985). "Mechanistic Seismic Damage Model for Reinforced Concrete." *Journal of Structural Engineering*, American Society of Civil Engineers, 111(4), 722–739.

Park, Y. J., Ang, A. H. S., and Wen, Y. K. (1985). "Seismic Damage Analysis of Reinforced Concrete Buildings." *Journal of Structural Engineering*, American Society of Civil Engineers, 111(4), 740–757.

Paterson, J., and Mechanics, A. (2001). *Seismic retrofit of reinforced concrete shearwalls*.

Paulay, T, and Priestley, M. J. N. (1982). "Ductility in earthquake resisting squat shear wall.pdf." *ACI Journal*, 79(4), 257–69.

Paulay, T., Priestley, M. J. N., and Synge, A. J. (1982). "Ductility in Earthquake Resisting Squat Shearwalls." *ACI Journal Proceedings*, 79(4), 257–69.

Pellissier, V. (2004). "Evaluation de stratégies pour la gestion du risque sismique du bâtiment." EPFL, Lausanne.

Pincheira, J. A., and Jirsa, J.O. (1995). "Seismic Response of RC Frames Retrofitted with Steel Braces or Walls." *Journal of Structural Engineering*, 121(8), 1225–1235.

Promis, G., Ferrier, E., and Hamelin, P. (2009). "Effect of external FRP retrofitting on reinforced concrete short columns for seismic strengthening." *Composite Structures*, Elsevier Ltd, 88(3), 367–379.

"Quake-hit express highway reopen." (2011). *Daily Yomiuri Online*, <http://www.yomiuri.co.jp/dy/> (Mar. 25, 1BC).

Rao, P. S., Sarma, B. S., Lakshmanan, N., and Stangenberg, F. (1998). "Damage Model for Reinforced Concrete Elements under Cyclic Loading." (95).

Ritter, W. (49AD). "Die Bauweise Hennebique." *Schweizerische Bauzeitung*, 33(7), 1899.

Rodriguez, M., and Park, R. (1994). "Seismic Load Tests on Reinforced Concrete Columns Strengthened by Jacketing." *ACI Structural Journal*, 91(2), 150–159.

Rogowsky, D. M., MacGregor, J. G., and Ong, S. Y. (1986). "Tests of Reinforced Concrete Deep Beams." *ACI Journal Proceedings*, 83(4), 614–623.

Rostasy, F. S. (1987). *Bonding of Steel and GFRP Plates in the Area of Coupling Joints. Talbrucke Kattenbusch*. Braunschweig, Germany.

Rothe, D. (1992). "Untersuchungen zum nichtlinearen Verhalten von Stahlbetonwandscheiben unter Erdbebenbeanspruchung, ." Institut für Massivbau, TH Darmstadt.

Roufaiel, M. S. L., and Meyer, C. (1987). "Analytical Modeling of Hysteretic Behavior of R/C Frames." *Journal of Structural Engineering*, American Society of Civil Engineers, 113(3), 429–444.

Rousseau, J. (1756). "Lettre à Voltaire sur la Providence, , Lettres sur divers sujets de philosophie, de morale et de politique."

Saatcioglu, M, Serrato, F., and Foo, S. (n.d.). "Seismic Performance of Masonry Infill Walls Retrofitted With CFRP Sheets." 341–354.

Sadeghi, K., Lamirault, J., and Sieffert, J. G. (1993). "Damage Indicator Improvement Applied on R/C Structures Subjected to Cyclic Loading." *Second EURODYN*, Trondheim, Norway, 129–136.

Salonikios, T.N., Kappos, A.J., Tegos, I. A., and Penelis, G. G. (1999). "Cyclic Load Behavior of Low-Slenderness Reinforced Concrete Walls : Design Basis and Test Results." *ACI Structural Journal*, 96(4), 649–660.

Salonikios, T.N., Kappos, A.J., Tegos, I. A., and Penelis, G. G. (2000). "Cyclic Load Behavior of Low-Slenderness Reinforced Concrete Walls: Failure Modes, Strength and Deformation Analysis, and Design Implications." *ACI Structural Journal*, 97(1), 132–142.

Schlaich, J., Schaefer, K., and Jennewein, M. (1987). "Towards a Consistent Design of Structural Concrete." *PCI*, 32(3), 74–150.

Sezen, H., Whittaker, A. S., Elwood, K. J., and Mosalam, K. M. (2003). "Performance of reinforced concrete buildings during the August 17, 1999 Kocaeli, Turkey earthquake, and seismic design and construction practise in Turkey." *Engineering Structures*, 25(1), 103–114.

Sittipunt, C., and Wood, S. L. (1996). "Influence of Web Reinforcement on the Cyclic Response of Structural Walls." *ACI Structural Journal*, 92(6), 745–756.

Sittipunt, C., Wood, S. L., Lukkunaprasit, P., and Pattararattanakul, P. (2001). "Cyclic Behavior of Reinforced Concrete Structural Walls with Diagonal Web Reinforcement." *ACI Structural Journal*, 98(4), 554–562.

Stephens, J. E., and Yao, J. T. P. (1987). "Damage Assessment Using Response Measurements." *Journal of Structural Engineering*, American Society of Civil Engineers, 113(4), 787–801.

Su, R. K. L., and Wong, S. M. (2007). "Seismic behaviour of slender reinforced concrete shear walls under high axial load ratio." *Engineering Structures*, 29(8), 1957–1965.

Takayanagi, T., and Schnobrich, W. C. (1976). *Computed Behaviour of R/C Coupled Shear Walls*. Urbana, 206.

Tena-Colunga, A., Gomez-Soberon, C., and Munoz-Loustaunau, A. (1997). "Seismic Isolation of Buildings Subjected to Typical Subduction Earthquake Motions for the Mexican Pacific Coast." *Earthquake Spectra*, 13(3), 505–532.

Teran-Gilmore, A., Bertero, V. V., and Youssef, N. (1995). *Seismic rehabilitation of framed buildings infilled with unreinforced masonry walls using post-tensioned steel braces*. (U. of C. at B. Earthquake Engineering Research Center, ed.), Earthquake Engineering Research Center, University of California at Berkeley, Berkeley, California, 267.

The Japan Times. (2011). "Gradual restoration of infrastructures continues at disaster areas."

Thermou, G. E., and Elnashai, a S. (2006). "Seismic retrofit schemes for RC structures and local-global consequences." *Progress in Structural Engineering and Materials*, 8(1), 1–15.

Thomas Paulay. (1975). "Design Aspects of Shear Walls for Seismic Areas." *Canadian Journal of Civil Engineering*, 2(3), 321–344.

Tjhin, T. N., and Kuchma, D. A. (2007). "Integrated analysis and design tool for the strut-and-tie method." *Engineering Structures*, 29(11), 3042–3052.

Tremblay, R., Léger, P., and Tu, J. (2001). "Inelastic seismic response of concrete shear walls considering P –delta effects." *Canadian Journal of Civil Engineering*, NRC Research Press Ottawa, Canada, 28(4), 640–655.

Uribe, C. M., and Alcocer, S. M. (2001). *Comportamiento de Vigas Peraltadas Dise adas con el Modelo de Puntales y Tensores*. Mexico, 247.

VARASTEHPOUR, H., and HAMELIN, P. (1996). "EXPERIMENTAL STUDY OF RC BEAMS STRENGTHENED WITH CFRP PLATE." *PROCEEDINGS OF THE 2ND INTERNATIONAL CONFERENCE ON ADVANCED COMPOSITE MATERIALS IN BRIDGES AND STRUCTURES, ACMBS-II, MONTREAL 1996*, M EL-BADRY, ed., CANADIAN SOCIETY FOR CIVIL ENGINEERING, MONTREAL, QUEBEC, 555–63.

Vulcano, A., Bertero, V. V., and Colotti, V. (1988). "Analytical Modeling of RC Structural Walls." *9th World Conference on Earthquake Engineering*, Tokyo-Kyoto, Japan, 41–46.

Walraven, J. (1994). "Rough Cracks Subjected to Earthquake Loading." *Journal of Structural Engineering*, American Society of Civil Engineers, 120(5), 1510–1524.

Wang, H., and Belarbi, A. (2011). "Ductility characteristics of fiber-reinforced-concrete beams reinforced with FRP rebars." *Construction and Building Materials*, 25(5), 2391–2401.

Wiradinata, S., and Saactioglu, M. (1986). “Tests of Squat Shear Walls under Lateral Load Reversals.” *Proceedings of the Third U.S. National Conference on Earthquake Engineering*, Earthquake Enginnering Research Institute, Charleston, 1395–1406.

Wolf, R., and Miessler, H. J. (1989). “HLV-Spannglieder in der Praxis.” *Erfahrungen Mit Glasfaserverbundstaben, Beton*, 2, 47–51.

Wu, Y., Liu, T., and Wang, L. (2008). “Experimental Investigation on Seismic Retrofitting of Square RC Columns by Carbon FRP Sheet Confinement Combined with Transverse Short Glass FRP Bars in Bored Holes.” (February), 53–60.

Wyllie, L. A., Abrahamson, N., Bolt, B., Castro, G., and Durkin, M. E. (1986). “The Chile Earthquake of March 3, 1985—Performance of Structures.” *Earthquake Spectra*, 2(2), 293–371.

Yalcin, Cem, Kaya, O., and Sinangil, M. (2008). “Seismic retrofitting of R/C columns having plain rebars using CFRP sheets for improved strength and ductility.” *Construction and Building Materials*, 22(3), 295–307.

Yuksel, E., Ozkaynak, H., Buyukozturk, O., Yalcin, C, a.a. Dindar, Surmeli, M., and Tastan, D. (2010). “Performance of alternative CFRP retrofitting schemes used in infilled RC frames.” *Construction and Building Materials*, Elsevier Ltd, 24(4), 596–609.

Zou, P. X. W. (2003). “Flexural Behavior and Deformability of Fiber Reinforced Polymer Prestressed Concrete Beams.” *Composites for Construction*, American Society of Civil Engineers, 7(4), 275–284.

List of Figures

List of Tables

FOLIO ADMINISTRATIF

THESE SOUTENUE DEVANT L'INSTITUT NATIONAL DES SCIENCES APPLIQUEES DE LYON

NOM : QAZI (avec précision du nom de jeune fille, le cas échéant) Prénoms : Samiullah	DATE de SOUTENANCE : 17 Janvier 2013
TITRE : COMPORTEMENT MÉCANIQUE SOUS SOLLICITATIONS ALTERNÉES DE VOILES BÉTON ARMÉ RENFORCÉS PAR MATÉRIAUX COMPOSITES	
NATURE : Doctorat Ecole doctorale : MEGA Spécialité : Génie CIVIL	Numéro d'ordre :
Code B.I.U. – Lyon : T 50/210/19 / et bis	CLASSE :

RESUME :
Les enquêtes récentes sur les séismes ont fait ressortir l'importance des murs en béton armé en tant que partie intégrante des structures. L'évolution des règlements prend en compte ces considérations, par contre le bâti existant doit subir des renforcements dans l'objectif de leur mise en conformité. Dans cette thèse une étude expérimentale faite sur douze murs (six élancés et six courts) renforcés par un collage externe en composite a été conduite. Les murs ont été conçus en étant sous-renforcés à la flexion et cisaillement. Quatre de ces six échantillons ont été renforcés par des bandes de PRFC collées. Deux spécimens, un témoin et un renforcé, ont été soumis à un test de chargement statique et quatre échantillons, l'un témoin et trois rénovés, ont été soumis à des essais de charge cyclique. La discussion et l'analyse des tests incluent la description de la fissuration, l'analyse de la rigidité, de la capacité de charge ultime, de la ductilité.

MOTS CLES :
voile - béton armé - renforcement par PRF – séisme – ancrage.

Laboratoire(s) de recherches :
Laboratoire de Génie Civil et d'Ingénierie Environnementale site BOHR

Directeur de thèse :
Pr. Emannual FERIIER, Maître de conférences. Laurent Michel

Président du jury :

Composition du jury

Nathalie ROY	Professeur, Université de Sherbrooke	Rapporteur
David BIGAUD	Professeur, Université d'Angers	Rapporteur
Joaquim BARROS	Professeur à l'Université de Minho	Examinateur
Ali LIMAM	Professeur, Insa Lyon	Examinateur
Marc QUIERTANT	Chargé de recherche, IFSTTAR	Invité
Patrice HAMELIN	Professeur émérite, Université Lyon 1	Invité
Emmanuel FERRIER	Professeur, Université Lyon 1	Directeur de thèse
Laurent MICHEL	Maitre de Conférences, Université Lyon 1	Co-directeur de thèse